

Ivie L. Conlon

ivieconlon@gmail.com (personal)
Baltimore, MD

Results-driven medicinal chemist with a strong passion for organic chemistry and experience in synthesis of heterocycles that target various protein-protein interactions involved in cancer.

Education

University of Maryland Baltimore, School of Pharmacy PhD Pharmaceutical Sciences

- Department of Pharmaceutical Sciences
Aug. 2015 – December 2020
- **Focus: Synthetic Organic/Medicinal Chemistry**

Georgia Regents University (Now Augusta University) B.S. Biology

- Augusta, GA
Aug. 2011 – May 2015
 - Undergraduate Research Assistant
2013 – 2015
-

Research Experience

GRADUATE RESEARCH ASSISTANT

University of Maryland, Baltimore, MD January 2016 – September 2020

- Under the direction of Dr. Steven Fletcher
- Design, synthesis, and biological evaluation of various small molecule alpha-helix mimetics using structure-based drug design.
- Libraries of compounds were developed that disrupt helix-mediated protein-protein interactions involved in cancer.
- Novel compounds developed targeting the Bcl-2 family anti-apoptotic proteins. Projects included:
 - Various heterocyclic scaffolds such as isoxazoles, pyrazoles, and indoles targeting Mcl-1,
 - Covalent inhibitors of Bfl-1 utilizing a variety of different electrophilic warheads, and
 - Bcl-2 PROTACs based on the Bcl-2 inhibitor venetoclax.
- Employed rationally-designed polypharmacology with isoxazole, pyrazole, imidazole, and thiazole scaffolds developed against two proteins: HDM2 and Mcl-1.
- Developed dual inhibitors that target BRD4 and HDAC6.

- Worked in a collaborative environment with numerous postdocs, cell biologists, and computational chemists, while mentoring undergraduates and PharmDs.

GRADUATE RESEARCH ASSISTANT

University of Maryland, Baltimore, MD

August 2015 – December 2016

- Under the direction of Dr. James Polli
- Evaluation of novel tri-fluorinated imaging agents, CA-lys-TFA and CA-sar-TFA, in WT mice and mice with impaired bile acid transport.
- Analyzed mouse gallbladder, liver, and blood samples with LC/MS/MS.

UNDERGRADUATE RESEARCH ASSISTANT

Georgia Regents University

August 2013 – May 2015

- Biological evaluation of analogues of persin, a microtubule stabilizing agent in MCF-7 cells.
- Evaluation performed with western blots and cell viability assays.

Skills and Techniques

- Synthetic organic and medicinal chemistry with experience in sensitive syntheses, automated and manual column chromatography, microwave reactors, and NMR for characterization
- Multi-step syntheses
- Heterocyclic chemistry
- Experience with molecular modeling software and methodology, including PyMOL, VMD, and Site Identification by Ligand Competitive Saturation (SILCS)
- Ability to work independently as well as in a team setting
- Excellent communication skills due to the collaborative work environment with both computer-aided drug design and biology groups, as well as group meetings with other chemistry labs
- Skilled at working in high pressure environments with careful attention to safety
- Excellent analytical thinking and problem-solving skills due to the nature of long organic syntheses
- Experience in protein purification and fluorescence polarization competition assays, analysis using GraphPad

Awards, Leadership, and Affiliations

- Department of Pharmaceutical Sciences Merit Award **Academic year 2019 –2020**
- ACS Travel Award **Spring 2020**
- ACS Travel Award **Spring 2018**
- Pharmacy Graduate Student Association 2nd year Graduate Representative **2016 – 2017**

- Royal Society of Chemistry, Rho Chi, American Chemical Society, American Association of Pharmaceutical Sciences, American Association for the Advancement of Science Member

Publications

Conlon, I.L., Drennen, B., Falat, A., MacKerell, A. D., Jr., Wilder, P.T., and Fletcher, S. “Design, synthesis, and biological evaluation of Mcl-1 selective inhibition using densely functionalized heterocycles” *Manuscript in prep.*

Conlon, I.L., Drennen, B., Lanning, M.E., Hughes, S., Rothhaas, R., MacKerell, A. D., Jr., Wilder, P.T., and Fletcher, S. “Rationally-designed polypharmacology: α -Helix mimetics as dual inhibitors of the oncoproteins Mcl-1 and HDM2” *ChemMedChem*, **2020**. *In Press.*

Conlon, I.L., Konsein, K., Morel, Y., Chan, A., and Fletcher, S. “Construction of 1H-indazoles from ortho-aminobenzoximes by the Mitsunobu reaction” *Tetrahedron Lett*, **2019**. *60*(37), 150929.

Conlon, I.L., Van Eker, D., Abdelmalak, S., Murphy, W.A., Bashir, H., Sun, M., Chauhan, J., Varney, K.M., Godoy-Ruiz, R., Wilder, P.T., and Fletcher, S. “Kröhnke pyridines: Rapid and facile access to Mcl-1 inhibitors” *Bioorg. Med. Chem Lett*, **2018**, *28*(10), 1949-1953.

Van Eker, D., Chauhan, J., Murphy, W.A., **Conlon, I.L.**, and Fletcher, S. “Chromatography-free, Mitsunobu-triggered heterocyclizations of salicylhydroxamic acids to 3-hydroxybenzisoxazoles” *Tetrahedron Lett*, **2016**, *57*(48), 5301-5303.

Patents

Conlon, I. L.; Drennen, B.; Lanning, M. E. and Fletcher, S. "Dual Inhibitors of the Bcl-2 and HDM2 Families Through Co-Mimicry of the BH3 and P53-Alpha-Helices." WO 2019040511A1, February 2019.

Conference Presentations

Conlon, I.L., Drennen, B., Wilder, P.T., MacKerell, A.D., Jr., Fletcher, S. “Rationally-designed polypharmacology: α -Helix mimetics as pan inhibitors of the oncoproteins Bcl-2, Mcl-1, and HDM2” Presented at the Gordon Research Seminar and Conference for Medicinal Chemistry, New London, NH, August 3-9, 2019. Poster.

Conlon, I.L., Drennen, B., Wilder, P.T., Mackerell, A.D., Fletcher, S. “Second Generation Isoxazoles and Pyrazoles Functioning as Pan Inhibitors Targeting Bcl-2, Mcl-1, and MDM2” Presented at the 7th RSC-BMCS Fragment-based Drug Discovery meeting, Cambridge, UK, March 24-26, 2019. Poster.

Conlon, I.L., Falat, A., Bowen, N.G., and Fletcher, S. “Dual Inhibition of Bcl-2/Mcl-1 and MDM2 with Novel α -helix Mimetics Based on a Densely-Functionalized Isoxazole Core” Presented at the 255rd ACS National Meeting, New Orleans, LA, March 18-22, 2018. Poster.

Conlon, I.L., Drennen, B., Lanning, M.E., Chen, L., Hughes, S., Wilder, P.T., and Fletcher, S. “Two-Faced Synthetic α -Helix Mimetics Based on Heterocyclic Cores as Dual Bcl-2/MDM2 Inhibitors.” Presented at the University of Maryland, Baltimore Research day, Baltimore, MD, April 12, 2017. Poster.

Conlon, I.L., Van Eker, D., Chauhan, J., and Fletcher, S. “Krohnke Pyridine Synthesis Permits Facile Access to Novel Mcl-1 Inhibitors.” Presented at the 253rd ACS National Meeting, San Francisco, CA April 2-6, 2017. Poster.

Jones, K.L., Clay, R.K., and **Conlon, I.L.** “Two Novel Compounds Induce Apoptosis in a Breast Cancer Cell Line.” Presented at the 15th Annual Phi Kappa Phi Student Research and Fine Arts Conference, Augusta, GA, March 19, 2014. Oral.

Abstract

Dissertation Title: Targeting Aberrant α -Helix Mediated Protein-Protein Interactions with Densely Functionalized Heterocycles

Ivie L. Conlon, Doctor of Philosophy, 2020

Dissertation Directed By: Dr. Steven Fletcher, Associate Professor, Pharmaceutical Sciences

Protein-protein interactions (PPIs) play crucial roles in cell proliferation, differentiation, and apoptosis. Apoptosis is a highly regulated process of cell death and its dysregulation can lead to a multitude of different pathophysiologies, such as cancer. In particular, the overexpression of pro-life Bcl-2 proteins, such as Bcl-2, Bfl-1, and Mcl-1, has been linked to cancer progression and tumorigenesis, as well as chemoresistance to a number of different chemotherapeutics. The binding counterparts of these proteins, pro-death Bcl-2 proteins such as Bim, and p53 transactivation domain (TAD), exert their effects through α -helix mediated PPIs with key residues i , $i+3/4$, and $i+7$ oriented on one side of the helix. In addition, HDM2, the E3 ubiquitin protein ligase responsible for the degradation of p53, is upregulated in numerous cancers, and given the similarities of the recognition profiles of Bim-BH3 and p53TAD, we have designed α -helix mimetic inhibitors that target Mcl-1 and HDM2. The first generation of compounds included various heterocyclic scaffolds, including isoxazoles, pyrazoles, and thiazoles, that project functional groups in a similar manner to the native α -helices. In addition, bicyclic scaffolds have been utilized in Mcl-1 selective inhibition. Therefore, we developed a second generation of compounds of isoxazoles, pyrazoles, and functionalized indoles to further explore the binding interface of Mcl-1. The recent resurgence of covalent

inhibition and targeted protein degradation has led to the development of successful Bcl-2 family inhibitors. We have designed two tris-aryl α -helix mimetic scaffolds targeting the Bfl-1 pro-life protein. A unique surface-accessible cysteine within the BH3 domain allows for the development of reversible and irreversible small molecule covalent inhibitors. In addition, we have also designed a venetoclax-based PROTAC targeting Bcl-2.

Targeting Aberrant alpha-Helix Mediated Protein-Protein Interactions with Densely
Functionalized Heterocycles

by
Ivie Conlon

Dissertation submitted to the Faculty of the Graduate School of the
University of Maryland, Baltimore in partial fulfillment
of the requirements for the degree of
Doctor of Philosophy
2020

Acknowledgements

First, I want to thank my advisor Dr. Steven Fletcher. I have learned how to be an independent researcher in this lab, generate ideas for myself, and work through problems on my own. I still have so much to learn, but I know I've been set up well for the future. The projects I had taught me so much chemistry. For that I am really thankful. I also appreciate all the conferences I've been able to attend and the amount of knowledge I've gained from them. I will be forever grateful for what I've learned throughout my graduate school career from Steve.

I would also like to thank my committee members: Drs. Andy Coop, Alex MacKerell, and Paul Shapiro. Individually, I have learned so much from them. Throughout group and individual meetings, I have learned so much chemistry from Andy. I also really value the insight and guidance he has given me over the past several years. I would also like to thank Alex, as he has given me a lot of guidance and help in learning SILCS as well as in terms of my career. I would also like to thank Paul Shapiro. Not only did he let me do protein work in his lab, but he helped my understanding of a lot of issues I was having at the time as well. Without these three faculties, I would not be the scientist I am today. I would also like to thank Dr. Takashi Tsukamoto for being on my committee. I would like to thank Dr. Paul Wilder for helping me learn the fluorescence polarization assay and answering any questions I had (which were a lot). I would also like to thank all the students in the department that helped me with the issues I had with protein purification and my assays, most notably Lizzie, Jordan, Ramon, and Amy. They were so extremely helpful. There are literally countless others. Lastly, I'd like

to thank Chad and Imran. They were so extremely nice and helpful throughout the years, and I really value the conversations and help I received from them.

I would also like to thank my lab (past and present): Lee, Maryanna, Brandon, Alex, and Chris. I had tons of fun with all the lab outings and conferences we've been to. I would also like to thank Katie Konsein. There's no one else I'd rather talk about marshmallow eggs with and eat loads of sweets with than you. Thank you to my absolute best friend Jennifer. You've always been there for me and given tons of support. I would also like to thank my bois Greg and Nathan. Who would've thought your year abroad would lead to a contractually obliged friendship? Our friendship has meant the world to me. So much so I can't even put it into words really-except for maybe a contract.

Lastly, I would like to thank my family: my mom, grandma, my two uncles-Wes and Richard, my aunt Robin, and Amanda. I have felt so much support and love from my family. I couldn't do this without them. I can't forget to thank my dog, Ellie. Red velvet church face daisy. Most importantly, my mom has done so much to make sure I've succeeded. She listens to everything with an open heart and is always there at the end of the day. I know she's sacrificed so much to make sure I am where I need to be- I really owe this all to her. I would also like to thank my grandma. She is always there to listen and has so much love to give. I wouldn't be where I am today without my mom and grandma.

Table of Contents

List of Tables	xi
List of Figures	xii
List of Abbreviations	xix
Chapter 1. The Bcl-2 Protein Family: Structure, Function, and Implication in Cancer	1
1.1. Introduction	1
1.2. The Bcl-2 family members: Structure and cellular localization	1
1.3. The Protein-Protein Interaction	4
1.4. The Bcl-2 Protein Family and Regulation of Apoptosis	6
1.4.1. BH3-only Protein Expression and Activation: The First Step in Apoptosis	6
1.4.2. The Direct Activation Model	7
1.4.3. BH3-only “Sensitizer” proteins	8
1.4.4. Multi-domain Pro-apoptotic Proteins Bak and Bax: Structure and Mitochondrial Localization	8
1.4.5. Structural changes of Bax	9
1.4.6. Mitochondrial Outer Membrane Permeabilization	9
1.5. Bcl-2 Proteins and Cancer	11
1.5.1. Targeting the Overexpression of Bcl-2 Anti-apoptotic Proteins with BH3 Mimetics	12
1.6. ABT-737, ABT-263, and the approval of ABT-199	14

1.6.1. Development of ABT-737	14
1.6.2. Development of Navitoclax (ABT-263).....	16
1.6.3. Development of Venetoclax (ABT-199).....	19
1.7. Bcl-2 Selective Inhibitors.....	21
1.7.1. S55746.....	21
1.7.2. Beigene Compounds.....	25
1.7.3. Ascentage Compounds	27
1.8. Bcl-2/Bcl-xL Dual Inhibitors	29
1.8.1. Ascentage Bcl-2/Bcl-xL dual inhibitor.....	29
1.9. Bcl-xL selective inhibition.....	31
1.9.1 Abbvie compounds.....	31
1.9. Mcl-1 selective inhibitors.....	36
1.9.1. AMG176 and AMG397.....	37
1.9.2. Servier and Vernalis	40
1.9.3. AZD5991	44
1.9.4. Abbvie compounds.....	47
1.10. Bfl-1 Inhibition.....	51
1.10.1. Structure and Function.....	52
1.10.2. Mode-of-Action.....	52
1.10.3. Implication in Cancer and Chemoresistance	53

1.11. Conclusions	54
1.12. References	55
Chapter 2. Rationally Designed Polypharmacology: α -Helix Mimetics as Dual Inhibitors of the Oncoproteins Mcl-1 and HDM2	67
2.1. Introduction	67
2.2. Results and Discussion.....	71
2.3. Computer aided drug design	75
2.4. Synthesis.....	77
2.5. Results	80
2.6. Conclusion.....	83
2.7 Supplementary Information.....	84
2.7.1. Chemistry.....	84
2.7.2. Biology	98
2.7.3. References	104
2.8. References	104
2.9. Acknowledgement.....	110
Chapter 3. Densely functionalized heterocycles selectively targeting Mcl-1	112
3.1. Introduction	112
3.2. α -Helix Mimicry.....	112
3.3. Design and Results- Series 1	114

3.3.1. Computer-Aided Drug Design.....	117
3.4. Synthesis.....	119
3.4.1. <i>Isoxazoles</i>	119
3.4.2. Pyrazoles.....	120
3.4.3. <i>3-substituted 2-acylsulfonamide 1-H indoles</i>	120
3.5. Series 1 Results	121
3.6. Design and Results-Series 2.....	124
3.7. Synthesis.....	125
3.7.1. <i>3-reverse sulfonamide 1H-indole</i>	125
3.8. Series 2 Results	126
3.9. Discussion	127
3.10. References	128
3.11. Supplementary Information.....	132
3.11.1. Chemistry.....	132
3.11.2. Biology	160
3.11.3. References	164
3.12. Acknowledgements	165
Chapter 4. Kröhnke pyridines: Rapid and facile access to Mcl-1 inhibitors	166
4.1. References	174
4.2. Supplementary Information.....	176

4.2.1. Chemistry: General.....	176
4.2.2. Biology	190
4.2.3. References	193
4.3. Acknowledgement.....	194
Chapter 5. Construction of 1 <i>H</i> -indazoles from <i>ortho</i> -aminobenzoximes by the Mitsunobu reaction.....	195
5.1. Conclusions	201
5.2. References	202
5.3. Supplementary Information.....	203
5.4. Acknowledgement.....	205
Chapter 6. Ongoing and future small molecule inhibitors targeting the Bcl-2 Anti-apoptotic Proteins.....	206
6.1. Introduction	206
6.2. Targeted Protein Degradation	206
6.3. Advantages and Disadvantages of PROTAC design	210
6.4. Venetoclax-based PROTACs.....	212
6.4.1. Venetoclax PROTAC approach.....	213
6.4.2. Design.....	214
6.5 Targeting the Bcl-2 family anti-apoptotic protein Bfl-1 through covalent inhibition	215

6.6. Current strategies to target Bfl-1	215
6.7. Stapled α -helix Covalent Inhibitors of Bfl-1	217
6.8. Design.....	219
6.8.1. JY-1-106	221
6.8.2. Triazene based scaffold	224
6.8.3. Electrophilic warheads	226
6.7. Discussion	228
6.8. Future Work and Introspection	228
6.9. Conclusion.....	229
6.9. References	231
Chapter 7. References	236

List of Tables

Table 2. 1. Inhibition of Mcl-1 and HDM2 with isoxazoles, pyrazoles, and thiazoles using fluorescence anisotropy competition assay (FACA). NA: no activity. Data are represented as the average of experiments performed in triplicate \pm SD. IC ₅₀ values were converted into K _i values by using the Nikolovska-Coleska equation ⁶¹	80
Table 3. 1. Series 1 fluorescence polarization data. IC ₅₀ 's were converted to K _i 's with the Nikolovska-Coleska equation ³⁴	122
Table 3. 2. Series 2 fluorescence polarization data. IC ₅₀ 's were converted to K _i 's with the Nikolovska-Coleska equation ³⁴	127
Table 4. 1. Mcl-1 inhibitory structure–activity relationships of Kröhnke pyridines. IC ₅₀ data from a fluorescence polarization assay with Mcl-1 ¹⁷²⁻³⁷¹ and TAMRA-labeled Bak-BH3 peptide were converted to K _i values using the Nikolovska-Coleska equation. ²⁶ ...	171
Table 5.1. Optimization of the Mitsunobu-triggered cyclodehydration. ^a isolated yield after purification by flash column chromatography.....	197
Table 5.2. Substrate scope for Mitsunobu reaction with NHBoc oximes. ^a Reagents and conditions: The oxime (1 eq) is dissolved in anhydrous THF (0.1 M), then PPh ₃ (2 eq) and DIAD (2 eq) are added. The reaction is heated at 60 °C for 4 h; ^b isolated yield after purification by flash column chromatography; ^c contaminated with DIAD-H ₂ , yield determined by NMR.	198
Table 5.3. Substrate scope for Mitsunobu reaction with NHR oximes utilizing optimized reaction conditions. ^a Isolated yield; ^b contaminated with DIAD-H ₂ , yield determined by ¹ H NMR; ^c ADDM substituted for DIAD.....	199

List of Figures

Figure 1. 1. The Bcl-2 protein family divided into the three subgroups that comprise the family.	2
Figure 1. 2. The globular structure of Bcl-xL (right) showcasing the nine α -helices. The interaction within the BH3 binding domain highlighted with Bcl-xL (cyan) and Bim (grey) protein-protein interaction. PDB 1PQ1.	2
Figure 1. 3. Experimental data from alanine scanning mutagenesis. Residues mutated to alanine are bolded and underlined. Yellow bars represent residues that caused significant loss in binding affinity.	5
Figure 1. 4. Critical residues and their positions within the α -helix of the Bak-BH3 peptide determined by alanine scanning mutagenesis. PDB 1BXL.	5
Figure 1. 5. The direct activation model.	7
Figure 1. 6. The extrinsic and intrinsic apoptosis pathways.	10
Figure 1. 7. The hallmarks of cancer.	11
Figure 1. 8. Non-primed cells (top) versus primed cells (bottom) when treated with multiple therapies such as chemotherapy and BH3 mimetics.	13
Figure 1. 9. The scales represent the delicate balance between anti- and pro-apoptotic proteins.	14
Figure 1. 10. Crystal structure of compounds 1 and 2 (top left). PDB 1YSG. Optimization led to compound 3. Site-specific replacements of compound 3 to reduce serum binding led to ABT-737. Co-crystal structure of ABT-737 and Bcl-xL (bottom right). PDB 2XYJ.	15

Figure 1. 11. Optimization of ABT-737 to the Bcl-2/Bcl-xL inhibitors ABT-263. The crystal structure of ABT-263 and Bcl-2. PDB 4LVT.	17
Figure 1. 12. Favorable interactions highlighted between an indole and Asp103 of Bcl-2, compounded by a pi-pi interaction with a phenyl group of an optimized compound (Left, PDB 4MAN). This led to the development of ABT-199 (center). The crystal structure of ABT-199 and Bcl-2 is represented on the right. PDB 6O0K.	20
Figure 1. 13. The co-crystal structure of S55746 and Bcl-2. PDB: 6GL8.....	22
Figure 1. 14. Bcl-2 selective inhibitors disclosed by Beigene in patent WO2019/210828.	25
Figure 1. 15. Bcl-2 selective inhibitors disclosed by Ascentage.	28
Figure 1. 16. Bcl-2/Bcl-xL dual inhibitors disclosed by Ascentage.	30
Figure 1. 17. The development of Bcl-xL selective inhibitor A-115463 from WEHI-539.	32
Figure 1. 18. The structure of A-115463 co-crystallized in Bcl-xL. PDB 4QVX.	33
Figure 1. 19. Development of A-1331852 from A-115463.	34
Figure 1. 20. The development of AMG176.....	38
Figure 1. 21. The SAR of Mcl-1 selective compounds described by Servier and Vernalis. Highlighted regions represent functional groups that were modified to increase affinity towards Mcl-1.	40
Figure 1. 22. The Mcl-1 selective compound S63845 co-crystallized with Mcl-1. PDB 5LOF.	42
Figure 1. 23. The development of the Mcl-1 selective inhibitor AZD5991. PDB 6FSO.	45
Figure 1. 24. The SAR leading to the development of A-1210477. PDB 5VKC.....	48

Figure 1. 25. The structure of Mcl-1 selective inhibitor A-1210477.....	49
Figure 1. 26. Structure of Bfl-1. PDB 5WHI.....	52
Figure 2. 1. A) Co-crystal structure of Bim-BH3 bound to Mcl-1 (PDB ID 2NL9). B) Hot spot residues highlighted in Bim-BH3 peptide. C) Co-crystal structure of p53TAD bound to HDM2 (PDB ID 1YCR). D) Hot spot residues highlighted in p53TAD.....	68
Figure 2. 2. Co-crystal structure of Novartis compound and HDM2 (PDB ID 4OQ3). Residue labels indicate the binding locations of the key residues in the p53TAD helix..	72
Figure 2. 3. Nutlin 3a co-crystallized with HDM2 (PDB ID 4 J3E).....	72
Figure 2. 4. Representative structures of Novartis patent CA2771936 A1 (left), Zhang et al. dual Bcl-2/HDM2 inhibitor (center), and our work presented in this manuscript (right).	73
Figure 2. 5. Energy minimization of OX0 in ChemDraw3D and overlaid with Bim-BH3 (center) and p53TAD (right) α -helices.	74
Figure 2. 6. OX0 docked in Mcl-1 (left) and HDM2 (right) with SILCS.	76
Figure 2. 7. SILCS MC docking with OX0 in A) Mcl-1 and B) HDM2.	76
Figure 2. 8. (i) NaN ₃ , DMF, r.t., 18hr; (ii) (4-OiPr)benzaldehyde, NaH, EtOH, -10°C, 4hr; (iii) NH ₂ OH·HCl, Pyridine, reflux, 1hr; (iv) Et ₃ N, NCS, DMF, rt to 90°C, 18hr; (v) LiOH·H ₂ O, THF/MeOH/H ₂ O, r.t.,18hr; (vi) hydrolysis prepared via (v) corresponding sulfonamide, isobutyl chloroformate, NMM, NaH, THF, -10°C to 0°C to r.t., 18hr.	77
Figure 2. 9. (ia) 2-iodopropane, K ₂ CO ₃ , DMF, r.t. to 60°C, 18hr; (ib) SnCl ₂ ·2H ₂ O, EtOAc, 50°C, 18hr; (iia) NaNO ₂ , H ₂ O, 0°C, 18hr; (iib) SnCl ₂ ·2H ₂ O, EtOAc, 50°C, o.n.; (iii) corresponding alcohol, K ₂ CO ₃ , DMF, 60°C, 18hr; (iv) diethyl oxalate, NaH, THF, 0°C to rt, 18hr; (v) AcOH, reflux, 18hr; (vi) LiOH·H ₂ O, THF/MeOH/H ₂ O, r.t., 18hr;	

(vii) hydrolysis prepared via (v), then corresponding sulfonamide, isobutyl chloroformate, NMM, NaH, THF, -10°C to 0°C to r.t., 18hr.....	78
Figure 2. 10. (i) NCS, ACN, 80°C, 18hr; (ii) t-BnONO, CuBr ₂ , ACN, 80°C, 18hr; (iii) 4-hydroxyphenylboronic acid, CsF, tetrakis ((triphenylphosphine)palladium(0)), DME/MeOH, 80°C, 18hr;(iv) 2-iodopropane, K ₂ CO ₃ , DMF, 50°C, 18hr; (v) LiOH·H ₂ O, THF/MeOH/H ₂ O, r.t., 18hr; (vi) corresponding sulfonamide, isobutyl chloroformate, NMM, NaH, THF, -10° to 0°C to r.t., 18hr.	79
Figure 3. 1. The Mcl-1/Bim-BH3 interaction (left). PDB 2NL9. Highlighted residues of Bim-BH3 (right).....	113
Figure 3. 2. The most potent isoxazole and pyrazole compounds from Chapter 2.....	114
Figure 3. 3. The general workflow of our isoxazole and pyrazole compounds.	115
Figure 3. 4. AZD5991 (left) and the crystal structure with key interactions highlighted. PDB 6FSO.	115
Figure 3. 5. The general workflow of our 2-acyl sulfonamide indole series.	116
Figure 3. 6. SILCS MC docking with OX0 (left) and highlighted FragMaps in Mcl-1 (center).	118
Figure 3. 7. SILCS MC docking with IN0	119
Figure 3. 8. (i) substituted ketones, diethyl oxalate, NaH, THF, 0°C to rt, 18hr, (ii) hydroxylamine HCl, EtOH, reflux, 18hr; (iii) NIS, TFA, rt, 18hr; (iv) substituted benzene boronic acids, CsF, Pd(PPh ₃) ₄ , DME/MeOH, 80°C, 18hr; (v) LiOH·H ₂ O, THF/H ₂ O/MeOH, rt, 18hr; (vi) corresponding sulfonamide, EDCI, DIPEA, DMF, rt, 18hr.	120

Figure 3. 9. (i) 6-chloro 2-ethyl ester 1H-indole, NBS, DMF, rt, 1hr; (ii) 3-chlorophenol, K ₂ CO ₃ , DMF, 100°C, 18hr; (iii) pinacol ester, Anh DMSO, 85°C, 2hr; (iv) PdCl ₂ (PPh ₃) ₂ , K ₂ CO ₃ , Anh. DMF, 110°C, 4hr; (v) LiOH H ₂ O, THF/MeOH/H ₂ O, rt, 18hr; (vi) 4-fluorobezenesulfonamide, EDCI, DMAP, DIPEA, DCM, rt, 18hr.....	121
Figure 3. 10. The crystal structure of Mcl-1 and FS0 . PDB 5IEZ.....	123
Figure 3. 11. SILCS MC docking with RS0 in Mcl-1 (left) with highlighted exclusion maps (center).....	125
Figure 3. 12. (i) H ₂ SO ₄ , Ac ₂ O,0°C to rt, 18hr; (ii) oxalyl chloride, DMF, DCM, rt to 45°C, 2hr; (iii) HNR ¹ R ² , DIPEA, Anh. DCM, rt, 18hr; (iv) LiOH H ₂ O, THF/MeOH/H ₂ O, rt, 18hr.....	126
Figure 4. 1. Some Mcl-1 inhibitors and the Bcl-x _L -selective inhibitor WEHI-539.....	168
Figure 4. 2. A. Generic inhibitor structure; B. MM2-energy minimized ligand 1 (R ¹ = R ² = OiPr, magenta, coloured by atom type) overlaid with Bim-BH3 α-helix (key residues highlighted).....	169
Figure 4. 3. A low-energy GOLD docking solution of 1 (magenta) with Mcl-1 extracted from PDB ID: 4HW2.....	169
Figure 4. 4. a) sodium pyruvate, NaOH, EtOH/H ₂ O, 1:1, RT, 1 h; b) I ₂ , pyridine, Δ, 16 h; c) NH ₄ OAc, MeOH, 60 °C, 16 h.....	170
Figure 4. 5. Two-dimensional ¹ H, ¹⁵ N-fast heteronuclear single quantum coherence (HSQC) spectra of MCL1 ¹⁷²⁻³²⁷ in the absence (black) and in the presence (red) of ILC-1-199.....	173
Figure 5.1. Drug molecules featuring a 1H-indazole motif.....	195

Figure 5.2. a) Boc ₂ O, EtOH, 50 °C, 48 h; (b) NH ₂ OH.HCl, pyridine; (c) DIAD, PPh ₃ , THF, 60 °C, 4 h; (d) TFA/CH ₂ Cl ₂ , rt, 1 h.....	197
Figure 5.3. Proposed mechanism for construction of the 1H-indazole nucleus under Mitsunobu conditions.....	200
Figure 6.1. The ubiquitin proteasome system (Ub = ubiquitin).....	207
Figure 6.2. PROTAC design (top) and the mechanism of the PROTAC technology (bottom).....	208
Figure 6.3. The first PROTAC developed by Sakamoto et al.....	209
Figure 6.4. Our venetoclax based PROTAC design. “L” represents linker.....	212
Figure 6.5. Mathieu <i>et al.</i> Bfl-1 inhibitors with corresponding binding affinities.....	215
Figure 6.6. Solvent accessible Cys highlighted in Bfl-1. PDB 3MPQ.	216
Figure 6.7. FDA approved covalent kinase inhibitors.	217
Figure 6.8. Noxa (cyan) C25 (yellow stick) and Bfl-1 C55 highlighted. PDB 3MPQ..	217
Figure 6.9. Representative acrylamide moieties used in Walensky et al. experiments.	218
Figure 6.10. D-nipepotic-acid-Noxa peptide-Bfl-1 complex. Sticks showcase the nipepotic acid moiety in contact with Bfl-1 C55 (yellow). PDB 5HWW.	219
Figure 6.11. Bim-BH3 with highlighted residues (left). Hamilton <i>et al.</i> representative terphenyl scaffold α -helix mimetic (right).....	220
Figure 6.12. Our general workflow of design. EW denotes electrophilic warhead.	221
Figure 6.13. Oligoamide-foldamer compounds with bifurcated hydrogen bonds.	221
Figure 6.14. Representative compound OA1 manually docked in Puma-Bfl-1. PDB 5UUL.	223
Figure 6.15 Oligoamide-foldamer based α -helix mimetic synthesis.	223

Figure 6.16. Triazene based α -helix mimetic synthesis.	225
Figure 6.17. Representative compound TR1 (pink) manually docked in Bfl-1-Puma- BH3. PDB 5UUL.	226
Figure 6.18. The electrophilic warheads we will use in our compound design. Acrylamide (left), pentafluorobenzenesulfonamide (center) and acrylonitrile (right). ..	227
Figure 6.19. E1cB mechanism describing thiol elimination of reversible α -cyanoacrylate covalent moiety.	227

List of Abbreviations

ADDM	Azidodicarbonyl Dimorpholide
ALL	Acute Lymphoblastic Leukemia
APAF1	Apoptotic Protease Activating Factor 1
AML	Acute Myeloid Leukemia
Bad	Bcl-2 Associated Death Promoter
Bak	Bcl-2 Homologous Antagonist Killer
Bax	Bcl-2 Associated X Protein
Bcl-2	B-Cell Lymphoma 2
Bcl-w	Bcl-2 Like Protein 2
Bcl-xL	B-Cell lymphoma Extra Large
Bim	Bcl-2 Like Protein 11
Bfl-1	Bcl-2-Related Gene Expressed in Fetal Liver
BH	B-Cell Homology
CADD	Computer-Aided Drug Design
CHOP	Cyclophosphamide, Doxorubicin, Vincristine, Prednisone
CLL	Chronic Lymphocytic Leukemia
clogP	Calculated Partition Coefficient
CML	Chronic Myeloid Leukemia
CR	Complete Remission
CRBN	Cereblon
CYP	Cytochrome P450
DEAD	Diethyl Azidocarboxylate
DIAD	Diisopropyl Azidocarboxylate
DDI	Drug-Drug Interaction
DIABLO	Diablo IAP-Binding Mitochondrial Protein
ERK	Extracellular Signal-Regulated Kinases
FADD	FAS-Associated Death Domain Protein

FDA	Federal Drug Administration
FITC	Fluorescein isothiocyanate
FOXO3A	Forkhead Box Protein O3a
FP	Fluorescence Polarization
GFE	Grid Free Energy
GM-CSF	Granulocyte Macrophage Colony Stimulating Factor
HDM2	Human Double Minute 2
HSA	Human Serum Albumin
HSQC	Heteronuclear Single Quantum Coherence Spectroscopy
IAP	Inhibitor of Apoptosis Proteins
LC/MS	Liquid Chromatography/Mass Spectrometry
MCL	Mantle Cell Lymphoma
MCL-1	Myeloid Cell Differentiation Protein
MD	Molecular Dynamics
MM	Multiple Myeloma
MOMP	Mitochondrial Outer Membrane Permeabilization
NFκB	Nuclear Factor Kappa B
NCI	National Cancer Institute
NSCLC	Non-Small Cell Lung Cancer
NHL	Non-Hodgkins Lymphoma
NMR	Nuclear Magnetic Resonance
NOE	Nuclear Overhauser Effect
NOSEY	Nuclear Overhauser Effect Spectroscopy
OMM	Outer Mitochondrial Membrane
PARP	Poly (ADP-ribose) polymerase
POI	Protein of Interest
PPI	Protein-Protein Interaction
PR	Partial Remission

PROTAC	Proteolysis Targeting Chimera
SAR	Structure Activity Relationship
SCID	Severe Combined Immunodeficiency
SCLC	Small Cell Lung Cancer
SD	Stable Disease
SIHE	Size-Independent Enthalpic Efficiency
SILCS	Site Identification by Ligand Competitive Saturation
SLL	Small Lymphocytic Leukemia
SMAC	Second Mitochondria-Derived Activator of Caspases
T-ALL	T-Cell Acute Lymphoblastic Leukemia
TAD	Transactivation Domain
TAMRA	Tetramethylrhodamine
TNF α	Tumor Necrosis Factor Alpha
TNFR	Tumor Necrosis Factor Receptor
TRAIL	TNF-Related Apoptosis-Inducing Ligand
TR-FRET	Time-Resolved Fluorescence Resonance Energy Transfer
UPS	Ubiquitin Proteasome System
VHL	Von Hippel-Lindau
WT	Wild Type

Chapter 1. The Bcl-2 Protein Family: Structure, Function, and Implication in Cancer

1.1. Introduction

This review encompasses detailed summaries of the discovery of small molecule inhibitors targeting the Bcl-2 family. The *Bcl2* (B-cell lymphoma 2) gene was first discovered in 1984. A breakpoint of the t(14;18) chromosome in follicular B-cell lymphoma caused translocations of immunoglobulin heavy chain enhancers near the *Bcl2* promoter, resulting in overexpression of the Bcl-2 protein^{1,2}. Further studies indicated Bcl-2 was involved in promoting hematopoietic cell survival³. More than 30 years later, the Bcl-2 protein family is still heavily researched in industrial and academic labs, owing to its complex interactions and importance during tumorigenesis and cancer progression. The compounds described within this chapter showcase the vast amount of information gained since its discovery. Progress in the field has been highlighted with the success of the development of venetoclax, the first Bcl-2 selective inhibitor approved by the FDA. Although venetoclax is the only small molecule inhibitor targeting the Bcl-2 family that has been FDA approved, there are many candidates in preclinical and clinical studies, both for mono- and combination therapies. A thorough examination of these inhibitors will highlight key functional groups and scaffolds that function as Bcl-2 family inhibitors as well as design strategies to prevent metabolic instability and increase pharmacokinetic properties, which can lead to a successful drug candidate. This includes learning what functional groups and molecular topologies will impart selectivity for each protein, as well as utilizing crystal structures to avoid unwanted pan-inhibition within the family.

1.2. The Bcl-2 family members: Structure and cellular localization

The Bcl-2 protein family comprises over 20 proteins divided into three subgroups, the anti-apoptotic, multi-domain pro-apoptotic, and BH3-only pro-apoptotic proteins, all of which possess one or more of the four BH (Bcl-2 homology) domains (Figure 1.1)⁴.

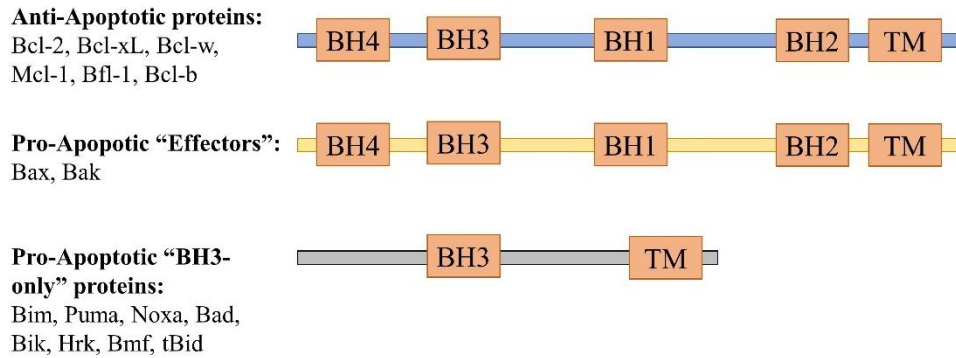


Figure 1. 1. The Bcl-2 protein family divided into the three subgroups that comprise the family.

Each protein takes part in highly regulated and tightly controlled series of α -helix mediated protein-protein interactions (PPIs)⁴⁻⁶.

The anti-apoptotic proteins include Bcl-2, Bcl-xL, Mcl-1, Bfl-1, Bcl-w, and Bcl-b. Structurally, they contain all four BH domains that take on a globular structure of internal hydrophobic α -helices surrounded by amphipathic helices (Figure 1.2)^{6,7}. A carboxy-terminal hydrophobic transmembrane domain anchors the proteins into the outer

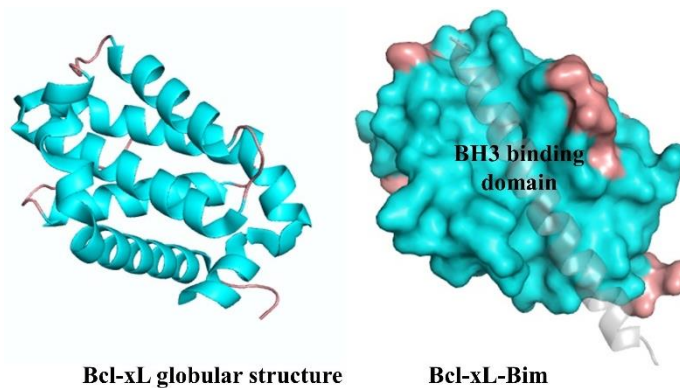


Figure 1. 2. The globular structure of Bcl-xL (right) showcasing the nine α -helices. The interaction within the BH3 binding domain highlighted with Bcl-xL (cyan) and Bim (grey) protein-protein interaction. PDB 1PQ1.

mitochondrial membrane (OMM)^{8,9}. The BH1-3 domains of the anti-apoptotic proteins form a pocket where the BH3 domain of the pro-apoptotic proteins bind (Figure 1.2, right)⁵.

The function of each anti-apoptotic protein is related to the different cell types and tissues where they are localized. Bcl-2 is required for the survival of mature lymphocytes, melanocyte stem cells, and renal epithelial stem cells; Bcl-xL for fetal erythroid progenitor and neuronal cells; Bcl-w for developing sperm cells; Bfl-1 for granulocytes and mast cells; and Mcl-1 for embryo implantation^{5,10}.

Multi-domain pro-apoptotic proteins consist of Bax and Bak, and structurally include BH domains 1,2, and 3 that take on a similar globular structure as their anti-apoptotic counterparts, as well as the carboxy-terminal hydrophobic transmembrane domain⁶. In addition, they also contain a lower homology BH4-like domain (Figure 1.1)¹¹. These proteins are crucial for outer mitochondrial membrane permeabilization (MOMP) during apoptotic events. Studies reveal that mice deficient for both of these proteins exhibit impaired apoptosis during development. Specifically, apoptosis is blocked at the mitochondrial permeabilization step, indicating these proteins are crucial for MOMP and thus commitment to apoptosis¹².

The last subgroup contains the pro-apoptotic BH3-only proteins including Bim, Puma, Bad, Noxa, Bik, Hrk, Bmf, and Bid. They share sequence homology within the BH3 domain and include the carboxy-terminal transmembrane domain present in all Bcl-2 family proteins (Figure 1.1). Although most are intrinsically disordered, upon binding (see Section 1.3) they adopt an amphipathic α -helical structure⁶. There are two subclasses within BH3-only proteins, classified by the multi-domain proteins they bind. The first

subclass includes the direct activators, including Bid, Bim, and Puma that not only bind to anti-apoptotic proteins, but also bind directly to pro-apoptotic proteins Bak and Bax. Second are the sensitizers that preferentially bind and occupy the BH3 binding domain of anti-apoptotic proteins and include Bad, Bmf, Hrk, and Noxa^{13,14}.

1.3. The Protein-Protein Interaction

The anti- and pro-apoptotic proteins exert their functions through α -helix mediated protein-protein interactions (PPIs). The α -helical BH3 domain of the pro-apoptotic proteins bind in the complementary binding pocket of the anti-apoptotic proteins. These PPI interfaces are large, shallow hydrophobic regions with noncontiguous contact points¹⁵. Tools such as alanine scanning mutagenesis has been used to probe these PPI interfaces and study the thermodynamics of a protein complex experimentally by identifying the key residues involved in the interaction. This technique involves the sequential mutation of each amino acid residue to alanine and the changes in the free energy of binding are then recorded¹⁶. Alanine is used because it does not introduce additional conformational freedom, whereas other simple residues such as glycine can¹⁷. A modification of binding can be mapped as each residue is mutated. Alanine scanning has revealed that PPIs such as the BH3-domain interactions depend on a few residues in positions termed “hot spots” that account for a large degree of the energetic stability of the complexes. These are residues where alanine mutations cause at least 2.0 kcal/mol increase in the binding free energy. In the BH3 domain, these residues occur at the i , $i + 3/4$, $i + 7$, and $i + 11$ positions, all hydrophobic in nature, and oriented on a single face of the helix^{8,15,18,19}. They occupy four pockets within the BH3-recognition interface of anti-apoptotic proteins that are formed by the BH1-3 domains (Figure 1.2, left). Typically, the

hydrophobic residues at these positions in pro-apoptotic proteins include leucine, isoleucine, valine, or phenylalanine²⁰.

One such study performed by Fesik *et al.* probed the Bcl-xL/Bak PPI with alanine

Peptide	Sequence	Binding Kd (uM)
Bak 72	GQVGRQLAIIGDDINRRYDSEFQ 94	0.20 ± 0.02
72	GQVGRQLAIIGDDINR 87	0.34 ± 0.03
Va74	GQ <u>A</u> GRQLAIIGDDINR	15 ± 3
	GQV <u>G</u> AQLAIIGDDINR	3.3 ± 1
Leu78	GQVGRQ <u>A</u> AIIGDDINR	270 ± 90
	GQVGRQLA <u>A</u> IIGDDINR	1.0 ± 0.2
Ile81	GQVGRQLAI <u>A</u> GDDINR	17 ± 6
	GQVGRQLAI <u>I</u> ADDINR	0.50 ± 0.1
Asp83	GQVGRQLAIIG <u>A</u> DINR	41 ± 4
	GQVGRQLAIIGD <u>A</u> INR	0.14 ± 0.02
Ile85	GQVGRQLAIIGDD <u>A</u> NR	93 ± 20

Figure 1. 3. Experimental data from alanine scanning mutagenesis. Residues mutated to alanine are bolded and underlined. Yellow bars represent residues that caused significant loss in binding affinity.

scanning mutagenesis. The residues within the BH3-domain of Bak were mutated (Figure 1.3). Leu78 mutation caused an 800-fold decrease in affinity of the Bak peptide to the protein and Asp83 mutation caused a 200-fold decrease. Subsequent studies have shown

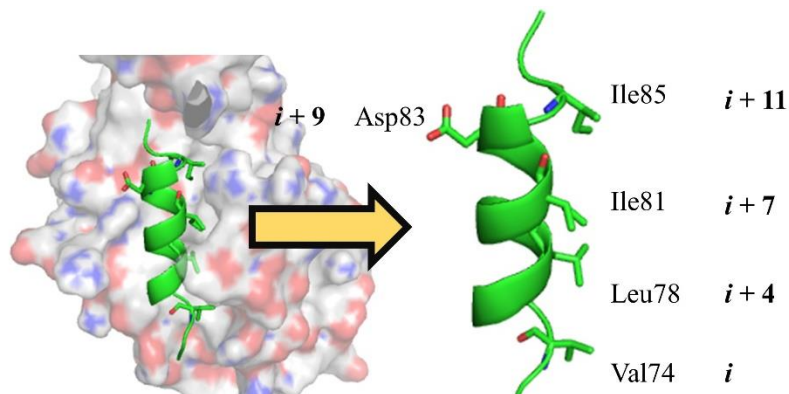


Figure 1. 4. Critical residues and their positions within the α -helix of the Bak-BH3 peptide determined by alanine scanning mutagenesis. PDB 1BXL.

this Asp is conserved within the Bcl-2 family and forms a salt bridge with conserved

arginine residues of anti-apoptotic proteins (Arg146, Arg139, and Arg263 for Bcl-2, Bcl-xL, and Mcl-1, respectively). Figure 1.4 showcases the critical residues of the Bak-BH3 peptide including Valine74 (*i*), Leucine78 (*i* +4), Ile81 (*i* +7), Ile85 (*i* +11)²¹. Such studies have proved instrumental in drug discovery, providing sound rationale for the development of synthetic BH3 mimetics.

1.4. The Bcl-2 Protein Family and Regulation of Apoptosis

Apoptosis is a highly controlled form of cell death that is important for tissue homeostasis and embryonic development²². It is comprised of the extrinsic and intrinsic pathway²³. The extrinsic pathway is triggered when ligands bind cell surface death receptors, initiating the caspase cascade, while the intrinsic pathway is governed by the Bcl-2 protein family²⁴. The intrinsic pathway is heavily reliant on the concentrations of Bcl-2 proteins at a given time at the face of the OMM^{5,14}.

1.4.1. BH3-only Protein Expression and Activation: The First Step in Apoptosis

The intrinsic apoptosis pathway is activated upon response from different stimuli such as viral infection, DNA damage, and growth factor deprivation^{5,14}. Upon activation from these cellular stressors BH3-only proteins are activated. Interestingly, different stressors induce expressions of different BH3-only proteins. For example, Noxa and Puma are both induced by the tumor suppressor protein p53 in response to DNA damage while Bim is induced by FOXO3A in response to growth factor deprivation and proteins related to endoplasmic reticulum stress. BH3-only proteins can also be activated by post-translational mechanisms. For example, the loss of phosphorylation in response to growth-factor deprivation leads to Bad expression. Interestingly, Bid provides a link to the extrinsic apoptotic pathway, as it is cleaved to activated tBid by the caspase-8

protease⁶. Bim may be activated by the release of the dynein motor complex or a loss of ERK-mediated phosphorylation⁵. These represent a few examples of how these proteins are tightly controlled by certain stress related events.

1.4.2. The Direct Activation Model

The direct activation model is a widely accepted and extensively studied apoptosis model describing the interactions between anti- and pro-apoptotic proteins. In this model the BH3-only proteins are defined by two subclasses based on their mode-of-action: direct activators or sensitizers^{5,6}. One proposed idea describes a “hit and run” model, where the BH3-only proteins transiently bind Bak or Bax. This causes a conformational change in Bak and Bax resulting in their activation, which then causes a release of the BH3-only

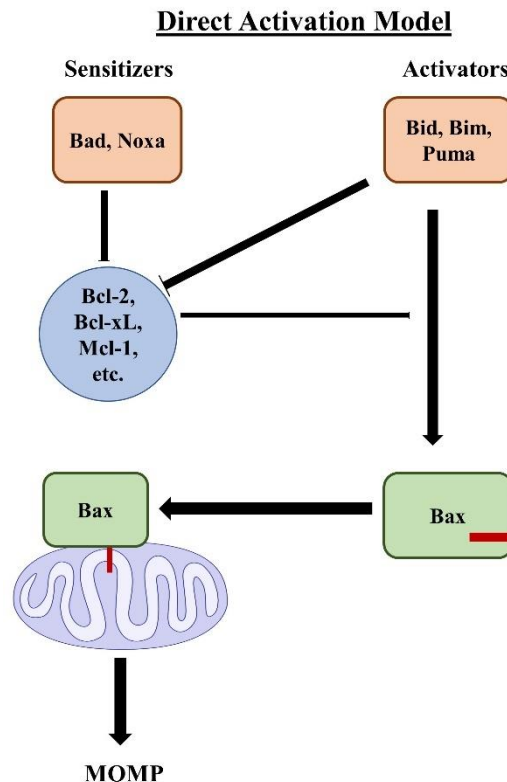


Figure 1. 5. The direct activation model.

proteins. The structural changes involve the N-terminus, the BH3 domain, and the α -5

and α -6 helices of Bak and Bax, as well as the α -9 helix of Bax (Figure 1.5, represented as a red line)²⁵. Once these structural changes occur, the BH3 domain of Bak and Bax are exposed and can undergo homo-dimerization leading to mitochondrial outer membrane permeabilization (MOMP) (Figure 1.5)²².

1.4.3. BH3-only “Sensitizer” proteins

The second subclass of BH3-only proteins includes the sensitizer proteins such as Bad and Noxa. They bind the anti-apoptotic proteins directly in the BH3 domain, neutralizing their anti-apoptotic activity, and displacing Bak and Bax, ultimately resulting in their activation¹⁴. Sensitizer BH3-only proteins have a certain selectivity profile for the anti-apoptotic proteins they bind. For example, Bad preferentially binds Bcl-2, Bcl-xL, and Bcl-w and Noxa preferentially binds Bfl-1 and Mcl-1⁵. Additionally, the “direct activator” BH3-only proteins can also function to bind all anti-apoptotic proteins to release Bak and Bax⁶. The complex and sometimes redundant nature of the interactions and their regulation highlight that these proteins work in concert to ensure the cellular environment remains under homeostatic conditions.

1.4.4. Multi-domain Pro-apoptotic Proteins Bak and Bax: Structure and Mitochondrial Localization

The multi-domain pro-apoptotic proteins Bak and Bax are critical to the cells commitment to death and thus must be tightly controlled^{6,25}. They are constitutively expressed in healthy cells and their cellular location and structure determine their activation state. Bak resides on the OMM, anchored into the membrane with the α -9 helix carboxy terminal transmembrane domain, but can also be bound to anti-apoptotic proteins Mcl-1 and Bcl-xL, which inactivate it^{5,6}. In contrast, Bax is mostly cytosolic, due to its

retro-translocation from the mitochondria to the cytosol by Bcl-xL²⁶. Of importance, the transmembrane domain is tucked into an internal hydrophobic space within the protein and is only revealed via conformation change upon death signals or activation from BH3-only proteins^{5,6,25}.

1.4.5. Structural changes of Bax

Further detail of this conformational change of Bax when activated by BH3-only proteins has been extensively studied. As stated previously, one conformational change of Bax is the eversion of the α -9 helix, allowing it to integrate into the OMM. Studies have indicated that BH3-only proteins bind into a rear pocket distant from the α -9 helix, and may provoke this exposure indirectly. In fact, an NMR study showed when a stapled Bim-BH3 peptide bound to this rear pocket of Bax, it induced chemical shifts directly related to the α -9 helix²⁵. Additionally, crystallographic studies revealed that when an activator BH3-only protein was complexed with Bax, cavities within the binding interface appeared that caused destabilization of the complex and released the core and BH3-domain²⁷. In contrast, Bak is localized at the OMM constitutively and biochemical studies suggest certain BH3 domains activate Bak upon binding to its surface groove²⁷. These changes are still under investigation²⁵. Ultimately, these structural changes result in the revealed BH3 domains of Bax and Bak, leading to their activation and eventual homo-dimerization²⁷.

1.4.6. Mitochondrial Outer Membrane Permeabilization

Once activated Bak and Bax homo-dimerize, they form pores on the OMM, inducing MOMP. The formation of these pores is still under investigation²⁵, however, one hypothesis includes the toroidal pore model. It states that the disruption of the

hydrophobic membrane bilayer has a high energetic cost. Activated Bak and Bax, under this model, stress the structural integrity of the membrane due to high protein concentration, and cause the formation of the pores. Experimentally, this has been shown in reconstituted Bax systems, revealing stabilized open pores. Additionally, cryo-electron microscopy images revealed holes (pores) in the membrane that were long lived in the presence of activated Bak and Bax²².

Pore formation represents a crucial step of apoptosis. It is characterized as a point of no return, committing the cell to death by releasing apoptogenic molecules such as cytochrome *c* to the cytosol. Cytochrome *c* goes on to bind APAF1, leading to the assembly of the apoptosome, which binds and activates pro-caspase-9 and SMAC/DIABLO, leading to the caspase cascade activation. Cytochrome *c* and

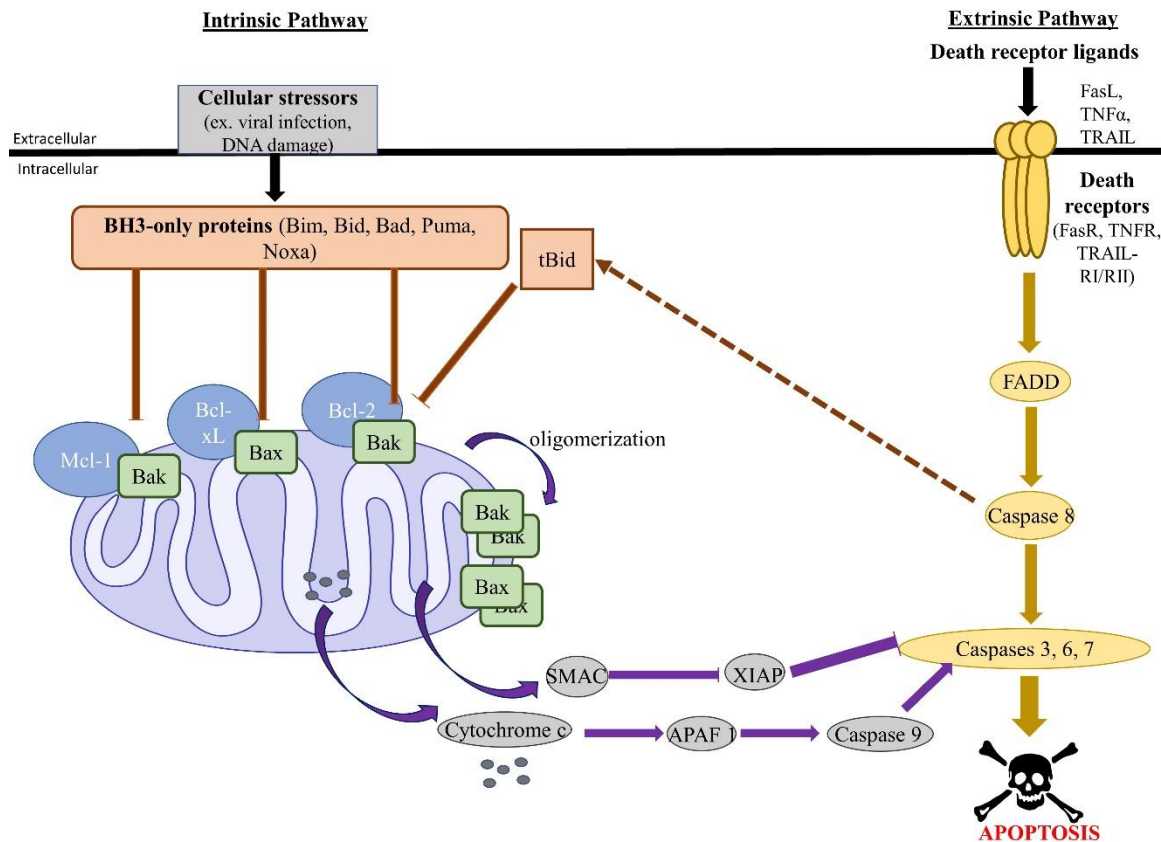


Figure 1. 6. The extrinsic and intrinsic apoptosis pathways.

SMAC/DIABLO are widely accepted to be crucial for caspase activation. An alternative APAF1-independent pathway involves inhibitor of apoptosis proteins (IAPs). These proteins inhibit caspase activation, but when SMAC/DIABLO is released from the mitochondria upon permeabilization, it binds IAPs and further allow for caspase activation⁵. The intrinsic and extrinsic pathway of apoptosis is summarized in Figure 1.6.

1.5. Bcl-2 Proteins and Cancer

The hallmarks of cancer represent many of the multiple underlying principles that describe the transformation of healthy cells to oncogenic cells (Figure 1.7). These include

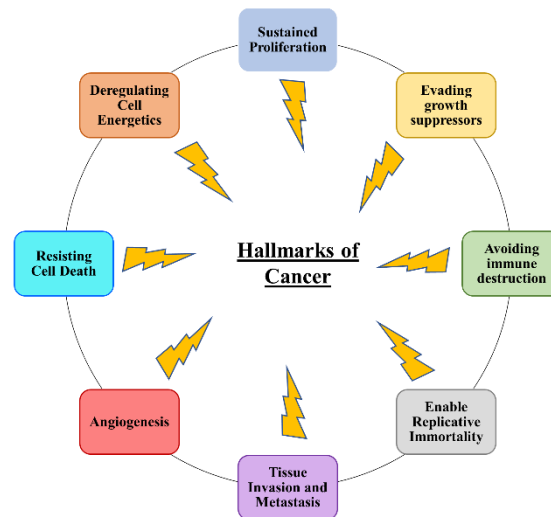


Figure 1. 7. The hallmarks of cancer.

examples such as sustained proliferation, evasion of growth suppression, tissue invasion and metastasis, sustained angiogenesis, enabling replication immortality, and evasion of cell death²⁸. The intrinsic pathway of apoptosis is implicated as a barrier to a multitude of different cancer pathogeneses including hematologic cancers such as acute myeloid leukemia (AML), chronic lymphocytic leukemia (CLL), and multiple myeloma (MM), as well as breast, lung, and neuroblastoma²⁹. Several cellular abnormalities described can

result in the evasion of cell death and can aid in sustained tumor growth and chemoresistance²⁴.

Overexpression of the Bcl-2 anti-apoptotic proteins and downregulation of pro-apoptotic proteins such as increasing the Bcl-2/Bax ratio, are hallmarks of cancer, which effectively block apoptosis in cancer cells^{28,30}. The overexpression of anti-apoptotic proteins can occur by a variety of mechanisms such as chromosomal translocation and increased gene expression and amplification. In fact, amplification of the *Mcl1* and *BclxL* genes is found in many solid cancers. A study of 3000 samples with 26 tumor types revealed that these genes were found to be the most frequently expressed²⁴. As a result, apoptosis is an intricate concert of highly controlled protein concentration, and the overexpression of anti-apoptotic proteins can be detrimental to the cell and lead to tumorigenesis.

1.5.1. Targeting the Overexpression of Bcl-2 Anti-apoptotic Proteins with BH3 Mimetics

A common misconception of oncogenic cells is that they are resistant to apoptosis. However, in reality they are often more sensitive to targeted apoptosis therapies in comparison to healthy cells because there is already stress induced by cancer such as hypoxia or reduced-nutrient availability placed on the system. Cells experiencing this sensitivity are termed as “primed” for death and can be revealed with BH3 profiling. This technique utilizes BH3-only peptides and can indicate which Bcl-2 anti-apoptotic proteins are required for the tumor cell to survive. Because of the concentrations of Bcl-2 proteins present for survival, the primed cells are closer to death, and adding an

additional stressor such as chemotherapy or a BH3 mimetic, can readily kill these cells compared to healthy cells and those that are not primed (Figure 1.8)³⁰.

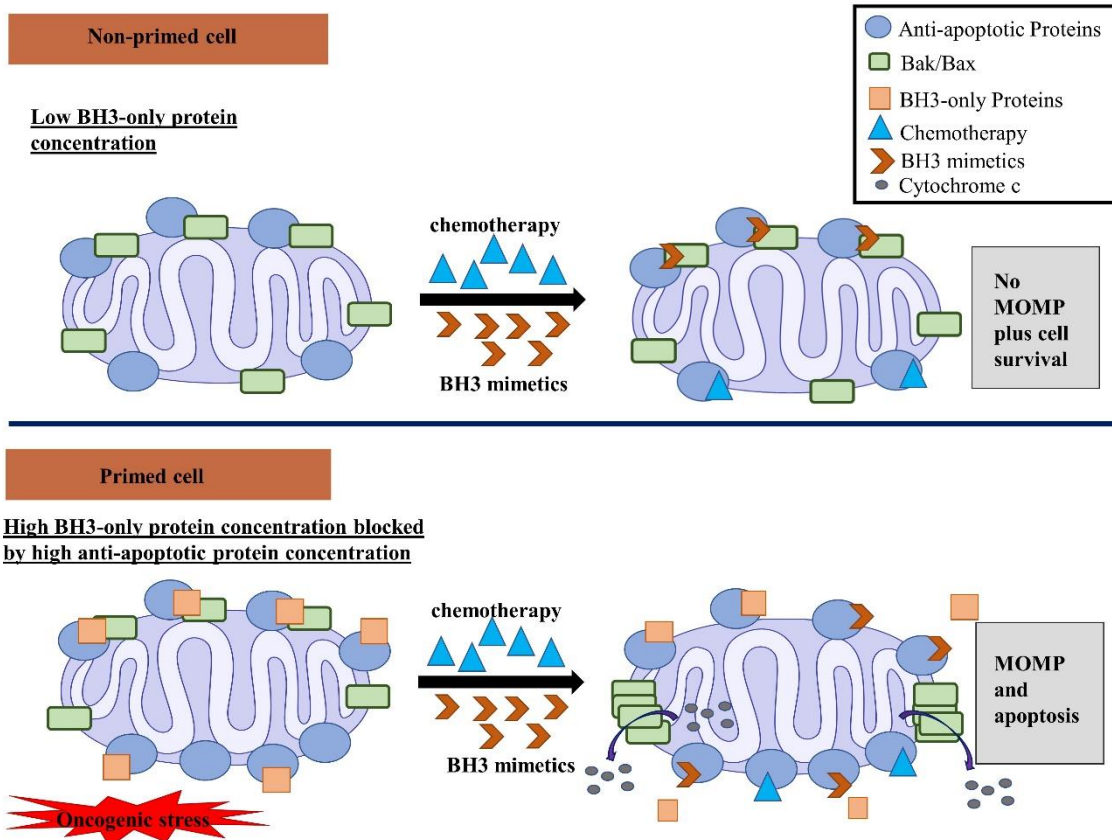


Figure 1. 8. Non-primed cells (top) versus primed cells (bottom) when treated with multiple therapies such as chemotherapy and BH3 mimetics.

BH3 mimetics are compounds that mimic the α -helical structural properties of the BH3 domain in pro-apoptotic proteins and function as inhibitors of the anti-apoptotic proteins. They are designed to mimic the spatial orientation of the α -helix of the BH3-only proteins as well as mimic the critical “hot spot” residues at the i , $i+3/4$, and $i+7$ positions. Additionally, mimicking the conserved aspartic acid residue that forms a salt bridge with the conserved arginine on anti-apoptotic proteins can increase contacts with the protein and produce a more effective inhibitor²⁰. These compounds are designed to increase the cellular concentration of pro-apoptotic proteins by binding to anti-apoptotic

proteins to displace Bak and Bax and induce cellular death in cancer cells (Figure 1.9)³¹.

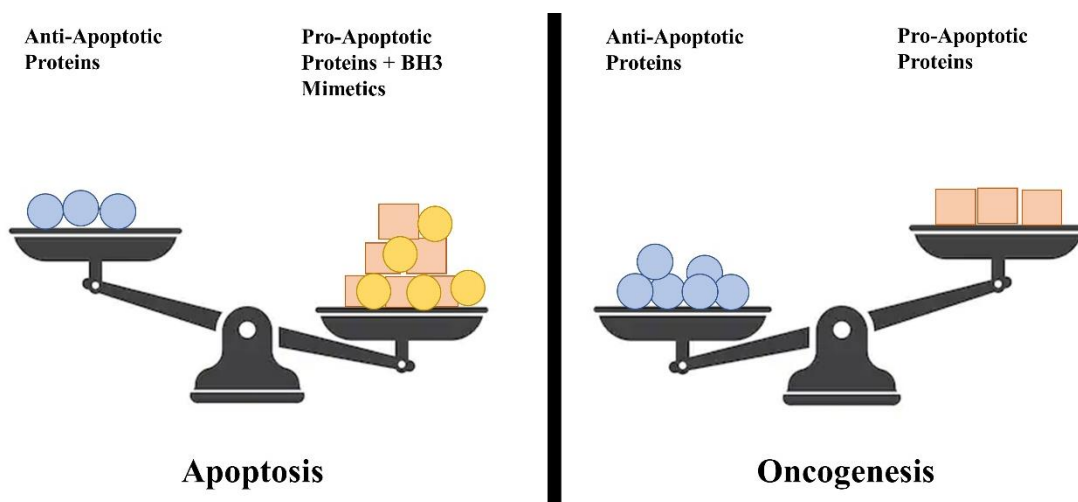


Figure 1. 9. The scales represent the delicate balance between anti- and pro-apoptotic proteins. Although overexpressed anti-apoptotic proteins can lead to cancer, introduction of BH3 mimetics can artificially increase pro-apoptotic protein members to induce apoptosis in the cancer cell.

Many academic and industrial groups have successfully developed BH3 mimetics, culminating in the FDA approved Bcl-2 selective inhibitor venetoclax, which is the first orally bioavailable small molecule drug approved for a PPI³².

This review describes the BH3 mimetics that pioneered the field, while focusing on compounds that are currently in clinical trials. These compounds will be separated based on the anti-apoptotic protein they inhibit: pan-selective, Bcl-2 selective, dual Bcl-2/Bcl-xL, Bcl-xL selective, and Mcl-1 selective.

1.6. ABT-737, ABT-263, and the approval of ABT-199

1.6.1. Development of ABT-737

In 2005, Abbott laboratories reported the discovery of ABT-737, a Bcl-2 family inhibitor, for the treatment of lymphoma and small cell lung cancer (SCLC). It selectively bound

Bcl-2, Bcl-xL, and Bcl-w with $K_i < 1$ nM with reduced binding to the other anti-apoptotic proteins Bcl-b, Mcl-1, and A1 ($K_i = 0.46 \pm 0.11$ μ M, >1 μ M, and >1 μ M, respectively). It was discovered by a high throughput NMR based method termed SAR by NMR³³, whereby fragments that bind proteins are identified and linked together according to their binding profiles to produce a functioning high-affinity compound that cumulatively binds all sites bound by the fragments³⁴. Two fragments, 4'-fluoro-biphenyl-4-carboxylic acid (**1**) and 5,6,7,8-tetrahydro-naphthalen-1-ol (**2**) were identified; the former occupying the same site as Leu78 in the Bak peptide, and the latter in the same region as Ile85 (Figure 1.10, top left). In addition, the carboxy group bound near Arg139 of Bcl-xL, similar to Asp83 of Bak (PDB 1YSG). Following the synthesis of compound **3** (Figure 1.10), it was discovered that the binding affinity decreased in the presence of 1% human serum

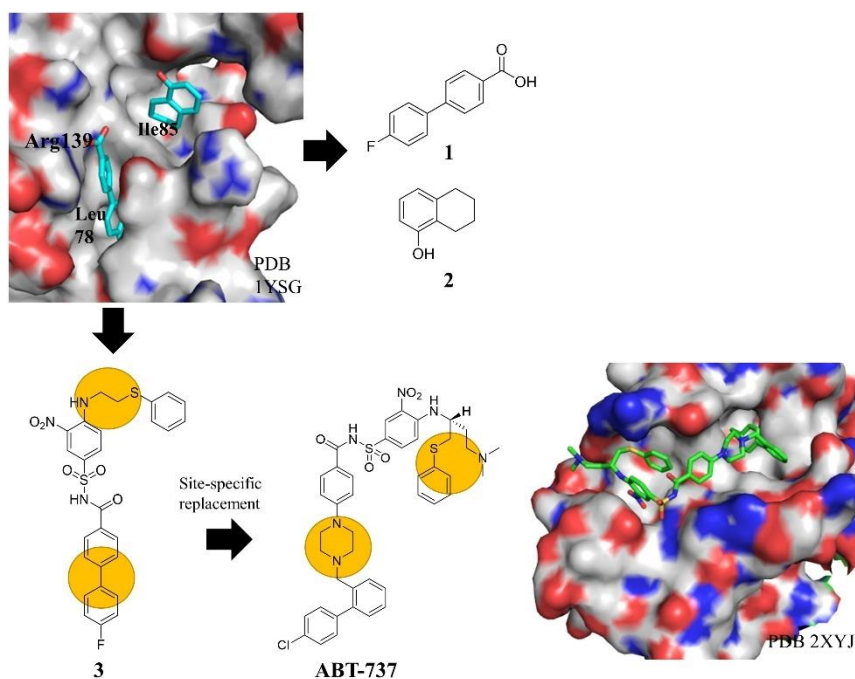


Figure 1. 10. Crystal structure of compounds **1** and **2** (top left). PDB 1YSG. Optimization led to compound **3**. Site-specific replacements of compound **3** to reduce serum binding led to ABT-737. Co-crystal structure of ABT-737 and Bcl-xL (bottom right). PDB 2XYJ.

albumin (HSA). Various site-specific replacements to polar substituents (highlighted in Figure 1.10) designed to decrease serum binding without losing affinity for Bcl-xL, ABT-737 was developed (Figure 1.10).

The crystal structure of ABT-737 in complex with Bcl-xL shows increased protein contacts while binding in similar pockets as the initial fragments (PDB 2XYJ). In fact, nanomolar affinity to Bcl-2, Bcl-xL, and Bcl-w was retained in the presence of 10% HSA. Additionally, tumor regression related to apoptosis was established with no increase in caspase-3 activation (an indicator of apoptosis) in healthy tissues such as the liver, heart, and intestine suggesting on-target effects³³.

However, ABT-737 had many shortcomings that needed to be addressed for a drug to advance to the clinic. Not only did it have low aqueous solubility that would make intravenous delivery difficult, it also showed poor oral bioavailability^{33,36}. If a drug can be delivered intravenously, it reaches the blood directly, which is assumed 100% bioavailability³⁵, but Abbott wanted to design an oral drug due to the flexibility it allows with dosing schedules³⁶. Additionally, high oral bioavailability allows for a reduced amount of drug needed to achieve the desired pharmacological effect³⁵. The poor pharmacokinetic properties of ABT-737 led to the development of the orally bioavailable drug ABT-263 (navitoclax).

1.6.2. Development of Navitoclax (ABT-263)

Designing an orally bioavailable drug targeting a PPI is difficult due to the large hydrophobic surface area of the binding pockets. Therefore, rather than a complete redesign of their lead compound, Abbott focused on small structural modifications of ABT-737 that would not disrupt the overall core and retain high binding affinity.

Fluorescence polarization (FP) assays are an *in vitro* tool to study the binding affinity of a compound and the protein-of-interest. However, in the development of ABT-263, SAR studies were driven by cellular efficacy instead of FP assays because the compounds binding affinities were below its limit of detection. The H146 cell line was used because of its dependence on Bcl-2 and Bcl-xL, and would also evaluate the relevance to human cancer. Additionally, these cytotoxicity assays were run in the presence of 10% HSA to more closely mimic *in vivo* environments.

Three regions of ABT-737 were targeted for modification: 1) the nitro group on the acyl sulfonamide, as it has a potential toxic metabolite, such as the corresponding hydroxylamine; 2) the 4-chlorobiphenyl moiety which has the potential for oxidative metabolism, forming a hydroxylated 4-chlorobiphenyl metabolite; and 3) the dimethylamino moiety as N-demethylation is a potential target of metabolism as well (highlighted in structures in Figure 1.11.)³⁶.

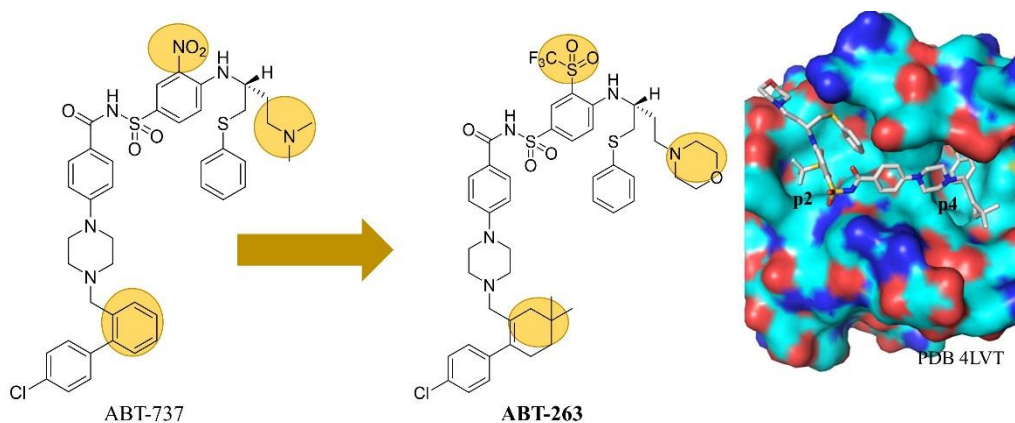


Figure 1. 11. Optimization of ABT-737 to the Bcl-2/Bcl-xL inhibitors ABT-263. The crystal structure of ABT-263 and Bcl-2. PDB 4LVT.

Nitro group SAR revealed that weaker electron withdrawing groups (less acidic cores) decreased cellular activity. It was not clear whether this was due to reduced cellular penetration, serum binding, or other reasons. However, when replaced with a

trifluoromethanesulfonyl group, it corresponded to a small increase in cellular efficacy, but a 7-fold increase in drug plasma concentrations, which may be attributed to the lower polar surface area compared to the nitro group³⁶.

Next, modifications of the internal aromatic ring replaced with cycloalkenyl groups of various ring sizes (5,6,7 and 8) were well tolerated. In fact, when modified to a gem-dimethylcyclohexene ring, an EC₅₀ value in Bcl-2 and Bcl-xL dependent FL6.12 cells was observed in subnanomolar range and thus the most efficacious of this series. Removal of the dimethylaminoethyl group resulted in drastically reduced cellular efficacy, which the researchers suggested was due to serum binding; when replaced with a morpholino group, 16% oral bioavailability was reached while retaining submicromolar cell activity. Accordingly, these functional groups were added to the main core one-by-one and an additive effect after addition of each modification was observed, and the resulting compound boasting all three modifications was named ABT-263, or Navitoclax³⁶. The crystal structure of ABT-263 and Bcl-2 shows the core acyl sulfonamide and thiophenyl moiety binding in the p4 pocket, while the 1-chloro-4-(4,4-dimethylcyclohex-1-enyl)benzene moiety binds in the p2 pocket of the proteins (Figure 1.11)³⁷.

ABT-263 disrupts the Bcl-2 and Bcl-xL interactions with pro-apoptotic proteins and leads to the initiation of apoptosis within two hours of treatment³⁸. Its pharmacokinetic profile displays low volumes of distribution values in mouse, rat, dog, and monkey with plasma elimination half-lives of 4.6 to 8.4 hours after intravenous dose. After oral gavage in these species, bioavailability was at 20%. Oral administration also induces complete tumor regression in SCLC and acute lymphoblastic leukemia (ALL)

xenograft models. Although Navitoclax possessed poor oral bioavailability at 20%, in lipid-based formulations the bioavailability increased to 50% and the half-life increased to 8.9 hours in dogs³⁸.

ABT-263 moved on to phase I clinical trials which showed a 50% response rate in patients with CLL³⁹. However, there was significant dose-limiting thrombocytopenia due to Bcl-xL inhibition, which is the primary survival factor in platelets^{31,37,39}. Due to this adverse event, there was a need to develop a Bcl-2 selective inhibitor to spare platelets, which prompted the development of ABT-199. Notably, although significant thrombocytopenia was reported in early clinical trials, navitoclax is still being assessed in combination therapies^{39,40}.

1.6.3. Development of Venetoclax (ABT-199)

In order to develop a Bcl-2 selective inhibitor, Abbvie reverse engineered navitoclax with systematic modifications of certain key binding moieties to decrease binding for Bcl-xL while retaining affinity for Bcl-2. For example, removal of the thiophenyl moiety revealed loss of binding affinity for Bcl-2, and subsequent co-crystallization with Bcl-2 protein showed the compound occupied a smaller volume within the p4 pocket. However, the complex crystallized as a protein dimer, and it was found that Trp30 from a second Bcl-2 protein bound into that same p4 pocket and formed pi-pi interactions with the nitroaryl moiety. Therefore, they initially incorporated a 5-substituted indole to the central core via an ether linkage, but found an additional electrostatic interaction was possible with Arg107. They also found the nitrogen of the indole of Trp30 formed a hydrogen bond with Asp103 of Bcl-2 (Figure 1.12, left). This was a key discovery, as this is one of the few differentiating amino acids between Bcl-2 and Bcl-xL; Bcl-xL has

Glu96 in the same position. Therefore, they replaced the indole with an azaindole, culminating in the development of ABT-199, or venetoclax (Figure 1.12). ABT-199 is a selective Bcl-2 inhibitor, with a $K_i < 0.010$ nM, and binds appreciably less to Bcl-xL,

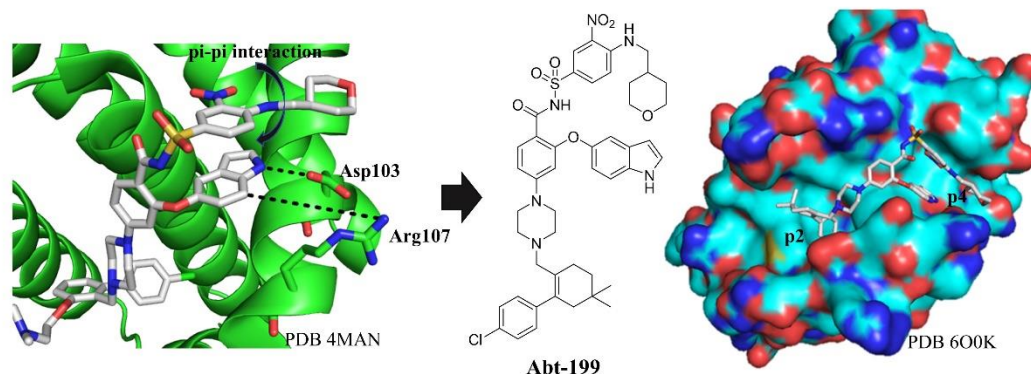


Figure 1. 12. Favorable interactions highlighted between an indole and Asp103 of Bcl-2, compounded by a pi-pi interaction with a phenyl group of an optimized compound (Left, PDB 4MAN). This led to the development of ABT-199 (center). The crystal structure of ABT-199 and Bcl-2 is represented on the right. PDB 600K.

Bcl-w, and Mcl-1 ($K_i = 48$ nM, 245 nM, and >444 nM, respectively)³⁷.

In vitro assays with interleukin-3-dependent mouse FL5.12 cells developed to rely on Bcl-2 or Bcl-xL showed ABT-199 potently killed Bcl-2 dependent cells ($EC_{50} = 4$ nM) and showed weaker activity against Bcl-xL dependent cells ($EC_{50} = 261$ nM). In addition, other *in vitro* assays revealed decreased cell killing in Bcl-xL dependent cell lines compared to Bcl-2 dependent cell lines and disrupted Bcl-2-Bim complexes while less effective against Bcl-xL-Bcl-xS and Mcl-1-Noxa interactions, further showcasing its selectivity. Many groups have additionally confirmed that ABT-199 induces Bak/Bax mediated apoptosis triggered specifically by Bim in a caspase-dependent manner. It also had anti-tumor activity against Non-Hodgkins lymphoma (NHL), CLL, and acute leukemias *in vitro*^{37,39}. Treatment in mouse xenografts also showed activity against aggressive lymphomas and acute leukemias³⁹.

Many clinical trials with venetoclax have been performed since its initial discovery in 2013⁴¹. In 2015, a phase II clinical study showed that nearly 80 percent of people with previously treated relapsed or refractory CLL with the 17p deletion--a hard to treat type of leukemia--responded to venetoclax⁴². By April 2017, the FDA approved venetoclax for those with CLL and the 17p deletion and were treated with at least one prior therapy. As of May 2019, venetoclax has been approved as a chemotherapy-free combination treatment with Obinutuzumab for previously untreated CLL or small lymphocytic leukemia (SLL) patients⁴³.

The approval of ABT-199 was a milestone for inhibitors of PPIs as they were once considered undruggable⁴⁴. Previously, small molecule inhibitor development was driven by the Lipinski rule of 5 (RO5) which predicts if a small molecule would be orally active. The RO5 is characterized by drugs with a molecular weight less than 500 Daltons, cLogP <5, five or less hydrogen bond donors, and 10 or less hydrogen bond acceptors⁴⁵. ABT-199 and its previous iterations violate the RO5 as they target large hydrophobic protein interfaces that are difficult to target with a small molecule. Larger more complex, and possibly lipophilic compounds are needed to disrupt these PPIs, as evidenced by these compounds.

1.7. Bcl-2 Selective Inhibitors

1.7.1. S55746

Vernalis and Servier developed S55746, an orally active Bcl-2 selective inhibitor. It is a *bona fide* BH3 mimetic, which is defined as a compound with high affinity to the protein target and induces Bax/Bak-dependent apoptosis⁴⁶. Compound design was initiated from an active literature compound search coupled with structure-based drug design. S55746

has a tetrahydroindolizine core that projects functional groups that direct into the proteins p1,2 and 3 pockets^{47,48}. The tertiary amide projects the phenyl group towards the p1 pocket and the 4-phenoxyphenyl group into the p2 pocket, where the phenol forms a hydrogen bond to the backbone carbonyl of A149 (Figure 1.13)⁴⁸.

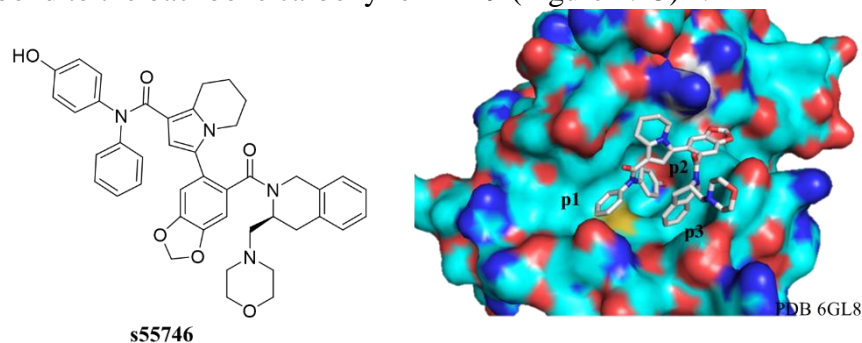


Figure 1. 13. The co-crystal structure of S55746 and Bcl-2. PDB 6GL8

They suggest that polar and van der Waals interactions in s55746 are optimal due to the size-independent enthalpic efficiency (SIHE), indicating highly specific binding to Bcl-2⁴⁸. The size-independent enthalpic efficiency ($SIHE = pK_H / 40xHA^{0.3}$) takes thermodynamics and heavy atom number into account during hit and lead selection as well as drug optimization. Heavy atoms (non-hydrogen atoms) are an important determinant for SIHE because of the important role polar interactions play in gaining binding enthalpy. During a ligand-protein binding event, the enthalpic component is dependent upon the specific interactions formed when the ligand binds the protein as well as the release of water molecule entropy. The specific interactions between the protein, ligand, and water molecules upon binding cause enthalpy gains, which can decrease with increasing ligand size⁴⁹.

They evaluated binding affinity with a fluorescence polarization assay and found it was highly potent and selective for Bcl-2 ($K_i = 1.3$ nM), with poor affinity to Bcl-xL and no significant binding to Mcl-1 or Bfl-1. Using the Bcl-2 dependent ALL cell line

RS4;11, S55746 potently induced cell death after 72 hours ($IC_{50} = 71.6 \text{ nM}$) while exhibiting a much weaker effect in the Bcl-xL dependent cell line H146 ($IC_{50} = 1.7 \text{ }\mu\text{M}$). It also induces apoptosis in a concentration-dependent manner, with caspase-3 and poly (ADP-ribose) polymerase PARP cleavage observed⁴⁸. These indicators are widely regarded as hallmarks of apoptosis⁵⁰.

Although *in vitro* S55746 acts as a potent and selective Bcl-2 inhibitor, it is important to ensure it is not affecting platelet count by inhibiting Bcl-xL. Isolated platelets from healthy volunteers exhibited insensitivity to S55746 treatment, suggesting the compound may not cause thrombocytopenia. It also caused significant, dose-dependent anti-tumor activity in SCID-bearing RS4;11 mice compared to untreated animals, with decreased tumor growth inhibition seventeen days after treatment. The highest dosed mice (100mg/kg) had complete tumor regression⁴⁸.

Importantly, a recent 2019 study highlighted that targeting Bcl-2 can result in the Bcl-2 mutant G101V. In fact, patients treated with the Bcl-2 selective inhibitor venetoclax for 19-42 months saw disease progression due to drug resistance caused by this mutant. Bcl-2_{G101V} results in a 180-fold decrease in binding affinity of venetoclax. Interestingly, the endogenous BH3-only proteins still bind to the mutant, albeit with moderately reduced affinity, and therefore the G101V mutant can still function as an anti-apoptotic protein. To explain the loss of affinity, Birkinshaw *et al.* performed crystallographic experiments between venetoclax with the wt and mutant Bcl-2 protein. Structurally, the G101V mutation is adjacent to the p4 pocket that engages either a Leu when Bax binds or the azaindole in venetoclax. They saw no change in the p4 pocket when venetoclax binds to the mutant, however, the bulk added from the valine mutation

saw a distinct rotamer change in Glu152 which caused a repositioning effect that was seen in the p2 pocket, specifically affecting the chlorophenyl moiety of venetoclax.

These experiments suggest that the G101V mutation cause changes in the p2 pocket. The deep penetration of the chlorophenyl moiety in the p2 pocket causes the dramatic decrease in binding, whereas the small Leu residue in Bak can still make contacts with the mutant, explaining why the endogenous BH3-peptides can still bind the mutant.

Due to this mutation and potential for resistance, Servier and Vernalis researchers generated crystal structures of S55746 with mutant Bcl-2 G101V and found the 4-hydroxyphenyl moiety that binds in the p2 pocket does not bind as deep as the chlorophenyl moiety of venetoclax, however it still loses 100-fold binding affinity. They suggest these changes may happen in the mutant prior to drug binding or other issues that were not detectable in the crystallographic structures. Nonetheless, these data suggest that in the event of the Bcl-2 G101V mutation, treatment with S55746 may also result in resistance⁵¹.

Results were published describing a phase I dose escalation study of S55746 in patients with refractory or relapsed CLL and B-cell NHL. Overall, 93.8% of patients reported at least one emergent adverse effect with the most common being anemia, cough, malignant neoplasm progression (10.8%), constipation, asthenia, nausea, vomiting, thrombocytopenia, diarrhea and headache. All patients withdrew from treatment due to the progression of their disease. In the end, Servier and Vernalis decided to halt treatment and discontinue the study. As a result, the maximum tolerated dose and

recommended dose was not established for further clinical study. There are currently no NCI-supported clinical trials with S55746⁴⁰.

1.7.2. Beigene Compounds

Beigene disclosed many compounds with general structure **4** in patent WO 2019/210828 A1 functioning as Bcl-2 selective inhibitors for apoptotic, proliferative, and neurodegenerative diseases (Figure 1.14). Authors Yunhang Guo *et al.* claimed bubbles A and B are cycloalkyl, cycloalkenyl, cycloalkynyl, aryl, heterocyclyl, or heteroaryl. Each are optionally substituted with 1 to 4 substituents, either R₁ and R₂, which may be hydrogen, halogen, alkyl, alkenyl, alkynyl, cycloalkyl, heterocyclyl, aryl, heteroaryl, oxo, or various amide, carbonyl, N, O, S, functional groups. R₃ and R₄ claims include hydrogen, halogen, C1-8 alkyl, C2-8 alkenyl, C2-8 alkynyl, cycloalkyl, aryl, heterocyclyl, or heteroaryl, each of said C1-8 alkyl, C2-8 alkenyl, C2-8 alkynyl, cycloalkyl, aryl, heterocyclyl, or heteroaryl is optionally substituted with 1 to 4 substituents R_{3a}. R_{3a} includes halogen, cyano, amide, carbonyl, N, O, S functional groups, alkyl, alkenyl, alkynyl, cyclo and heterocyclic compounds. R₅ claims are alkyl, alkenyl, alkynyl, O, S, N functional groups, amide and carbonyl groups. L1-4 are each

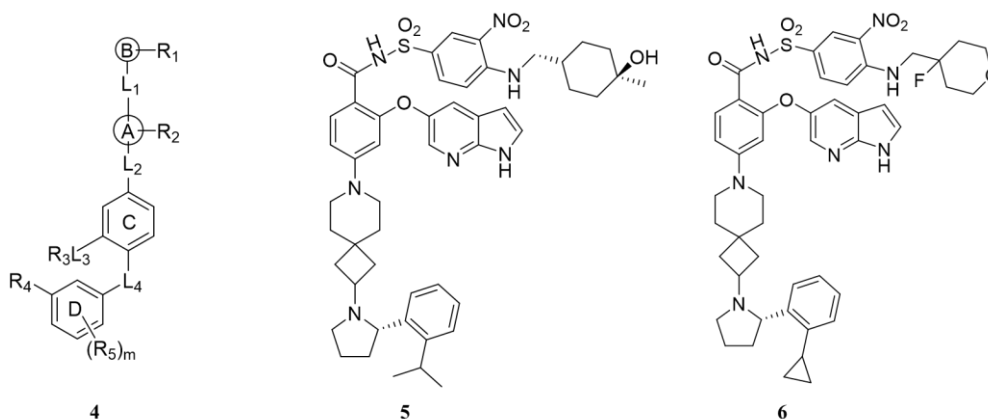


Figure 1. 14. Bcl-2 selective inhibitors disclosed by Beigene in patent WO2019/210828.

independently a direct bond including alkyl, alkenyl, alkynyl, carbonyl, amide, S, O, or N functional groups. Examples of these compounds are **5** and **6**.

Compounds were tested with either an FP or time-resolved fluorescence resonance energy transfer (TR-FRET) assay to evaluate binding affinities and Bcl-2 selectivity. Many of their compounds were in the low picomolar range. The most potent compound (**5**) inhibited Bcl-2 and Bcl-xL with $IC_{50} = 0.015$ nM and 18 nM, respectively, and exhibited high potency and selectivity in a cell proliferation assay in the Bcl-2 dependent cell line RS4;11 ($IC_{50} = 0.41$ nM) in contrast to a Bcl-xL dependent cell line ($IC_{50} = 2.52$ μ M) (Figure 1.14).

As stated previously, patients treated with venetoclax can develop resistance due to the novel mutation G101V in Bcl-2. In a TR-FRET assay against this mutant, most of their compounds displayed $IC_{50} < 3$ nM, whereas venetoclax binds with an $IC_{50} = 28$ nM. This indicates that their compounds may overcome the resistant Bcl-2 G101V mutant in the clinic.

CYP2C9 is an important enzyme of the cytochrome P450 family. It is abundant in the liver and largely contributes to the metabolism of various drugs and xenobiotic compounds⁵². In order to evaluate the risk of inhibition of CYP2C9, which has a potential to cause drug-drug interactions (DDIs), Beigene tested these compounds against this isoform. For reference, venetoclax binds CYP2C9 $IC_{50} = 1.7$ μ M, whereas many of these compounds are significantly less potent, with $IC_{50} > 10$ μ M, indicating they may potentially have a lower indication of DDIs.

In addition to *in vitro* and *in cell* assays, an unpublished crystal structure was generated of Bcl-2 and **6** (Bcl-2 $IC_{50} = 0.032$ nM) of which three interactions are noted

(Figure 1.14). First, the 2-(2-cyclopropylphenyl)-pyrrolidinyl moiety of **6** creates an extra subpocket in the protein, which is induced by different conformations of residues around the p2 pocket of Bcl-2. Next, a water bridge with Val133 is formed with the nitrogen of the pyrrolidinyl ring, which is void in the venetoclax crystal structure. Lastly, a sulfur-pi interaction between Met115 and the 2-cyclopropylphenyl is apparent. Structurally, this may explain the significant potency for Bcl-2. The inventors of this patent found the compounds potently inhibit Bcl-2 and the Bcl-2 G101V mutation, suggesting these inhibitors as a new therapeutic Bcl-2 selective inhibitor with no resistance concern compared to venetoclax⁵³.

Of interest, Beigene is currently recruiting for a Phase 1a/1b trial in patients with mature B-cell malignancies with their Bcl-2 selective inhibitor BGB-11417⁵⁴. Although this compound has yet to be disclosed, the compounds described within this patent showcase promising highly potent and selective Bcl-2 inhibitors developed from Beigene.

1.7.3. Ascentage Compounds

Ascentage published three patents in early 2020, each disclosing Bcl-2 selective inhibitors in combination with different chemotherapeutic drugs for the treatment of different diseases. The compounds disclosed within these patents is illustrated in general structure **7** (Figure 1.15). The claims for A represent a mono- or bicyclic moiety, E is either C where the adjacent bond is either a single or double bond, or N, with the adjacent bond being a single bond. X_{1,2} and X₃ are independently selected from a group consisting of: -CR= (R is H or a halogen) and -N=. The C attached to R_{1a} and R_{1b} form a 3,4, or 5

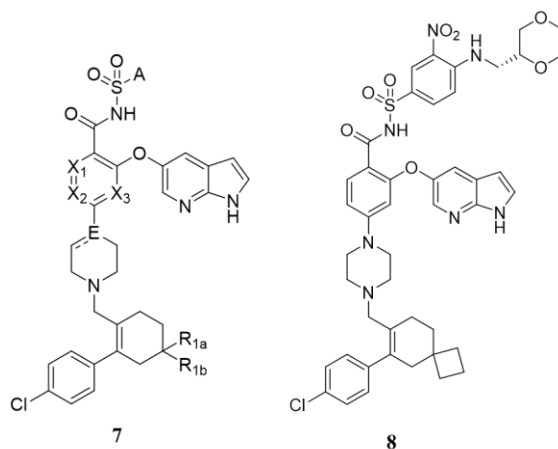


Figure 1. 15. Bcl-2 selective inhibitors disclosed by Ascentage.

membered optionally substituted aliphatic ring, or a 4 or 5 membered optionally substituted heterocyclic ring. Examples of these compounds are represented here.

The effects of the combination of **8** and the topoisomerase inhibitor topotecan in SCLC mice xenograft tumors derived from human H146 tumor cells was evaluated. At the end of the 21st day of treatment, the group with monotherapy with **8** showed moderate anti-tumor activity, with no complete remission (CR), partial (PR), or stable disease (SD) while the topotecan group showed potent anti-tumor activity (remission rate 100%). However, in the combination group, all five mice treated showed CR with a 100% remission rate. On the 46th day post treatment, remission rates of **8** alone, topotecan alone, and combination therapy changed to 0%, 40%, and 100%, respectively, which confirmed the efficacy of the combination therapy. Additionally, mice had no significant body weight change. These studies suggest that combination therapy had no significant side effects with increased anti-tumor effects *in vivo*⁵⁵.

Additional experiments were disclosed utilizing APG-115, an MDM2 inhibitor, that showed enhanced anti-leukemic activity in combination therapy with **8**. They performed cell viability assays using MM and AML malignant cell lines. In combination

treatment, **8** decreases cell proliferation when combined with APG-115 in these cell lines and suggest they work synergistically *in vitro*. Additionally, mouse xenograft experiments were carried out with the RS4;11 (ALL) cell line. Both APG-115 and **8** do not achieve CR alone, but together the combination was able to achieve PR and CR with no significant side effects. These experiments were also carried out in hematologic xenograft models. Due to the results disclosed in these patents, Ascentage suggests further clinical investigation is deserving as **8** in combination with APG-115 causes anti-leukemic effects in multiple tumor xenografts experiments⁵⁶. Similar experiments with other combination therapies such as CHOP were performed. These results can be found in patent WO 2020/02826 A1⁵⁷.

Encouragingly, Ascentage Pharma has begun Phase Ib/II clinical studies of APG-2575, an orally available Bcl-2 selective inhibitor as a single agent or in combination for the treatment of relapsed/refractory CLL or SLL. As of March 2020, the first patient has been dosed⁵⁸. Additionally, a Phase I study of APG-2575 in hematologic malignancies in the US and Australia showed no dose-limiting toxicity or tumorlysis syndrome suggesting it may have a favorable safety profile⁵⁹. APG-2575 is a proprietary compound of Ascentage, and has neither been published nor outwardly disclosed in any patents.

1.8. Bcl-2/Bcl-xL Dual Inhibitors

1.8.1. Ascentage Bcl-2/Bcl-xL dual inhibitor

In patent WO 2020024966 A1, published in early 2020, Ascentage also disclosed a Bcl-2/Bcl-xL dual inhibitor for the treatment of cancer. This compound, **9**, (Figure 1.16) binds with high affinity to Bcl-2, Bcl-xL, and Bcl-w ($IC_{50} = 1.6$ nM, 4.4 nM, and 9.3 nM, respectively). It experimentally reduces platelet toxicity and induces enzyme activation in

tissues to kill tumor cells. **10** is the active metabolite of **9** (Figure 1.16)⁶⁰. Currently, Ascentage has published data on dual Bcl-2/Bcl-xL inhibitors APG-1252 and its active

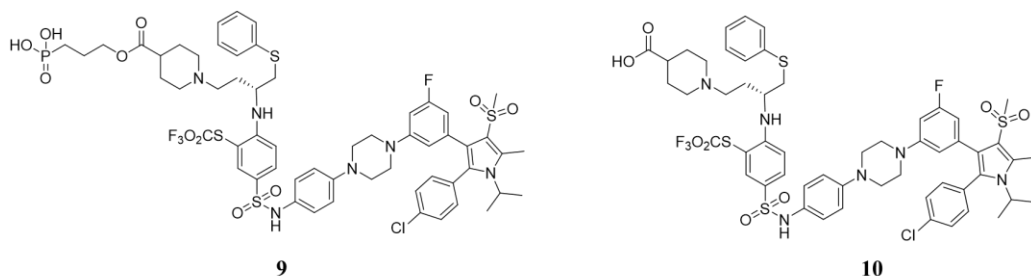


Figure 1. 16. Bcl-2/Bcl-xL dual inhibitors disclosed by Ascentage.

metabolite APG-1252-M1 which is currently in clinical trials. The structures have not been disclosed, but **9** and **10** provide examples of structures of Ascentage Bcl-2/Bcl-xL dual inhibitors.

APG-1252 was developed with a strategy that would enable a drug to limit the cell permeation in platelets, while converting into an active metabolite in tumor tissue in order to limit the toxic thrombocytopenia seen with ABT-263. Experimentally, Ascentage developed APG-1252, which converts into the active metabolite APG-1252-M1 *in vivo*. Both compounds bind to Bcl-2 and Bcl-xL with $K_i < 1$ nM, but APG-1252 is more than 10 times less active than APG-1252-M1 in a cell growth assay⁶¹. APG-1252-M1 was tested in five AML cell lines and shows that the viability of the cells decreases significantly in a time and dose- dependent manner⁶². The active metabolite induces Bax/Bak-dependent apoptosis in an MEF/MCL1-/- model cell line and both compounds can achieve complete tumor regression in human cancer animal models⁶¹. Additionally, APG-1252 achieved complete tumor regression in H146 and H1963 SCLC xenograft models while avoiding thrombocytopenia. Data also suggested that the active metabolite induces apoptosis in a Bcl-2 family dependent manner, due to the cleavage and activation of caspase-3 and PARP in HL-60 cells.

Patients with advanced SCLC or other solid tumors were treated with APG-1252 in a phase I study. 13 patients received the drug intravenously twice weekly for 3 weeks in a 28-day cycle. The maximum tolerated dose was not identified and the most common adverse events included arthralgia, AST/ALT increase, vomiting, and fatigue. No adverse events nor thrombocytopenia were observed. It was well tolerated over all dose levels (100-400mg) with no hematologic toxicity reported⁶³. Other phase I clinical trials including dose escalation and combination therapy studies are currently ongoing with APG-1252⁶⁴⁻⁶⁷.

1.9. Bcl-xL selective inhibition

1.9.1 Abbvie compounds

Clinical trials with navitoclax revealed that targeting Bcl-xL resulted in thrombocytopenia because platelets are dependent on Bcl-xL for survival³⁸. However, Bcl-xL overexpression has been correlated with drug resistance and hematological cancer progression as well as solid tumors⁶⁸. Combination therapies with navitoclax showed that synergy was primarily driven by Bcl-xL inhibition in solid tumors and selective Bcl-xL inhibition can potentially offer decreased immunosuppressive effects compared to dual Bcl-x/Bcl-xL inhibition⁶⁸. These data drove the discovery of the Bcl-xL inhibitor A-1155463.

Abbvie began with the optimization of Bcl-xL selective inhibitor WEHI-539 (Figure 1.17). Its use was limited clinically due to the potentially toxic hydrazone moiety

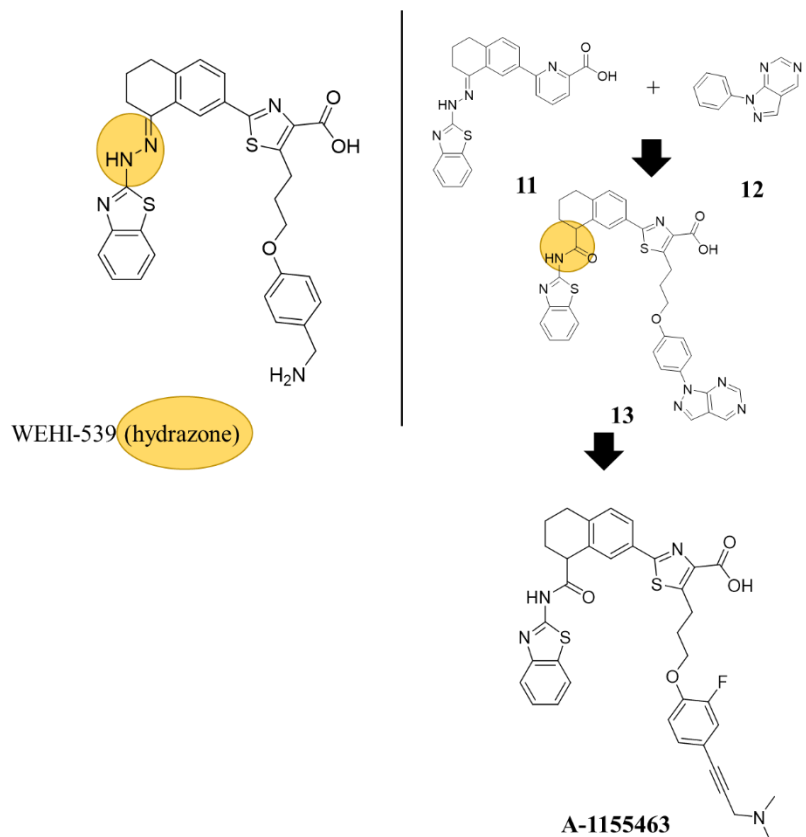


Figure 1. 17. The development of *Bcl-xL* selective inhibitor A-115463 from WEHI-539.

present (highlighted). They replaced this group with an amide, which caused a loss of affinity, but acceptable pharmacokinetics were favorable in comparison and had no liabilities. Concurrently, they utilized a fragment-based NMR approach to identify additional fragments that may bind in the BH3 binding domain. For their first site ligand, **11** was used due to its higher solubility in aqueous conditions, which is required for NMR. In the presence of **11**, a second site ligand **12** (Figure 1.17) was identified, which showed good affinity ($K_d = 4$ mM). A NOSEY experiment was conducted with these ligands and suggested that a short linker could attach the two molecules and retain affinity.

After a targeted SAR, a 4-atom linker in the para position offered a subnanomolar K_i with >4000-fold selectivity over Bcl-2, **13** ($K_i = 0.042$ nM Bcl-xL, 170 nM Bcl-2). However, it showed poor binding in a cell viability assay in the presence of HSA. A co-crystal structure was obtained with **13** and found it projected into the p2 pocket and the carboxylic acid formed a hydrogen bond with Arg139. Additionally, the pyrimidine moiety bound in the p4 pocket while making favorable pi-stacking interactions. They incorporated tethered amine groups and halogens to offset serum binding and increase cell permeability and metabolic stability, which eventually led to the development of A-1155463. The co-crystal structure of this compound with Bcl-xL showed the 2-fluoro moiety sat within the p4 pocket while making van der waals contacts with the surrounding residues (Figure 1.18). It offered picomolar binding with >1000-fold weaker

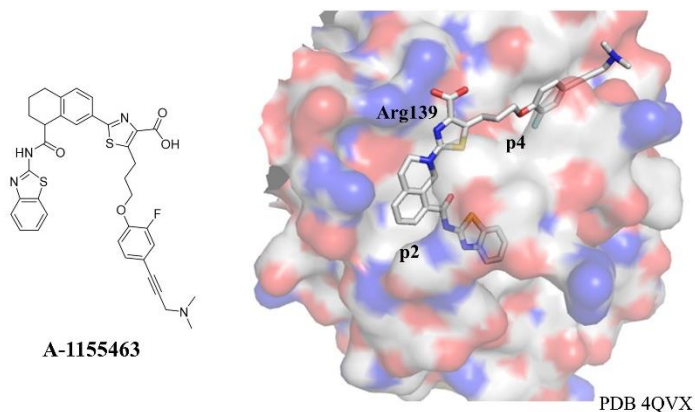


Figure 1. 18. The structure of A-1155463 co-crystallized in Bcl-xL. PDB 4QVX.

binding to Bcl-2, Bcl-w, and Mcl-1. In the Bcl-xL dependent cell line H146 with 10% HSA, the EC_{50} of A-1155463 was 0.065 μ M. Non-tumor bearing SCID-beige mice were treated with a single dose of A-1155463 (5 mg/kg) and although platelet counts fell drastically after 6h, the mice rebounded to normal levels within 72 h indicating dosing schedules will be critical⁶⁸.

However, A-1155463 had poor solubility and oral absorption that ultimately limited its use in more *in vivo* experiments. Therefore, they developed the oral compound A-1331852 (Figure 1.19)⁶⁹. They began by revisiting the tetrahydroisoquinoline (THIQ)-thiazole core in A-1155463. The THIQ-thiazole had poor oral pharmacokinetic properties, but if replaced with a THIQ-pyridine core, the molecule showed superior pharmacokinetics in rats and lower measured logD, even though it had lower affinity towards Bcl-xL in a FRET assay ($K_i = 65$ nM THIQ-thiazole, 164 nM THIQ-pyridine). They elected to move this forward and began a targeted SAR. A crystal structure of A-115463 revealed that the propyloxy linker had a destabilizing arrangement of atoms within the p4 pocket, so they wanted to decrease the number of rotatable bonds, which would also impart a more drug-like property to the compound. They also incorporated 5-membered heterocycles as they believed it would be optimal for binding within the p4 pocket. The most potent compound of this series was **14**, $K_i = 0.296$ nM⁶⁹ (Figure 1.19).

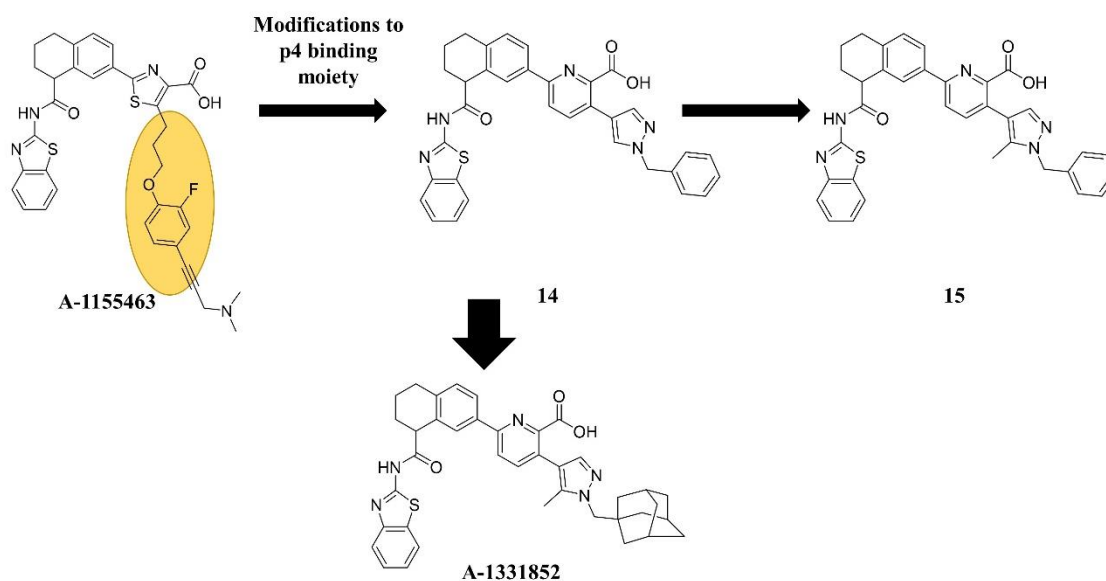


Figure 1. 19. Development of A-1331852 from A-115463.

Next, they methylated the pyrazole and found substitution at the 5-position afforded $K_i = 0.027$ nM as well as modest potency in MOLT-4 cells (Bcl-xL dependent cell line) with 10% HSA ($EC_{50} = 1,610$ nM) (Figure 1.19). Lastly, they introduced sp³-rich cycloalkyl groups as it would increase the overall sp³-fraction of the pharmacophore, and could improve the properties of the compound. They introduced a cyclohexane, which afforded $K_i = 0.027$ nM Bcl-xL, but incorporation of adamantane led to the most potent compound of the series, named A-1331852 (Figure 1.19), with $K_i = < 0.010$ nM Bcl-xL and $EC_{50} = 0.3$ nM MOLT-4 cells⁶⁹.

A-1331852 binds Bcl-xL with a $K_i = < 0.010$ nM and 10- to 50-fold more potent than A-115543 and navitoclax in cells. It disrupts the Bcl-xL-Bim complex and induces hallmarks of apoptosis in a Bcl-xL dependent manner. In xenograft models it offers tumor regression as a single agent and recapitulates the efficacy of navitoclax in combination with venetoclax. In a separate experiment, male Sprague-dawley rats treated with docetaxel, a chemotherapy agent, decreased neutrophil counts significantly, whereas monotherapy of A-1331852 exhibited increased neutrophil counts, while the combination offered no statistical significance in reductions. A-1331852 does induce significant reductions in circulating platelets. According to these studies, this suggests that Bcl-2 inhibition may account for the neutropenia induced by docetaxel in these combination therapies. This may suggest that Bcl-xL selective inhibitors can avoid dose-limiting neutropenia, which has been seen in the clinic with combination therapies of navitoclax and docetaxel⁶⁹.

Although A-1331852 is currently not in clinical trials, these studies show that Bcl-xL inhibitors may be efficacious in the clinic as a monotherapy or in combination for

solid tumors or other cancers dependent on the protein. However, more extensive studies need to be carried out to avoid the dose-limiting thrombocytopenia side effect of navitoclax⁷⁰.

1.9. Mcl-1 selective inhibitors

Mcl-1 is an anti-apoptotic protein related to Bcl-2 and Bcl-xL, and a critical factor for the survival of both healthy and malignant tissues. It is required for implantation and is also a survival factor for hematopoietic stem cells as well as progenitor B and T lymphoid cells⁷¹. It was originally cloned from the myeloid cell line ML-1 as an early induction gene during differentiation. It has a short half-life due to its amino-terminal PEST domain that targets proteins for proteasomal degradation⁷². Additionally, it is tightly controlled by a variety of mechanisms including transcription and post-translational regulation. For example, phosphorylation at the specific residues Thr92 and Thr163 prolongs its half-life, phosphorylation at Ser159 enhances Mcl-1 ubiquitylation and degradation, and once phosphorylated at Ser121 and Thr163, it becomes inactivated in response to oxidative stress. Its rapid turnover is regulated by caspases and proteasome-dependent degradation in response to different death stimuli such as cytokine deprivation⁷³. It can also be upregulated post-translationally to inhibit cell death⁶.

Mcl-1 has been implicated in cancer progression through a variety of different mechanisms. Due to its instability and rapid turnover, cancer cells can utilize different mechanisms to stabilize Mcl-1 and increase survival³⁰. It is one of the most overamplified genes and overexpressed proteins in cancers including hematological malignancies and solid tumors including breast, NSCLC , ovarian, prostate, and pancreatic cancers^{71,74,75}. Mcl-1 has also been shown to mediate survival for MM, AML,

NSCLC, and MYC-driven lymphomas⁷⁶, and act as an essential survival protein for MM cells⁷⁷. This overexpression is associated with poor prognosis as well as resistance to different anti-cancer drugs including Taxol, cisplatin, vincristine, and other standard chemotherapy drugs^{75,78}. Interestingly, many cancers upregulate Mcl-1 in response to Bcl-2/Bcl-xL inhibition and is primarily responsible for venetoclax resistance^{78,79}.

Mcl-1 differs structurally from other anti-apoptotic proteins. They have similar globular structures⁷², however, Mcl-1 only shares around 25% sequence identity with other members of the protein family. Additionally, its BH3 binding groove is more shallow, rigid, and more electropositive, differing in a number of different residues^{80,81}. Due to its importance in healthy tissues, one concern is that selectively targeting it can cause side effects in healthy cells. The importance of targeting Mcl-1 has been recognized and its structure, expression, and regulation represent the difficulty of developing selective inhibitors. The compounds presented in this section review these difficulties and describe current efforts towards developing potent, selective Mcl-1 inhibitors.

1.9.1. AMG176 and AMG397

Amgen developed the orally bioavailable Mcl-1 selective inhibitor AMG176 by utilizing structure-based drug design guided by X-ray crystallography and small molecule conformational analysis, the latter used for optimization to increase selectivity and pharmacokinetic properties of the compounds. First, they employed a high-throughput screen of 248,090 compounds that would specifically disrupt the Mcl-1/Bim interaction. The screen identified a series of spiro-macrocyclic molecules, such as compound **16** (IC₅₀ = 3.4 μM) in Figure 1.20. The enantiomers were separated and the ring was expanded to

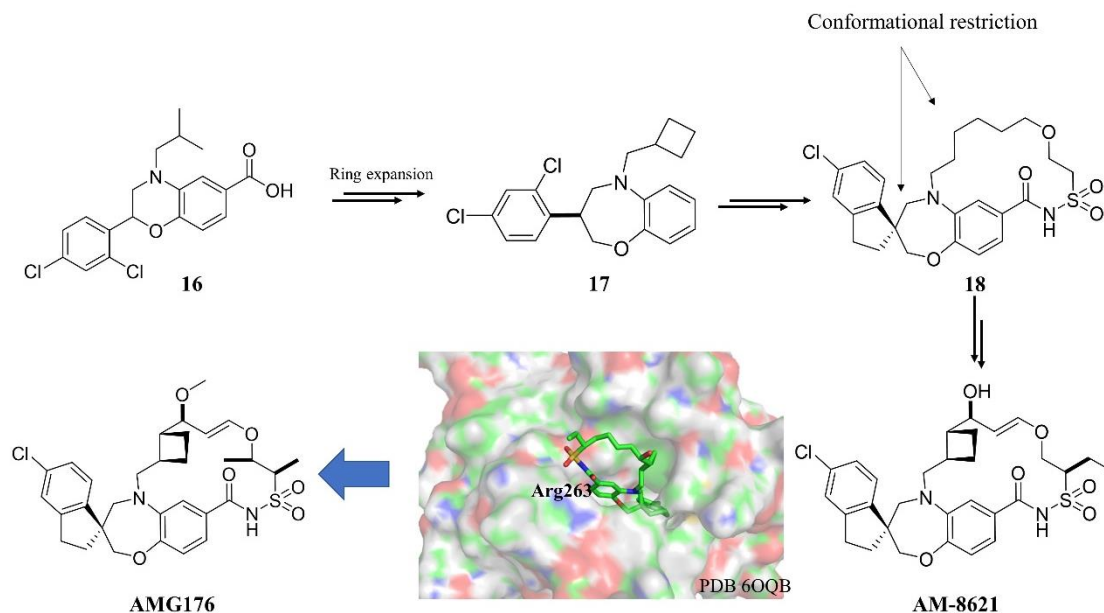


Figure 1. 20. The development of AMG176.

7- and 8- membered rings, ultimately resulting in compound **17** ($IC_{50} = 0.3 \mu M$). Co-crystallization with **17** showed a binding pocket that was not present in the co-crystal structure of Mcl-1 and Bim. To fill this pocket, they introduced an ethylene in place of the 2-chloro group that would introduce conformational restriction and a macrocyclic ring utilizing an acyl sulfonamide that afforded compound **18** ($IC_{50} = 0.1 \mu M$). Further development and conformational restraint, including O-methylation to increase oral bioavailability and the pharmacokinetic profile, led to AMG176 (Figure 1.20). It has $K_i = 0.06 \text{ nM}$, $0.7 \mu M$, and $0.95 \mu M$ for Mcl-1, Bcl-xL, and Bcl-2, respectively, showcasing its selectivity for Mcl-1 over other anti-apoptotic proteins.

Amgen chose AM-8621 ($K_i = 0.05 \text{ nM}$, Figure 1.20), an analog of AMG176, for cell-based assays. In the NSCLC cell line A427, AM-8621 disrupted Mcl-1 and Bim in a dose- and time dependent manner. In a panel of AM-8621 sensitive cell lines, treatment showed increased activated Bak levels, as well as caspase 3- and 7 activation. Cell

viability also decreased and showed a near-maximal cell death response within 8 hours of treatment. They also profiled AM-8621 against 952 tumor cell lines, which showed hematologic malignancies had greater sensitivity to treatment⁸².

In xenograft studies, they used AMG176 due to its superior pharmacokinetic profile over AM-8621. Activated Bak, cleaved caspase-3 and PARP were all detected two hours after administration indicating apoptosis-dependent cell death. Additionally, mice treated twice weekly with a 30mg/kg dose achieved 54% tumor growth inhibition, while 60 mg/kg dose showed 21% tumor growth inhibition. Daily administration saw 84% regression and 100% regression, respectively. Similar studies were done with human gene *MCL1* knock-in mice, as AMG176 was unable to inhibit mouse Mcl-1. Oral administration at 30 and 60 mg/kg saw dose-dependent decreases in B cells, monocytes, and neutrophils with no evidence of systemic toxicity. Additionally, they evaluated combination therapy with AMG176 and carfilzomib, a drug used for people who previously received one or more treatments for relapsed MM⁸³. Mice were treated once daily with AMG176 (20 mg/kg) and twice-weekly with carfilzomib (3 mg/kg), which achieved significant tumor inhibition relative to monotherapy⁸².

In a phase I, first in-human clinical trial, AMG176 was evaluated in relapsed or refractory MM patients. 26 patients were treated, but 22 discontinued treatment due to progression of disease. Adverse events related to treatment included neutropenia, nausea, diarrhea, and anemia. No appreciable drug accumulation was observed and release of Bak and activation of caspase-3 in peripheral blood monocytes was observed⁸⁴. AMG397 is an additional Mcl-1 selective inhibitor developed by Amgen that has not been disclosed. In September 2019, during a phase I dose escalation clinical trial of AMG397 in patients

with MM, NHL, and AML, the trial was halted by Amgen due to cardiac toxicity. Amgen noted that preclinical research suggests Mcl-1 may be required for normal cardiac myocyte mitochondrial activity and severe, sudden heart failure is not an acceptable liability⁸⁵. As a result, Amgen put a voluntary hold on the AMG 176 clinical trial⁸⁶.

1.9.2. Servier and Vernalis

Servier and Vernalis published a detailed SAR describing the development of compounds leading to S63845 and S64315, the latter of which is currently in clinical trials. Initially, a fragment screen identified carboxylic acid containing compounds with a thienopyrimidine core. Compound **19**, their initial hit, binds Mcl-1 and Bcl-2 with $K_i = 50 \mu\text{M}$ and $74 \mu\text{M}$, respectively, with no measurable affinity to Bcl-xL. They performed rigorous SAR studies, with many modifications failing to gain appreciable selectivity or potency for Mcl-1. For example, modifications at the 2- and 6- position, variation of the amino acid substituent, and chirality differences were tolerated, but had no significant

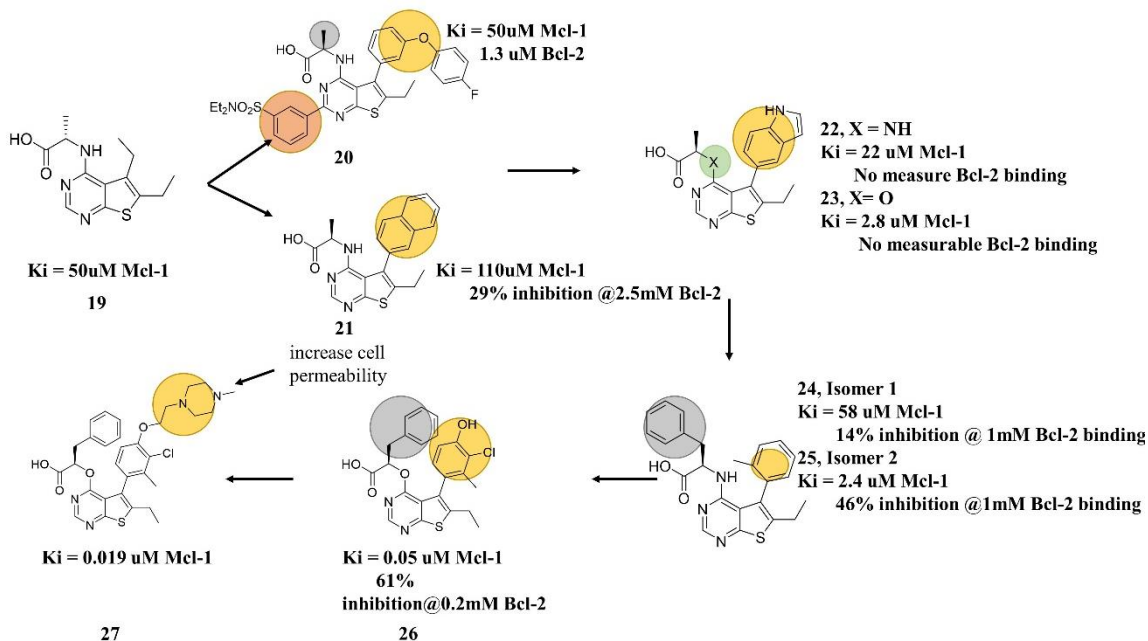


Figure 1. 21. The SAR of Mcl-1 selective compounds described by Servier and Vernalis. Highlighted regions represent functional groups that were modified to increase affinity towards Mcl-1.

influence on affinity. Examples of these include compounds **20** and **21**⁸⁸ (Figure 1.21. highlighted examples of modifications).

Next, Nuclear Overhauser Effect (NOE)-based methods were utilized to probe binding interactions⁸⁸. NOEs are NMR based experiments used in drug design to assess the protein-ligand interaction distance and help elucidate the binding mode⁸⁷. NOE experiments with compound **21** showed the naphthyl ring and one of the two methyl groups made contact with Mcl-1, indicated by experimental residue perturbations, which suggested it was in a similar location as Leu10 and Ile13 of Bim-BH3. Driven by NOEs and molecular docking data, they further explored the p2 pocket with indolyl derivatives, represented with **22** and **23** (Figure 1.21). Of note, the atropisomers generated of these compounds offered similar affinities and were not further characterized. Interestingly, replacement of the nitrogen linker with oxygen improved Mcl-1 binding by 6-8-fold ($K_i = 22 \mu\text{M}$ (**22**), $K_i = 2.8 \mu\text{M}$ (**23**)). They hypothesized that aryl ethers have a different rotational barrier compared to anilines, and suggested that the oxygen within the linker may offer a preferable conformational profile for Mcl-1 binding⁸⁸.

Crystal structures with these compounds and Mcl-1 were generated, and found the 2-indolyl group pointing towards solvent, while additional modifications could increase specificity and potency. D-phenylalanine replaced the glycine in compound **23**, giving separable diastereoisomers that offered submicromolar affinity and high selectivity for Mcl-1 ($K_i = 0.49 - 1.6 \mu\text{M}$ Mcl-1). **24** and **25** shown in Figure 1.21 exhibit $K_i = 58 \mu\text{M}$ and $2.4 \mu\text{M}$ to Mcl-1, revealing the differences in affinities of these atropisomers. An X-ray structure revealed the methyl substituent of **25** points towards with protein, making additional hydrophobic contacts. In addition, halogen substituted phenyl groups were

introduced next in place of indolyl derivatives. Compound **26** showed significantly increased inhibition and selectivity for Mcl-1, $K_i = 0.051 \mu\text{M}$ (61% inhibition of Bcl-2 at 0.2mM).

26 was assessed in cell viability assays in H929 cells, an MM Mcl-1 dependent cell line, and showed no cellular activity. They suggest this is due to the poor cell penetrance, and therefore introduced basic groups such as tertiary amines. This led to the

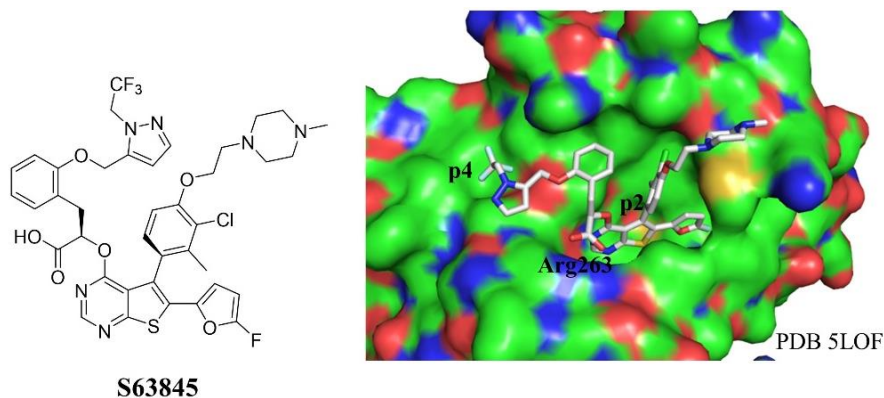


Figure 1. 22. The Mcl-1 selective compound S63845 co-crystallized with Mcl-1. PDB 5LOF.

isolation of atropisomers of **27**, one of which showed superior affinity for Mcl-1 ($K_i = 0.019 \mu\text{M}$) in FP and cell viability assays ($\text{IC}_{50} = 5.6 \mu\text{M}$ and $1.0 \mu\text{M}$ for 10% and 0.1% serum levels). X-ray crystal structures of the potent atropisomer also showed the methylpiperazine group projected towards the solvent, while the methyl and chlorine interact with the protein. Additionally, **27** disrupted the Mcl-1/Bak complex, and induced PARP and caspase 3 cleavage, suggesting it demonstrates on target cell killing through activation of apoptosis. Drug-drug interaction potential was evaluated with five different human CYP450 enzymes and showed $\text{IC}_{50} = 20 \mu\text{M}$. This low binding affinity may suggest reduced DDI liability. This compound led to the discovery of S63845 (Figure 1.22)⁸⁸.

S63845 binds human Mcl-1 with $K_d = 0.19$ nM, determined by surface plasmon resonance, a 6-fold lower affinity to mouse Mcl-1, and no appreciable binding to Bcl-2 or Bcl-xL. X-ray crystallography reveals it binds in the BH3-binding groove of Mcl-1 and the carboxylate group forms interactions with Arg263. The aromatic scaffold binds in the p2 pocket while the trifluoromethyl group stretches across the p4 pocket (Figure 1.22). Cell viability assays demonstrated S63845 potently killed H929 cells with little impact on Bcl-2 and Bcl-xL dependent H146 SCLC cells. It also disrupts binding of Bak and Bax interactions with Mcl-1 and induced cleavage of caspase-3 and PARP, suggesting it kills cells in an apoptosis-dependent manner. Many different cell lines including MM, lymphomas, CML, and AML demonstrated sensitivity to the compound. In human MM xenografts, immunocompromised mice showed tumor growth inhibition over 100%. Additionally, at the therapeutically efficacious dose of 25 mg/kg, S63845 induced complete tumor regression in 7 out of 8 mice after 100 days of treatment. It was tolerated well with no histomorphological changes to liver, heart, kidney, skeletal muscle, or other organs⁷⁴.

As an Mcl-1 inhibitor, S63845 has the potential to act synergistically with the Bcl-2 selective inhibitor venetoclax in cell lines that are resistant or nonresponsive to venetoclax treatment. Li *et al.* treated 11 T-ALL cell lines with S63845 and found four were sensitive to treatment and western blot analysis showed PARP cleavage, indicating Mcl-1 plays an important role in maintaining survival for some T-ALL cells. Combination treatment of S63845 and venetoclax in cells revealed the two agents were highly synergistic in four T-ALL cell lines as well as in a zebrafish model⁸⁹. In clinical trials with MCL patients, resistance developed to venetoclax monotherapy, and Prukova

et al. showed that the upregulation of Mcl-1 conferred resistance. They demonstrated that the combination of venetoclax and S63845 in mantle cell lymphoma (MCL) xenografts, derived from patients with chemotherapy refractory diseases, showed long-term lymphoma free survival⁹⁰.

Although S63845 was not chosen for further clinical evaluation, the closely related S64315 has begun clinical trials^{91,92}. The structure of the clinical candidate S64315 is undisclosed, however, the experimental impact its precursor shows in various preclinical models showcases the potential these compounds have as selective Mcl-1 inhibitors. Phase I studies currently ongoing include dose escalation studies, and further assessing the tolerability and anti-tumor activity in AML, myelodysplastic syndrome (NCT02979366), and refractory or relapsed lymphoma or MM (NCT02992483). Additionally, a phase I dose escalation study of S64315 in combination with venetoclax in patients with AML is currently ongoing (NCT03672695).

1.9.3. AZD5991

AstraZeneca developed AZD5991, an indole 2-carboxylic acid macrocyclic Mcl-1 selective inhibitor. Four different strategies were used in the design including fragment-based lead generation, DNA-encoded library screen, building from known compounds and covalent inhibition, as well as structure-based drug design.

They started with compound **28** from the literature (Figure 1.23), and generated a co-crystal structure with Mcl-1. Interestingly, two of the compounds bound in the BH3 domain: carboxylic acid interacted with Arg263 while the naphthyl group occupied an induced-fit in the pocket. Binding of a second compound was in close proximity to the first, resulting in a conformational change in the protein to accommodate both

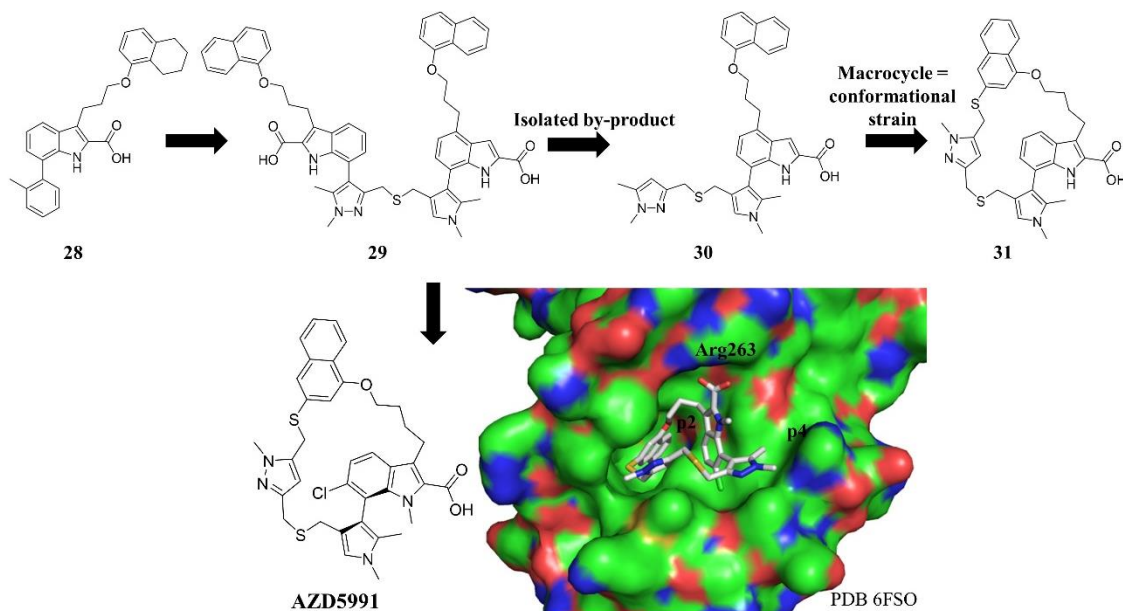


Figure 1.23. The development of the Mcl-1 selective inhibitor AZD5991. PDB 6FSO

compounds. To increase solubility, the 2-methylphenyl group was replaced with 1,3,5-trimethylpyrazole and the two monomers were linked together (**29**). This compound yielded an Mcl-1 $IC_{50} = 0.77 \mu M$ in a TR-FRET assay. A byproduct of compound **29** was isolated (**30**) and had an improved potency towards Mcl-1 with $IC_{50} = 0.042 \mu M$. A co-crystal structure with **30** revealed a U-shaped conformation within the pocket and they hypothesized that a macrocycle would constrain the molecule and thus give an entropic benefit upon binding (Figure 1.23). It also revealed that the pyrazole ring was well accommodated by the protein, by further opening the induced-fit pocket and increasing contacts with the protein. Additionally, it was suggested a polar heteroatom linker would cause a desolvation penalty, and thus **31** was synthesized ($IC_{50} = 42 \text{ nM Mcl-1}$)⁸¹.

After multiple modifications including addition of the 6-chloro and N-methyl substituents, atropisomers were isolated due to the restricted rotation around the biaryl bond, resulting in the discovery of AZD5991 (the “R” atropisomer) (Figure 1.23). NMR

experiments revealed that the compound adopts the bioactive free ligand conformation, and its potent affinity is driven by rapid on-rate kinetics. A surface plasmon resonance assay validated binding affinity ($K_d = 170$ pM) as well as the rapid on-rate binding kinetics. AZD5991 was also evaluated in a panel of Mcl-1 dependent cell line and displayed superior potency. They also assessed selectivity in lymphoma cell lines, which express Mcl-1, Bcl-2, Bcl-xL, Bfl-1, or Bcl-w. Activity of AZD5991 was blocked by the overexpression of the other Bcl-2 pro-apoptotic proteins and expression of Bcl-xL in the sensitive cell line NCI-H23 showed resistance to the compound. A thermal melt shift assay demonstrated that in MV4-11 cells, the compound stabilized Mcl-1 and additional assays showed that AZD5991 relies on Bak for apoptosis induction, disrupts the Bak/Mcl-1 complex, and leads to cleavage of caspase-3. These data represent the compound is sensitive to Mcl-1 and induces apoptosis via Mcl-1 inhibition in a Bak-dependent manner⁸¹.

In MOLP-8 tumors, a single intravenous dose of the compound led to dose-dependent tumor growth inhibition and regression. Ten days post treatment, there was 52% and 93% tumor growth inhibition in 10 and 30 mg/kg doses, whereas 60 mg/kg caused 99% tumor regression with no detectable tumors in 6 out of 7 mice. The compound was well tolerated with no considerable body weight loss in all mice. In combination with bortezomib, anti-tumor activity was achieved in MM models, while combinations with venetoclax offered enhanced sensitivity to AZD5991 in AML models, including those that were resistant to venetoclax. It exhibited potent anti-tumor activity with complete tumor regression in MM and AML mouse and rat xenograft models, which additionally showed induction of apoptosis from caspase-3 and PARP cleavage⁸¹.

Recruiting for a phase I clinical trial with AZD5991 is currently underway. It includes a three-part dose-escalation study to assess safety, tolerability, pharmacokinetics, and anti-tumor activity in patients with relapsed or refractory hematologic malignancies including MM, NHL, TCL, CLL, SLL, and Richter's syndrome^{92,93}. It is estimated to be completed in 2022⁹⁴.

1.9.4. Abbvie compounds

ABBV-467 is an Mcl-1 selective inhibitor that will begin a phase I clinical trial assessing the safety and tolerability in adult patients with relapsed/refractory MM. Its estimated completion date is in 2023⁹³. Although its structure has not been disclosed, here I will discuss the discovery of Abbvie's 7-substituted indole 2-carboxylic acid scaffolds, which includes the Mcl-1 selective inhibitor A-1210477, that was not selected for clinical studies. These 7-substituted indoles including macrocyclic Mcl-1 inhibitors have been disclosed in a number of patents^{95,96}.

A high-throughput screen led to the identification and generation of **32** (Figure 1.24) that was then incubated with Mcl-1 in a C¹³- Heteronuclear Singular Quantum Coherence (HSQC) NMR experiment to evaluate protein-ligand interactions. Chemical shift perturbations indicated Mcl-1 binding, leading to further modifications of the compound. Linker length and polar moieties in place of the cyclohexyl group were deleterious to binding. Next, 4-(1-naphthoxypropyl) group was installed (**33**), resulting in a 10-fold increase in binding affinity. Overlay with Bim showed it occupied the p2 pocket with the naphthyl group penetrating deep into the pocket. Co-crystallization showed the carboxylic acid interacted with Arg263 in the BH3 binding groove. Addition

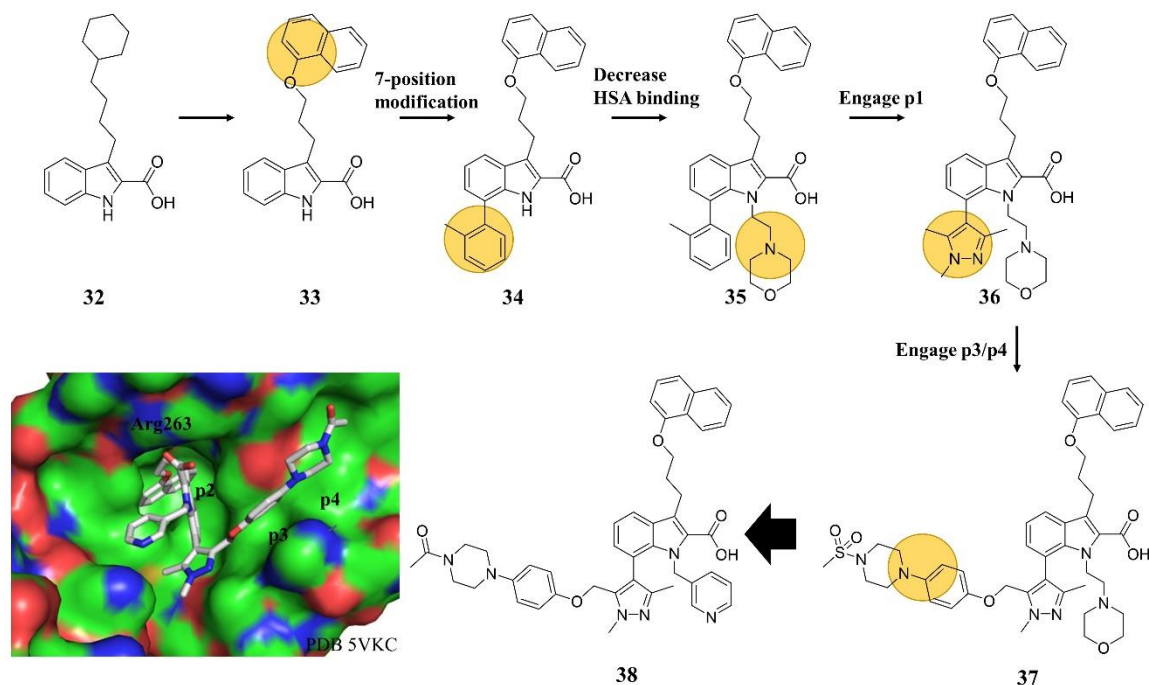


Figure 1.24. The SAR leading to the development of A-1210477. PDB 5VKC

of an *o*-tolyl group (**34**) at the 7- position afforded a 2-fold affinity gain. At this point, it was imperative to test the inhibitor in an FP assay in the presence of HSA, as serum depletes in a cellular context, Mcl-1 levels also decrease. All binding affinities to Mcl-1 decreased in the presence of serum.

To alleviate this serum binding, various polar groups were added to the N-1 position. Addition of morpholinoethyl group (**35**) afforded improved affinity to Mcl-1 ($K_i = 9$ nM Mcl-1, $K_i = 470$ nM Mcl-1 with 1% HSA). Co-crystal structure of **35** with Mcl-1 showed the morpholine group projected towards the solvent, while the C7-*o*-tolyl methyl group pointed towards the p3 and p4 pockets. However, they noticed the 6- position on the C7-*o*-tolyl ring pointed towards the p1 pocket, and an appropriate disubstituted 5-membered ring could afford optimal geometry to engage both p1 and p3/p4 pocket.

Installation of 1,3,5-trimethyl-1H-pyrazole ring at the 7 position (**36**) resulted in below detectable limits in the FP assay. Therefore, they turned to a TR-FRET assay, which is able to accurately measure affinities to 10pM. The K_i of **36** was 1.5 nM in Mcl-1 and 35 nM in the presence of 10% HSA in the TR-FRET assay. Guided by these results, they extended the 5-membered ring at the ortho position to engage the p3/p4 pocket, and eventually developed **37** ($K_i = 1.8$ nM Mcl-1, $K_i = 98$ nM 10% HSA). A co-crystal structure showed the N-acetylpiperazine binds along the p3/p4 pocket, while the 5-substituted methyl group projects into the p1 pocket.

38 ($K_i = 0.43$ nM Mcl-1, $K_i = 6$ nM Mcl-1 1% HSA) (Figure 1.24) was used for additional assays because it achieved picomolar inhibition of Mcl-1. **38** exhibited good selectivity, with the TR-FRET assay ($K_i > 0.66$ μ M for other anti-apoptotic protein members Bcl-2, Bcl-xL, Bcl-w, and A1). In an Mcl-1 dependent MM cell line (H929), **38** induced caspase activation and decreased cell viability within 4 h⁹⁷.

This led to the development of A-1210477 (Figure 1.25), an analog of **37**. It binds Mcl-1 with $K_i = 0.454$ nM in a TR-FRET assay with selectivity over Bcl-2 and Bcl-xL ($K_i = 0.132$ μ M and >0.660 μ M, respectively). In various cancer cell lines, A-1210477 caused Mcl-1 elevation, indicating the compound directly binds and targets Mcl-1. They

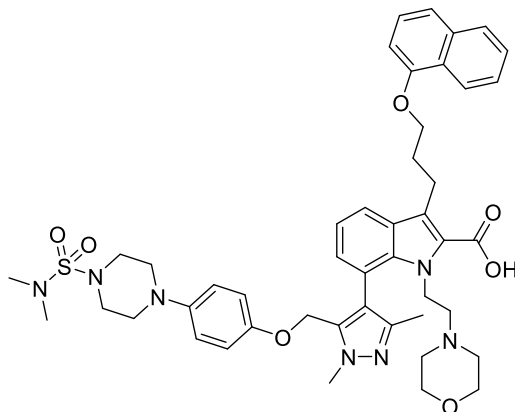


Figure 1. 25. The structure of Mcl-1 selective inhibitor A-1210477.

also observe cytochrome *c* fractions in the cytosol and caspase-3 activation, indicating it can induce apoptosis in Mcl-1 dependent cell lines. It also caused a dose-dependent reduction in co-immunoprecipitated Bim with Mcl-1 as well as Mcl-1-NOXA interactions, while showing no effect on Bcl-2-Bim or Bcl-xL-Xs. In a live cell assay using a mammalian two-hybrid assay, they saw disruption of Mcl-1-Noxa and Mcl-1-Bim2a. Additionally, it selectively killed multiple Mcl-1 dependent cancer cell lines while synergistically acting with navitoclax to decrease cell viability in cell lines that are dependent on Mcl-1 and Bcl-xL. These data show that A-1210477 acts on-target and induces mitochondrial apoptosis in an Mcl-1 dependent manner⁷⁶. It has been reported that addition of an Mcl-1 or Bcl-xL selective inhibitor in cell lines resistant to Bcl-2 selective inhibitors could potentially be re-sensitized by the administration of these inhibitors. Indeed, synergy was observed in co-administration of ABT-199 and A-1210477 in AML resistant cell lines⁹⁸.

Although the structure of ABBV-467 has yet to be disclosed, the promising data from these studies suggest that Abbvie's Mcl-1 selective compounds have the potential for treatment as a monotherapy as well as combination therapy for a variety of different cancers.

Mcl-1 selective inhibitors are difficult to develop due to the various structural differences of the protein such as a flatter topology compared to the other anti-apoptotic proteins, however, the compounds discussed have shown that targeting Mcl-1 is possible with a small molecule inhibitor in picomolar ranges with on-target effects. Mcl-1 is a crucial anti-apoptotic protein, with many cancers dependent on its expression coupled with its implication in chemoresistance. However, these inhibitors have suggested that

targeting Mcl-1 may be efficacious as a cancer therapeutic, but their viability in the clinic will be tested with the numerous Mcl-1 monotherapy and combination therapy clinical trials ongoing.

1.10. Bfl-1 Inhibition

Bfl-1/A1 is one of the least extensively studied Bcl-2 family proteins. The lack of antibodies and loss-of-function mouse models, coupled with the redundant anti-apoptotic function upon overexpression further validates the lack of published material⁹⁹⁻¹⁰¹.

Recently, numerous studies have elucidated its structure and function, including the development of a Bfl-1 specific antibody capable of detecting endogenous proteins and a crystal structure of Bfl-1 complexed with the pro-apoptotic protein Noxa^{101,102}.

Murine A1 was initially discovered in 1991 as a granulocyte and macrophage colony stimulating factor (GM-CSF) early response gene. A few years later the human gene, which shares 72% sequence identity with murine A1, was discovered separately by three different groups⁹⁹. In 1995, it was initially discovered as a gene found to be overexpressed in stomach cancer that resulted in disease development and progression and subsequently identified in fetal liver, hence the name Bfl-1 (Bcl-2 related gene expressed in fetal liver), implicating its involvement in early hematopoiesis^{99,103,104}. It was later reported as a direct transcriptional target of NF- κ B, suggesting a role in inflammation¹⁰⁵. In addition, it was discovered as a gene involved in genomic translocation in patients with chronic myeloid leukemia (CML)⁹⁹.

Since its discovery, Bfl-1 has been found in a variety of cell and tissue types, including hematopoietic cells, lung, small intestine, testis, and smooth muscle cells, as

well as playing a role in the regulation and survival of activated lymphocytes, macrophages, and neutrophils^{103,106,107}.

1.10.1. Structure and Function

Structurally, Bfl-1 is an anti-apoptotic Bcl-2 protein with four BH domains and nine α -helices, consistent with the other anti-apoptotic proteins (Figure 5.1), yet differs

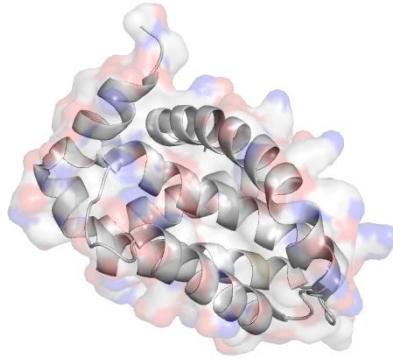


Figure 1.26. Structure of Bfl-1. PDB 5WHI

structurally in its C terminal end, where it contains a stretch of hydrophilic residues. This amphipathic domain is responsible for the ubiquitination and degradation by the ubiquitin proteasome system (UPS), owing to the short half-life of Bfl-1⁹⁹. To date, no E3 ligase has been identified¹⁰³. In addition to post-translational regulation by the UPS, it is also regulated at the transcriptional level. It is induced by TNF- α , GM-CSF, lipopolysaccharide-stimulated macrophages, and antigen receptor stimulation^{103,108}. As represented here, Bfl-1 is extensively regulated by a number of different cellular mechanisms, owing to the complex nature of the protein.

1.10.2. Mode-of-Action

Its mode-of-action remains unclear because Bfl-1 can act as a pro- and anti-apoptotic protein. Studies have explained the interchangeable function of Bfl-1 using the concentrations of CL/CLox apoptosis-related lipids, which reside on the outer

mitochondrial membrane (OMM). These studies revealed that if CL/CLox lipids were expressed in low levels, Bfl-1 exerted anti-apoptotic function, but upon accumulation of the lipids, pro-apoptotic function occurred through self-assembly of homocomplexes¹⁰⁰. When functioning as an anti-apoptotic protein, it is capable of binding both pro-apoptotic proteins Bak and Bax and strongly interacts with BH3-only proteins tBid, Bim, Puma, and Noxa^{100,103}. Interestingly, the pro-apoptotic function is regulated by two essential proteolytic events: the first involves modification of the C-terminal domain via the ubiquitin-dependent proteasome turnover of Bfl-1; second includes the μ -calpain cleavage at the N-terminal BH4 motif^{100,103}. Although the mode-of-action of Bfl-1 remains unclear, it is important to note that the overexpression of the anti-apoptotic function of Bfl-1 is implicated in both cancer development and progression as well as chemoresistance^{106,109,110}.

1.10.3. Implication in Cancer and Chemoresistance

Bfl-1 is highly regulated by many different proteins and environmental stressors. However, dysregulations of these mechanisms can lead to its overexpression^{1,4}. For example, hyperoxia and low levels of reactive oxygen species can increase its transcription and lead to protein overexpression^{103,108}. Additionally, *in vivo* studies have reported that mutations that inhibit Bfl-1 ubiquitination (thus increasing its half-life) has led to increased tumorigenesis¹⁰³. The overexpression of Bfl-1 has been implicated in the development and progression of many solid tumors and cancers including acute lymphoblastic leukemia (ALL) and chronic lymphocytic leukemia (CLL), anaplastic large cell lymphoma, mantle cell lymphoma, and multiple types of large B-cell lymphoma^{103,111}. Additionally, it has also been associated with stomach, colon, bladder,

and breast cancers, as well as melanoma, hepatocellular and squamous cell carcinoma^{103,104}. Interestingly, the overexpression of Bfl-1 has been implicated in the chemoresistance of a number of chemotherapeutics including the Bcl-2 selective inhibitor venetoclax, etoposide, staurosporine, and cisplatin¹¹². In fact, many *in vivo* studies reveal increased levels of Bfl-1 are correlated with more severe cases in CLL and breast cancer due to these resistance factors^{103,111}. Importantly, the oncogenesis and chemoresistance linked to Bfl-1 overexpression reveals the therapeutic need to target the anti-apoptotic protein. There are no drugs in clinical trials targeting Bfl-1, however, for a more detailed analysis at the current progress made towards developing Bfl-1 inhibitors, see Chapter 5.

1.11. Conclusions

Significant progress has been made towards the development of Bcl-2 family inhibitors since the discovery of venetoclax. Dose-limiting thrombocytopenia and protein mutations showcase the difficulty in targeting these PPIs. However, significant strides have been made within this field utilizing BH3 mimetics, which operate to displace the pro-apoptotic proteins by binding in the BH3 binding domain of anti-apoptotic proteins. All of the compounds within this chapter have large, hydrophobic heterocyclic scaffolds that serve as highly potent inhibitors of the Bcl-2 anti-apoptotic proteins. However, efforts from various groups such as Beigene, Ascentage, Abbvie, and Servier and Vernalis showcase the progress made, represented by the numerous Bcl-2 and Mcl-1 selective inhibitors currently in clinical trials. My thesis herein describes my work towards developing inhibitors targeting various anti-apoptotic proteins utilizing highly functionalized heterocyclic scaffolds.

1.12. References

- (1) Pentimalli, F. BCL2: A 30-Year Tale of Life, Death and Much More to Come. *Cell Death Differ.* **2018**, *25* (1), 7–9.
- (2) Tzifi, F.; Economopoulou, C.; Gourgiotis, D.; Ardavanis, A.; Papageorgiou, S.; Scorilas, A. The Role of BCL2 Family of Apoptosis Regulator Proteins in Acute and Chronic Leukemias <https://www.hindawi.com/journals/ah/2012/524308/> (accessed Mar 21, 2020).
- (3) Vaux, D. L.; Cory, S.; Adams, J. M. Bcl-2 Gene Promotes Haemopoietic Cell Survival and Cooperates with c-Myc to Immortalize Pre-B Cells. *Nature* **1988**, *335* (6189), 440–442.
- (4) Hardwick, J. M.; Soane, L. Multiple Functions of BCL-2 Family Proteins. *Cold Spring Harb. Perspect. Biol.* **2013**, *5* (2).
- (5) Youle, R. J.; Strasser, A. The BCL-2 Protein Family: Opposing Activities That Mediate Cell Death. *Nat. Rev. Mol. Cell Biol.* **2008**, *9* (1), 47–59.
- (6) Czabotar, P. E.; Lessene, G.; Strasser, A.; Adams, J. M. Control of Apoptosis by the BCL-2 Protein Family: Implications for Physiology and Therapy. *Nat. Rev. Mol. Cell Biol.* **2014**, *15* (1), 49–63.
- (7) Muchmore, S. W.; Sattler, M.; Liang, H.; Meadows, R. P.; Harlan, J. E.; Yoon, H. S.; Nettlesheim, D.; Chang, B. S.; Thompson, C. B.; Wong, S.-L.; Ng, S.-C.; Fesik, S. W. X-Ray and NMR Structure of Human Bcl-x L , an Inhibitor of Programmed Cell Death. *Nature* **1996**, *381* (6580), 335–341.
- (8) Petros, A. M.; Olejniczak, E. T.; Fesik, S. W. Structural Biology of the Bcl-2 Family of Proteins. *Biochim. Biophys. Acta* **2004**, *1644* (2–3), 83–94.
- (9) Wong, C.; Anderson, D. J.; Lee, E. F.; Fairlie, W. D.; Ludlam, M. J. C. Direct Visualization of Bcl-2 Family Protein Interactions Using Live Cell Fluorescent Protein Redistribution Assays. *Cell Death Dis.* **2012**, *3* (3), e288.
- (10) van Delft, M. F.; Huang, D. C. S. How the Bcl-2 Family of Proteins Interact to Regulate Apoptosis. *Cell Res.* **2006**, *16* (2), 203–213.
- (11) Shimizu, S.; Konishi, A.; Kodama, T.; Tsujimoto, Y. BH4 Domain of Antiapoptotic Bcl-2 Family Members Closes Voltage-Dependent Anion Channel and Inhibits Apoptotic Mitochondrial Changes and Cell Death. *Proc. Natl. Acad. Sci. U. S. A.* **2000**, *97* (7), 3100–3105.

- (12) Dewson, G.; Kluck, R. M. Mechanisms by Which Bak and Bax Permeabilise Mitochondria during Apoptosis. *J. Cell Sci.* **2009**, *122* (16), 2801–2808.
- (13) Letai, A.; Bassik, M. C.; Walensky, L. D.; Sorcinelli, M. D.; Weiler, S.; Korsmeyer, S. J. Distinct BH3 Domains Either Sensitize or Activate Mitochondrial Apoptosis, Serving as Prototype Cancer Therapeutics. *Cancer Cell* **2002**, *2* (3), 183–192.
- (14) Willis, S. N.; Fletcher, J. I.; Kaufmann, T.; van Delft, M. F.; Chen, L.; Czabotar, P. E.; Ierino, H.; Lee, E. F.; Fairlie, W. D.; Bouillet, P.; Strasser, A.; Kluck, R. M.; Adams, J. M.; Huang, D. C. S. Apoptosis Initiated When BH3 Ligands Engage Multiple Bcl-2 Homologs, Not Bax or Bak. *Science* **2007**, *315* (5813), 856–859.
- (15) Lanning, M. E.; Fletcher, S. Recapitulating the α -Helix: Nonpeptidic, Low-Molecular-Weight Ligands for the Modulation of Helix-Mediated Protein–Protein Interactions. *Future Med. Chem.* **2013**, *5* (18), 2157–2174.
- (16) Boersma, M. D.; Sadowsky, J. D.; Tomita, Y. A.; Gellman, S. H. Hydrophile Scanning as a Complement to Alanine Scanning for Exploring and Manipulating Protein–Protein Recognition: Application to the Bim BH3 Domain. *Protein Sci. Publ. Protein Soc.* **2008**, *17* (7), 1232–1240.
- (17) Moreira, I. S.; Fernandes, P. A.; Ramos, M. J. Hot Spots--a Review of the Protein-Protein Interface Determinant Amino-Acid Residues. *Proteins* **2007**, *68* (4), 803–812.
- (18) Azzarito, V.; Long, K.; Murphy, N. S.; Wilson, A. J. Inhibition of α -Helix-Mediated Protein-Protein Interactions Using Designed Molecules. *Nat. Chem.* **2013**, *5* (3), 161–173.
- (19) Barnard, A.; Long, K.; Yeo, D. J.; Miles, J. A.; Azzarito, V.; Burslem, G. M.; Prabhakaran, P.; A Edwards, T.; Wilson, A. J. Orthogonal Functionalisation of α -Helix Mimetics. *Org. Biomol. Chem.* **2014**, *12* (35), 6794–6799.
- (20) Drennen, B.; Scheenstra, J. A.; Yap, J. L.; Chen, L.; Lanning, M. E.; Roth, B. M.; Wilder, P. T.; Fletcher, S. Structural Re-Engineering of the α -Helix Mimetic JY-1-106 into Small-Molecules: Disruption of the Mcl-1–Bak-BH3 Protein–Protein Interaction with 2,6-Di-Substituted Nicotinates. *ChemMedChem* **2016**, *11* (8), 827–833.
- (21) Sattler, M.; Liang, H.; Nettlesheim, D.; Meadows, R. P.; Harlan, J. E.; Eberstadt, M.; Yoon, H. S.; Shuker, S. B.; Chang, B. S.; Minn, A. J.; Thompson, C. B.; Fesik, S. W. Structure of Bcl-XL-Bak Peptide Complex: Recognition Between Regulators of Apoptosis. *Science* **1997**, *275* (5302), 983–986.
- (22) Cosentino, K.; García-Sáez, A. J. Bax and Bak Pores: Are We Closing the Circle? *Trends Cell Biol.* **2017**, *27* (4), 266–275.

- (23) Renehan, A. G.; Booth, C.; Potten, C. S. What Is Apoptosis, and Why Is It Important? *BMJ* **2001**, *322* (7301), 1536–1538.
- (24) Campbell, K. J.; Tait, S. W. G. Targeting BCL-2 Regulated Apoptosis in Cancer. *Open Biol.* **2018**, *8* (5).
- (25) Westphal, D.; Kluck, R. M.; Dewson, G. Building Blocks of the Apoptotic Pore: How Bax and Bak Are Activated and Oligomerize during Apoptosis. *Cell Death Differ.* **2014**, *21* (2), 196–205.
- (26) Flores-Romero, H.; Landeta, O.; Ugarte-Uribe, B.; Cosentino, K.; García-Porras, M.; García-Sáez, A. J.; Basañez, G. BFL1 Modulates Apoptosis at the Membrane Level through a Bifunctional and Multimodal Mechanism Showing Key Differences with BCLXL. *Cell Death Differ.* **2019**, *26* (10), 1880–1894.
- (27) Czabotar, P. E.; Westphal, D.; Dewson, G.; Ma, S.; Hockings, C.; Fairlie, W. D.; Lee, E. F.; Yao, S.; Robin, A. Y.; Smith, B. J.; Huang, D. C. S.; Kluck, R. M.; Adams, J. M.; Colman, P. M. Bax Crystal Structures Reveal How BH3 Domains Activate Bax and Nucleate Its Oligomerization to Induce Apoptosis. *Cell* **2013**, *152* (3), 519–531.
- (28) Hanahan, D.; Weinberg, R. A. Hallmarks of Cancer: The next Generation. *Cell* **2011**, *144* (5), 646–674.
- (29) Um, H.-D. Bcl-2 Family Proteins as Regulators of Cancer Cell Invasion and Metastasis: A Review Focusing on Mitochondrial Respiration and Reactive Oxygen Species. *Oncotarget* **2015**, *7* (5), 5193–5203.
- (30) Lopez, J.; Tait, S. W. G. Mitochondrial Apoptosis: Killing Cancer Using the Enemy Within. *Br. J. Cancer* **2015**, *112* (6), 957–962.
- (31) Ortíz-Maldonado, V.; Mozas, P.; Delgado, J. The Biology behind B-Cell Lymphoma 2 as a Target in Chronic Lymphocytic Leukemia. *Ther. Adv. Hematol.* **2016**, *7* (6), 321–329.
- (32) Green, D. R. A BH3 Mimetic for Killing Cancer Cells. *Cell* **2016**, *165* (7), 1560.
- (33) Oltersdorf, T.; Elmore, S. W.; Shoemaker, A. R.; Armstrong, R. C.; Augeri, D. J.; Belli, B. A.; Bruncko, M.; Deckwerth, T. L.; Dinges, J.; Hajduk, P. J.; Joseph, M. K.; Kitada, S.; Korsmeyer, S. J.; Kunzer, A. R.; Letai, A.; Li, C.; Mitten, M. J.; Nettlesheim, D. G.; Ng, S.; Nimmer, P. M.; O'Connor, J. M.; Oleksijew, A.; Petros, A. M.; Reed, J. C.; Shen, W.; Tahir, S. K.; Thompson, C. B.; Tomaselli, K. J.; Wang, B.; Wendt, M. D.; Zhang, H.; Fesik, S. W.; Rosenberg, S. H. An Inhibitor of Bcl-2 Family Proteins Induces Regression of Solid Tumours. *Nature* **2005**, *435* (7042), 677–681.

- (34) Shuker, S. B.; Hajduk, P. J.; Meadows, R. P.; Fesik, S. W. Discovering High-Affinity Ligands for Proteins: SAR by NMR. *Science* **1996**, *274* (5292), 1531–1534.
- (35) Oral Bioavailability (F%)
https://www.pharmainformatic.com/html/oral_bioavailability__f__.html (accessed Mar 25, 2020).
- (36) Park, C.-M.; Bruncko, M.; Adickes, J.; Bauch, J.; Ding, H.; Kunzer, A.; Marsh, K. C.; Nimmer, P.; Shoemaker, A. R.; Song, X.; Tahir, S. K.; Tse, C.; Wang, X.; Wendt, M. D.; Yang, X.; Zhang, H.; Fesik, S. W.; Rosenberg, S. H.; Elmore, S. W. Discovery of an Orally Bioavailable Small Molecule Inhibitor of Prosurvival B-Cell Lymphoma 2 Proteins. *J. Med. Chem.* **2008**, *51* (21), 6902–6915.
- (37) Souers, A. J.; Levenson, J. D.; Boghaert, E. R.; Ackler, S. L.; Catron, N. D.; Chen, J.; Dayton, B. D.; Ding, H.; Enschede, S. H.; Fairbrother, W. J.; Huang, D. C. S.; Hymowitz, S. G.; Jin, S.; Khaw, S. L.; Kovar, P. J.; Lam, L. T.; Lee, J.; Maecker, H. L.; Marsh, K. C.; Mason, K. D.; Mitten, M. J.; Nimmer, P. M.; Oleksijew, A.; Park, C. H.; Park, C.-M.; Phillips, D. C.; Roberts, A. W.; Sampath, D.; Seymour, J. F.; Smith, M. L.; Sullivan, G. M.; Tahir, S. K.; Tse, C.; Wendt, M. D.; Xiao, Y.; Xue, J. C.; Zhang, H.; Humerickhouse, R. A.; Rosenberg, S. H.; Elmore, S. W. ABT-199, a Potent and Selective BCL-2 Inhibitor, Achieves Antitumor Activity While Sparing Platelets. *Nat. Med.* **2013**, *19* (2), 202–208.
- (38) Tse, C.; Shoemaker, A. R.; Adickes, J.; Anderson, M. G.; Chen, J.; Jin, S.; Johnson, E. F.; Marsh, K. C.; Mitten, M. J.; Nimmer, P.; Roberts, L.; Tahir, S. K.; Xiao, Y.; Yang, X.; Zhang, H.; Fesik, S.; Rosenberg, S. H.; Elmore, S. W. ABT-263: A Potent and Orally Bioavailable Bcl-2 Family Inhibitor. *Cancer Res.* **2008**, *68* (9), 3421–3428.
- (39) Cang, S.; Iragavarapu, C.; Savooji, J.; Song, Y.; Liu, D. ABT-199 (Venetoclax) and BCL-2 Inhibitors in Clinical Development. *J. Hematol. Oncol. J Hematol Oncol* **2015**, *8*.
- (40) Clinical Study Report Synopsis S55746, **2019**. <https://clinicaltrials.servier.com/wp-content/uploads/CL1-55746-001-anonymisedsynopsis-2019.09.16-1.pdf>
- (41) Juárez-Salcedo, L. M.; Desai, V.; Dalia, S. Venetoclax: Evidence to Date and Clinical Potential. *Drugs Context* **2019**, *8*.
- (42) Pivotal Phase II Study Showed Nearly 80 Percent of People with Hard-to-treat Type of Chronic Lymphocytic Leukemia Responded to Investigational Medicine Venetoclax https://www.drugs.com/nda/venetoclax_151206.html (accessed Mar 26, 2020).
- (43) AbbVie Announces US FDA Approval of Venclexta (venetoclax) as a Chemotherapy-Free Combination Regimen for Previously Untreated Chronic

Lymphocytic Leukemia Patients <https://www.drugs.com/newdrugs/abbvie-announces-us-fda-approval-venclerxa-venetoclax-chemotherapy-free-combination-regimen-4974.html>

- (44) Ran, X.; Gestwicki, J. E. Inhibitors of Protein-Protein Interactions (PPIs): An Analysis of Scaffold Choices and Buried Surface Area. *Curr. Opin. Chem. Biol.* **2018**, *44*, 75–86.
- (45) Lipinski, C. A. Rule of Five in 2015 and beyond: Target and Ligand Structural Limitations, Ligand Chemistry Structure and Drug Discovery Project Decisions. *Adv. Drug Deliv. Rev.* **2016**, *101*, 34–41.
- (46) Lessene, G.; Czabotar, P. E.; Colman, P. M. BCL-2 Family Antagonists for Cancer Therapy. *Nat. Rev. Drug Discov.* **2008**, *7* (12), 989–1000.
- (47) Diguarher, T. L.; Casara, P.; STARCK, J.-B.; Henlin, J.-M.; Davidson, J. E. P.; Murray, J. B.; Graham, C. J.; Chen, I.-J.; Geneste, O.; Hickman, J.; Depil, S.; Tiran, A. L.; Nyerges, M.; Nanteuil, G. D. New Indolizine Derivatives, Method for Preparing Same and Pharmaceutical Compositions Containing Same. WO2013110890A1, August 1, 2013.
- (48) Casara, P.; Davidson, J.; Claperon, A.; Le Toumelin-Braizat, G.; Vogler, M.; Bruno, A.; Chanrion, M.; Lysiak-Auvity, G.; Le Diguarher, T.; Starck, J.-B.; Chen, I.; Whitehead, N.; Graham, C.; Matassova, N.; Dokurno, P.; Pedder, C.; Wang, Y.; Qiu, S.; Girard, A.-M.; Schneider, E.; Gravé, F.; Studeny, A.; Guasconi, G.; Rocchetti, F.; Maïga, S.; Henlin, J.-M.; Colland, F.; Kraus-Berthier, L.; Le Gouill, S.; Dyer, M. J. S.; Hubbard, R.; Wood, M.; Amiot, M.; Cohen, G. M.; Hickman, J. A.; Morris, E.; Murray, J.; Geneste, O. S55746 Is a Novel Orally Active BCL-2 Selective and Potent Inhibitor That Impairs Hematological Tumor Growth. *Oncotarget* **2018**, *9* (28), 20075–20088.
- (49) Ferenczy, G. G.; Keserű, G. M. Enthalpic Efficiency of Ligand Binding. *J. Chem. Inf. Model.* **2010**, *50* (9), 1536–1541.
- (50) Yang, Y.; Zhao, S.; Song, J. Caspase-Dependent Apoptosis and -Independent Poly(ADP-Ribose) Polymerase Cleavage Induced by Transforming Growth Factor B1. *Int. J. Biochem. Cell Biol.* **2004**, *36* (2), 223–234.
- (51) Birkinshaw, R. W.; Gong, J.; Luo, C. S.; Lio, D.; White, C. A.; Anderson, M. A.; Blombery, P.; Lessene, G.; Majewski, I. J.; Thijssen, R.; Roberts, A. W.; Huang, D. C. S.; Colman, P. M.; Czabotar, P. E. Structures of BCL-2 in Complex with Venetoclax Reveal the Molecular Basis of Resistance Mutations. *Nat. Commun.* **2019**, *10* (1), 1–10.

- (52) Daly, A. K. Chapter 24 - Pharmacogenomics of Warfarin. In *Handbook of Pharmacogenomics and Stratified Medicine*; Padmanabhan, S., Ed.; Academic Press: San Diego, 2014; pp 497–507.
- (53) GUO, Y.; Xue, H.; Wang, Z.; SUN, H. Bcl-2 INHIBITORS. WO2019210828A1, November 7, 2019.
- (54) Study of Bcl-2 Inhibitor BGB-11417 in Participants With Mature B-Cell Malignancies - Full Text View - ClinicalTrials.gov
<https://clinicaltrials.gov/ct2/show/NCT04277637>
- (55) Yang, D.; Zhai, Y.; Wang, G. Combination Product of Bcl-2 Inhibitor and Chemotherapeutic Agent and Use Thereof in the Prevention and/or Treatment of Diseases. WO2020024834A1, February 6, 2020.
- (56) Yang, D.; Zhai, Y.; TANG, Q.; Fang, D. D. Combination Product of Bcl-2 Inhibitor and Mdm2 Inhibitor and Use Thereof in the Prevention and/or Treatment of Diseases. WO2020024820A1, February 6, 2020.
- (57) Yang, D.; Zhai, Y.; Wang, G. Synergistic Antitumor Effect of Bcl-2 Inhibitor Combined with Rituximab and/or Bendamustine or Bcl-2 Inhibitor Combined with Chop. WO2020024826A1, February 6, 2020.
- (58) Ascentage Pharma Announces First Patient Dosed in the Global Phase Ib/II Clinical Study of Bcl-2 Inhibitor APG-2575 in the United States
<https://www.biospace.com/article/ascentage-pharma-announces-first-patient-dosed-in-the-global-phase-ib-ii-clinical-study-of-bcl-2-inhibitor-apg-2575-in-the-united-states/> (accessed Mar 27, 2020).
- (59) Pharma, A. Ascentage Pharma Announces Clearances for Three Phase Ib/II Clinical Studies of APG-2575 in China and the U.S., Beginning Simultaneous Clinical Development in Three Hematologic Malignancy Indications
<https://www.prnewswire.com/news-releases/ascentage-pharma-announces-clearances-for-three-phase-ib-ii-clinical-studies-of-apg-2575-in-china-and-the-us-beginning-simultaneous-clinical-development-in-three-hematologic-malignancy-indications-301019683.html>
- (60) Yang, D.; Zhai, Y.; Wang, G.; Fang, D. D.; DENG, J.; QIU, M.; Zhang, L. Combination of Bcl-2/Bcl-xL Inhibitors and Chemotherapeutic Agent and Use Thereof. WO2020024976A1, February 6, 2020.
- (61) Bai, L.; Chen, J.; Liu, L.; McEachern, D.; Aguilar, A.; Zhou, H.; Yang, C. Y.; Wang, H.; Wen, J.; Wang, G.; Zhai, Y.; Guo, M.; Yang, D.; Wang, S. 338 BM-1252 (APG-1252): A Potent Dual Specific Bcl-2/Bcl-XL Inhibitor That Achieves Complete Tumor Regression with Minimal Platelet Toxicity. *Eur. J. Cancer* **2014**, *50*, 109–110.

- (62) Wang, J.; Yang, D.; Luo, Q.; Qiu, M.; Zhang, L.; Li, B.; Chen, H.; Yi, H.; Yan, X.; Li, S.; Sun, J. APG-1252-12A Induces Mitochondria-Dependent Apoptosis through Inhibiting the Antiapoptotic Proteins Bcl-2/Bcl-xL in HL-60 Cells. *Int. J. Oncol.* **2017**, *51* (2), 563–572.
- (63) Lakhani, N. J.; Rasco, D. W.; Tolcher, A. W.; Huang, Y.; Ji, J.; Wang, H.; Dong, Q.; Men, L.; O'Rourke, T. J.; Chandana, S. R.; Amaya, A.; Cole, Y.; Kaiser, B.; Mays, T. A.; Patnaik, A.; Papadopoulos, K. P.; Yang, D.; Zhai, Y. A Phase I Study of Novel Dual Bcl-2/Bcl-XL Inhibitor APG-1252 in Patients with Advanced Small Cell Lung Cancer (SCLC) or Other Solid Tumor. *J. Clin. Oncol.* **2018**, *36*, 2594–2594.
- (64) Study of Combination APG-1252 Plus Paclitaxel in Patients With Relapsed/Refractory Small Cell Lung Cancer - Full Text View - ClinicalTrials.gov <https://clinicaltrials.gov/ct2/show/NCT04210037>
- (65) A Study of APG-1252 in Patients With SCLC or Other Solid Tumors - Full Text View - ClinicalTrials.gov <https://clinicaltrials.gov/ct2/show/NCT03080311>
- (66) APG-1252 in Patients With SCLC or Advanced Solid Tumors - Full Text View - ClinicalTrials.gov <https://clinicaltrials.gov/ct2/show/NCT03387332>
- (67) A Study of APG-1252 Plus Osimertinib(AZD9291) in EGFR TKI Resistant NSCLC Patients - Full Text View - ClinicalTrials.gov <https://clinicaltrials.gov/ct2/show/NCT04001777>
- (68) Tao, Z.-F.; Hasvold, L.; Wang, L.; Wang, X.; Petros, A. M.; Park, C. H.; Boghaert, E. R.; Catron, N. D.; Chen, J.; Colman, P. M.; Czabotar, P. E.; Deshayes, K.; Fairbrother, W. J.; Flygare, J. A.; Hymowitz, S. G.; Jin, S.; Judge, R. A.; Koehler, M. F. T.; Kovar, P. J.; Lessene, G.; Mitten, M. J.; Ndubaku, C. O.; Nimmer, P.; Purkey, H. E.; Oleksijew, A.; Phillips, D. C.; Sleeb, B. E.; Smith, B. J.; Smith, M. L.; Tahir, S. K.; Watson, K. G.; Xiao, Y.; Xue, J.; Zhang, H.; Zobel, K.; Rosenberg, S. H.; Tse, C.; Levenson, J. D.; Elmore, S. W.; Souers, A. J. Discovery of a Potent and Selective BCL-XL Inhibitor with in Vivo Activity. *ACS Med. Chem. Lett.* **2014**, *5* (10), 1088–1093.
- (69) Wang, L.; Doherty, G. A.; Judd, A. S.; Tao, Z.-F.; Hansen, T. M.; Frey, R. R.; Song, X.; Bruncko, M.; Kunzer, A. R.; Wang, X.; Wendt, M. D.; Flygare, J. A.; Catron, N. D.; Judge, R. A.; Park, C. H.; Shekhar, S.; Phillips, D. C.; Nimmer, P.; Smith, M. L.; Tahir, S. K.; Xiao, Y.; Xue, J.; Zhang, H.; Le, P. N.; Mitten, M. J.; Boghaert, E. R.; Gao, W.; Kovar, P.; Choo, E. F.; Diaz, D.; Fairbrother, W. J.; Elmore, S. W.; Sampath, D.; Levenson, J. D.; Souers, A. J. Discovery of A-1331852, a First-in-Class, Potent, and Orally-Bioavailable BCL-X_L Inhibitor. *ACS Med. Chem. Lett.* **2020**.

- (70) Levenson, J. D.; Phillips, D. C.; Mitten, M. J.; Boghaert, E. R.; Diaz, D.; Tahir, S. K.; Belmont, L. D.; Nimmer, P.; Xiao, Y.; Ma, X. M.; Lowes, K. N.; Kovar, P.; Chen, J.; Jin, S.; Smith, M.; Xue, J.; Zhang, H.; Oleksijew, A.; Magoc, T. J.; Vaidya, K. S.; Albert, D. H.; Tarrant, J. M.; La, N.; Wang, L.; Tao, Z.-F.; Wendt, M. D.; Sampath, D.; Rosenberg, S. H.; Tse, C.; Huang, D. C. S.; Fairbrother, W. J.; Elmore, S. W.; Souers, A. J. Exploiting Selective BCL-2 Family Inhibitors to Dissect Cell Survival Dependencies and Define Improved Strategies for Cancer Therapy. *Sci. Transl. Med.* **2015**, *7* (279), 279ra40-279ra40.
- (71) Besbes, S.; Pocard, M.; Mirshahi, M.; Billard, C. The First MCL-1-Selective BH3 Mimetics Have Therapeutic Potential for Chronic Lymphocytic Leukemia. *Crit. Rev. Oncol. Hematol.* **2016**, *100* (Supplement C), 32–36.
- (72) Fire, E.; Gullá, S. V.; Grant, R. A.; Keating, A. E. Mcl-1–Bim Complexes Accommodate Surprising Point Mutations via Minor Structural Changes. *Protein Sci. Publ. Protein Soc.* **2010**, *19* (3), 507–519.
- (73) Akgul, C. Mcl-1 Is a Potential Therapeutic Target in Multiple Types of Cancer. *Cell. Mol. Life Sci.* **2009**, *66* (8), 1326–1336.
- (74) Kotschy, A.; Szlavik, Z.; Murray, J.; Davidson, J.; Maragno, A. L.; Le Toumelin-Braizat, G.; Chanrion, M.; Kelly, G. L.; Gong, J.-N.; Moujalled, D. M.; Bruno, A.; Csekei, M.; Paczal, A.; Szabo, Z. B.; Sipos, S.; Radics, G.; Prosenyak, A.; Balint, B.; Ondi, L.; Blasko, G.; Robertson, A.; Surgenor, A.; Dokurno, P.; Chen, I.; Matassova, N.; Smith, J.; Pedder, C.; Graham, C.; Studeny, A.; Lysiak-Auvity, G.; Girard, A.-M.; Gravé, F.; Segal, D.; Riffkin, C. D.; Pomilio, G.; Galbraith, L. C. A.; Aubrey, B. J.; Brennan, M. S.; Herold, M. J.; Chang, C.; Guasconi, G.; Cauquil, N.; Melchiorre, F.; Guigal-Stephan, N.; Lockhart, B.; Colland, F.; Hickman, J. A.; Roberts, A. W.; Huang, D. C. S.; Wei, A. H.; Strasser, A.; Lessene, G.; Geneste, O. The MCL1 Inhibitor S63845 Is Tolerable and Effective in Diverse Cancer Models. *Nature* **2016**, *538* (7626), 477–482.
- (75) Xiang, W.; Yang, C.-Y.; Bai, L. MCL-1 Inhibition in Cancer Treatment. *OncoTargets Ther.* **2018**, *11*, 7301–7314.
- (76) Levenson, J. D.; Zhang, H.; Chen, J.; Tahir, S. K.; Phillips, D. C.; Xue, J.; Nimmer, P.; Jin, S.; Smith, M.; Xiao, Y.; Kovar, P.; Tanaka, A.; Bruncko, M.; Sheppard, G. S.; Wang, L.; Gierke, S.; Kategaya, L.; Anderson, D. J.; Wong, C.; Eastham-Anderson, J.; Ludlam, M. J. C.; Sampath, D.; Fairbrother, W. J.; Wertz, I.; Rosenberg, S. H.; Tse, C.; Elmore, S. W.; Souers, A. J. Potent and Selective Small-Molecule MCL-1 Inhibitors Demonstrate on-Target Cancer Cell Killing Activity as Single Agents and in Combination with ABT-263 (Navitoclax). *Cell Death Dis.* **2015**, *6* (1), e1590.
- (77) Derenne, S.; Monia, B.; Dean, N. M.; Taylor, J. K.; Rapp, M.-J.; Harousseau, J.-L.; Bataille, R.; Amiot, M. Antisense Strategy Shows That Mcl-1 Rather than Bcl-2 or

Bcl-x(L) Is an Essential Survival Protein of Human Myeloma Cells. *Blood* **2002**, *100* (1), 194–199.

- (78) Chen, L.; Fletcher, S. Mcl-1 Inhibitors: A Patent Review. *Expert Opin. Ther. Pat.* **2017**, *27* (2), 163–178.
- (79) Ramsey, H. E.; Fischer, M. A.; Lee, T.; Gorska, A. E.; Arrate, M. P.; Fuller, L.; Boyd, K. L.; Strickland, S. A.; Sensintaffar, J.; Hogdal, L. J.; Ayers, G. D.; Olejniczak, E. T.; Fesik, S. W.; Savona, M. R. A Novel MCL1 Inhibitor Combined with Venetoclax Rescues Venetoclax-Resistant Acute Myelogenous Leukemia. *Cancer Discov.* **2018**, *8* (12), 1566–1581.
- (80) Beekman, A. M.; Howell, L. A. Small-Molecule and Peptide Inhibitors of the Pro-Survival Protein Mcl-1. *Chemmedchem* **2016**, *11* (8), 802–813.
- (81) Tron, A. E.; Belmonte, M. A.; Adam, A.; Aquila, B. M.; Boise, L. H.; Chiarparin, E.; Cidado, J.; Embrey, K. J.; Gangl, E.; Gibbons, F. D.; Gregory, G. P.; Hargreaves, D.; Hendricks, J. A.; Johannes, J. W.; Johnstone, R. W.; Kazmirski, S. L.; Kettle, J. G.; Lamb, M. L.; Matulis, S. M.; Nooka, A. K.; Packer, M. J.; Peng, B.; Rawlins, P. B.; Robbins, D. W.; Schuller, A. G.; Su, N.; Yang, W.; Ye, Q.; Zheng, X.; Secrist, J. P.; Clark, E. A.; Wilson, D. M.; Fawell, S. E.; Hird, A. W. Discovery of Mcl-1-Specific Inhibitor AZD5991 and Preclinical Activity in Multiple Myeloma and Acute Myeloid Leukemia. *Nat. Commun.* **2018**, *9*.
- (82) Caenepeel, S.; Brown, S. P.; Belmontes, B.; Moody, G.; Keegan, K. S.; Chui, D.; Whittington, D. A.; Huang, X.; Poppe, L.; Cheng, A. C.; Cardozo, M.; Houze, J.; Li, Y.; Lucas, B.; Paras, N. A.; Wang, X.; Taygerly, J. P.; Vimolratana, M.; Zancanella, M.; Zhu, L.; Cajulis, E.; Osgood, T.; Sun, J.; Damon, L.; Egan, R. K.; Greninger, P.; McClanaghan, J. D.; Gong, J.; Moujalled, D.; Pomilio, G.; Beltran, P.; Benes, C. H.; Roberts, A. W.; Huang, D. C.; Wei, A.; Canon, J.; Coxon, A.; Hughes, P. E. AMG 176, a Selective MCL1 Inhibitor, Is Effective in Hematologic Cancer Models Alone and in Combination with Established Therapies. *Cancer Discov.* **2018**, *8* (12), 1582–1597.
- (83) KYPROLIS® (carfilzomib) for Relapsed Multiple Myeloma Treatment
<https://www.kyprolis.com/>
- (84) Spencer, A.; Rosenberg, A. S.; Jakubowiak, A.; Raje, N.; Chatterjee, M.; Trudel, S.; Bahlis, N. J.; Siegel, D. S.; Wilop, S.; Harrison, S. J.; NagaKrishna, M.; Dhuria, S.; Hindoyan, A.; McIver, Z.; Henary, H.; Morrow, P. K.; Roberts, A. A Phase 1, First-in-Human Study of AMG 176, a Selective MCL-1 Inhibitor, in Patients With Relapsed or Refractory Multiple Myeloma. *Clin. Lymphoma Myeloma Leuk.* **2019**, *19* (10), e53–e54.

- (85) Safety, Tolerability, Pharmacokinetics and Efficacy of AMG 397 in Subjects With Multiple Myeloma, NHL, and AML - Full Text View - ClinicalTrials.gov <https://clinicaltrials.gov/ct2/show/NCT03465540>
- (86) Amgen shares hit after analysts expose buried FDA trial halt <https://www.fiercebitech.com/biotech/amgen-shares-hit-after-analysts-expose-buried-fda-trial-halt>
- (87) Agrawal, P. NMR Spectroscopy in Drug Discovery and Development. *Mater. Methods* **2019**.
- (88) Szlávik, Z.; Ondi, L.; Csékei, M.; Paczal, A.; Szabó, Z. B.; Radics, G.; Murray, J.; Davidson, J.; Chen, I.; Davis, B.; Hubbard, R. E.; Pedder, C.; Dokurno, P.; Surgenor, A.; Smith, J.; Robertson, A.; LeToumelin-Braizat, G.; Cauquil, N.; Zarka, M.; Demarles, D.; Perron-Sierra, F.; Claperon, A.; Colland, F.; Geneste, O.; Kotschy, A. Structure-Guided Discovery of a Selective Mcl-1 Inhibitor with Cellular Activity. *J. Med. Chem.* **2019**, *62* (15), 6913–6924.
- (89) Li, Z.; He, S.; Look, A. T. The MCL1-Specific Inhibitor S63845 Acts Synergistically with Venetoclax/ABT-199 to Induce Apoptosis in T-Cell Acute Lymphoblastic Leukemia Cells. *Leukemia* **2019**, *33* (1), 262–266.
- (90) Prukova, D.; Andera, L.; Nahacka, Z.; Karolova, J.; Svaton, M.; Klanova, M.; Havranek, O.; Soukup, J.; Svobodova, K.; Zemanova, Z.; Tuskova, D.; Pokorna, E.; Helman, K.; Forsterova, K.; Pacheco-Blanco, M.; Vockova, P.; Berkova, A.; Fronkova, E.; Trneny, M.; Klener, P. Co-Targeting of BCL2 with Venetoclax and MCL1 with S63845 Is Synthetically Lethal in Vivo in Relapsed Mantle Cell Lymphoma. *Clin. Cancer Res.* **2019**.
- (91) Wei, A. H.; Roberts, A. W.; Spencer, A.; Rosenberg, A. S.; Siegel, D.; Walter, R. B.; Caenepeel, S.; Hughes, P.; McIver, Z.; Mezzi, K.; Morrow, P. K.; Stein, A. Targeting MCL-1 in Hematologic Malignancies: Rationale and Progress. *Blood Rev.* **2020**, 100672.
- (92) Hird, A. W.; Tron, A. E. Recent Advances in the Development of Mcl-1 Inhibitors for Cancer Therapy. *Pharmacol. Ther.* **2019**, *198*, 59–67.
- (93) Study of AZD5991 in Relapsed or Refractory Haematologic Malignancies. - Full Text View - ClinicalTrials.gov <https://clinicaltrials.gov/ct2/show/NCT03218683> (accessed Apr 2, 2020).
- (94) A Study of the Safety and Tolerability of ABBV-467 in Adult Participants With Relapsed/Refractory Multiple Myeloma - Full Text View - ClinicalTrials.gov <https://clinicaltrials.gov/ct2/show/NCT04178902>

- (95) Brady, P. B.; Braje, W.; Dai, Y.; Doherty, G. A.; Gong, J.; Jantos, K.; Ji, C.; Judd, A. S.; Kunzer, A. R.; Lai, C.; Mastracchio, A.; Risi, R. M.; Song, X.; Souers, A. J.; Sullivan, G. M.; Tao, Z.-F.; Teske, J. A.; Wang, X.; Wendt, M. D.; Yu, Y.; Zhu, G.; Penning, T. D. Macrocyclic MCL-1 Inhibitors and Methods of Use. US20200010480A1, January 9, 2020.
- (96) Elmore, S. W.; Souers, A. J.; Bruncko, M.; Song, X.; Wang, X.; Hasvold, L. A.; Wang, L.; Kunzer, A. R.; Park, C.-M.; Wendt, M. D.; Tao, Z.-F.; Madar, D. 7-Substituted Indole as Mcl-1 Inhibitors. EP3243814B1, October 17, 2018.
- (97) Bruncko, M.; Wang, L.; Sheppard, G. S.; Phillips, D. C.; Tahir, S. K.; Xue, J.; Erickson, S.; Fidanze, S.; Fry, E.; Hasvold, L.; Jenkins, G. J.; Jin, S.; Judge, R. A.; Kovar, P. J.; Madar, D.; Nimmer, P.; Park, C.; Petros, A. M.; Rosenberg, S. H.; Smith, M. L.; Song, X.; Sun, C.; Tao, Z.-F.; Wang, X.; Xiao, Y.; Zhang, H.; Tse, C.; Levenson, J. D.; Elmore, S. W.; Souers, A. J. Structure-Guided Design of a Series of MCL-1 Inhibitors with High Affinity and Selectivity. *J. Med. Chem.* **2015**, *58* (5), 2180–2194.
- (98) Wang, Q.; Hao, S. A-1210477, a Selective MCL-1 Inhibitor, Overcomes ABT-737 Resistance in AML. *Oncol. Lett.* **2019**, *18* (5), 5481–5489.
- (99) Ottina, E.; Tischner, D.; Herold, M. J.; Villunger, A. A1/Bfl-1 in Leukocyte Development and Cell Death. *Exp. Cell Res.* **2012**, *318* (11), 1291–1303.
- (100) Flores-Romero, H.; Landeta, O.; Ugarte-Uribe, B.; Cosentino, K.; García-Porras, M.; García-Sáez, A. J.; Basañez, G. BFL1 Modulates Apoptosis at the Membrane Level through a Bifunctional and Multimodal Mechanism Showing Key Differences with BCLXL. *Cell Death Differ.* **2019**, *26* (10), 1880–1894.
- (101) Gangoda, L.; Teh, C. E.; Dengler, M. A.; Best, S. A.; Weeden, C. E.; Tai, L.; Lee, E. F.; Fairlie, W. D.; Sutherland, K. D.; Harrison, L. C.; Gray, D. H.; Strasser, A.; Herold, M. J. Characterization of a Novel Human BFL-1-Specific Monoclonal Antibody. *Cell Death Differ.* **2020**, *27* (2), 826–828.
- (102) Barile, E.; Marconi, G. D.; De, S. K.; Baggio, C.; Gambini, L.; Salem, A. F.; Kashyap, M. K.; Castro, J. E.; Kipps, T. J.; Pellicchia, M. HBfl-1/HNOXA Interaction Studies Provide New Insights on the Role of Bfl-1 in Cancer Cell Resistance and for the Design of Novel Anticancer Agents. *ACS Chem. Biol.* **2017**, *12* (2), 444–455.
- (103) Vogler, M. BCL2A1: The Underdog in the BCL2 Family. *Cell Death Differ.* **2012**, *19* (1), 67–74.
- (104) Choi, S. S.; Park, I. C.; Yun, J. W.; Sung, Y. C.; Hong, S. I.; Shin, H. S. A Novel Bcl-2 Related Gene, Bfl-1, Is Overexpressed in Stomach Cancer and Preferentially Expressed in Bone Marrow. *Oncogene* **1995**, *11* (9), 1693–1698.

- (105) Zong, W.-X.; Edelman, L. C.; Chen, C.; Bash, J.; Gélinas, C. The Prosurvival Bcl-2 Homolog Bfl-1/A1 Is a Direct Transcriptional Target of NF- κ B That Blocks TNF α -Induced Apoptosis. *Genes Dev.* **1999**, *13* (4), 382–387.
- (106) Fan, G.; Simmons, M. J.; Ge, S.; Dutta-Simmons, J.; Kucharczak, J.; Ron, Y.; Weissmann, D.; Chen, C.-C.; Mukherjee, C.; White, E.; Gélinas, C. Defective Ubiquitin-Mediated Degradation of Antiapoptotic Bfl-1 Predisposes to Lymphoma. *Blood* **2010**, *115* (17), 3559–3569.
- (107) Vier, J.; Groth, M.; Sochalska, M.; Kirschnek, S. The Anti-Apoptotic Bcl-2 Family Protein A1/Bfl-1 Regulates Neutrophil Survival and Homeostasis and Is Controlled via PI3K and JAK/STAT Signaling. *Cell Death Dis.* **2016**, *7*, e2103.
- (108) Herman, M. D.; Nyman, T.; Welin, M.; Lehtiö, L.; Flodin, S.; Trésaugues, L.; Kotenyova, T.; Flores, A.; Nordlund, P. Completing the Family Portrait of the Anti-Apoptotic Bcl-2 Proteins: Crystal Structure of Human Bfl-1 in Complex with Bim. *FEBS Lett.* **2008**, *582* (25–26), 3590–3594.
- (109) Olsson, A.; Norberg, M.; ökvist, A.; Derkow, K.; Choudhury, A.; Tobin, G.; Celsing, F.; österborg, A.; Rosenquist, R.; Jondal, M.; Osorio, L. M. Upregulation of Bfl-1 Is a Potential Mechanism of Chemoresistance in B-Cell Chronic Lymphocytic Leukaemia. *Br. J. Cancer* **2007**, *97* (6), 769–777.
- (110) Huhn, A. J.; Guerra, R. M.; Harvey, E. P.; Bird, G. H.; Walensky, L. D. Selective Covalent Targeting of Anti-Apoptotic BFL-1 by Cysteine-Reactive Stapled Peptide Inhibitors. *Cell Chem. Biol.* **2016**, *23* (9), 1123–1134.
- (111) Mathieu, A.-L.; Sperandio, O.; Pottiez, V.; Balzarín, S.; Herlédan, A.; Elkäim, J. O.; Fogeron, M.-L.; Piveteau, C.; Dassonneville, S.; Deprez, B.; Villoutreix, B. O.; Bonnefoy, N.; Leroux, F. Identification of Small Inhibitory Molecules Targeting the Bfl-1 Anti-Apoptotic Protein That Alleviates Resistance to ABT-737. *J. Biomol. Screen.* **2014**, *19* (7), 1035–1046.
- (112) Esteve-Arenys, A.; Roue, G. BFL-1 Expression Determines the Efficacy of Venetoclax in MYC+/BCL2+ Double Hit Lymphoma. *Oncoscience* **2018**, *5* (3–4), 59–61.

Chapter 2. Rationally Designed Polypharmacology: α -Helix Mimetics as Dual Inhibitors of the Oncoproteins Mcl-1 and HDM2

2.1. Introduction

Protein-protein interactions (PPIs) are involved in crucial cellular pathways including proliferation, differentiation, and apoptosis^{1,2}. Dysregulations of PPIs cause a host of different diseases, including cancer, neurodegenerative disorders, autoimmunity complications and diabetes¹⁻⁵. Typically, PPI interfaces cover large surface areas and consist of flat hydrophobic regions with noncontiguous contact points, rendering drug design challenging⁶⁻⁹. However, many academic and industrial groups have successfully targeted these interactions with small molecules, several of which in various stages of clinical trials¹⁰⁻¹³. Tools such as alanine scanning mutagenesis have been instrumental in identifying key residues located in “hot spots” that account for a large degree of the energetic stability of the complexes. In α -helix-mediated PPIs, these “hot spots” often involve the i , $i+3/4$, and $i+7$ residues that are oriented on one side of the helix¹⁴⁻¹⁶.

The B-cell lymphoma-2 (Bcl-2) family and human double minute 2 (HDM2) engage in such α -helix-mediated PPIs and their aberrant regulations are directly associated with tumorigenesis^{17,18}. The Bcl-2 family of proteins are key regulators of cell life and death, and constitute the intrinsic pathway of apoptosis^{17,19}. The family comprises three subgroups: the antiapoptotic proteins myeloid cell leukemia-1 (Mcl-1), Bcl-2, Bcl-xL, Bcl-w and Bfl-1; multidomain pro-apoptotic proteins Bak and Bax; and BH3-only pro-apoptotic proteins including Bim, Bid, PUMA, and NOXA. When the cell receives apoptotic stimuli due to different stressors such as DNA damage or growth-factor deprivation, BH3-only proteins are upregulated and, through their α -helical BH3 “death”

domains (Figure 2.1A), bind the antiapoptotic proteins to release Bak and Bax, leading to homodimerization of these proteins^{17,19}. In turn, this leads to mitochondrial outer-

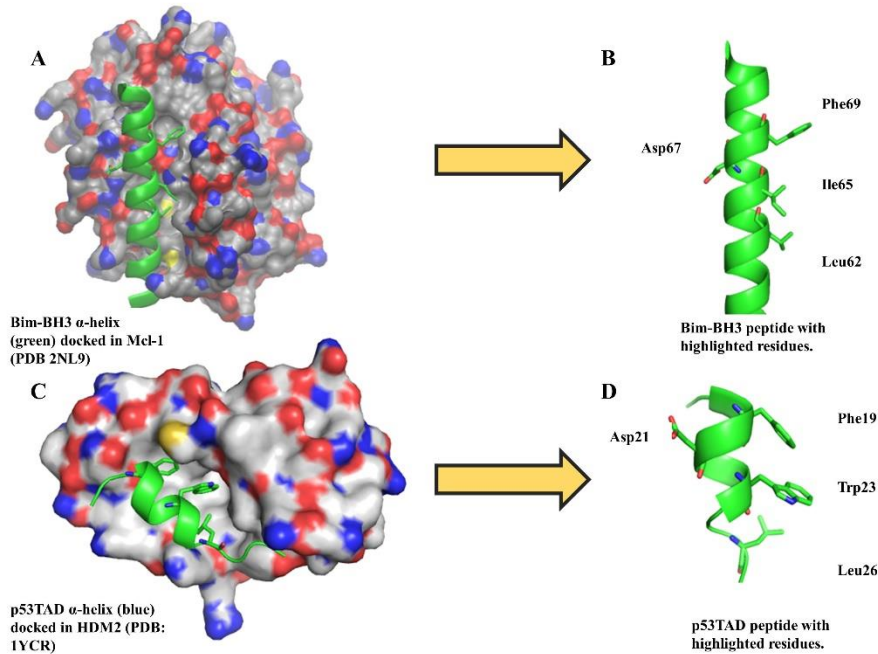


Figure 2. 1. A) Co-crystal structure of Bim-BH3 bound to Mcl-1 (PDB ID: 2NL9). B) Hot spot residues highlighted in Bim-BH3 peptide. C) Co-crystal structure of p53TAD bound to HDM2 (PDB ID: 1YCR). D) Hot spot residues highlighted in p53TAD.

membrane permeabilization (MOMP), ultimately allowing the release of apoptosis-inducing proteins such as cytochrome *c*^{17,19}. During the formation of malignancies dependent on Bcl-2 proteins, the anti-apoptotic proteins are overexpressed and the BH3-only proteins are unable to compensate, causing cell immortality¹⁷⁻²⁰.

HDM2 is an E3 ubiquitin protein ligase responsible for the degradation of the tumor-suppressor protein p53 through binding its α -helical transactivation domain (TAD; Figure 2.1C)^{21,22}. p53 is a short-lived protein whose concentration at any given time is controlled by the rate at which it is degraded²³. It is coined the “guardian of the genome” due to its involvement in a variety of cellular pathways, notably the transcription of genes during cell stress events involved in apoptosis, DNA repair, senescence, and metabolic

homeostasis. In turn it is negatively regulated by HDM2^{22,24}. During tumorigenesis, HDM2 can be overexpressed, thus inhibiting the activation of p53 and decreasing cell death²⁵. p53 regulates apoptosis with both the transcription-dependent and -independent pathways, crossing paths with Bcl-2 proteins²³. Within the transcription-dependent pathway, it transcribes genes necessary for cell senescence and apoptosis such as p21 and the BH3-only protein PUMA¹⁸. Importantly, this pathway involves the translocation of p53 from the nucleus to the mitochondria, allowing interactions with various members of the Bcl-2 family²⁶. p53 can bind anti-apoptotic proteins directly or disrupt pro- and anti-apoptotic interactions such as the Bak/ Mcl-1²⁷. Additionally, it can directly bind Bax, which can then translocate and homodimerize on the mitochondrial outer membrane, leading to MOMP^{17,23,27-29}. Together these interactions indirectly cause apoptosis within the cell^{20,23,24}.

Consequently, these proteins have been the target of intense medicinal chemistry efforts towards the discovery of new treatments for cancer^{22,30-35}. Although clinical trials are ongoing, to date there are no FDA-approved Mcl-1 or HDM2 inhibitors, with only one Bcl-2 selective inhibitor, venetoclax, that has reached the clinic³⁶. However, studies have shown that venetoclax-treated cancer cells develop chemoresistance by overexpressing other anti-apoptotic proteins, most notably Mcl1, re-affirming the unmet medical need of developing Mcl-1 inhibitors^{37,38}.

In a phase II study evaluating venetoclax in patients with relapsed/refractory acute myeloid leukemia (AML), a 19% response rate was observed. 34% of patients in this study escalated to 1200 mg of venetoclax due to lack of response at the initial 800 mg dose, which did not achieve additional response³⁹. Next, a phase Ib clinical trial was

employed to assess a combination therapy of venetoclax and idasanutlin, an HDM2 inhibitor, in relapsed/refractory acute myeloid leukemia (AML) due to the modest monotherapy response rate. This combination was explored due to the overexpression of Mcl-1 in venetoclax-resistant cells, compounded with the knowledge that the inhibition of HDM2 and subsequent activation of p53 can result in Mcl-1 degradation. They reported 35.9% of patients responded to treatment. Of 39 patients treated, 14 exhibited antileukemic response which include complete and partial remission⁴⁰. Currently, a phase I/II study is ongoing to determine the safety, tolerability, pharmacokinetics of the combination therapy in pediatric and young adult patients with relapsed/refractory acute leukemias or solid tumors (NCT04029688). Additionally, a recent study involving the Mcl-1 selective inhibitor S63845 and the HDM2 inhibitor HDM201 evaluated the cell viability of combination treatments in AML cells⁴¹. MOLM-13 and OCI-AML-3 cells were susceptible to S63845 monotherapy with 60–70% viability, while OCI-AML-2 cells were 95% viable. In contrast, OCI-AML-2 AND MOLM-13 cells were susceptible to HDM201 monotherapy with 80% viability, whereas OCI-AML-3 showed no reduction. All three cell lines showed synergistic effects, with the combination index (CI)= 0.2–0.5 when treated with both drugs, while OCI-AML-3 exhibited a strong synergy effect with CI= 0.2–0.3⁴¹. These studies represent the efficacy of combination therapies of an anti-apoptotic protein inhibitor with an HDM2 inhibitor.

An alternative strategy to these polypharmacy regimens is polypharmacology, in which one drug is fashioned to recognize multiple targets. Polypharmacology is an emerging field of research and could provide multiple benefits to the patient, including increased patient compliance, eliminated drug-drug interactions, and reduced side effects,

not only through a reduction in drug cocktail complexity but also broadened therapeutic windows through greater therapeutic efficacies with reduced doses^{42,43}. In light of these studies, coupled with the multifactorial nature of cancer that suggests multiple drugs, or a single drug presenting multiple pharmacophores, will be required for an effective pharmacotherapy, we herein describe a polypharmacology approach to address the unmet need of Mcl-1 and HDM2 inhibitors in the clinic using synthetic α -helix mimicry.

2.2. Results and Discussion

Both the Bim-BH3 and p53TAD α -helices project similar hydrophobic character at “hot spot” residues i , $i+3/4$, and $i+7$: Leu62, Ile65, and Phe69 in Bim (Figure 2.1), and Phe19, Trp23, and Leu26 in p53TAD (Figure 2.1)^{44–46}. Importantly, there is a conserved arginine residue on pro-life proteins (Arg263 in Mcl1) that forms a salt bridge with Asp67 on the Bim α -helix at the $i+5$ position⁴⁷. Additionally, there is an aspartate residue in an analogous location ($i+2$) in p53TAD (Asp21), that helps maintain the integrity of the helix rather than engage in recognition⁴⁸. We set out to capitalize on these similarities across both α -helices towards the discovery of dual inhibitors of Mcl-1 and HDM2.

Monocyclic scaffolds such as terphenyl, imidazoline, and pyrazole scaffolds have been used as scaffolds to effectively mimic either the BH3 or the p53 α -helices^{4,13,49}. Roche introduced small molecules based on cis-imidazolines as inhibitors of HDM2, leading to the discovery of the nanomolar inhibitor Nutlin-3a⁵⁰. As evidenced by a co-crystal structure of Nutlin-3a and HDM2, the isopropoxyphenyl group mimics Phe19, while the two 4-chlorophenyl groups projected in a cis1,2-fuctionalization from the imidazoline scaffold mimic Trp23 and Leu26 (PDB ID: 4 J3E; Figure 2.2)²².

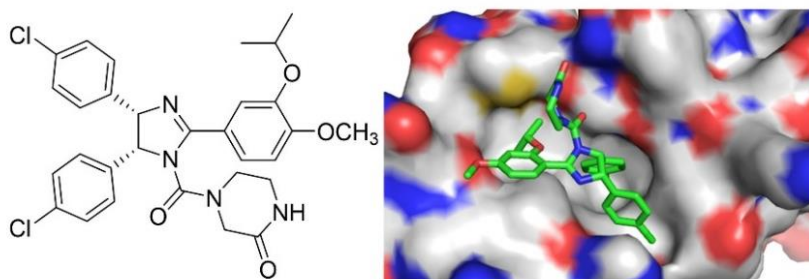


Figure 2. 2. Nutlin 3a co-crystallized with HDM2 (PDB ID: 4 J3E).

Given Nutlin 3a's effective mimicry of the p53TAD helix, which resembles the Bim-BH3 helix, perhaps it is unsurprising that it also exhibits low micromolar inhibition of Bcl-2²². In patent CA2771936 A1, Novartis describes sub-nanomolar inhibitors of HDM2 based on tetra-substituted heteroaryl scaffolds including imidazoles, pyrazoles, and pyrroles. The most potent compounds project aryl functional groups in a 1,2,3-substitution pattern, indicating a clustered projection appears optimal⁵¹. PDB ID 4OQ3 illustrates the co-crystal structure of one of these imidazole-based inhibitors with HDM2 (Figure 2.3).

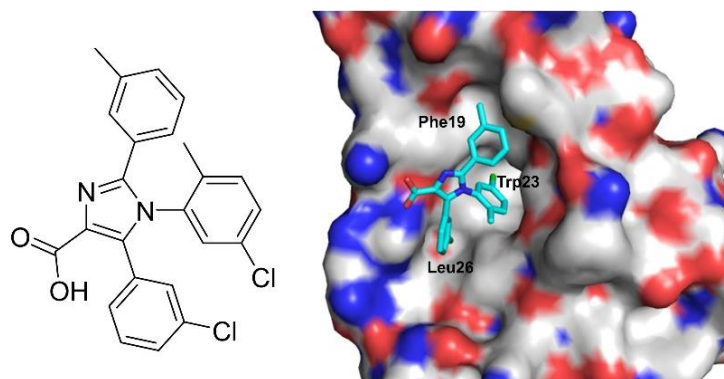


Figure 2. 3. Co-crystal structure of Novartis compound and HDM2 (PDB ID: 4OQ3). Residue labels indicate the binding locations of the key residues in the p53TAD helix.

The three functional groups engage in multiple contacts with the protein with each functional group projected into the respective pockets: 3-chlorophenyl in a π - π interaction with His96 while mimicking Leu26, 2-methyl, 5-chlorophenyl sitting in the Trp23 pocket, and the 3-methylphenyl functional group mimicking Phe19⁴⁶. More recently, Zhang *et al.* developed a dual Bcl-2/ HDM2 inhibitor based on a pyrazole scaffold (Figure 2.4, center structure)⁴⁵. As shown in Figure 2.3, their work is very closely related to the corresponding pyrazoles from Novartis (Figure 2.4, left structure) with a noticeable departure being the incorporation of an amide group between the pyrazole core and one of the aryl side chains. The authors reasoned this flexible amide bond was incorporated to promote mimicry of the less structured p53TAD α -helix, while retaining effective mimicry of the BH3 α -helix. The most potent Bcl-2, Mcl-1, and HDM2 achieved affinities of $K_i = 0.140, 0.161, \text{ and } 0.107 \mu\text{M}$, respectively⁴⁵.

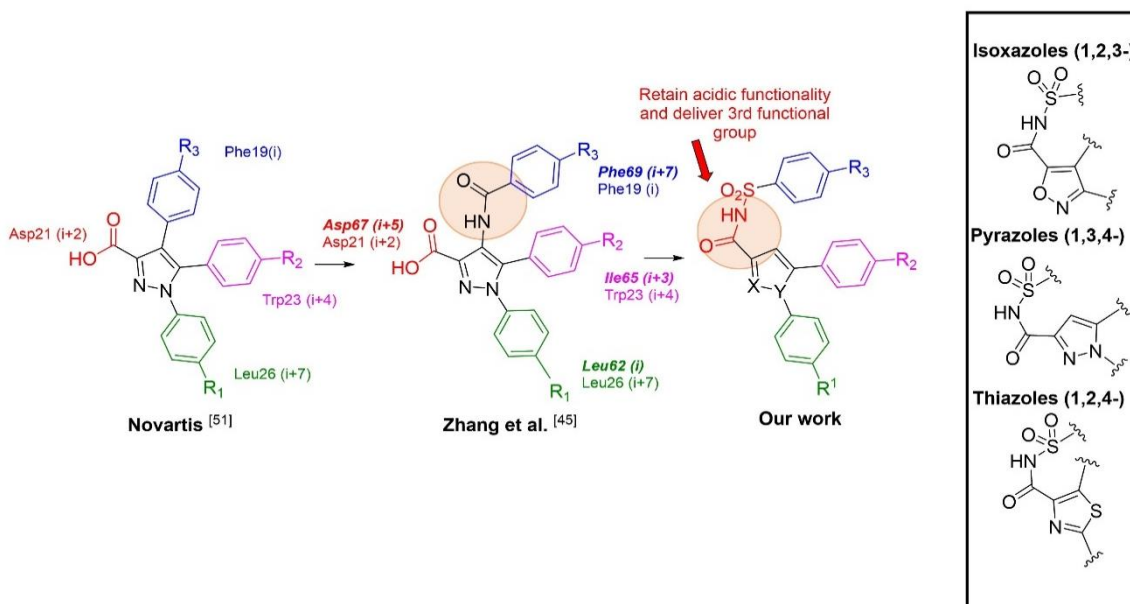


Figure 2. 4. Representative structures of Novartis patent CA2771936 A1⁵¹ (left), Zhang *et al.*⁴⁵ dual Bcl-2/HDM2 inhibitor (center), and our work presented in this manuscript (right). Normal font represents p53TAD residues; bold, italic font represents Bim-BH3 residues.

Leveraging the successes from Novartis and Zhang with heavily functionalized pyrazoles to inhibit the Bcl-2 family of proteins and HDM2, coupled with the effective deployment of the acyl sulfonamide functional group as a carboxylic acid bioisostere in Mcl-1 inhibitors elsewhere, we designed a library of three novel, densely functionalized scaffolds to mimic the BH3 binding domain and p53TAD: isoxazoles, pyrazoles, and thiazoles (Figure 2.4, right structure), which are all present in pharmacologically active drug molecules⁵²⁻⁵⁵. Each scaffold will allow us to explore the protein binding interfaces with different substitution patterns: isoxazoles represent a 1,2,3-functionalization (with the numbering starting with the acyl substituent), pyrazoles represent a 1,3,4-functionalization, and thiazoles a 1,2,4-functionalization. In addition to sustaining the acidic functionality needed to make contacts with Arg263 of Mcl-1, incorporation of the acyl sulfonamide functional group – akin to the amide in Zhang’s work – is hypothesized to ensure delivery of the third aryl group to both Mcl-1 and MDM2 by providing additional flexibility that permits effective mimicry of the more rigid BH3 α -helix and equally the less-structured p53 α -helix. Figure 2.5 shows the overlay of an energy-

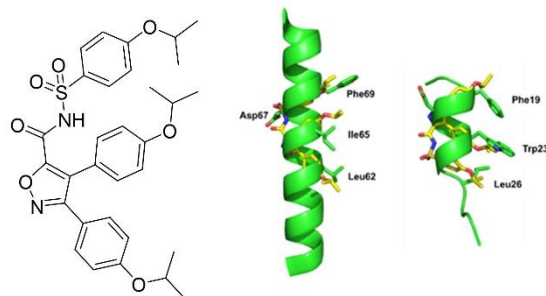


Figure 2. 5. Energy minimization of *OX0* in ChemDraw3D and overlaid with *Bim-BH3* (center) and *p53TAD* (right) α -helices.

minimized conformation of acyl sulfonamide isoxazole **OX0** in which all R groups were fixed as isopropyl groups.

Good mimicry of the key side chains (highlighted) of both helical peptides is suggested, which is expected to translate into potent inhibition of Mcl-1 and HDM2. Since the acyl sulfonamide portion is intended to emulate the carboxylic acid on one face of the helix as well as a hydrophobic group on the opposing face, while the R¹ and R² are intended to emulate adjacent hydrophobic groups on the same face of the helix, we hypothesize that the isoxazoles and pyrazoles will be more potent inhibitors than the corresponding thiazoles which carry an inferior substitution pattern.

2.3. Computer aided drug design

We employed computer-aided drug design (CADD) using SILCS, site identification by ligand competitive saturation, to assist in compound library design efforts⁵⁶⁻⁵⁸. Unlike other CADD methods, SILCS takes protein flexibility and desolvation into account. SILCS initially involves molecular dynamics (MD) simulations of the target protein in the presence of organic solutes immersed in an aqueous environment, which compete for binding sites on the protein. Analysis of the distribution of organic solutes yields 3D residence fragment probability distributions that are used to map functional group affinity patterns, termed FragMaps. These FragMaps include aliphatic, aromatic, hydrogen bond donors and acceptors, heterocycles and charged functional groups that are converted into grid free energies (GFEs)⁵⁹. Visualization of the FragMaps allows for the identification of synthetically accessible specific functional groups that will maximize interactions with proteins. SILCS Monte-Carlo (SILCS-MC) sampling can be used in conjunction with the FragMaps for ligand docking from which Ligand-GFE (LGFE)

scores are obtained, providing a quantitative ranking of different ligands⁶⁰. This aids in the design of functional group modifications on the inhibitors to increase affinity for the target protein. In the present study the SILCS approach is used simultaneously on Mcl-1 and HDM2 to identify functional groups that will maximize affinity for the two proteins in the context of a rational polypharmacology design approach.

Next, **OX0** was docked into Mcl-1 (Figure 2.6A) and HDM2 (Figure 2.6B) by using SILCS to show the binding mode of our compounds and determine their ability to occupy regions that are favorable for binding of the design functional groups.

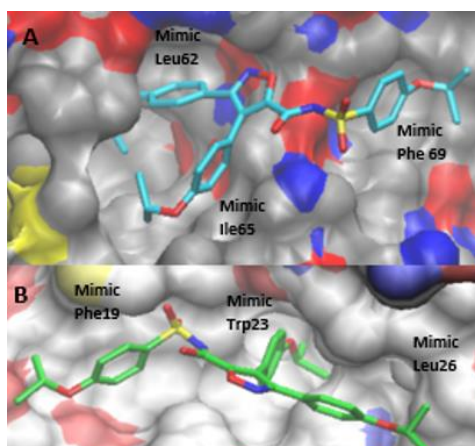


Figure 2. 6. SILCS MC docking with **OX0** in A) Mcl-1 and B) HDM2.

Figure 2.7 shows the SILCS-MC docked orientations of **OX0** in Mcl-1 (left) and HMD2 (right), along with FragMaps for aliphatic (green) and aromatic (purple) functional groups. This informs us where additional moieties should be grafted onto our

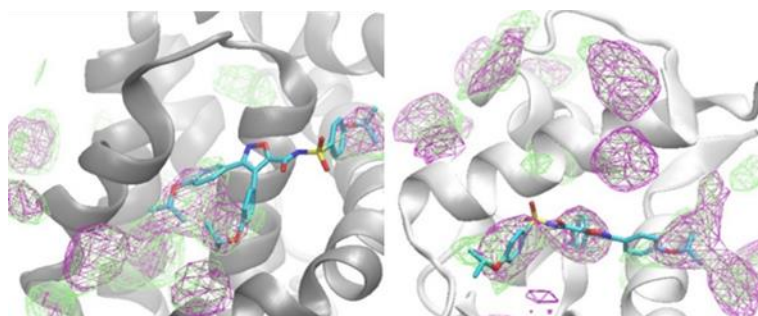


Figure 2. 7. **OX0** docked in Mcl-1 (left) and HDM2 (right) with SILCS. Aliphatic FragMaps are purple and aromatic FragMaps are green.

inhibitors to ensure more favorable contacts with the proteins. In both proteins, the hydrophobic functional groups projected from the core scaffold are encased almost entirely within the FragMaps indicating that they are in the correct orientation to mimic the native ligand and thereby improve the binding affinity.

2.4. Synthesis

Target molecules based on the generic structures shown in Figure 2.4 (right), were accessed as depicted in Scheme 1–3. In order to evaluate our design strategy, the R¹, R² and R³ groups were restricted to a focus set of hydrophobic side chains, including isopropyl and phenyl.

Isoxazoles: Azidation of ethylbromoacetate (**1**) followed by a Knoevenagel condensation with 4-isopropoxybenzaldehyde (**2**) delivered ethyl (Z)-2-azido-3-(4-isopropoxyphenyl) acrylate (**3**). Meanwhile, various 4-substituted benzaldehydes **4** were

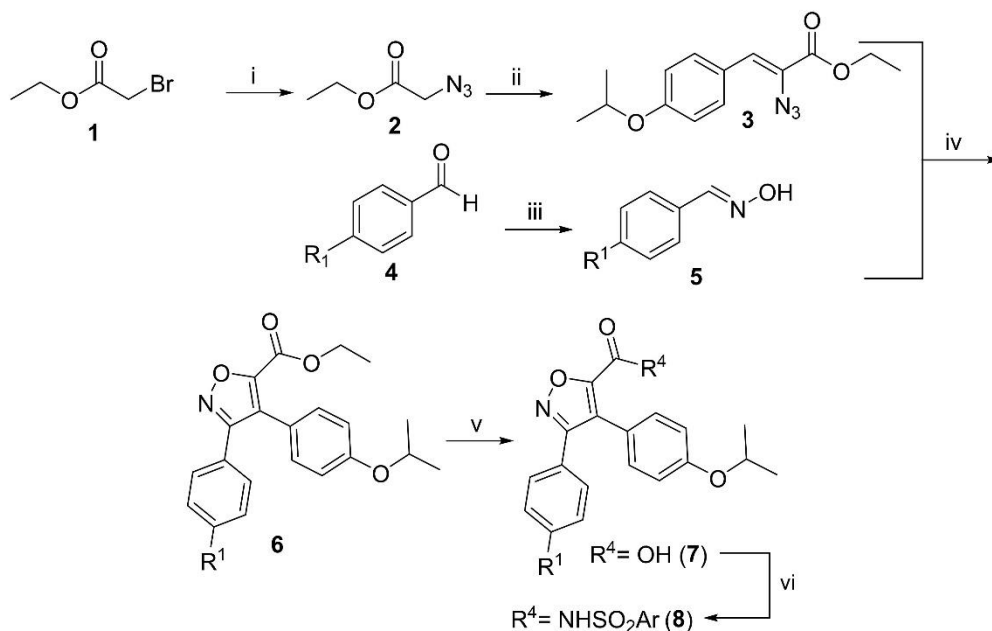


Figure 2.8. (i) NaN₃, DMF, r.t., 18hr; (ii) (4-OiPr)benzaldehyde, NaH, EtOH, -10°C, 4hr; (iii) NH₂OH·HCl, Pyridine, reflux, 1hr; (iv) Et₃N, NCS, DMF, rt to 90°C, 18hr; (v) LiOH·H₂O, THF/MeOH/H₂O, r.t., 18hr; (vi) hydrolysis prepared via (v) corresponding sulfonamide, isobutyl chloroformate, NMM, NaH, THF, -10°C to 0°C to r.t., 18hr.

transformed into (*E*)-benzaldehyde oximes **5** under standard conditions. Subsequently, *N*-chlorosuccinimide mediated the cyclization of acrylates **3** with oximes **5** to construct the isoxazole scaffold in compounds **6**. Saponification of the ethyl esters revealed the carboxylic acids **7**, which were finally coupled with various sulfonamides to afford the 1,2,3-functionalized isoxazole acyl sulfonamides **8**.

Pyrazoles: Isopropylation of 4-nitrophenol (**9**) followed by reduction with tin(II) chloride yielded 4-isopropoxyaniline (**10**), which was subsequently transformed into hydrazine **11**. Meanwhile, 4-fluoroacetophenone (**12**) underwent S_NAr reactions with isopropanol or phenol to furnish the 4-substituted phenol ethers **13**, which underwent Claisen ester condensations with diethyl oxalate to deliver β -keto esters **14**. In an application of the Knorr pyrazole synthesis, hydrazines **11** were condensed with β -keto

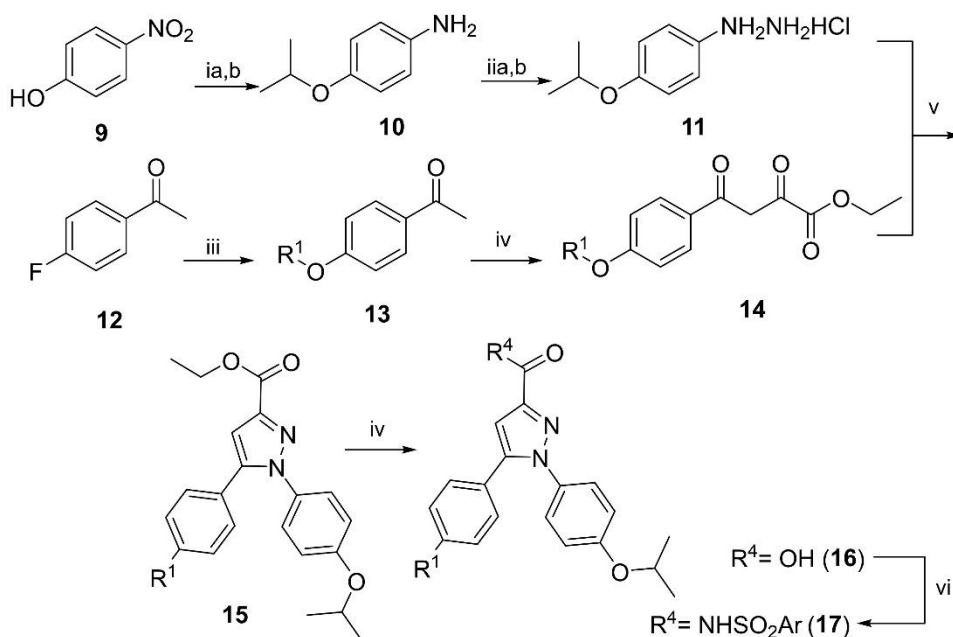


Figure 2.9. (ia) 2-iodopropane, K_2CO_3 , DMF, r.t. to $60^\circ C$, 18hr; (ib) $SnCl_2 \cdot 2H_2O$, EtOAc, $50^\circ C$, 18hr; (iia) $NaNO_2$, H_2O , $0^\circ C$, 18hr; (iib) $SnCl_2 \cdot 2H_2O$, EtOAc, $50^\circ C$, o.n.; (iii) corresponding alcohol, K_2CO_3 , DMF, $60^\circ C$, 18hr; (iv) diethyl oxalate, NaH, THF, $0^\circ C$ to rt, 18hr; (v) AcOH, reflux, 18hr; (vi) LiOH·H₂O, THF/MeOH/H₂O, r.t., 18hr; (vii) hydrolysis prepared via (v), then corresponding sulfonamide, isobutyl chloroformate, NMM, NaH, THF, $-10^\circ C$ to $0^\circ C$ to r.t., 18hr.

esters to yield the 1,2,4-trisubstituted pyrazoles **15**. Saponification as before delivered the corresponding carboxylic acids **16**, which were subsequently coupled to the library of sulfonamides to furnish the 1,3,4-trisubstituted pyrazole acyl sulfonamides **17**.

Thiazoles: Briefly, ethyl-2-aminothiazole-4-carboxylate (**18**) was chlorinated in the remaining aromatic position and then subjected to a Sandmeyer transformation to deliver the 2-bromo-5-chlorothiazole-2-carboxylate derivative **20**. Both halogens were displaced in a double Suzuki reaction employing an excess of 4-hydroxybenzeneboronic acid, and then both phenols were alkylated with isopropyl iodide to yield **22**. Saponification as before delivered the carboxylic acid **23**, and conjugation to our library of sulfonamides furnished the target molecules, 1,2,4-tri-substituted thiazole acyl sulfonamides **24**.

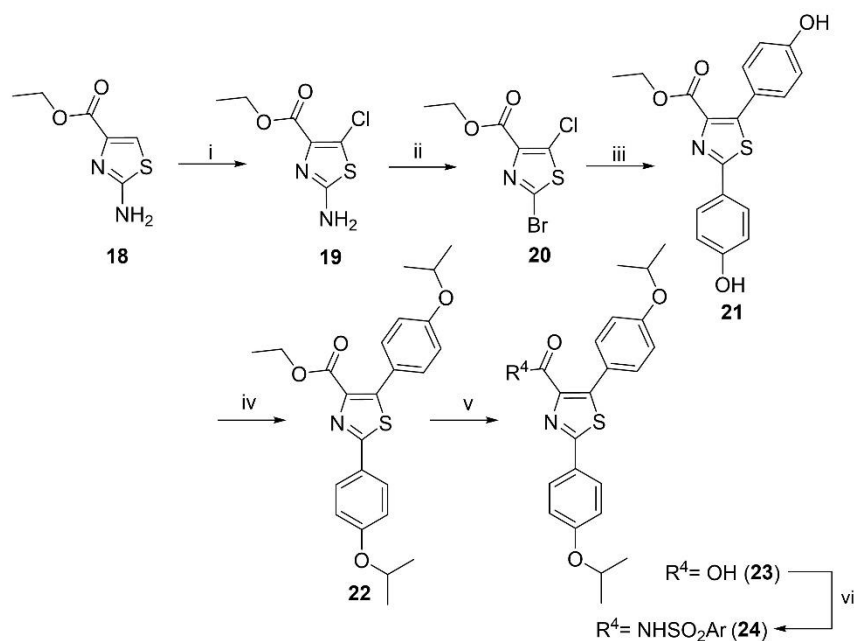
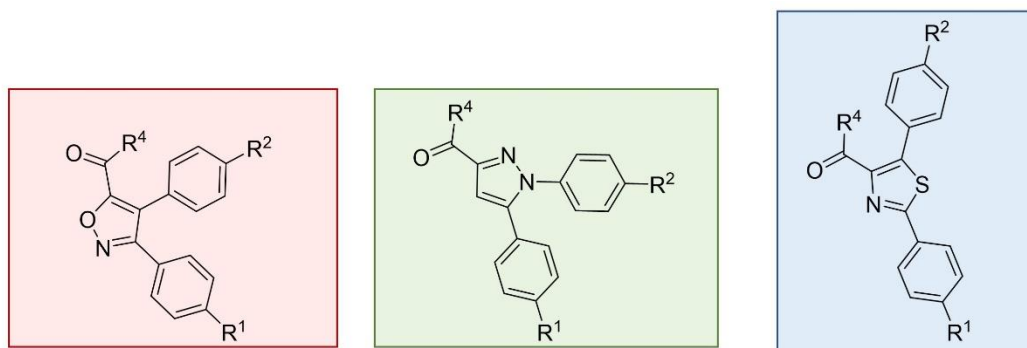


Figure 2. 10. (i) NCS, ACN, 80°C, 18hr; (ii) *t*-BnONO, CuBr₂, ACN, 80°C, 18hr; (iii) 4-hydroxyphenylboronic acid, CsF, tetrakis ((triphenylphosphine)palladium(0)), DME/MeOH, 80°C, 18hr; (iv) 2-iodopropane, K₂CO₃, DMF, 50°C, 18hr; (v) LiOH·H₂O, THF/MeOH/H₂O, r.t., 18hr; (vi) corresponding sulfonamide, isobutyl chloroformate, NMM, NaH, THF, -10° to 0°C to r.t., 18hr.

2.5. Results

Binding affinities of target molecules to Mcl-1 and HDM2 were determined by a standard fluorescence anisotropy competition assay using FITC (fluorescein isothiocyanate)-labeled Bak-BH3 for Mcl-1 or TAMRA (tetramethylrhodamine)-labeled p53 for HDM2; these data are presented in Table 2.1. As we prepared a focused set of inhibitors, it would be premature at this stage to delve into a detailed discussion on R¹, R² and R⁴ side chains, and that will be reserved for a follow-up full paper with a larger library of compounds.

However, it is clear that in every case, compounds were more potent inhibitors of Mcl-1



Compound Number	R ¹	R ²	R ⁴	K _i (μM)	
				Mcl-1	HDM2
7a	-OiPr	-OiPr	-OH	11.4 ± 1.0	85.8 ± 16.2
7b	-OPh	-OiPr	-OH	2.83 ± 0.30	18.6 ± 3.9
16a	-OiPr	-OiPr	-OH	10.6 ± 0.7	84.4 ± 16.9
16b	-OPh	-OiPr	-OH	3.12 ± 7	15.4 ± 2.9
23	-OiPr	-OiPr	-OH	10.4 ± 0.8	27.9 ± 5.1
8a	-OiPr	-OiPr	-NHSO ₂ (4-OCF ₃)Ph	2.91 ± 0.11	41.5 ± 8.3
8b	-OPh	-OiPr	-NHSO ₂ (4-OCF ₃)Ph	0.263 ± 0.018	NA
8c	-OPh	-OiPr	-NHSO ₂ (4-OPh)Ph	0.355 ± 0.02	33.4 ± 4.2
8d	-OPh	-OiPr	-NHSO ₂ (2-naphthyl)	NA	NA
17a	-OiPr	-OiPr	-NHSO ₂ (4-OCF ₃)Ph	5.89 ± 0.03	41.0 ± 7.4
17b	-OPh	-OiPr	-NHSO ₂ (4-OPh)Ph	2.05 ± 1.62	16.5 ± 2.1
17c	-OPh	-OiPr	-NHSO ₂ (4-OCF ₃)Ph	0.433 ± 0.033	11.5 ± 1.7
17d	-OPh	-OiPr	-NHSO ₂ (2-naphthyl)	0.561 ± 0.072	39.2 ± 8.3
24a	-OiPr	-OiPr	-NHSO ₂ (4-OCF ₃)Ph	5.14 ± 0.59	141 ± 26
24b	-OiPr	-OiPr	-NHSO ₂ (4-OPh)Ph	30.9 ± 7.26	263 ± 54
24c	-OiPr	-OiPr	-NHSO ₂ (2-naphthyl)	19.1 ± 2.2	NA

Table 2. 1. Inhibition of Mcl-1 and HDM2 with isoxazoles, pyrazoles, and thiazoles using fluorescence anisotropy competition assay (FACA). NA: no activity. Data are represented as the average of experiments performed in triplicate ± SD. IC₅₀ values were converted into K_i values by using the Nikolovska-Coleska equation⁶¹.

than HDM2, ranging from around three-fold to >100-fold better. Furthermore, the isoxazoles and pyrazoles were, generally, the most potent dual inhibitors, and, likely owing to the inferior substitution pattern that was referred to earlier, the thiazoles were the worst inhibitors. Of course, we cannot rule out that the identity and location of the heteroatoms in each core did not impact binding affinity, as well, and this will be investigated at a later date. It is noteworthy that the more potent isoxazoles and pyrazoles have a more clustered projection of “side chains” similar to the potent HDM2 inhibitor Nutlin-3a, and a co-crystal structure of Nutlin-3a/HDM2 reveals the three sub-pockets on HDM2 are close together (PDB ID: 4 J3E). This superior functionality is present in both the Novartis patent and the Zhang et al. dual inhibitor^{45,51}.

We hypothesized that the conversion of the carboxylic acid to an acyl sulfonamide would offer greater inhibition, accomplishing mimicry of the third hydrophobic side chain. While the poor activity of the thiazole acid **23** could not be rescued in this way, the data for the isoxazoles and pyrazoles proved this hypothesis true in almost every case with Mcl-1 and in some of the cases with HDM2. This can be seen, for example, by comparing acid **7a** ($K_i = 11.4 \mu\text{M}$ (Mcl-1), $85.8 \mu\text{M}$ (HDM2)) with its corresponding acyl sulfonamide **8a** ($K_i = 2.91 \mu\text{M}$ (Mcl-1), $41.5 \mu\text{M}$ (HDM2)), as well as acid **16a** ($K_i = 10.6 \mu\text{M}$ (Mcl-1), $84.4 \mu\text{M}$ (HDM2)) with the analogous acyl sulfonamide **17a** ($K_i = 5.89 \mu\text{M}$ (Mcl-1), $41.0 \mu\text{M}$ (HDM2)). We attribute this to a combination of the retention of an acidic functionality needed to engage with Arg263 of Mcl-1, but also the excellent delivery of the third functional group R^4 that is seen to overlap with the FragMaps in **OX0** (Figure 2.6) in the modeling studies with both proteins, indicating their contribution to improved affinity. It should be noted that although **OX0** was not synthesized, it is very

similar to **8a**, and the intention of the FragMaps was to suggest analogues based on the modeled compound, such as **8a**. Closer inspection of the data suggests that the strategy of converting a carboxylic acid into a structurally more elaborate acyl sulfonamide had a greater beneficial impact on Mcl-1 inhibition than on HDM2 inhibition, and in some cases – predominantly isoxazoles – this actually proved detrimental to HDM2 inhibition. Of all compounds tested, our most potent dual inhibitor was pyrazole **17c** with K_i values of 433 nM and 11.5 μ M for Mcl-1 and HDM2, respectively. Inadvertently, we may have identified a new scaffold for the development of selective Mcl-1 inhibitors, since some of our isoxazoles were potent against Mcl-1 with limited or no activity against HDM2, for example **8b** with a K_i of 263 nM for Mcl-1 and inactive against HDM2.

One of the challenges with developing dual inhibitors – through the same recognition motif – of Mcl-1 and HDM2 by α -helix mimicry is the size mismatch between analogous side chains. Particularly, the middle side chain of the region of Bim-BH3 that is being emulated is relatively small (Ile65), whereas the corresponding residue in p53TAD is much larger (Trp23), and the respective pockets that bind these side chains do not appear malleable from crystal structures. On the other hand, Fesik's group has demonstrated that the p2 pocket on Mcl-1 that binds Leu62 of Bim-BH3 is somewhat plastic, and can accommodate larger groups³⁷; indeed, this appears to be a significant source of ligand affinity. Thus, for an effective dual inhibitor, a large R^1 group is required for Mcl-1 inhibition, but a large R^2 group is required for HDM2 inhibition. The isoxazole scaffold cannot effectively meet these criteria simultaneously. However, the pyrazole scaffold can because the R^1 and R^2 groups are interchangeable with respect to the third substituent at the acyl sulfonamide functionality through rotation about the pyrazole-acyl

bond, and this may be one reason why, in general, the pyrazole acyl sulfonamides fared better as dual inhibitors than the corresponding isoxazole acyl sulfonamides. In other words, the large R¹ phenyl group in the pyrazole series can serve as an effective mimic of Leu62 at the located at the periphery of the BH3 α -helix and bind the plastic p2 pocket of Mcl-1, yet, on the other hand through pyrazole-acyl bond rotation, is also able to mimic the Trp23 in the middle of the p53TAD α -helix.

2.6. Conclusion

The discovery of targeted anticancer agents is an intense field of research that is constantly being met with defeat due to the development of resistance. Polypharmacology represents a paradigm shift in the treatment of multi-factorial diseases, such as cancer. Recognizing that Mcl-1 and HDM2 are both upregulated in similar cancers and their anticancer activities are regulated by similarly functionalized α -helical domains in their partner proteins, we hypothesized that suitably functionalized heterocycles could be designed to simultaneously inhibit both Mcl-1 and HDM2. In summary, we have demonstrated that acyl sulfonamides of triply substituted isoxazoles and pyrazoles are effective dual α -helix mimetics of the Bim-BH3 and p53TAD domains, inhibiting Mcl-1 and HDM2, respectively. Although our data presently indicate that the isoxazoles might be better suited to the development of selective Mcl-1 inhibitors, further optimization of the pyrazole core may lead to more potent dual inhibitors. Particularly, since conversion of the pyrazole acids to their corresponding acyl sulfonamides was more impactful for Mcl-1 than HDM2, we intend to first optimize the pyrazole acid predominantly to HDM2, and then anticipate a greater improvement in Mcl-1 affinity upon converting the acids to acyl sulfonamides.

2.7 Supplementary Information

2.7.1. Chemistry

General. Unless otherwise stated, all reactions were performed under an inert atmosphere (N₂). Reagents and solvents were ACS grade, and purchased from Sigma-Aldrich, Alfa Aesar, Oakwood and TCI America. Anhydrous solvents were used as provided from Sigma-Aldrich. Reactions were monitored by thin-layer chromatography (TLC), visualizing with a UV lamp and/or KMnO₄ stain. Flash column chromatography was performed with silica gel 60 A (70-230 mesh, Merck). ¹H and ¹³C NMR spectra were recorded on a Varian INOVA 400 MHz NMR spectrometer at 25 °C. Chemical shifts are reported in parts per million (ppm). Data for ¹H NMR are reported thus: chemical shift (δ ppm) (multiplicity, coupling constant (Hz), integration), where multiplicities are: s = singlet, d = doublet, t = triplet, m = multiplet. The residual solvent peak was used as an internal reference: CDCl₃ (δ_H 7.26; δ_C 77.21) and *d*₆-DMSO (δ_H 2.50; δ_C 39.51).

Isoxazoles

General Procedure A: Synthesis of ethyl 2-azidoacetate. Ethyl bromoacetate (1eq) and sodium azide (1 eq) were dissolved in DMF (0.1M) stirring at room temperature for 18 hours. A TLC in 1:1 Hexane/EtOAc indicated the reaction was complete. EtOAc (50mL) was added to the reaction, washed with H₂O (5x, 75mL) and brine (1x, 50mL), dried with Na₂SO₄, filtered, and concentrated in vacuo. Azeotroping with CHCl₃ yielded ethyl 2-azidoacetate (quantitative yield).

General Procedure B: Synthesis of (Z)-2-azido-3-(4-isoxpropoxyphenyl) acrylate.

Anhydrous EtOH (0.5M) was cooled to -10°C under N₂. NaH (5 eq) was added and stirred at -10°C for 30 minutes. Next, a mixture of ethyl-2-azidoacetate (1 eq) and 4-

isopropoxybenzaldehyde (1 eq) in 1mL of anhydrous EtOH was added dropwise to the reaction over 30 minutes and the reaction was stirred at -10°C for four hours. A TLC in 1:1 Hexane/EtOAc indicated the reaction was complete. The reaction was quenched with 1mL of H₂O and EtOAc (50mL) was added to the reaction and washed with 1M HCl (2x, 75mL) and brine (1x, 75mL), dried with Na₂SO₄, filtered, concentrated in vacuo, and azeotroped with CHCl₃ yielded 4-substituted (Z)-2-azido-3-(4-isoxpropoxyphenyl) acrylate (quantitative yield).

General Procedure C: Synthesis of aryl aldehydes. 4-phenoxybenzaldehyde (1eq) and K₂CO₃ (1.5 eq) were dissolved in DMF (0.1M). 2-iodopropane (4a) or phenol (4b) (1.5 eq) was added dropwise to the reaction and it was stirred at room temperature for 18 hours. A TLC in Hexane/EtOAc revealed the reaction was complete. EtOAc (50mL) was added and the reaction was washed with H₂O (5x, 75mL) and brine (1x, 75mL). The organics were dried with Na₂SO₄, concentrated in vacuo, and azeotroped to reveal aryl aldehydes.

General Procedure D: Synthesis of substituted aryl oximes. A substituted benzaldehyde (1 eq) and NH₂OH · HCl (1.1 eq) were dissolved in pyridine (0.1 M) and refluxed for 1 hour. A TLC in 1:1 Hexane/EtOAc indicated the reaction was complete. EtOAc (30mL) was added to the reaction and washed with H₂O (x5, 50 mL) and brine (x1, 50mL), dried with Na₂SO₄, filtered, and concentrated. It was columned on an Isolera in 4:1 Hex/EtOAc, concentrated in vacuo, and azeotroped CHCl₃ yielded substituted aryl oximes.

General Procedure E: Synthesis of isoxazole ethyl esters. A substituted aryl oxime (1 eq) was reacted with N-chlorosuccinimide (1.2 eq) in DMF (0.1 M) stirring at room

temperature for four hours. A TLC in 2:1 Hexane/EtOAc indicated the reaction was complete. Then, a substituted methyl azidoacrylate (1 eq) was added in 1mL DMF, followed by TEA (1 eq, 2.81 mmol) stirring overnight at 90°C. A TLC in 4:1 Hexane/EtOAc indicated the reaction was complete. EtOAc (30mL) was added to the reaction and washed with H₂O (x5, 50 mL) and brine (x1, 50mL), dried with Na₂SO₄, filtered, and concentrated. It was columned on an Isolera in 4:1 Hex/EtOAc, concentrated in vacuo and azeotropered to give the isoxazole ethyl ester compounds with (29% yield).

General Procedure F: Synthesis of isoxazole carboxylic acids. The isoxazole ethyl ester (1 eq) was reacted with LiOH · H₂O (4 eq) in 3:1:1 THF/H₂O/MeOH (0.1 M) at room temperature overnight. A TLC in 92:7:1 CH₂Cl₂/MeOH/Acetic acid indicated the reaction was complete. EtOAc (30mL) was added to the reaction, washed with 1M HCl (x3, 50mL), dried with Na₂SO₄, filtered, and concentrated in vacuo. The crude product was columned in 92:7:1 CH₂Cl₂/MeOH/Acetic acid, concentrated in vacuo to reveal the isoxazole carboxylic acid (55% yield).

General Procedure G: Synthesis of isoxazole acyl sulfonamides. An isoxazole carboxylic acid (1 eq) was dissolved in THF (0.1 M), brought to -10°C, when isobutylchloroformate (1.1 eq) followed by NMM (1.1 eq) was added. The reaction stirred for 1 hour at -10°C. Then, at 0°C, a substituted sulfonamide (1.5 eq) was added, followed by NaH (3 eq). Then, the reaction warmed up to room temperature and stirred overnight. A TLC in 79:9:1 CH₂Cl₂/MeOH/H₂O showed the reaction was complete. EtOAc (15mL) was added to the reaction, washed with 1M HCl (x3, 30mL), dried with Na₂SO₄, filtered, and concentrated in vacuo. The crude product was columned in 79:9:1

CH₂Cl₂/MeOH/H₂O, concentrated in vacuo to reveal a 3,4,5-trisubstituted isoxazole acyl sulfonamide (75% yield).

General Procedure H: Synthesis of functionalized sulfonamides. The sulfonyl chloride (1 eq) was added to a reaction flask and dissolved in dioxane (0.1M). The reaction was cooled to 0°C and NH₄OH (10 eq) was added slowly to the reaction mixture. The reaction was heated to room temperature and stirred for 1 hour. Completion of the reaction was monitored via TLC with a gradient of Hexanes/EtOAc. Once completed, the solvent was evaporated off and the crude material was dissolved in EtOAc. The organic layer was washed 1M HCl three times and collected, dried with Na₂SO₄, filtered, concentrated down and azeotroped with CHCl₃ to yield the functionalized sulfonamides (80-90% yield).

Pyrazoles

General Procedure I: Synthesis of the arylhydrazines. An aniline (1 eq) was added to a reaction flask followed by the addition of 1M HCl (0.1 M) and stirred at 0°C. The reaction stirred for 5 minutes and then was brought to room temperature. The reaction stirred for 20 minutes and then was cooled to -5°C. NaNO₂ (1.05 eq.) dissolved in H₂O was added dropwise to reaction. The reaction stirred for 15 minutes and then SnCl₂ (4.0 eq.) was added to the reaction. The reaction stirred at room temperature for 3 hours and a precipitate formed. The precipitate was filtered out of the reaction and washed with cold H₂O to isolate the desired arylhydrazine (60-70% yield).

General Procedure J: Synthesis of the 2,4-dioxobutanoates. A ketone (1 eq) was added to a reaction flask and solubilized in a mixture of 5:1 anhydrous toluene/anhydrous THF (0.1 M). The reaction was cooled to 0°C and NaH (2 eq) was then added to the

reaction. The reactions stirred for 10 minutes and then diethyl oxalate (1.2 eq) was added. The reaction was then heated to 60°C and stirred for 2 hours. Completion of the reaction was monitored via TLC in a gradient of Hexanes/EtOAc. Once complete, the crude mixture was partitioned between 1M HCl and EtOAc. The organic layer was extracted, dried with Na₂SO₄, filtered and concentrated down. The crude material was then dry loaded onto silica gel and purified via column chromatography. The fractions containing the product were combined, concentrated down and azeotroped with CHCl₃ to yield the 2,4-dioxobutanoates (60-85% yield).

General Procedure K: Synthesis of pyrazole ethyl esters. An arylhydrazine (1 eq) and 2,4- dioxobutanoate (1.2 eq) were added into a reaction flask and solubilized in MeOH (0.1 M). The reaction was refluxed for 3 hours at 65°C. Completion of the reaction was monitored via TLC in a gradient of Hexanes/EtOAc. Once complete, the crude mixture was partitioned between 1M NaOH and EtOAc. The organic layer was extracted, dried with Na₂SO₄, filtered and concentrated down. The crude material was then dry loaded onto silica gel and purified via column. The fractions containing the product were collected, combined, concentrated down and azeotroped with CHCl₃ to yield the pyrazole ethyl esters (80-90% yield).

General Procedure L: Synthesis of pyrazole carboxylic acids. A pyrazole ethyl ester (1 eq) was placed into a reaction flask and solubilized in a 3:1:1 mixture of THF/H₂O/MeOH (0.1 M). LiOH monohydrate (3 eq) was then added and the reaction stirred at room temperature for 3 hours. Additional MeOH and THF were added when needed to homogenize the reaction mixture. Completion of the reaction was monitored via TLC in a gradient of 92:7:1 DCM/MeOH/Acetic acid. Once complete, the crude

mixture was partitioned between 1M NaOH and EtOAc. The aqueous layer was collected and then acidified to a pH of 3. EtOAc was added to the acidified aqueous layer. The organic layer was then extracted, dried with Na₂SO₄, filtered, concentrated down and azeotroped with CHCl₃ to yield the pyrazole carboxylic acids (90-95% yield).

General Procedure M: Synthesis of 3-acyl sulfonamide pyrazoles. A pyrazole carboxylic acid (1 eq) was placed into a reaction flask and solubilized in SOCl₂ (0.3 M). The reaction was refluxed for 3 hours to create the acid chloride. Formation of acid chloride was determined via TLC in a gradient of 92:7:1 DCM/MeOH/Acetic acid by performing a mini-workup in MeOH. Once all the starting acid had become the acid chloride, the SOCl₂ was vacuum evaporated and the acid chloride was re-solubilized in anhydrous DCE (0.3 M). Sulfonamides (1.2 eq) were then added to the reaction followed by DMAP (0.5 eq). The reaction stirred at room temperature for 16 hours. Completion of the reaction was monitored via TLC in a gradient of 92:7:1 DCM/MeOH/H₂O. Once complete, the DCE was evaporated and the crude mixture was dry loaded onto silica gel. The product was purified via column chromatography in a gradient of 92:7:1 DCM/MeOH/H₂O. The product fractions were collected, combined, concentrated down and azeotroped with CHCl₃ to yield the 3-acylsulfonamide pyrazoles (40-65% yield).

Thiazoles

General Procedure N: Synthesis of ethyl-2-amino-5-chlorothiazole-4-carboxylate.

Ethyl 2- aminothiazole-4-carboxylate (1 eq) and N-chlorosuccinimide (1.1 eq) were dissolved in Acetonitrile (0.5 M). The reaction was stirred at 80°C for 18 hours. The reaction mixture was cooled to 0°C and the precipitate was filtered and washed with cold iPrOH (2x, 5mL). The HCl salt was taken up in H₂O (10mL) and 1M NaOH (10mL) and

extracted with CH₂Cl₂ (20mL). The organic layers were combined and concentrated in vacuo and azeotroped to reveal ethyl-2- amino-5-chlorothiazole-4-carboxylate.

General Procedure O: Synthesis of ethyl-2-bromo-5-chlorothiazole-4-carboxylate.

Ethyl-2-amino-5-chlorothiazole-4-carboxylate (1eq) was added to a solution of tert-butyl nitrite (1.5 eq) and copper (II) bromide (1.5eq). The reaction was stirred at 80C for 18 hours. The mixture was cooled and partitioned between CH₂Cl₂ (50mL) and 1M HCl (75mL). The aqueous layer was extracted with CH₂Cl₂ (2x, 50mL) and the combined organics were dried over Na₂SO₄, filtered, and concentrated in vacuo. The crude product was columned via flash column chromatography on an Isolera in 4:1 Hexane/EtOAc, concentrated, azeotrope to give ethyl-2-bromo-5-chlorothiazole-4-carboxylate.

General Procedure P: Synthesis of ethyl 2,5-bis (4-hydroxyphenyl)thiazole-4-carboxylate.

Ethyl-2-bromo-5-chlorothiazole-4-carboxylate (1 eq) was dissolved in a mixture of DME/MeOH (0.1M). 4-ydroxyphenylboronic acid (1 eq), and CsF (1.5 eq) were added to the reaction and was subsequently degassed with N₂. Lastly, tetrakis (10 mol %) was added and the reaction was stirred at 80°C for 18 hours under N₂. A TLC in 4:1 Hexane/EtOAc revealed the reaction was complete. EtOAc (50mL) was added and the reaction was washed with H₂O (3x, 75mL) and brine (1x, 75mL). The organics were dried with Na₂SO₄ and concentrated in vacuo. The crude product was columned in flash column chromatography on an Isolera in 4: 1 Hexane/EtOAc, concentrated in vacuo, and azeotroped to reveal the ethyl 2,5-bis (4- hydroxyphenyl)thiazole-4-carboxylate.

General Procedure Q: Synthesis of ethyl 2,5-bis(4-isopropoxyphenyl)thiazole-4-

carboxylate. 2,5-bis(4-hydroxyphenyl)thiazole-4-carboxylate (1eq) and K_2CO_3 (3 eq) were dissolved in DMF (0.1M). 2-iodopropane (2.5 eq) was added dropwise to the reaction and it was stirred at 50°C for 18 hours. A TLC in Hexane/EtOAc revealed the reaction was complete. EtOAc (50mL) was added and the reaction was washed with H_2O (5x, 75mL) and brine (1x, 75mL). The organics were dried with Na_2SO_4 and concentrated in vacuo. The crude product was purified by flash column chromatography in 9:1 Hexane/EtOAc, concentrated in vacuo, and azeotroped to reveal ethyl 2,5-bis(4-isopropoxyphenyl)thiazole-4-carboxylate.

General Procedure R: Synthesis of 2,5-bis(4-isopropoxyphenyl)thiazole-4-carboxylic acid. 2,5-bis(4-isopropoxyphenyl)thiazole-4-carboxylate (1 eq) was reacted with $LiOH \cdot H_2O$ (4 eq) in 3:1:1 THF/ H_2O /MeOH (0.1M) and stirred at room temperature overnight. A TLC in 92:7:1 CH_2Cl_2 /MeOH/Acetic acid indicated the reaction was complete. EtOAc (30mL) was added to the reaction, washed with 1M HCl (x3, 50mL), dried with Na_2SO_4 , filtered, and concentrated in vacuo. The crude product was columned in 92:7:1 CH_2Cl_2 /MeOH/Acetic acid, concentrated in vacuo to reveal 2,5-bis(4-isopropoxyphenyl)thiazole-4-carboxylic acid.

General Procedure S: Synthesis of acyl sulfonamide thiazoles. The 2,5-bis(4-isopropoxyphenyl)thiazole-4-carboxylic acid (1 eq) was dissolved in THF (0.1M), brought to -10°C, when isobutylchloroformate (1.1 eq) followed by NMM (1.1 eq) was added. The reaction stirred for 1 hour at -10°C. Then, at 0°C, a substituted sulfonamide (1.5 eq) was added, followed by NaH (3 eq). Then, the reaction warmed up to room temperature and stirred overnight. A TLC in 79:9:1 CH_2Cl_2 /MeOH/ H_2O showed the reaction was complete. EtOAc (50mL) was added to the reaction, washed with 1M HCl

(x3, 75mL), dried with Na₂SO₄, filtered, and concentrated in vacuo. The crude product was columned in 79:9:1 CH₂Cl₂/MeOH/H₂O, concentrated in vacuo to reveal the tri-substituted thiazole.

Ethyl 2-azidoacetate (2). General procedure A. (Quantitative); δ_{H} (400 MHz, CDCl₃) 4.28-4.23 (m, 2H, CH₂CH₃), 3.85 (s, 2H, CH₂N₃), 1.30 (t, 3H, (CH₂CH₃), $J = 7$ Hz).

(Z)-2-azido-3-(4-isopropoxyphenyl) acrylate (3). General procedure B. (31%) δ_{H} (400 MHz, CDCl₃) 7.78 (d, 2H, Ar, $J = 8.8$ Hz), 6.88 (t, 3H, Ar, $J = 3.8$ Hz), 4.62-4.59 (m, 1H, CH(CH₃)₂), 4.38-4.33 (m, 2H, CH₂CH₃), 1.40 (d, 3H, (CH₂CH₃), $J = 6.8$ Hz), 1.35 (d, 6H, (CH(CH₃)₂), $J = 5.2$ Hz).

4-isopropoxybenzaldehyde (4a). General procedure C with 2-iodopropane. (Quantitative) δ_{H} (400 MHz, CDCl₃) 9.87 (s, 1H, Ar), 7.81 (d, 2H, Ar, $J = 8.8$ Hz), 6.97 (d, 2H, Ar, $J = 8.4$ Hz), 4.68-4.65 (m, 1H, CH(CH₃)₂), 1.38 (d, 6H, (CH(CH₃)₂), $J = 5.6$ Hz)

4-phenoxybenzaldehyde (4b). General procedure C with phenol. (Quantitative) δ_{H} (400 MHz, CDCl₃) 9.92 (s, 1H, Ar), 7.85 (d, 2H, Ar, $J = 8.4$ Hz), 7.42 (t, 2H, Ar, $J = 7.4$ Hz), 7.26-7.21 (m, 1H, Ar), 7.09 (d, 2H, Ar, $J = 8.8$ Hz), 7.06 (d, 2H, Ar, $J = 8.4$ Hz)

(E)-4-isopropoxybenzaldehyde oxime (5a). General procedure D. (82%) δ_{H} (400 MHz, CDCl₃) 8.09 (s, 1H, Ar), 7.49 (d, 2H, Ar, $J = 8.8$ Hz), 6.88 (d, 2H, Ar, $J = 8.4$ Hz), 4.60-4.57 (m, 1H, CH(CH₃)₂), 1.35 (d, 6H, (CH(CH₃)₂), $J = 5.2$ Hz)

(E)-4-phenoxybenzaldehyde oxime (5b). General procedure D. (67%) δ_{H} (400 MHz, CDCl₃) 8.14 (s, 1H, Ar), 7.55 (d, 2H, Ar, $J = 8.8$ Hz), 7.37 (t, 2H, Ar, $J = 7.8$ Hz), 7.16 (t, 1H, Ar, $J = 7.4$ Hz), 7.05 (d, 2H, Ar, $J = 8.4$ Hz), 7.00 (d, 2H, Ar, $J = 8.8$ Hz)

Ethyl 3,4-bis(4-isopropoxyphenyl)isoxazole-5-carboxylate (6a). General procedure E with **5a**. (29%). Was used immediately in the next step.

Ethyl 4-(4-isopropoxyphenyl)-3-(4-phenoxyphenyl)isoxazole-5-carboxylate (6b). General procedure E with **5b**. (25%). Was used immediately in the next step.

3,4-bis(4-isopropoxyphenyl)isoxazole-5-carboxylic acid (7a). General procedure F with **6a**. (56%) δ_{H} (400 MHz, d_6 -DMSO) 7.23 (d, 2H, Ar, $J = 8.8$ Hz), 7.15 (d, 2H, Ar, $J = 7.6$ Hz), 6.90- 6.84 (m, 4H, Ar), 4.64-4.59 (m, 1H, $\text{CH}(\text{CH}_3)_2$), 1.28-1.24 (m, 12H, $\text{CH}(\text{CH}_3)_3$)

4-(4-isopropoxyphenyl)-3-(4-phenoxyphenyl)isoxazole-5-carboxylic acid (7b). General procedure F with **6b**. (12%) δ_{H} (400 MHz, DMSO- d_6) 7.83 (d, 2H, Ar, $J = 8.4$ Hz), 7.39 (d, 2H, Ar, $J = 8.4$ Hz), 7.19 (d, 2H, Ar, $J = 8.4$ Hz), 7.03 (d, 2H, Ar, $J = 8.8$ Hz), 6.87 (d, 2H, Ar, $J = 8.4$ Hz), 6.79(d, 2H, Ar, $J = 8.4$ Hz), 4.63-4.55 (m, 2H, $\text{CH}(\text{CH}_3)_2$), 1.27-1.23 (m, 12H, $\text{CH}(\text{CH}_3)_3$); δ_{C} (400 MHz, d_6 -DMSO) 161.4, 158.7, 157.2, 149.7, 144.7, 131.9, 130.0, 129.5, 129.4, 121.8, 121.0, 120.6, 120.5, 117.8, 115.7, 115.1, 98.0, 69.5, 69.4, 22.3, 22.2

3,4-bis(4-isopropoxyphenyl)-N-((4-(trifluoromethoxy)phenyl)sulfonyl)isoxazole-5-carboxamide (OX3). General procedure G with **7a** and 4-(trifluoromethyl)benzenesulfonamide. (75%) δ_{H} (400 MHz, CDCl_3) 7.35 (d, 4H, Ar, $J = 6.8$ Hz), 7.14 (t, 3H, Ar, $J = 14$ Hz), 7.03 (d, 2H, Ar, $J = 8$ Hz), 6.9 (t, 4H, Ar, $J = 21$ Hz), 4.56 (s, 1H, $\text{CH}(\text{CH}_3)_2$), 1.34 (s, 6H, $\text{CH}(\text{CH}_3)_3$); δ_{C} (400 MHz, d_6 -DMSO) 160.6, 159.1, 158.3, 149.3, 131.5, 130.1, 129.8, 128.8, 124.1, 124.0, 122.2, 119.7, 119.6, 118.5, 118.0, 115.4, 69.8, 22.0

4-(4-isopropoxyphenyl)-3-(4-phenoxyphenyl)-N-((4-(trifluoromethoxy)phenyl)sulfonyl)isoxazole-5-carboxamide (OX4). General procedure G with **7b** and 4-(trifluoromethyl)benzenesulfonamide. (37%) δ_{H} (400 MHz, CDCl_3) 7.35

(d, 4H, Ar, $J = 6.8$ Hz), 7.14 (t, 3H, Ar, $J = 14$ Hz), 7.03 (d, 2H, Ar, $J = 8$ Hz), 6.9 (t, 4H, Ar, $J = 21$ Hz), 4.56 (s, 1H, $\underline{\text{C}}\text{H}(\text{CH}_3)_2$), 1.34 (s, 6H, $\text{CH}(\underline{\text{C}}\text{H}_3)_3$); δ_{C} (400 MHz, d_6 -DMSO) 160.6, 159.1, 158.3, 149.3, 131.5, 130.1, 129.8, 128.8, 124.1, 124.0, 122.2, 119.7, 119.6, 118.5, 118.0, 115.4, 69.8, 22.0 *4-(4-isopropoxyphenyl)-3-(4-phenoxyphenyl)-N-((4-phenoxyphenyl)sulfonyl)isoxazole-5-carboxamide (OX5)*. General procedure G with **7b** and 4-phenoxybenzenesulfonamide. (55%) δ_{H} (400 MHz, d_6 -DMSO) 7.80 (d, 2H, Ar, $J = 8.4$ Hz), 7.47-7.40 (m, 4H, Ar), 7.31 (d, 2H, Ar, $J = 8.8$ Hz), 7.23-7.19 (m, 2H, Ar), 7.11 (d, 2H, Ar, $J = 7.6$ Hz), 7.07 (d, 4H, Ar, $J = 8.4$ Hz), 7.02 (d, 2H, Ar, $J = 8.4$ Hz), 6.97 (d, 2H, Ar, $J = 8.4$ Hz), 6.83 (d, 2H, Ar, $J = 8.4$ Hz), 4.62-4.59 (m, 1H, $\underline{\text{C}}\text{H}(\text{CH}_3)_2$), 1.26 (d, 6H, $\text{CH}(\underline{\text{C}}\text{H}_3)_3$, $J = 5.2$ Hz)

4-(4-isopropoxyphenyl)-N-(naphthalen-2-ylsulfonyl)-3-(4-phenoxyphenyl)isoxazole-5-carboxamide (OX6). General procedure G with **7b** and naphthalene-2-sulfonamide. (50%) δ_{H} (400 MHz, d_6 -DMSO) 8.43 (s, 1H, Ar), 8.11 (d, 1H, Ar, $J = 6.8$ Hz), 8.01 (t, 2H, Ar, $J = 7.6$ Hz), 7.84 (d, 1H, Ar, $J = 8.4$ Hz), 7.67-7.62 (m, 2H, Ar), 7.39 (t, 2H, Ar, $J = 7.8$ Hz), 7.30 (d, 2H, Ar, $J = 8.4$ Hz), 7.19 (t, 1H, Ar, $J = 7.4$ Hz), 7.06 (d, 2H, Ar, $J = 7.6$ Hz), 7.01 (d, 2H, Ar, $J = 8.4$ Hz), 6.96 (d, 2H, Ar, $J = 8.4$ Hz), 6.73 (d, 2H, Ar, $J = 8.4$ Hz), 4.53-4.50 (m, 1H, $\underline{\text{C}}\text{H}(\text{CH}_3)_2$), 1.24 (d, 6H, $\text{CH}(\underline{\text{C}}\text{H}_3)_3$, $J = 6.4$ Hz)

4-(trifluoromethyl)benzenesulfonamide: Followed General Procedure H with 4-(trifluoromethyl)benzenesulfonyl chloride (83%). δ_{H} (400MHz, d_6 -DMSO) 7.97 (d, $J = 8.8$ Hz, 2H), 7.61 (d, $J = 8.4$ Hz, 2H), 7.53 (s, 2H).

4-phenoxybenzenesulfonamide: Followed General Procedure H with 4-phenoxybenzenesulfonyl chloride (90%). δ_{H} (400MHz, CDCl_3) 7.88 (d, $J = 8.8$ Hz, 2H), 7.42 (t, $J = 7.8$ Hz, 2H), 7.23 (t, $J = 7.4$ Hz, 1H), 7.06 (t, $J = 9.0$ Hz, 4H), 4.83 (s, 2H).

naphthalene-2-sulfonamide: Followed General Procedure H with 4-phenoxybenzenesulfonyl chloride (90%). ^1H NMR was consistent with the literature (*4-isopropoxyphenyl*)hydrazine (**10**). Followed General Procedure I with 4-isopropoxyaniline (65%). δ_{H} (400MHz, d_6 -DMSO) 10.00 (s, 2H), 6.97 (d, $J = 8.4$ Hz, 2H), 6.88 (d, $J = 8.4$ Hz, 2H), 4.55-4.49 (m, 1H), 1.23 (d, $J = 5.6$ Hz, 6H).

4-(4-isopropoxyphenyl)-2,4-dioxobutanoate (**14a**): Followed General Procedure J with 1-(4-isopropoxyphenyl)ethan-1-one (72%). δ_{H} (400MHz, CDCl_3) 7.97 (d, $J = 8.8$ Hz, 2H), 7.03 (s, 1H), 6.94 (d, $J = 8.8$ Hz, 2H), 4.69-4.66 (m, 1H), 4.39 (q, $J = 6.8$ Hz, 2H), 1.43-1.37 (m, 9H).

Ethyl 2,4-dioxo-4-(4-phenoxyphenyl)butanoate (**14b**): Followed General Procedure J with 1-(4-phenoxyphenyl)ethan-1-one (85%). δ_{H} (400MHz, CDCl_3) 7.99 (d, $J = 6.8$ Hz, 2H), 7.42 (bs, 2H), 7.27-7.23 (m, 1H), 7.09 (d, $J = 7.2$ Hz, 2H), 7.04 (bs, 3H), 4.38 (q, $J = 6.4$ Hz, 2H), 1.41 (t, $J = 6.2$ Hz, 3H).

Ethyl 1,5-bis(4-isopropoxyphenyl)-1H-pyrazole-3-carboxylate (**15a**): Followed General Procedure K with **11a** and **14a**. (80%). δ_{H} (400MHz, CDCl_3) 7.15 (d, $J = 8.4$ Hz, 2H), 7.03 (d, $J = 8.8$ Hz, 2H), 6.75 (d, $J = 8.4$ Hz, 2H), 6.70 (d, $J = 8.4$ Hz, 2H), 4.47-4.42 (m, 2H), 4.35 (q, $J = 6.8$ Hz, 2H), 1.32 (t, $J = 7.0$ Hz, 3H), 1.24-1.22 (m, 12H).

Ethyl 1-(4-isopropoxyphenyl)-5-(4-phenoxyphenyl)-1H-pyrazole-3-carboxylate (**15b**): Followed General Procedure K with **11a** and **14b**. (83%). δ_{H} (400MHz, CDCl_3) 7.35 (t, $J = 7.8$ Hz, 2H), 7.23 (d, $J = 8.8$ Hz, 2H), 7.18-7.12 (m, 3H), 7.03-7.00 (m, 3H), 6.90 (d, $J = 8.0$ Hz, 2H), 6.84 (d, $J = 8.4$ Hz, 2H), 4.58-4.52 (m, 1H), 4.46 (q, $J = 7.2$ Hz, 2H), 1.42 (t, $J = 7.0$ Hz, 3H), 1.33 (d, $J = 5.6$ Hz, 6H).

1,5-bis(4-isopropoxyphenyl)-1H-pyrazole-3-carboxylic acid (16a): Followed General Procedure L with **15a** (92%). δ_{H} (400 MHz, d_6 -DMSO) 7.19 (d, 2H, Ar, $J = 8.8$ Hz), 7.12 (d, 2H, Ar, $J = 8.4$ Hz), 6.93 (d, 2H, Ar, $J = 8.4$ Hz), 6.86 (d, 2H, Ar, 8.4 Hz), 6.71 (s, 1H, Ar), 4.66-4.58 (m, 2H, CH(CH₃)₃), 1.26 (t, 12H, CH(CH₃)₃, $J = 14$ Hz); δ_{C} (400 MHz, d_6 -DMSO) 165.4, 157.7, 157.1, 150.4, 143.2, 133.1, 130.1, 127.2, 122.4, 115.9, 115.7, 108.5, 69.8, 69.5, 22.2, 22.1

1-(4-isopropoxyphenyl)-5-(4-phenoxyphenyl)-1H-pyrazole-3-carboxylic acid (16b): Followed General Procedure L with **15b** (97%). δ_{H} (400 MHz, d_6 -DMSO) 7.41 (t, 2H, Ar, $J = 7.8$ Hz), 7.21 (t, 5H, Ar, $J = 8.4$ Hz), 7.05 (d, 2H, Ar, $J = 7.6$ Hz), 6.93 (d, 2H, Ar, $J = 8.8$ Hz), 6.74 (s, 1H, Ar), 4.66-4.60 (m, 1H, CH(CH₃)₃), 1.26 (d, 6H, CH(CH₃)₃, $J = 5.2$ Hz); δ_{C} (400 MHz, d_6 -DMSO) 170.3, 162.1, 162.0, 147.5, 138.0, 135.5, 132.2, 130.5, 129.4, 124.6, 123.4, 120.9, 113.8, 74.8, 27.1

1,5-bis(4-isopropoxyphenyl)-N-((4-(trifluoromethoxy)phenyl)sulfonyl)-1H-pyrazole-3-carboxamide (17a): Followed General Procedure M with **16a** and 4-(trifluoromethyl)benzenesulfonamide: (54%). δ_{H} (400 MHz, CDCl₃) 8.23 (d, 2H, Ar, $J = 8.8$ Hz), 7.36 (d, 2H, Ar, $J = 8.8$ Hz), 7.17 (d, 2H, Ar, $J = 9.6$ Hz), 7.06 (d, 2H, Ar, 8.4 Hz), 6.91 (s, 1H, Ar), 6.87 (d, 2H, Ar, $J = 9.2$ Hz), 6.78 (d, 2H, Ar, $J = 8.4$ Hz), 4.58-4.51 (m, 2H, CH(CH₃)₃), 1.35 (d, 6H, CH(CH₃)₃, $J = 6$ Hz), 1.32 (d, 6H, CH(CH₃)₃, $J = 6.4$ Hz)

1-(4-isopropoxyphenyl)-5-(4-phenoxyphenyl)-N-((4-(trifluoromethoxy)phenyl)sulfonyl)-1Hpyrazole-3-carboxamide (17b): Followed General Procedure M with **16b** and 4-(trifluoromethyl)benzenesulfonamide: (65%). δ_{H} (400MHz, CDCl₃) 9.41 (s, 1H), 8.23 (d, $J = 8.8$ Hz, 2H), 7.36 (t, $J = 7.8$ Hz, 4H), 7.17 (t, $J = 7.0$ Hz, 3H), 7.11 (d, $J = 8.4$ Hz,

2H), 7.02 (d, $J = 8.4$ Hz, 2H), 6.95 (s, 1H), 6.90-6.87 (m, 4H), 4.58-4.56 (m, 1H), 1.36 (d, $J = 6.0$ Hz, 6H).

1-(4-isopropoxyphenyl)-5-(4-phenoxyphenyl)-N-((4-phenoxyphenyl)sulfonyl)-1H-pyrazole-3-carboxamide (17c): Followed *General Procedure 5* with **16b** and 4-phenoxybenzenesulfonamide (58%). δ_{H} (400 MHz, d_6 -DMSO) 8.00 (d, 2H, Ar, $J = 8.8$ Hz), 7.48 (t, 2H, Ar, $J = 8$ Hz), 7.41 (d, 2H, Ar, $J = 8$ Hz), 7.30-7.23 (m, 6H, Ar), 7.16 (t, 4H, Ar, $J = 8.6$ Hz), 7.06 (t, 3H, Ar, $J = 10.2$ Hz), 6.97 (t, 4H, Ar, $J = 10.2$ Hz), 4.68-4.63 (m, 1H, $\text{CH}(\text{CH}_3)_3$), 1.27 (d, 6H, $\text{CH}(\text{CH}_3)_3$, $J = 6.4$ Hz); δ_{C} (400 MHz, CDCl_3) 162.6, 158.6, 158.0, 154.8, 145.3, 144.0, 131.7, 131.4, 130.9, 130.1, 126.6, 126.3, 125.1, 124.1, 123.4, 120.5, 119.9, 119.7, 118.0, 117.9, 117.2, 115.9, 107.9, 70.3, 21.9

1-(4-isopropoxyphenyl)-N-(naphthalen-2-ylsulfonyl)-5-(4-phenoxyphenyl)-1H-pyrazole-3-carboxamide (17d): Followed *General Procedure 5* with **16b** and naphthalene-2-sulfonamide (49%). δ_{H} (400 MHz, d_6 -DMSO) 8.14 (d, 2H, Ar, $J = 8.8$ Hz), 7.95 (d, 1H, Ar, $J = 8.8$ Hz), 7.66 (d, 2H, Ar, $J = 7.6$ Hz), 7.59 (d, 1H, Ar, $J = 8.8$ Hz), 7.51 (s, 1H, Ar), 7.42 (t, 2H, Ar, $J = 7.8$ Hz), 7.25 (t, 3H, Ar, $J = 10.2$), 7.19 (t, 2H, Ar, $J = 7.4$ Hz), 7.07 (t, 3H, Ar, $J = 14$ Hz), 7.01-6.94 (m, 4H, Ar), 4.68-4.63 (m, 1H, $\text{CH}(\text{CH}_3)_3$), 1.27 (d, 6H, $\text{CH}(\text{CH}_3)_3$, $J = 5.6$ Hz); δ_{C} (400 MHz, d_6 -DMSO) 160.3, 157.8, 144.5, 136.9, 135.1, 134.3, 132.1, 131.8, 130.8, 129.9, 129.7, 129.5, 128.7, 128.2, 127.5, 126.1, 124.6, 124.0, 122.9, 122.5, 119.8, 116.1, 108.6, 70.0, 22.1

ethyl 2,5-bis(4-isopropoxyphenyl)thiazole-4-carboxylate (22): Prepared analogously to those compounds in: Hodgetts, Kevin J. and Kershaw, Mark T., *Organic Letters*, 4(8), 1363-1365; 2002

2,5-bis(4-isopropoxyphenyl)thiazole-4-carboxylic acid (23): Followed General Procedure R. δ_{H} (400 MHz, CDCl₃) 7.84 (d, 2H, Ar, $J = 7.6$ Hz), 7.63 (d, 2H, Ar, $J = 8.8$ Hz), 6.94 (t, 4H, Ar, $J = 9$ Hz), 4.65-4.60 (m, 2H, CH(CH₃)₃), 1.38-1.36 (m, 12H, CH(CH₃)₃)

2,5-bis(4-isopropoxyphenyl)-N-((4-(trifluoromethoxy)phenyl)sulfonyl)thiazole-4-carboxamide (24a): Followed General Procedure S. δ_{H} (400 MHz, CDCl₃) 8.21 (d, 2H, Ar, $J = 9.2$ Hz), 7.82 (d, 2H, Ar, $J = 8.8$ Hz), 7.54 (d, 2H, Ar, $J = 8.8$ Hz), 7.33 (d, 2H, Ar, $J = 8.4$ Hz), 6.96 (d, 2H, Ar, $J = 8.8$ Hz), 6.88 (d, 2H, Ar, $J = 8.8$ Hz), 4.66-4.58 (m, 2H, CH(CH₃)₃), 1.39-1.35 (m, 12H, CH(CH₃)₃); δ_{C} (400 MHz, CDCl₃) 164.6, 160.3, 159.2, 158.1, 152.8, 147.5, 137.7, 137.1, 131.5, 130.7, 128.1, 124.3, 120.5, 115.9, 15.2, 70.1, 69.9, 21.9, 21.9

2,5-bis(4-isopropoxyphenyl)-N-((4-phenoxyphenyl)sulfonyl)thiazole-4-carboxamide (24b): Followed General Procedure S. δ_{H} (400 MHz, CDCl₃) 8.08 (d, 2H, Ar, $J = 8.4$ Hz), 7.83 (d, 2H, Ar, $J = 8.8$ Hz), 7.56 (d, 2H, Ar, $J = 8.4$ Hz), 7.39 (t, 2H, Ar, $J = 7.8$ Hz), 7.21 (t, 1H, Ar, $J = 7.4$ Hz), 7.05 (d, 2H, Ar, $J = 7.6$ Hz), 7.01 (d, 2H, Ar, $J = 8.4$ Hz), 6.96 (d, 2H, Ar, $J = 8.8$ Hz), 6.86 (d, 2H, Ar, $J = 8.4$ Hz), 4.66-4.58 (m, 2H, CH(CH₃)₃), 1.39-1.35 (m, 12H, CH(CH₃)₃)

2,5-bis(4-isopropoxyphenyl)-N-(naphthalen-2-ylsulfonyl)thiazole-4-carboxamide (24c): Followed General Procedure S. δ_{H} (400 MHz, CDCl₃) 8.73 (s, 1H, Ar), 8.08 (d, 1H, Ar, $J = 8.8$ Hz), 8.00 (d, 1H, Ar, $J = 8$ Hz), 7.95 (d, 1H, Ar, $J = 8.4$ Hz), 7.88 (d, 1H, Ar, $J = 7.6$ Hz), 7.83 (d, 2H, Ar, $J = 8.4$ Hz), 7.65-7.57 (m, 2H, Ar), 7.51 (d, 2H, Ar, $J = 8.4$ Hz), 6.96 (d, 2H, Ar, $J = 8.4$ Hz), 6.84 (d, 2H, Ar, $J = 8.4$ Hz), 4.66-4.53 (m, 2H, CH(CH₃)₃), 1.39 (d, 6H, CH(CH₃)₃), $J = 6.4$ Hz), 1.34 (d, 6H, CH(CH₃)₃), $J = 6.4$ Hz)

2.7.2. Biology

Materials. All chemical reagents were ACS grade or higher unless otherwise indicated.

The D₂O, D₆-DMSO, and ¹⁵NH₄Cl were purchased from Cambridge Isotope Laboratories, Inc. (Andover, MA). All other chemicals were purchased from Sigma-Aldrich (St. Louis, MO).

Proteins. The pET30a expression vector (EMD Millipore, Billerica, MA) was used to express N-terminal His6-tagged Hdm2 N-terminal domain residues 1 to 155 (Hdm21-115) in HMS174 (DE3) cells (EMD Millipore). Briefly, the ¹⁵N-labeled protein was purified (>98% final) from inclusion bodies by initial solubilizing in 6 M guanidium chloride in PBS, pH 7.4, with 0.5 mM TCEP. The denatured protein was refolded by rapid dilution into 6-fold volume of PBS, pH 7.4, with 0.5 mM TCEP. The folded protein was then captured on Q-sepharose resin and eluted with a linear gradient of 0 to 2 M NaCl in 10 mM Na₃PO₄, pH 7.0, and 1 mM DTT. Then (NH₄)₂SO₄ powder was added to reach a final concentration of 0.8 M by slow addition over 30 minutes and stirring for an additional 30 minutes. The sample was added to a butyl sepharose column preconditioned with 0.8 M (NH₄)₂SO₄, 10 mM Na₃PO₄, pH 7.0, and 1 mM DTT buffer. The sample was eluted with a linear gradient of decreasing (NH₄)₂SO₄ to a final buffer of 10 mM Na₃PO₄, pH 7.0, and 1 mM DTT. The protein was concentrated using a 10,000 MWCO centrifugal filter concentrator (EMD Millipore) and the concentrate stored frozen in the same buffer. The pLM302 expression vector was constructed to produce His6-MBP (maltose binding protein) tagged recombinant human Mcl-1 residues 172 to 327 (Mcl-1 172-327) in HMS174 (DE3) cells (EMD Millipore) using either LB or minimal media supplemented with ¹⁵NH₄Cl to produce unlabeled or ¹⁵N-labeled Mcl-1, respectively. The tagged protein was initially purified from the crude cell lysate by IMAC chromatography (GE Healthcare Life Sciences), and after dialysis to remove the imidazole the affinity tag was cleaved using PreScission Protease (GE

Healthcare Life Sciences). A Sephacryl S-200 size exclusion column was used as a final purification step before the protein was concentrated with a 10,000 MWCO centrifugal filter concentrator (EMD Millipore). The concentrations of the proteins were determined using the Bio-Rad Protein Assay (Bio-Rad Inc., Hercules, CA) using BSA of a known concentration as the standard (Pierce). The purity of the protein was confirmed using SDS-PAGE analysis and NMR HSQC experiments were done to confirm the protein was properly folded (data not shown).

Peptides. A 6-aminohexanoic acid linker was conjugated to the N-terminus of the Bak BH3 peptide (GQVGRQLAIIGDDINR), capped with fluorescein (on the amino group of the linker), and the peptide was amidated on the C-terminus to give FITC-Ahx-GQVGRQLAIIGDDINR-CONH₂, hereafter referred to as “FITC-Bak⁷¹⁻⁸⁹” (synthesized by Neo BioScience in >95% purity). The p53 peptides were derived from the N-terminal human p53, residues 15-29 (SQETFSDLWKLLPEN) with TAMRA-labeled (TAMRA-p53¹⁵⁻²⁹) N-terminus. Each peptide was soluble and stored in H₂O at pH 7. The concentration of the stock solution of unlabeled peptides were determined by quantitative amino acid analysis (Biosynthesis Inc., Lewisville, TX), the concentration of FITC peptides was determined at pH 8.0 using the extinction coefficient for amide-linked FITC, $\epsilon_{494} = 68,000 \text{ cm}^{-1}\text{M}^{-1}$, and the concentration of the TAMRA peptide was determined using the extinction coefficient for TAMRA, $\epsilon_{547} = 65,000 \text{ cm}^{-1}\text{M}^{-1}$. All peptides were synthesized using solid-state peptide synthesis and their purity was determined to be >95% by high pressure liquid chromatography and mass spectrometry.

Fluorescence anisotropy experiments. Fluorescence anisotropy experiments were conducted using a PHERAstar FS (BMG Labtech) multimode microplate reader equipped with two PMTs for simultaneous measurements of the perpendicular and parallel fluorescence emission. In addition, the absolute anisotropy measurements were made on a

Cary Eclipse Fluorescence Spectrophotometer (Agilent Technologies) equipped with automated polarizers.

The fluorescence anisotropy assays were performed in black polypropylene 384-well microplate (Costar) with a final volume of 20 μ L. Initially the affinity (K_d) of the FITC-Bak⁷¹⁻⁸⁹ peptide was determined by titrating Mcl-1¹⁷²⁻³²⁷ into 10 nM FITC-Bak⁷¹⁻⁸⁹ peptide in 20 mM HEPES, pH 6.8, 50 mM NaCl, 3 mM DTT, 0.01% Triton X-100 and 5% DMSO at room temperature while monitoring the perpendicular and parallel fluorescence emission with a 485 nm excitation and 520 nm emission filters. The fluorescence anisotropy competition assay was performed using 100 nM Mcl-1¹⁷²⁻³²⁷ in the same buffer (10 nM FITC-Bak⁷¹⁻⁸⁹ peptide in 20 mM HEPES, pH 6.8, 50 mM NaCl, 3 mM DTT, 0.01% Triton X-100 and 5% DMSO) with varying concentrations of either unlabeled peptide or experimental compounds.

Similarly, the affinity of TAMRA-p53¹⁵⁻²⁹ was determined by the titration of Hdm2¹⁻¹¹⁵ into 10 nM TAMRA-p53¹⁵⁻²⁹ peptide in PBS with 0.01% Triton X-100 and 5% DMSO at room temperature with a 544 nm excitation and 590 nm emission filters. The fluorescence polarization assays (FPCA) were performed using 10 μ M Hdm2¹⁻¹¹⁵ in the same buffer (PBS with 0.01% Triton X-100 and 5% DMSO) with varying concentrations of unlabeled p53¹⁵⁻²⁹ peptide or experimental compounds.

The initial binding affinities (K_d) were determined by fitting the binding data to the Dose Response function in the Origin software (OriginLab, Northampton, MA): $y = A_1 + (A_2 - A_1) / (1 + 10^{(\text{LOG}x^0 - x)p})$ such that dynamic range = abs ($A_1 - A_2$) and the $K_d = 10^{\text{LOG}x^0}$. The IC_{50} in the competition assays were determined by fitting the binding data to the One Site

Competition function in the Origin software (OriginLab, Northampton, MA): $y = A_2 + (A_1 - A_2) / (1 + 10^{(x - \log x_0)})$ such that dynamic range = $\text{abs}(A_1 - A_2)$ and the $IC_{50} = 10^{\log x_0}$. It has been shown that each of the proteins used here binds a single target peptide (1:1 stoichiometry) at the concentrations used in the competition assays¹⁻³. Therefore, we are able to use an equation derived by Nikolovska-Coleska et al.⁴ to calculate the K_d from the IC_{50} from the anisotropy competition assays. The affinity (K_d) of TAMRA-p53¹⁵⁻²⁹ for Hdm²¹⁻¹¹⁵ was determined to be $6.51 \pm 0.44 \mu\text{M}$, and the affinity of FITC-Bak⁷¹⁻⁸⁹ for Mcl-1¹⁷²⁻³²⁷ was determined to be $41.96 \pm 2.78 \text{ nM}$ and $6.67 \pm 0.05 \text{ nM}$, respectively, in the assay conditions used.

The quality and suitability of the fluorescence anisotropy competition assays were evaluated using the Z-factor developed by Zhang et al.⁵ The Z-factor = $1 - (3SD_b + 3SD_f) / (|\mu_b - \mu_f|)$ where μ_b and μ_f are the mean anisotropy (mA) values of the bound and free probe, respectively, and SD_b and SD_f are the standard deviations of those values for bound and free probe, respectively. The Z-factor can be any value ≤ 1 , with a value of 1 being an ideal assay, ≥ 0.5 but < 1.0 being an excellent assay, and a value < 0.5 being unacceptable for our application.

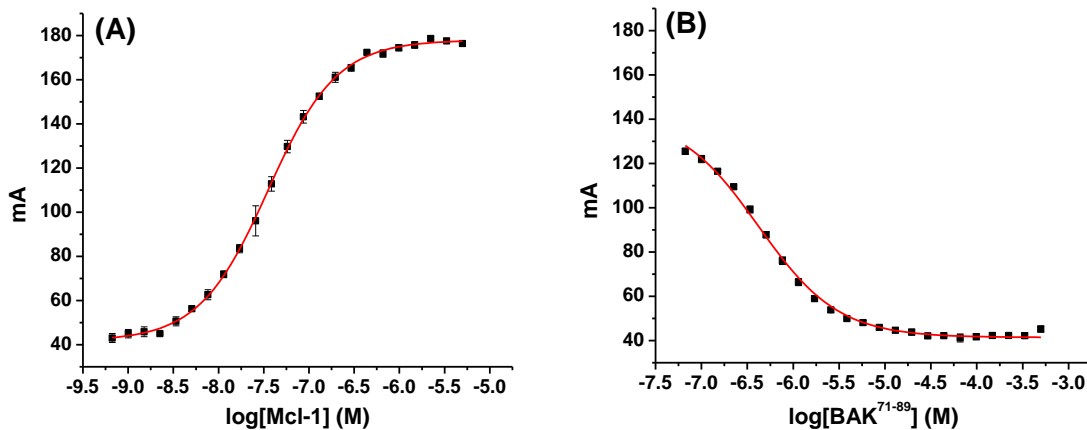


Figure S1. (A) Titration of Mcl-1¹⁷²⁻³²⁷ into 10 nM FITC-BAK⁷¹⁻⁸⁹ gives a K_D of 41.96 ± 2.78 nM with the free FITC-BAK peptide having an absolute anisotropy value of 41.4 ± 1.4 mA (this is the same as Mcl-1 assay b/c same peptide, buffer and conditions) and the Mcl-1 bound peptide 178.0 ± 1.4 mA. (B) The FITC-BAK⁷¹⁻⁸⁹ was competed off Mcl-1¹⁷²⁻³²⁷ with unlabeled BAK⁷¹⁻⁸⁹ peptide with an IC_{50} of 418.19 ± 37.77 nM giving a calculated K_D of 101.84 ± 12.37 nM. For this competition assay 60 nM Mcl-1¹⁷²⁻³²⁷ was used and gives an excellent Z-factor of 0.79 with a dynamic range of 86.96 ± 0.32 mA.

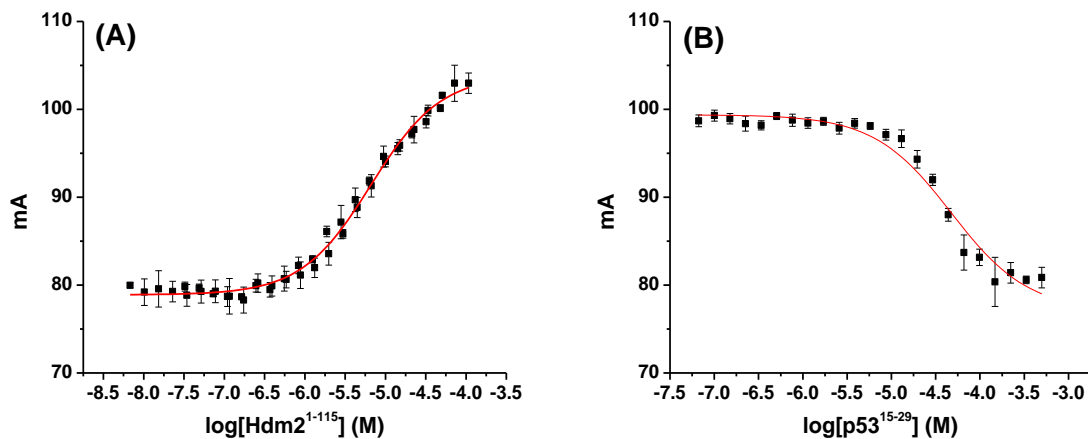


Figure S2. (A) Titration of Hdm2¹⁻¹¹⁵ into 10 nM TAMRA-p53¹⁵⁻²⁹ gives a K_d of 6.51 ± 0.44 μ M with the free TAMRA-p53¹⁵⁻²⁹ peptide having an absolute anisotropy value of 80.1 ± 1.3 mA and the Hdm2¹⁻¹¹⁵ bound peptide 102.9 ± 1.5 mA. (B) The TAMRA-p53¹⁵⁻²⁹ was competed with unlabeled p53¹⁵⁻²⁹ with an IC_{50} of 49.36 ± 1.13 μ M giving a calculated K_d of 16.64 ± 0.44 μ M. Using 10 μ M Hdm2¹⁻¹¹⁵ for the competition assay gives a good Z-factor of 0.58 and a dynamic

range of 19.57 ± 0.64 mA. The same conditions were used to test all compounds but no competition was seen.

2.7.3. References

- (1) Willis S.N., Chen, L., Dewson, G., Wei, A., Naik E., Fletcher J. I., Adams, J. M., Huang, D. C. S. Proapoptotic Bak is sequestered by Mcl-1 and Bcl-xL, but not Bcl-2, until displaced by BH3-only proteins. *Genes Dev.* **2005**, *19* (11), 1294-1305.
- (2) Stewart, M. L., Fire, E., Keating, A. E., Walensky, L. D. The Mcl-1 BH3 helix is an exclusive Mcl-1 inhibitor and apoptosis sensitizer. *Nat Chem Biol.* **2010**, *6* (8), 595-601.
- (3) Popowicz G.M., Czarna A., Holak T.A.. Structure of the human Mdmx protein bound to the p53 tumor suppressor transactivation domain. *Cell Cycle.* **2008**, *7*(15), 2441-3.
- (4) Nikolovska-Coleska Z., Wang R., Fang X., Pan H., Tomita Y., Li P., et al. Development and optimization of a binding assay for the XIAP BIR3 domain using fluorescence polarization. *Anal Biochem.* **2004**, *332* (2), 261-73.
- (5) Zhang J.H., Chung T.D., Oldenburg K.R. A Simple Statistical Parameter for Use in Evaluation and Validation of High Throughput Screening Assays. *J Biomol Screen.* **1999**, *4* (2), 67-73.

2.8. References

- (1) Janda, A. L. G. and K. D. Protein-Protein Interactions and Cancer: Targeting the Central Dogma <http://www.eurekaselect.com/87258/article>
- (2) Mabonga, L.; Kappo, A. P. Protein-Protein Interaction Modulators: Advances, Successes and Remaining Challenges. *Biophys. Rev.* **2019**, *11* (4), 559–581.
- (3) Akhtar, R. S.; Ness, J. M.; Roth, K. A. Bcl-2 Family Regulation of Neuronal Development and Neurodegeneration. *Biochim. Biophys. Acta BBA - Mol. Cell Res.* **2004**, *1644* (2), 189–203.
- (4) Sassone, J.; Maraschi, A.; Sassone, F.; Silani, V.; Ciammola, A. Defining the Role of the Bcl-2 Family Proteins in Huntington’s Disease. *Cell Death Dis.* **2013**, *4* (8), 772–772.
- (5) Luciani, D. S.; White, S. A.; Widenmaier, S. B.; Saran, V. V.; Taghizadeh, F.; Hu, X.; Allard, M. F.; Johnson, J. D. Bcl-2 and Bcl-XL Suppress Glucose Signaling in Pancreatic β -Cells. *Diabetes* **2013**, *62* (1), 170–182.

- (6) Fletcher, S.; Hamilton, A. D. Protein Surface Recognition and Proteomimetics: Mimics of Protein Surface Structure and Function. *Curr. Opin. Chem. Biol.* **2005**, *9* (6), 632–638.
- (7) Lanning, M. E.; Fletcher, S. Recapitulating the α -Helix: Nonpeptidic, Low-Molecular-Weight Ligands for the Modulation of Helix-Mediated Protein–Protein Interactions. *Future Med. Chem.* **2013**, *5* (18), 2157–2174.
- (8) Azzarito, V.; Long, K.; Murphy, N. S.; Wilson, A. J. Inhibition of α -Helix-Mediated Protein-Protein Interactions Using Designed Molecules. *Nat. Chem.* **2013**, *5* (3), 161–173.
- (9) Arkin, M. Protein–Protein Interactions and Cancer: Small Molecules Going in for the Kill. *Curr. Opin. Chem. Biol.* **2005**, *9* (3), 317–324.
- (10) Lampson, B. L.; Davids, M. S. The Development and Current Use of BCL-2 Inhibitors for the Treatment of Chronic Lymphocytic Leukemia. *Curr. Hematol. Malig. Rep.* **2017**, *12* (1), 11–19.
- (11) Tisato, V.; Voltan, R.; Gonelli, A.; Secchiero, P.; Zauli, G. MDM2/X Inhibitors under Clinical Evaluation: Perspectives for the Management of Hematological Malignancies and Pediatric Cancer. *J. Hematol. Oncol. J Hematol Oncol* **2017**, *10* (1), 133.
- (12) Phase I Study of MIK665, a Mcl-1 Inhibitor, in Patients With Refractory or Relapsed Lymphoma or Multiple Myeloma. <https://clinicaltrials.gov/ct2/show/NCT02992483>
- (13) Study of Safety and Efficacy of HDM201 in Combination With LEE011 in Patients With Liposarcoma. <https://clinicaltrials.gov/ct2/show/NCT02343172>
- (14) Lanning, M. E.; Wilder, P. T.; Bailey, H.; Drennen, B.; Cavalier, M.; Chen, L.; Yap, J. L.; Raje, M.; Fletcher, S. Towards More Drug-like Proteomimetics: Two-Faced, Synthetic α -Helix Mimetics Based on a Purine Scaffold. *Org. Biomol. Chem.* **2015**, *13* (32), 8642–8646.
- (15) Petros, A. M.; Olejniczak, E. T.; Fesik, S. W. Structural Biology of the Bcl-2 Family of Proteins. *Biochim. Biophys. Acta* **2004**, *1644* (2–3), 83–94.
- (16) Barnard, A.; Long, K.; Yeo, D. J.; Miles, J. A.; Azzarito, V.; Burslem, G. M.; Prabhakaran, P.; A Edwards, T.; Wilson, A. J. Orthogonal Functionalisation of α -Helix Mimetics. *Org. Biomol. Chem.* **2014**, *12* (35), 6794–6799.

- (17) Czabotar, P. E.; Lessene, G.; Strasser, A.; Adams, J. M. Control of Apoptosis by the BCL-2 Protein Family: Implications for Physiology and Therapy. *Nat. Rev. Mol. Cell Biol.* **2014**, *15* (1), 49–63.
- (18) Vousden, K. H.; Lane, D. P. P53 in Health and Disease. *Nat. Rev. Mol. Cell Biol.* **2007**, *8* (4), 275–283.
- (19) Youle, R. J.; Strasser, A. The BCL-2 Protein Family: Opposing Activities That Mediate Cell Death. *Nat. Rev. Mol. Cell Biol.* **2008**, *9* (1), 47–59.
- (20) Adams, C. M.; Clark-Garvey, S.; Porcu, P.; Eischen, C. M. Targeting the Bcl-2 Family in B Cell Lymphoma. *Front. Oncol.* **2019**, *8*.
- (21) Lee, M.-S.; Ha, J.-H.; Yoon, H. S.; Lee, C.-K.; Chi, S.-W. Structural Basis for the Conserved Binding Mechanism of MDM2-Inhibiting Peptides and Anti-Apoptotic Bcl-2 Family Proteins. *Biochem. Biophys. Res. Commun.* **2014**, *445* (1), 120–125.
- (22) Vu, B.; Wovkulich, P.; Pizzolato, G.; Lovey, A.; Ding, Q.; Jiang, N.; Liu, J.-J.; Zhao, C.; Glenn, K.; Wen, Y.; Tovar, C.; Packman, K.; Vassilev, L.; Graves, B. Discovery of RG7112: A Small-Molecule MDM2 Inhibitor in Clinical Development. *ACS Med. Chem. Lett.* **2013**, *4* (5), 466–469.
- (23) Saha, M. N.; Jiang, H.; Chang, H. Molecular Mechanisms of Nutlin-Induced Apoptosis in Multiple Myeloma. *Cancer Biol. Ther.* **2010**, *10* (6), 567–578.
- (24) Toufekhtchan, E.; Toledo, F. The Guardian of the Genome Revisited: P53 Downregulates Genes Required for Telomere Maintenance, DNA Repair, and Centromere Structure. *Cancers* **2018**, *10* (5).
- (25) Teoh, G.; Urashima, M.; Ogata, A.; Chauhan, D.; DeCaprio, J. A.; Treon, S. P.; Schlossman, R. L.; Anderson, K. C. MDM2 Protein Overexpression Promotes Proliferation and Survival of Multiple Myeloma Cells. *Blood* **1997**, *90* (5), 1982–1992.
- (26) Kojima, K.; Konopleva, M.; McQueen, T.; O’Brien, S.; Plunkett, W.; Andreeff, M. Mdm2 Inhibitor Nutlin-3a Induces P53-Mediated Apoptosis by Transcription-Dependent and Transcription-Independent Mechanisms and May Overcome Atm-Mediated Resistance to Fludarabine in Chronic Lymphocytic Leukemia. *Blood* **2006**, *108* (3), 993–1000.
- (27) Leu, J. I.-J.; Dumont, P.; Hafey, M.; Murphy, M. E.; George, D. L. Mitochondrial P53 Activates Bak and Causes Disruption of a Bak–Mcl1 Complex. *Nat. Cell Biol.* **2004**, *6* (5), 443–450.
- (28) Kojima, K.; McQueen, T.; Chen, Y.; Jacamo, R.; Konopleva, M.; Shinojima, N.; Shpall, E.; Huang, X.; Andreeff, M. P53 Activation of Mesenchymal Stromal Cells

Partially Abrogates Microenvironment-Mediated Resistance to FLT3 Inhibition in AML through HIF-1 α -Mediated down-Regulation of CXCL12. *Blood* **2011**, *118* (16), 4431–4439.

- (29) Chipuk, J. E.; Kuwana, T.; Bouchier-Hayes, L.; Droin, N. M.; Newmeyer, D. D.; Schuler, M.; Green, D. R. Direct Activation of Bax by P53 Mediates Mitochondrial Membrane Permeabilization and Apoptosis. *Science* **2004**, *303* (5660), 1010–1014.
- (30) Besbes, S.; Billard, C. First MCL-1-Selective BH3 Mimetics as Potential Therapeutics for Targeted Treatment of Cancer. *Cell Death Dis.* **2015**, *6* (7), e1810–e1810.
- (31) Kotschy, A.; Szlavik, Z.; Murray, J.; Davidson, J.; Maragno, A. L.; Le Toumelin-Braizat, G.; Chanrion, M.; Kelly, G. L.; Gong, J.-N.; Moujalled, D. M.; Bruno, A.; Csekei, M.; Paczal, A.; Szabo, Z. B.; Sipos, S.; Radics, G.; Proszenyak, A.; Balint, B.; Ondi, L.; Blasko, G.; Robertson, A.; Surgenor, A.; Dokurno, P.; Chen, I.; Matassova, N.; Smith, J.; Pedder, C.; Graham, C.; Studeny, A.; Lysiak-Auvity, G.; Girard, A.-M.; Gravé, F.; Segal, D.; Riffkin, C. D.; Pomilio, G.; Galbraith, L. C. A.; Aubrey, B. J.; Brennan, M. S.; Herold, M. J.; Chang, C.; Guasconi, G.; Cauquil, N.; Melchiorre, F.; Guigal-Stephan, N.; Lockhart, B.; Colland, F.; Hickman, J. A.; Roberts, A. W.; Huang, D. C. S.; Wei, A. H.; Strasser, A.; Lessene, G.; Geneste, O. The MCL1 Inhibitor S63845 Is Tolerable and Effective in Diverse Cancer Models. *Nature* **2016**, *538* (7626), 477–482.
- (32) Carry, J.-C.; Garcia-Echeverria, C. Inhibitors of the P53/Hdm2 Protein–Protein Interaction—Path to the Clinic. *Bioorg. Med. Chem. Lett.* **2013**, *23* (9), 2480–2485.
- (33) Drennen, B.; Scheenstra, J. A.; Yap, J. L.; Chen, L.; Lanning, M. E.; Roth, B. M.; Wilder, P. T.; Fletcher, S. Structural Re-Engineering of the α -Helix Mimetic JY-1-106 into Small-Molecules: Disruption of the Mcl-1–Bak-BH3 Protein–Protein Interaction with 2,6-Di-Substituted Nicotinates. *ChemMedChem* **2016**, *11* (8), 827–833; E. Whiting, M. R. Raje, J. Chauhan, P. T. Wilder, D. Van Eker, S. J. Hughes, N. G. Bowen, G. E. A. Vickers, I. C. Fenimore, S. Fletcher, Discovery of Mcl-1 inhibitors based on a thiazolidine-2,4-dione scaffold. *Bioorg. Med. Chem. Lett.* **2018**, *28*, 523–528; I. L. Conlon, D. Van Eker, S. Abdelmalak, W. A. Murphy, H. Bashir, M. Sun, J. Chauhan, K. M. Varney, R. GodoyRuiz, P. T. Wilder, S. Fletcher, Kröhnke pyridines: Rapid and facile access to Mcl-1 inhibitors. *Bioorg. Med. Chem. Lett.* **2018**, *28*, 1949–1953; M. E. Lanning, W. Yu, J. L. Yap, J. Chauhan, L. Chen, E. Whiting, L. S. Pidugu, T. Atkinson, H. Bailey, W. Li, B. M. Roth, L. Hynicka, K. Chesko, E. A. Toth, P. Shapiro, A. D. MacKerell Jr, P. T. Wilder, S. Fletcher, Structure-based design of N-substituted 1-hydroxy-4-sulfamoyl-2-naphthoates as selective inhibitors of the Mcl-1 oncoprotein. *Eur. J. Med. Chem.* **2016**, *113*, 273–292; M. E. Lanning, P. T. Wilder, H. Bailey, B. Drennen, M. Cavalier, L. Chen, J. L. Yap, M. Raje, S. Fletcher, Towards more drug-like proteomimetics: two-faced, synthetic α -helix mimetics based on a purine scaffold. *Org. Biomol. Chem.* **2015**, *13*, 8642–8646.

- (34) Fletcher, S. MCL-1 Inhibitors - Where Are We Now (2019)? *Expert Opin. Ther. Pat.* **2019**, *29* (11), 909–919; J. L. Yap, L. Chen, M. E. Lanning, S. Fletcher, *J. Med. Chem.* **2017**, *60*, 821–838.
- (35) Beloglazkina, A.; Zyk, N.; Majouga, A.; Beloglazkina, E. Recent Small-Molecule Inhibitors of the P53–MDM2 Protein–Protein Interaction. *Molecules* **2020**, *25* (5) <https://doi.org/10.3390/molecules25051211>.
- (36) AbbVie Announces US FDA Approval of Venetoclax (venetoclax) as a Chemotherapy-Free Combination Regimen for Previously Untreated Chronic Lymphocytic Leukemia Patients <https://www.drugs.com/newdrugs/abbvie-announces-us-fda-approval-venetoclax-venetoclax-chemotherapy-free-combination-regimen-4974.html>
- (37) Friberg, A.; Vigil, D.; Zhao, B.; Daniels, R. N.; Burke, J. P.; Garcia-Barrantes, P. M.; Camper, D.; Chauder, B. A.; Lee, T.; Olejniczak, E. T.; Fesik, S. W. Discovery of Potent Myeloid Cell Leukemia 1 (Mcl-1) Inhibitors Using Fragment-Based Methods and Structure-Based Design. *J. Med. Chem.* **2013**, *56* (1), 15–30.
- (38) Punnoose, E. A.; Levenson, J. D.; Peale, F.; Boghaert, E. R.; Belmont, L. D.; Tan, N.; Young, A.; Mitten, M.; Ingalla, E.; Darbonne, W. C.; Oleksijew, A.; Tapang, P.; Yue, P.; Oeh, J.; Lee, L.; Maiga, S.; Fairbrother, W. J.; Amiot, M.; Souers, A. J.; Sampath, D. Expression Profile of BCL-2, BCL-XL, and MCL-1 Predicts Pharmacological Response to the BCL-2 Selective Antagonist Venetoclax in Multiple Myeloma Models. *Mol. Cancer Ther.* **2016**, *15* (5), 1132–1144.
- (39) Konopleva, M.; Pollyea, D. A.; Potluri, J.; Chyla, B.; Hogdal, L.; Busman, T.; McKeegan, E.; Salem, A. H.; Zhu, M.; Ricker, J. L.; Blum, W.; DiNardo, C. D.; Kadia, T.; Dunbar, M.; Kirby, R.; Falotico, N.; Levenson, J.; Humerickhouse, R.; Mabry, M.; Stone, R.; Kantarjian, H.; Letai, A. Efficacy and Biological Correlates of Response in a Phase II Study of Venetoclax Monotherapy in Patients with Acute Myelogenous Leukemia. *Cancer Discov.* **2016**, *6* (10), 1106–1117.
- (40) Research, A. A. for C. BCL2/MDM2 Inhibitor Combo Effective in AML. *Cancer Discov.* **2019**, *9* (2), 156–156.
- (41) Seipel, K.; Schmitter, K.; Bacher, U.; Pabst, T. Rationale for a Combination Therapy Consisting of MCL1- and MEK-Inhibitors in Acute Myeloid Leukemia. *Cancers* **2019**, *11* (11). <https://doi.org/10.3390/cancers11111779>.
- (42) Reddy, A. S.; Zhang, S. Polypharmacology: Drug Discovery for the Future. *Expert Rev. Clin. Pharmacol.* **2013**, *6* (1). <https://doi.org/10.1586/ecp.12.74>.
- (43) Anighoro, A.; Bajorath, J.; Rastelli, G. Polypharmacology: Challenges and Opportunities in Drug Discovery. *J. Med. Chem.* **2014**, *57* (19), 7874–7887.

- (44) Rautureau, G. J. P.; Yabal, M.; Yang, H.; Huang, D. C. S.; Kvensakul, M.; Hinds, M. G. The Restricted Binding Repertoire of Bcl-B Leaves Bim as the Universal BH3-Only Prosurvival Bcl-2 Protein Antagonist. *Cell Death Dis.* **2012**, *3* (12), e443.
- (45) Wang, Z.; Song, T.; Feng, Y.; Guo, Z.; Fan, Y.; Xu, W.; Liu, L.; Wang, A.; Zhang, Z. Bcl-2/MDM2 Dual Inhibitors Based on Universal Pyramid-Like α -Helical Mimetics. *J. Med. Chem.* **2016**, *59* (7), 3152–3162.
- (46) Vaupel, A.; Bold, G.; De Pover, A.; Stachyra-Valat, T.; Hergovich Lisztwan, J.; Kallen, J.; Masuya, K.; Furet, P. Tetra-Substituted Imidazoles as a New Class of Inhibitors of the P53–MDM2 Interaction. *Bioorg. Med. Chem. Lett.* **2014**, *24* (9), 2110–2114.
- (47) Mady, A. S. A.; Liao, C.; Bajwa, N.; Kump, K. J.; Abulwerdi, F. A.; Lev, K. L.; Miao, L.; Grigsby, S. M.; Perdih, A.; Stuckey, J. A.; Du, Y.; Fu, H.; Nikolovska-Coleska, Z. Discovery of Mcl-1 Inhibitors from Integrated High Throughput and Virtual Screening. *Sci. Rep.* **2018**, *8*. <https://doi.org/10.1038/s41598-018-27899-9>.
- (48) Li, C.; Pazgier, M.; Li, C.; Yuan, W.; Liu, M.; Wei, G.; Lu, W.-Y.; Lu, W. Systematic Mutational Analysis of Peptide Inhibition of the P53-MDM2/MDMX Interactions. *J. Mol. Biol.* **2010**, *398* (2), 200–213.
- (49) Yin, H.; Lee, G.; Sedey, K. A.; Kutzki, O.; Park, H. S.; Orner, B. P.; Ernst, J. T.; Wang, H.-G.; Sebti, S. M.; Hamilton, A. D. Terphenyl-Based Bak BH3 α -Helical Proteomimetics as Low-Molecular-Weight Antagonists of Bcl-XL. *J. Am. Chem. Soc.* **2005**, *127* (29), 10191–10196.
- (50) Vassilev, L. T.; Vu, B. T.; Graves, B.; Carvajal, D.; Podlaski, F.; Filipovic, Z.; Kong, N.; Kammlott, U.; Lukacs, C.; Klein, C.; Fotouhi, N.; Liu, E. A. In Vivo Activation of the P53 Pathway by Small-Molecule Antagonists of MDM2. *Science* **2004**, *303* (5659), 844–848.
- (51) Bold, G.; Furet, P.; Gessier, F.; Kallen, J.; Lisztwan, J. H.; Masuya, K.; Vaupel, A. Tetra-Substituted Heteroaryl Compounds and Their Use as Mdm2 and/or Mdm4 Modulators. CA2771936A1, March 3, 2011.
- (52) Pelz, N. F.; Bian, Z.; Zhao, B.; Shaw, S.; Tarr, J. C.; Belmar, J.; Gregg, C.; Camper, D. V.; Goodwin, C. M.; Arnold, A. L.; Sensintaffar, J. L.; Friberg, A.; Rossanese, O. W.; Lee, T.; Olejniczak, E. T.; Fesik, S. W. Discovery of 2-Indole-Acylsulfonamide Myeloid Cell Leukemia 1 (Mcl-1) Inhibitors Using Fragment-Based Methods. *J. Med. Chem.* **2016**, *59* (5), 2054–2066.

- (53) Kapadiya, Dr. K.; Kavadia, K.; Manvar, P.; Kotadiya, R.; Kothari, R.; Ranjan, K. Catalyst Free Synthesis of Thiazole Derivatives Bearing Azo Imine Linkageas Antimicrobial Agents. *Chem. Biol. Interface* **2015**, *5*, 258–266.
- (54) Miyamoto, D. K.; Flaxman, H. A.; Wu, H.-Y.; Gao, J.; Woo, C. M. Discovery of a Celecoxib Binding Site on Prostaglandin E Synthase (PTGES) with a Cleavable Chelation-Assisted Biotin Probe. *ACS Chem. Biol.* **2019**, *14* (12), 2527–2532.
- (55) Gierse, J. K.; Zhang, Y.; Hood, W. F.; Walker, M. C.; Trigg, J. S.; Maziasz, T. J.; Koboldt, C. M.; Muhammad, J. L.; Zweifel, B. S.; Masferrer, J. L.; Isakson, P. C.; Seibert, K. Valdecoxib: Assessment of Cyclooxygenase-2 Potency and Selectivity. *J. Pharmacol. Exp. Ther.* **2005**, *312* (3), 1206–1212.
- (56) Guvench, O.; Jr, A. D. M. Computational Fragment-Based Binding Site Identification by Ligand Competitive Saturation. *PLOS Comput. Biol.* **2009**, *5* (7), e1000435.
- (57) Raman, E. P.; Yu, W.; Lakkaraju, S. K.; MacKerell, A. D. Inclusion of Multiple Fragment Types in the Site Identification by Ligand Competitive Saturation (SILCS) Approach. *J. Chem. Inf. Model.* **2013**, *53* (12), 3384–3398.
- (58) Ustach, V. D.; Lakkaraju, S. K.; Jo, S.; Yu, W.; Jiang, W.; MacKerell, A. D. Optimization and Evaluation of Site-Identification by Ligand Competitive Saturation (SILCS) as a Tool for Target-Based Ligand Optimization. *J. Chem. Inf. Model.* **2019**, *59* (6), 3018–3035.
- (59) Raman, E. P.; Yu, W.; Guvench, O.; MacKerell, A. D. Reproducing Crystal Binding Modes of Ligand Functional Groups Using Site-Identification by Ligand Competitive Saturation (SILCS) Simulations. *J. Chem. Inf. Model.* **2011**, *51* (4), 877–896.
- (60) Small, M.; MacKerell, A. D. Force Field Representation of Biomolecular Systems. In *In Silico Drug Discovery and Design: Theory, Methods, Challenges, and Applications*; Cavasotto, C. N., Series Ed.; CRC Press, 2015.
- (61) Z. Nikolovska-Coleska, R. Wang, X. Fang, H. Pan, Y. Tomita, P. Li, P. P. Roller, K. Krajewski, N. G. Saito, J. A. Stuckey, S. Wang, *Anal. Biochem.* 2004, *332*, 261-273..

2.9. Acknowledgement

I would like to thank Dr. Paul T. Wilder for performing the fluorescence polarization competition assay, Dr. Maryanna Lanning for synthesizing the thiazoles, Dr. Brandon

Drennen for synthesizing the pyrazoles, and Dr. Alexander MacKerell Jr.'s lab for performing SILCS.

Reproduced with permission from I.L. Conlon, B. Drennen, M.E. Lanning, S. Hughes, R. Rothhaas, P.T. Wilder, A.D. MacKerell Jr., and S. Fletcher. *Chemmedchem*, 2020, 15, 1-9. Copyright © 2020 John Wiley and Sons. Published by John Wiley and Sons. All rights Reserved.

Chapter 3. Densely functionalized heterocycles selectively targeting Mcl-1

3.1. Introduction

Mcl-1 is a vital anti-apoptotic protein due to its importance in a variety of healthy tissues (see Chapter 1.9). Its overexpression is linked to numerous cancers including breast, ovarian, prostate, pancreatic, and hematological cancers such as multiple myeloma (MM) and acute myeloid leukemia (AML)¹⁻⁴. Cancer is an incredibly complex disease that remains evasive and primed to develop resistance to single drugs owing to its complex network of PPIs. For example, the overexpression of Mcl-1 has been associated with poor prognosis and resistance to numerous drugs such as venetoclax as well as the widely used chemotherapeutic drugs paclitaxel, cisplatin, gemcitabine, and vincristine, among others⁵⁻⁷. Although significant strides have been made in the field of Mcl-1 selective inhibitors with many in clinical trials, none have successfully reached the clinic^{8,9}. Due to the urgent need of Mcl-1 selective inhibitors, we have described the development of mono- and bicyclic scaffolds that target Mcl-1.

3.2. α -Helix Mimicry

Targeting α -helix mediated PPIs such as the Mcl-1/Bim interaction has proved challenging due to the inherent flexibility of proteins and is compounded by the large, shallow hydrophobic surface of the binding grooves¹⁰. Many successful small molecules have been developed to probe these interactions, yet many have failed to yield successful drug candidates^{11,12}. However, utilizing BH3 mimetics represents a validated, targeted strategy to inhibit these interactions. BH3 mimetics are small molecules that mimic the α -helix of pro-apoptotic proteins, such as Bim. An ideal α -helix mimetic projects functional groups in a way that mimics the peptides natural helix. It mimics residues that bind in the

“hot spot” regions of the protein that are vital for the interaction and largely account for the binding free energy of the protein complex^{10,13–15}. In pro-apoptotic proteins, these residues are located at the i , $i+3$ (or $i+4$), and $i+7$ positions oriented on the hydrophobic face of the α -helix^{16,17}. Terphenyls, oligoamides, purines, and benzodiazepines have all been used as successful α -helix mimetics, with computational studies and X-ray crystal structures validating their functional reproduction of correct spatial orientation and mimicry of the critical residues of the α -helix^{16,18–22}.

In the Bim-BH3 α -helix, these residues include Leu62(i), Ile65 ($i+3$), and Phe69 ($i+7$) (Figure 3.1). Additionally, the critical residue Arg263 in Mcl-1, forms a salt bridge interaction with a conserved Asp residue (Asp67 in Bim) in the pro-apoptotic proteins.

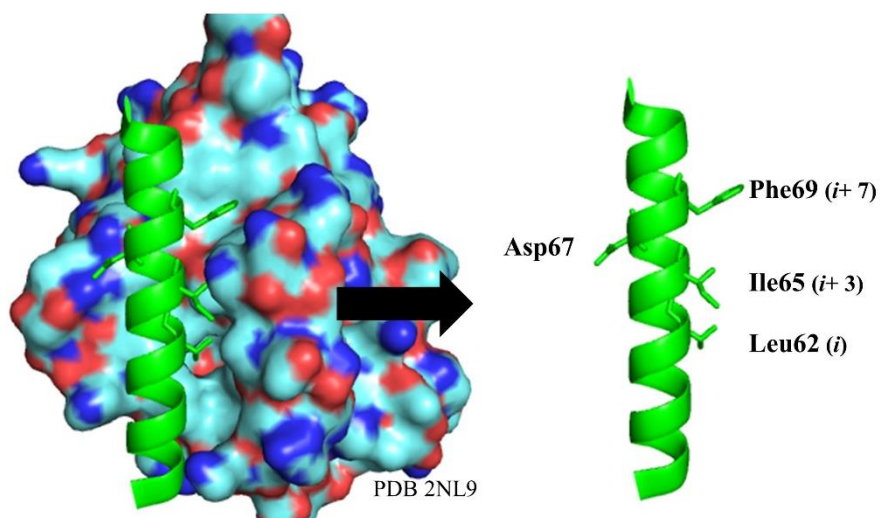


Figure 3. 1. The Mcl-1/Bim-BH3 interaction (left). Highlighted residues of Bim-BH3 (right). PDB 2NL9

Studies have shown that retaining this acidic functionality in a small molecule inhibitor contributes to increased binding affinity towards Mcl-1⁷. Both academic and industrial research labs have successfully developed potent Mcl-1 inhibitors despite its rigid, hydrophobic BH3 binding groove^{12,23}. Indole, picolinic acid, thienopyrimidine, and

pyrazole cores among others have been used in BH3 mimetics targeting Mcl-1, with both mono- and bicyclic scaffolds advancing in clinical trials^{5,7,24-26}.

Our lab has previously utilized a polypharmacology-based design describing dual Mcl-1/HDM2 inhibitors with mono-cyclic scaffolds isoxazoles, pyrazoles, and thiazoles (Refer to Chapter 2)²⁷. The computer-aided drug design methodology SILCS (Site Identification by Ligand Competitive Saturation) was employed and revealed excellent mimicry of both the BH3 and p53 α -helices. Overall, the most potent compounds were the isoxazoles and pyrazoles and although our most potent HDM2 inhibition was modest ($K_i = 11.5\mu\text{M}$), we were able to achieve low nanomolar inhibitors of Mcl-1, **OX** and **PZ** ($K_i = 263\text{nM}$ and 433nM) (Figure 3.2). This work encouraged our development of a second generation of Mcl-1 inhibitors²⁷.

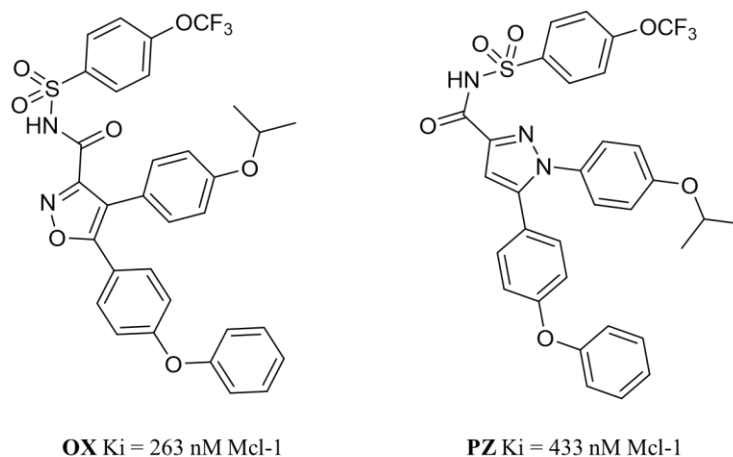


Figure 3.2. The most potent isoxazole and pyrazole compounds from Chapter 2.

3.3. Design and Results- Series 1

Based on the results from our first generation of compounds, we elected to move forward in a more detailed SAR study with the isoxazole and pyrazole scaffolds, both of which offer a unique functional group relationship to probe the Mcl-1-ligand interface:

isoxazoles offer a clustered functionalization with groups projected in a 1,2,3- position, while the pyrazoles offer a 1,2,4 functionalization (Figure 3.3)²⁷.

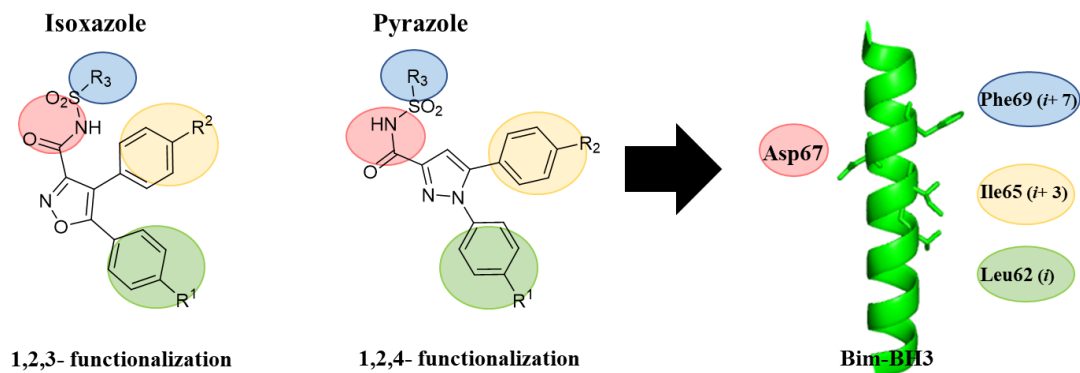


Figure 3.3. The general workflow of our isoxazole and pyrazole compounds.

To accomplish a more detailed study with these scaffolds, we wanted to include more diverse groups in the second generation of compounds, while taking advantage of the differences within each binding pocket of Mcl-1. These have been characterized previously as pockets p2, p3, and p4. An NMR based fragment screen performed by Fesik *et al.* revealed that the p2 pocket of Mcl-1 is flexible and accommodating of larger groups with the development of their indoles scaffolds that possess a 4-chloro-3,5-dimethyl phenyl moiety functionalized via an alkyl chain at the 3-position of the indole. Therefore, we have introduced larger groups at the R¹ position such as halogen-

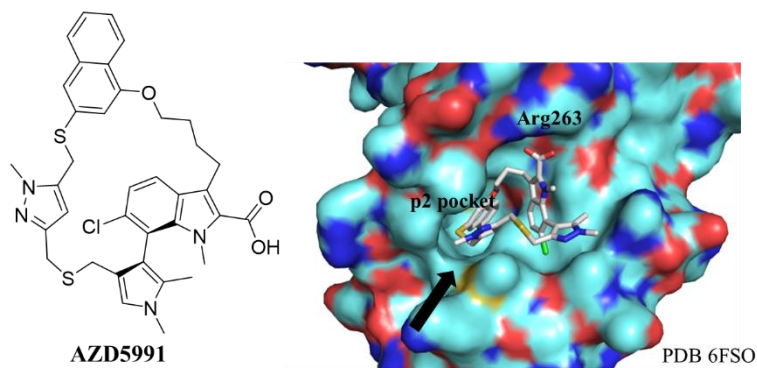


Figure 3.4. AZD5991 (left) and the crystal structure with key interactions highlighted. PDB 6FSO

substituted phenyl rings and biphenyl ethers to further explore the plasticity of the p2 pocket.

The p3 pocket of Mcl-1 is rather small, which interacts with Ile65 of the Bim-BH3 peptide. However, a crystal structure with the Mcl-1 selective inhibitor AZD5991, developed by AstraZeneca, revealed increased protein contacts through an opened pocket (Figure 3.4). The macrocyclic 6-chloroindole compound offers picomolar inhibition by interaction of various key functional groups. In fact, the crystal structure revealed that in addition to an induced fit of the naphthyl group in the p2 pocket, a previously unknown hydrophobic pocket was revealed to accommodate the pyrazole ring of the compound (represented by the black arrow in Figure 3.4)²³. To capitalize on this, we introduced both halogen-substituted phenyl rings as well as bicyclic functional groups such as substituted indoles to further probe the p3 pocket. Similar to our first generation inhibitors, we have grafted on acyl sulfonamides to function as a bioisostere of the carboxylic acid to serve three purposes: 1) deliver a third functional group, which is absent in compounds with a carboxylic acid; 2) retain acidic functionality to interact with Arg263 of Mcl-1; and 3) increase solubility.

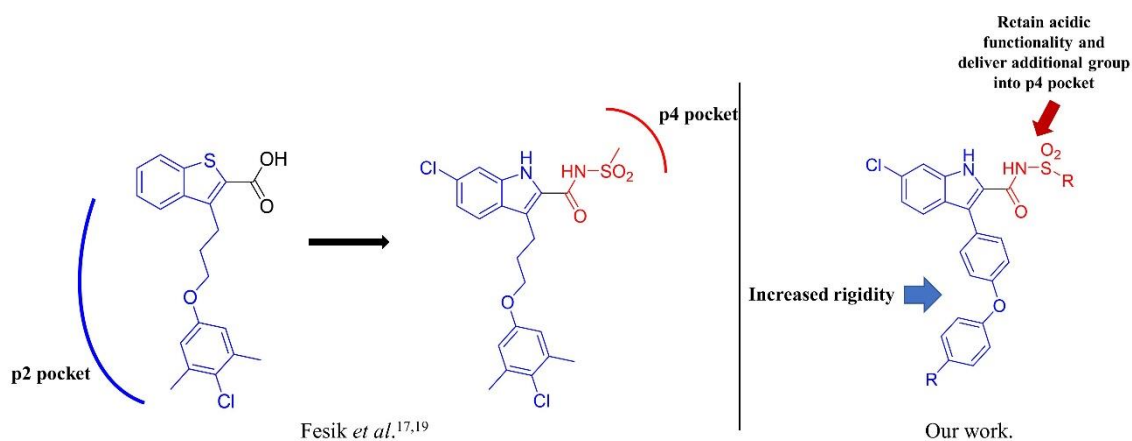


Figure 3. 5. The general workflow of our 2-acyl sulfonamide indole series.

In addition, we have also introduced an indole scaffold to probe the Mcl-1 binding interface (Figure 3.5). Bicyclic scaffolds are heavily featured in Mcl-1 selective inhibitors, many of which are currently in clinical trials (See Chapter 1.9)^{8,9,23,28}. For example, AZD5991 features a densely functionalized indole scaffold²³. Fesik's laboratory has driven the field of Mcl-1 selective inhibitors utilizing bicyclic scaffolds, including benzothiophenes and indoles^{5,7}. Their initial fragment based drug design and NMR based studies showed that the p2 pocket of Mcl-1 accommodated both the benzothiophene as well as the phenol group (Figure 3.5, left), revealing the flexibility of the pocket, as stated previously. They further introduced indoles, functionalized at the 2 position with an acyl sulfonamide that was capable of interacting with the p4 pocket of the protein. From this work, we have introduced a 3-functionalized indole scaffold to probe the p2 and p4 pockets of Mcl-1^{5,7}. As seen in Figure 3.5, the long alkyl chain of the Fesik compounds at the 3-position introduces additional flexibility in the scaffold, therefore, to further probe the p2 pocket, we have introduced larger, biaryl groups that will function to increase the rigidity at the 3-position of the indole to see if any further increase in affinity can be accomplished. In addition, we will further functionalize the carboxylic acid at the 2-position with a functionalized acyl sulfonamide to retain acidic functionality to engage with Arg263 of Mcl-1, while increasing hydrophobic contacts with the p4 pocket (Figure 3.5, right).

3.3.1. Computer-Aided Drug Design

We employed SILCS methodology to aid in the development of our compounds. SILCS evaluates the free energy contribution of different functional groups in the protein of interest (POI), taking desolvation and flexibility of the protein into account^{29,30}. Docking

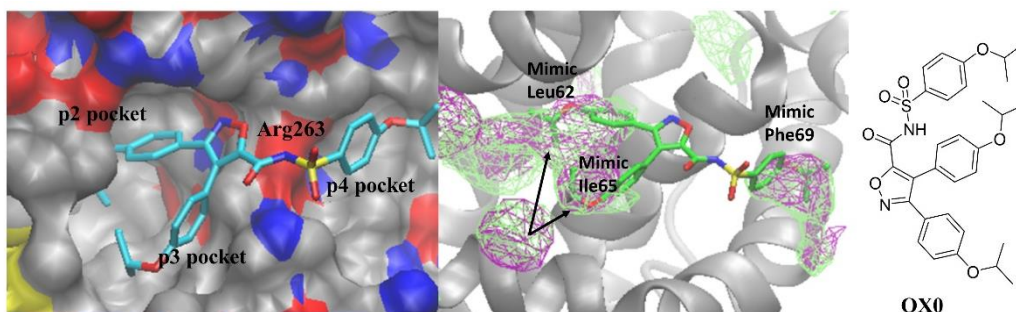


Figure 3. 6. *SILCS MC docking with OX0 (left) and highlighted FragMaps (Aromatic FragMaps are purple and Aliphatic are green) in Mcl-1 (center).*

of General Isoxazole **OX0** in Mcl-1 using SILCS Monte Carlo (SILCS-MC) (Figure 3.6, left) shows effective delivery of the functional groups into the p2, p3, and p4 pockets of the protein for the isoxazoles with the acyl sulfonamide in contact with Arg263.

Additionally, these figures showcase that the acyl sulfonamide functions as a comparable carboxylic acid bioisostere, capable of interacting with Arg263 while delivering the third functional group to the p4 pocket. However, we will also introduce different linkers to probe this interaction, including acyl sulfonamides with varying linker lengths as well as amides.

In addition, FragMaps were also generated, which are developed when the POI is immersed in an aqueous environment of various solutes that are utilized to represent different functional groups such as benzene, propane, methanol, imidazole, formamide, acetaldehyde, methylammonium, acetate, and water. FragMaps provide information that can help visualize which regions of the protein can accommodate different functional groups³¹. Figure 3.6 shows a representative isoxazole compound **OX0** residing within the areas of the protein interface where aliphatic (purple) and aromatic (green) groups are favored. In fact, the FragMaps of Figure 3.6 (left) reveal that larger groups may be favorable in the 3 and 4 positions of the core (arrows), which bind in the p2 and p3 pockets of Mcl-1, and can potentially increase affinity to Mcl-1. Therefore, in our design

we will incorporate larger groups in these positions. These *in silico* experiments suggest that our compounds act as functional mimetics of the pro-apoptotic proteins and bind in the BH3 binding domain of Mcl-1.

SILCS was also performed on the 2-acylsulfonamide indole scaffold. In Figure 3.7, docking with the **IN0** reveals a large amount of protein surface interaction in both the p2 and p4 pockets, which may result in potent binding affinity.

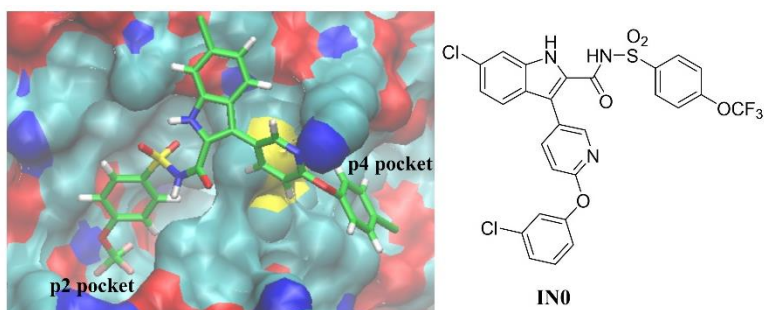


Figure 3.7. SILCS MC docking with **IN0**.

3.4. Synthesis

3.4.1. Isoxazoles

First, substituted aryl ketones **1** were reacted with diethyl oxalate in a Claisen condensation reaction to give β -keto esters **2**. **2** was cyclized with hydroxylamine HCl to give **3**, which was iodinated at the 4-position to give the 4-iodosubstituted isoxazole **4**. A Suzuki reaction with various substituted boronic acids furnished the tri-substituted isoxazole **5**. **5** was saponified under standard conditions to give **6** and coupled with sulfonamides and EDCI to give the final acyl sulfonamide isoxazole compounds **7**.

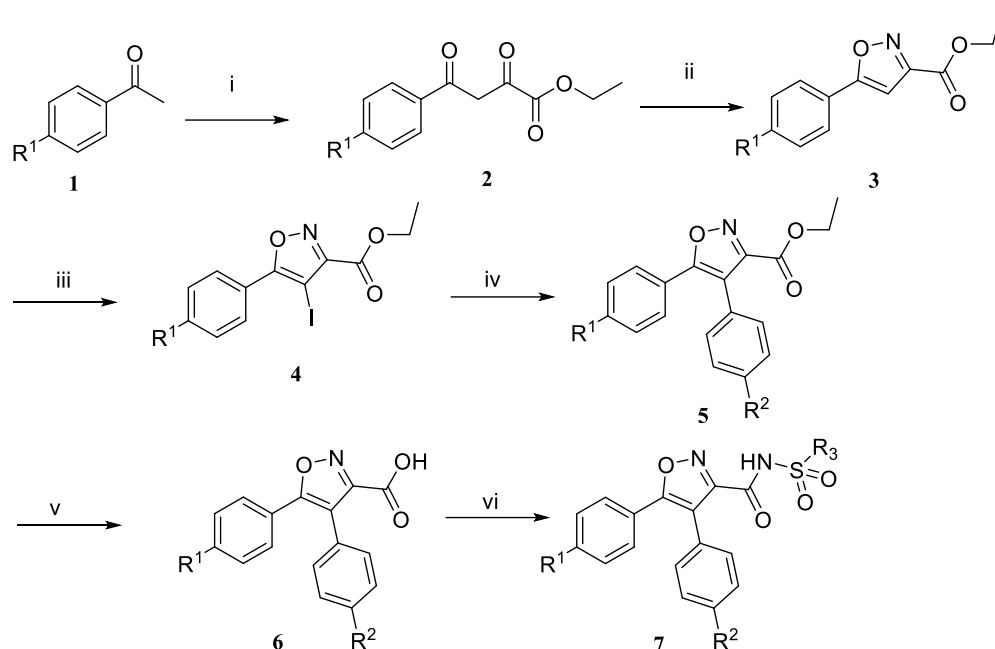


Figure 3. 8. (i) substituted ketones, diethyl oxalate, NaH, THF, 0°C to rt, 18hr, (ii) hydroxylamine HCl, EtOH, reflux, 18hr; (iii) NIS, TFA, rt, 18hr; (iv) substituted benzene boronic acids, CsF, Pd(PPh₃)₄, DME/MeOH, 80°C, 18hr; (v) LiOH·H₂O, THF/H₂O/MeOH, rt, 18hr; (vi) corresponding sulfonamide, EDCl, DIPEA, DMF, rt, 18hr.

3.4.2. Pyrazoles

See Chapter 2.4 for pyrazole synthesis.

3.4.3. 3-substituted 2-acylsulfonamide 1-H indoles

6-chloro 2-ethyl ester 1H-indole **8** was brominated at the 3-position with NBS to give **9**. Meanwhile, 4-bromo 2-fluoropyridine **10** underwent an S_NAr with 3-chlorophenol to give the brominated biphenyl ether **11**. **11** was subsequently reacted with bis(pinacolato)diboron to furnish the boronic ester **12**. The 3-bromoindole **9** and **12** underwent a Suzuki reaction to give the 3-functionalized 1H-indole **13**, that was hydrolyzed under standard conditions and coupled with 4-fluorobenzenesulfonamide to give the 2-acylsulfonamide 1H indole **15**.

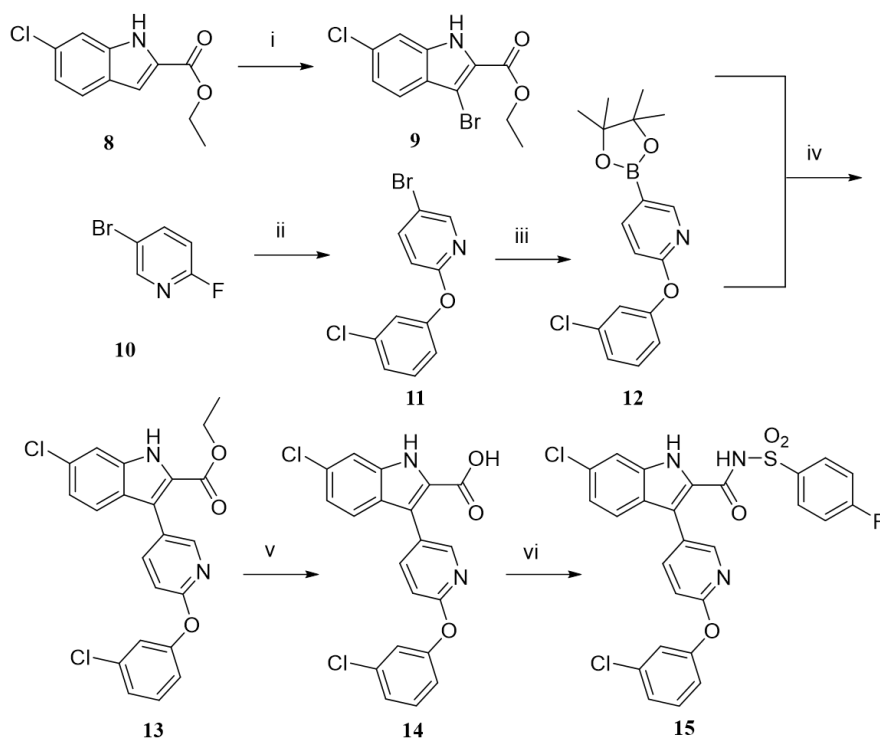


Figure 3. 9. (i) 6-chloro 2-ethyl ester 1H-indole, NBS, DMF, rt, 1hr; (ii) 3-chlorophenol, K_2CO_3 , DMF, 100°C, 18hr; (iii) pinacol ester, Anh DMSO, 85°C, 2hr; (iv) $PdCl_2(PPh_3)_2$, K_2CO_3 , Anh. DMF, 110°C, 4hr; (v) LiOH H_2O , THF/MeOH/ H_2O , rt, 18hr; (vi) 4-fluorobenzenesulfonamide, EDCI, DMAP, DIPEA, DCM, rt, 18hr.

3.5. Series 1 Results

Binding affinities were determined by a standard fluorescence polarization competition assay with Mcl-1 and a fluorescein (FITC)-labelled Bak-BH3 peptide. IC_{50} values were converted to K_i 's using the Nikolovska-Coleska equation³⁴. Data for Series 1 compounds are represented in Table 3.1.

In general, isoxazoles were the most potent Mcl-1 inhibitors, with most having K_i 's <600nM. In fact, our most potent compound, **7f**, had a $K_i = 473$ nM. The conversion of carboxylic acids to acyl sulfonamides resulted in an increase in binding affinity in almost every compound. For example, isoxazole **7a** had a $K_i = 11.37\mu M$, while the 4-OCF₃-phenyl acyl sulfonamide group of **7f** led to over a 20-fold increase in binding affinity, with $K_i = 473$ nM. Similarly, isoxazole **7b** had a $K_i = 3.21\mu M$, and conversion to

the acyl sulfonamide, **7g**, led to a 6-fold increase in binding affinity. This trend held true for pyrazoles as well. The carboxylic acid **PZ1** had $K_i = 10.89 \mu\text{M}$ and its acyl

Code Name	R ¹	R ²	R ³	Mel-1 K _i (μM)
7a	-3,4diCl	-OiPr	-OH	11.37 ± 0.773
7b	-3,4diCl	-6-Me(1Hindole)	-OH	3.21 ± 0.327
7c	-3,4diCl	-6-Me(Boc-indole)	-OH	4.81 ± 0.493
7d	-2-(3Cl-OPh)Pyr	-2,4diCl	-OH	0.481 ± .034
7e	-2-(3Cl-OPh)Pyr	-3,4diCl	-OH	3.58 ± 0.343
7f	-3,4diCl	-OiPr	-NHSO ₂ (4-OCF ₃)Ph	0.473 ± 0.03
7g	-3,4diCl	-6-Me(1Hindole)	-NHSO ₂ (4-OCF ₃)Ph	0.482 ± 0.035
7h	-2-(3Cl-OPh)Pyr	-2,4diCl	-NHSO ₂ (4-OCF ₃)Ph	0.730 ± 0.039
7i	-2-(3Cl-OPh)Pyr	-3,4diCl	-NHSO ₂ (4-OCF ₃)Ph	0.558 ± 0.035
7j	-3,4diCl	-3,4diCl	-NHPh(3-COOH)	1.93 ± 0.11
PZ1	-3,4diCl	-1Hindole	-OH	10.89 ± 0.871
PZ2	-O(3-ClPh)	-3,4diCl	-OH	8.94 ± 1.45
PZ3	-3,4diCl	-1Hindole	-NHSO ₂ (4-Cl)Ph	1.75 ± 0.134
PZ4	-O(3-ClPh)	-3,4diCl	-NHSO ₂ (4-Cl)Ph	1.03 ± 0.088
PZ5	-O(3-ClPh)	-3,4diCl	-NHSO ₂ (CH ₂ CH ₂ NHCO(3-F1,4-Cl)Ph)	0.530 ± 0.02
14	-2-(3Cl-OPh)Pyr	-	-OH	1.32 ± 0.170
15	-2-(3Cl-OPh)Pyr	-	-NHSO ₂ (4-F)Ph	1.35 ± 0.074

Table 3. 1. Series 1 fluorescence polarization data. IC_{50} 's were converted to K_i 's with the Nikolovska-Coleska equation³⁴.

sulfonamide counterpart, **PZ2**, had a $K_i = 1.75 \mu\text{M}$, a 6-fold increase in affinity.

To further probe the plasticity of the p3 pocket based on the crystal structure from AZD5991²³ (Figure 3.4), we elected to introduce larger bicyclic groups such as indoles within the molecules. Although these are mimicking Ile65 in Bim, and is known to bind within a shallow pocket, we see that the indoles are well tolerated in both our isoxazole and pyrazole scaffolds. This correlates with Leu78 in the Bak peptide, suggesting larger groups can be accommodated in this pocket. For example, isoxazole **7g** has an indole at the R² position and offered one of our most potent compounds of the series, with $K_i = 482\text{nM}$. This suggests this region of the protein may be somewhat malleable to

accommodate these larger groups, supported by the induced fit of the pyrazole of AZD5991²³. This further increased protein contacts and thus increased binding affinity.

The NMR studies by the Fesik laboratory revealed the flexibility of the p2 pocket of Mcl-1. To test this theory within our compounds, we grafted on biphenyl ethers in both our isoxazole and pyrazole scaffolds. As seen in every case (refer to compounds **7d**, **e**, **h**, **i**), these functional groups were well tolerated, further indicating the p2 pocket of the protein may be flexible and accommodate larger functional groups.

We also introduced different carbonyl linkers in our molecules, such as a longer acyl sulfonamides and amide linkers, as these have previously shown good inhibitory activity in Mcl-1^{5,7,32}. Conversion to an amide linker, **7j**, led to $K_i = 1.93 \mu\text{M}$. Although acidic functionality is not retained to engage with Arg263 of Mcl-1 an X-ray structure of an Mcl-1 inhibitor developed with Fesik with an amide linker with Mcl-1 revealed the carbonyl of **FS0** can maintain interactions with Arg263, while the phenyl group forms a cation-pi stacking interaction (Figure 3.10)³². Fesik's laboratory introduced long acyl

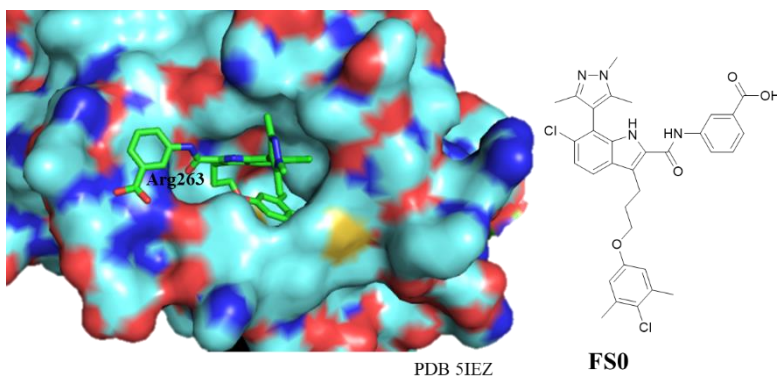


Figure 3.10. The crystal structure of Mcl-1 and FS0. PDB 5IEZ

sulfonamide linkers during an SAR of their indole compounds. Therefore, we also utilized this linker to hopefully increase binding contacts with Mcl-1. The carboxylic acid was transformed into the long acyl sulfonamide linker to give **PZ5**. Surprisingly, this

transformation led to nanomolar binding affinity of $K_i = 530\text{nM}$ and was the most potent pyrazole compound of the series.

For the 3-substituted 2-acyl sulfonamide 1H indole compounds, rigidity was introduced into the molecule with the biphenyl ether at the 3-position to further probe the p2 pocket of Mcl-1 as stated previously. As we see with both compounds, the rigidity was not well accommodated, with both compounds $K_i > 1\mu\text{M}$. It is surprising that **14** and **15** had no difference in binding affinity because 88 had an additional acyl sulfonamide projecting a 4-fluorophenyl moiety. One explanation may be that reduced flexibility of the biaryl group at the 3-position may introduce too much rigidity and be deleterious to protein binding. In the future, we will perform additional structural studies at the 3-position to further explain this.

3.6. Design and Results-Series 2

We see with our series 1 indole scaffold we had modest Mcl-1 data. As previously described, AZD5991 has an indole scaffold that achieved picomolar binding affinity in Mcl-1. Due to the increased hydrophobic contacts around the p2 pocket with the naphthyl and pyrazole moieties, we wanted to further probe this region of the protein. Therefore, we developed the reverse sulfonamide 1H-indole scaffold. Given that Mcl-1 accommodates the pyrazole of AZD5991 by further opening the hydrophobic pocket of the protein, we hypothesized that the indole scaffold could have additional interactions with the branched reverse sulfonamide group. In addition, we saw no change when the acid was converted to the acyl sulfonamide in our series 1 indole scaffold, so we elected to not functionalize the acid for this scaffold.

Figure 3.11 (left) represents SILCS MC docking with the **RS0**, revealing it binds within the p2 pocket of Mcl-1, which we hypothesized due to Fesik indoles and AZD5991 binding in the same region.

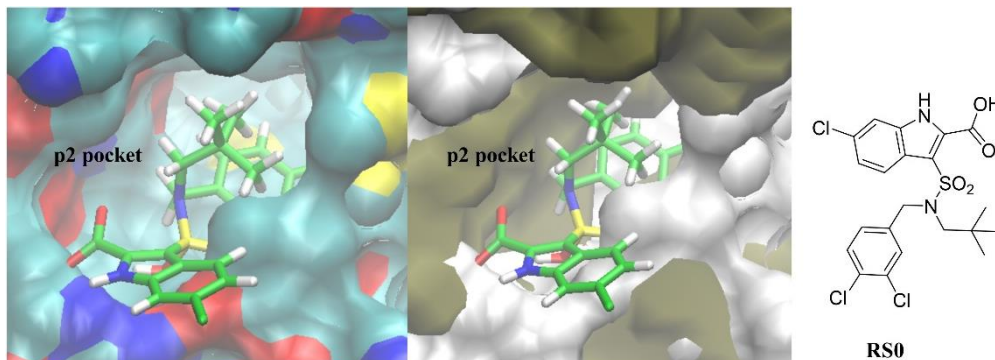


Figure 3. 11. SILCS MC docking with **RS0** in Mcl-1 (left) with highlighted exclusion maps (center).

In addition to FragMaps and docking experiments, exclusions maps were generated. These represent regions of the protein where there is an absence of probe or water molecules. These are generated because many protein binding interfaces have regions that are inaccessible due to the flexibility of the protein³³. These maps are dark green and represented Figure 3.11 (center), showing where compound design should be exempt. These exclusion maps showcase the sulfonamide scaffold interacting within the p2 pocket of Mcl-1. Surprisingly, the carboxylic acid points towards the inside of the pocket as this is a hydrophobic pocket. However, the exclusion maps in Figure 3.11 showcase the fluidity of the protein interface, as the acidic moiety binds in an agreeable position to the generated maps. Additionally, the sulfonamide functional group offers flexibility and rotation, so the carboxylic acid at any point in time can be pointed out towards the solvent while the core indole itself is buried into the pocket.

3.7. Synthesis

3.7.1. 3-reverse sulfonamide 1H-indole

6-chloro 2-ethyl ester 1H indole **16** was sulfonylated with sulfuric acid and acetic anhydride to furnish **17** and was further reacted with oxalyl chloride to give the sulfonyl chloride **18**. Then, various secondary amines were reacted with **18** to give the functionalized reverse sulfonamide **19** and was subsequently saponified under standard conditions to give the final compounds **20**.

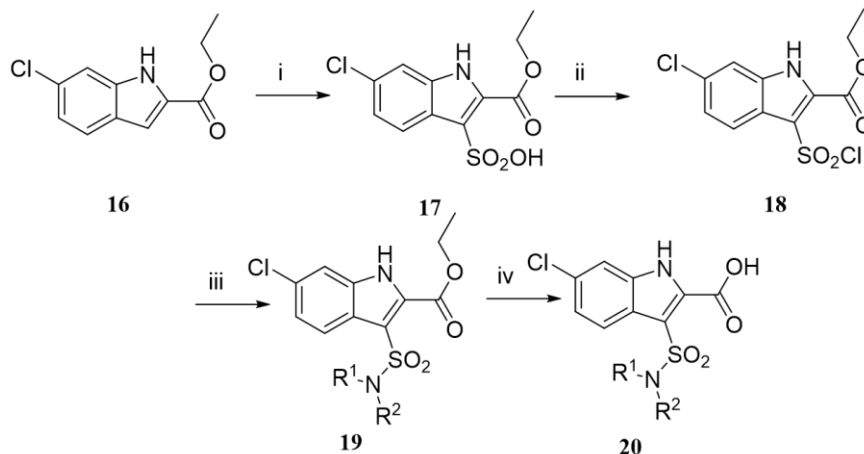


Figure 3. 12. (i) H_2SO_4 , Ac_2O , $0^\circ C$ to rt , 18hr; (ii) oxalyl chloride, DMF, DCM, rt to $45^\circ C$, 2hr; (iii) HNR^1R^2 , DIPEA, Anh. DCM, rt , 18hr; (iv) $LiOH$ H_2O , THF/MeOH/ H_2O , rt , 18hr.

3.8. Series 2 Results

Table 3.2 shows the fluorescence polarization data of our indole library. SAR with the indole scaffolds were comparable in binding affinity with the mono-cyclic scaffolds. The reverse sulfonamide indole scaffold provided the most potent bicyclic inhibitors of our series. Although no trends were apparent with the data with respect to functional group differences, all compounds had a $K_i < 2\mu M$, with the most potent compound, **20f**, had a $K_i = 733nM$. It is revealed with these data that large groups at the R^1 and R^2 positions are well tolerated, as none are deleterious to binding and all of these compounds fall within a 2-fold difference in binding affinity. It can be inferred that these bind within the p2 pocket based on the CADD data. In future studies, the carboxylic acid can be converted

into an acyl sulfonamide to potentially increase binding affinity to Mcl-1 by increasing protein contacts through interaction at the p4 pocket.



20a-g

Code Name	R ¹	R ²	Mcl-1 μ M)
20a	-(4-Cl)Ph	-Bn	0.960 \pm 0.096
20b	-(4-Cl)Ph	-tert-butyl	1.47 \pm 0.183
20c	-(3,4Cl)Ph	-CH ₂ (furan)	1.59 \pm 0.507
20d	-(3,4Cl)Ph	-tert-butyl	0.771 \pm 0.794
20e	-(4-Br)Ph	-tert-butyl	1.28 \pm 0.197
20f	-(4-Br)Ph	-CH ₂ (cyclohexane)	0.733 \pm 0.059
20g	-(3-Br)Ph	-CH ₂ CH ₂ (4-Cl)Ph	0.790 \pm 0.143

Table 3. 2. Series 2 fluorescence polarization data. IC₅₀'s were converted to Ki's with the Nikolovska-Coleska equation³⁴.

3.9. Discussion

Targeting Mcl-1 has proven challenging due to the shallow, hydrophobic nature of the BH3 binding pocket, however, its importance in cancer development and progression reveals the therapeutic need of an Mcl-1 selective inhibitor. In summary, the detailed SAR study outlined in this chapter showcases the difficulty in maintaining high binding affinity in both mono- and bicyclic scaffolds. We have demonstrated that both isoxazoles and pyrazoles are effective Mcl-1 inhibitors, in particular when functionalized with an acyl sulfonamide. In addition, larger groups that interact in both the p2 and p3 pockets of Mcl-1 offer increased binding affinity. Although the indole series demonstrates modest inhibition in Mcl-1, a further exploration of these compounds at both the 2- and 3-position can offer additional insights in binding affinity, in particular, functionalizing the carboxylic acid of the reverse sulfonamide scaffold with an acyl sulfonamide.

3.10. References

- (1) Akgul, C. Mcl-1 Is a Potential Therapeutic Target in Multiple Types of Cancer. *Cellular and Molecular Life Sciences* **2009**, *66* (8), 1326–1336.
- (2) Lee, E. F.; Harris, T. J.; Tran, S.; Evangelista, M.; Arulananda, S.; John, T.; Ramnac, C.; Hobbs, C.; Zhu, H.; Gunasingh, G.; Segal, D.; Behren, A.; Cebon, J.; Dobrovic, A.; Mariadason, J. M.; Strasser, A.; Rohrbeck, L.; Haass, N. K.; Herold, M. J.; Fairlie, W. D. BCL-XL and MCL-1 Are the Key BCL-2 Family Proteins in Melanoma Cell Survival. *Cell Death Dis* **2019**, *10* (5), 342.
- (3) Derenne, S.; Monia, B.; Dean, N. M.; Taylor, J. K.; Rapp, M.-J.; Harousseau, J.-L.; Bataille, R.; Amiot, M. Antisense Strategy Shows That Mcl-1 Rather than Bcl-2 or Bcl-x(L) Is an Essential Survival Protein of Human Myeloma Cells. *Blood* **2002**, *100* (1), 194–199.
- (4) Abulwerdi, F.; Liao, C.; Liu, M.; Azmi, A. S.; Aboukameel, A.; Mady, A. S. A.; Gulappa, T.; Cierpicki, T.; Owens, S.; Zhang, T.; Sun, D.; Stuckey, J. A.; Mohammad, R. M.; Nikolovska-Coleska, Z. A Novel Small-Molecule Inhibitor of Mcl-1 Blocks Pancreatic Cancer Growth in Vitro and in Vivo. *Mol. Cancer Ther.* **2014**, *13* (3), 565–575.
- (5) Friberg, A.; Vigil, D.; Zhao, B.; Daniels, R. N.; Burke, J. P.; Garcia-Barrantes, P. M.; Camper, D.; Chauder, B. A.; Lee, T.; Olejniczak, E. T.; Fesik, S. W. Discovery of Potent Myeloid Cell Leukemia 1 (Mcl-1) Inhibitors Using Fragment-Based Methods and Structure-Based Design. *J. Med. Chem.* **2013**, *56* (1), 15–30.
- (6) Punnoose, E. A.; Levenson, J. D.; Peale, F.; Boghaert, E. R.; Belmont, L. D.; Tan, N.; Young, A.; Mitten, M.; Ingalla, E.; Darbonne, W. C.; Oleksijew, A.; Tapang, P.; Yue, P.; Oeh, J.; Lee, L.; Maiga, S.; Fairbrother, W. J.; Amiot, M.; Souers, A. J.; Sampath, D. Expression Profile of BCL-2, BCL-XL, and MCL-1 Predicts Pharmacological Response to the BCL-2 Selective Antagonist Venetoclax in Multiple Myeloma Models. *Mol Cancer Ther* **2016**, *15* (5), 1132–1144.
- (7) Pelz, N. F.; Bian, Z.; Zhao, B.; Shaw, S.; Tarr, J. C.; Belmar, J.; Gregg, C.; Camper, D. V.; Goodwin, C. M.; Arnold, A. L.; Sensintaffar, J. L.; Friberg, A.; Rossanese, O. W.; Lee, T.; Olejniczak, E. T.; Fesik, S. W. Discovery of 2-Indole-Acylsulfonamide Myeloid Cell Leukemia 1 (Mcl-1) Inhibitors Using Fragment-Based Methods. *J. Med. Chem.* **2016**, *59* (5), 2054–2066.
- (8) Phase I Study of S64315 Administred Intravenously in Patients With Acute Myeloid Leukaemia or Myelodysplastic Syndrome - Full Text View - ClinicalTrials.gov <https://clinicaltrials.gov/ct2/show/NCT02979366>

- (9) Phase I Study of MIK665, a Mcl-1 Inhibitor, in Patients With Refractory or Relapsed Lymphoma or Multiple Myeloma - Full Text View - ClinicalTrials.gov <https://clinicaltrials.gov/ct2/show/NCT02992483>
- (10) Lanning, M. E.; Fletcher, S. Recapitulating the α -Helix: Nonpeptidic, Low-Molecular-Weight Ligands for the Modulation of Helix-Mediated Protein-Protein Interactions. *Future Medicinal Chemistry* **2013**, *5* (18), 2157–2174.
- (11) Amgen halts trials on cardiac toxicity <https://www.evaluate.com/vantage/articles/news/snippets/amgen-halts-trials-cardiac-toxicity>
- (12) Beekman, A. M.; Howell, L. A. Small-Molecule and Peptide Inhibitors of the Pro-Survival Protein Mcl-1. *ChemMedChem* **2016**, *11* (8), 802–813.
- (13) Barnard, A.; Long, K.; Yeo, D. J.; Miles, J. A.; Azzarito, V.; Burslem, G. M.; Prabhakaran, P.; A Edwards, T.; Wilson, A. J. Orthogonal Functionalisation of α -Helix Mimetics. *Org. Biomol. Chem.* **2014**, *12* (35), 6794–6799.
- (14) Petros, A. M.; Olejniczak, E. T.; Fesik, S. W. Structural Biology of the Bcl-2 Family of Proteins. *Biochim. Biophys. Acta* **2004**, *1644* (2–3), 83–94.
- (15) Azzarito, V.; Long, K.; Murphy, N. S.; Wilson, A. J. Inhibition of α -Helix-Mediated Protein-Protein Interactions Using Designed Molecules. *Nat Chem* **2013**, *5* (3), 161–173.
- (16) Lanning, M. E.; Fletcher, S. Multi-Facial, Non-Peptidic α -Helix Mimetics. *Biology (Basel)* **2015**, *4* (3), 540–555.
- (17) Jayatunga, M. K. P.; Thompson, S.; Hamilton, A. D. α -Helix Mimetics: Outwards and Upwards. *Bioorganic & Medicinal Chemistry Letters* **2014**, *24* (3), 717–724.
- (18) Yin, H.; Lee, G.-I.; Sedey, K. A.; Kutzki, O.; Park, H. S.; Orner, B. P.; Ernst, J. T.; Wang, H.-G.; Sebti, S. M.; Hamilton, A. D. Terphenyl-Based Bak BH3 Alpha-Helical Proteomimetics as Low-Molecular-Weight Antagonists of Bcl-XL. *J. Am. Chem. Soc.* **2005**, *127* (29), 10191–10196.
- (19) Kazi, A.; Sun, J.; Doi, K.; Sung, S.-S.; Takahashi, Y.; Yin, H.; Rodriguez, J. M.; Becerril, J.; Berndt, N.; Hamilton, A. D.; Wang, H.-G.; Sebti, S. M. The BH3 α -Helical Mimic BH3-M6 Disrupts Bcl-XL, Bcl-2, and MCL-1 Protein-Protein Interactions with Bax, Bak, Bad, or Bim and Induces Apoptosis in a Bax- and Bim-Dependent Manner. *J Biol Chem* **2011**, *286* (11), 9382–9392.
- (20) Yap, J. L.; Cao, X.; Vanommeslaeghe, K.; Jung, K.-Y.; Peddaboina, C.; Wilder, P. T.; Nan, A.; MacKerell, A. D.; Smythe, W. R.; Fletcher, S. Relaxation of the Rigid Backbone of an Oligoamide-Foldamer-Based α -Helix Mimetic:

- Identification of Potent Bcl-XL Inhibitors. *Org. Biomol. Chem.* **2012**, *10* (15), 2928–2933.
- (21) Drennen, B.; Scheenstra, J. A.; Yap, J. L.; Chen, L.; Lanning, M. E.; Roth, B. M.; Wilder, P. T.; Fletcher, S. Structural Re-Engineering of the α -Helix Mimetic JY-1-106 into Small-Molecules: Disruption of the Mcl-1–Bak-BH3 Protein–Protein Interaction with 2,6-Di-Substituted Nicotinates. *ChemMedChem* **2016**, *11* (8), 827–833.
- (22) Lanning, M. E.; Wilder, P. T.; Bailey, H.; Drennen, B.; Cavalier, M.; Chen, L.; Yap, J. L.; Raje, M.; Fletcher, S. Towards More Drug-like Proteomimetics: Two-Faced, Synthetic α -Helix Mimetics Based on a Purine Scaffold. *Org. Biomol. Chem.* **2015**, *13* (32), 8642–8646.
- (23) Tron, A. E.; Belmonte, M. A.; Adam, A.; Aquila, B. M.; Boise, L. H.; Chiarparin, E.; Cidado, J.; Embrey, K. J.; Gangl, E.; Gibbons, F. D.; Gregory, G. P.; Hargreaves, D.; Hendricks, J. A.; Johannes, J. W.; Johnstone, R. W.; Kazmirski, S. L.; Kettle, J. G.; Lamb, M. L.; Matulis, S. M.; Nooka, A. K.; Packer, M. J.; Peng, B.; Rawlins, P. B.; Robbins, D. W.; Schuller, A. G.; Su, N.; Yang, W.; Ye, Q.; Zheng, X.; Secrist, J. P.; Clark, E. A.; Wilson, D. M.; Fawell, S. E.; Hird, A. W. Discovery of Mcl-1-Specific Inhibitor AZD5991 and Preclinical Activity in Multiple Myeloma and Acute Myeloid Leukemia. *Nat Commun* **2018**, *9*.
- (24) Wang, Z.; Song, T.; Feng, Y.; Guo, Z.; Fan, Y.; Xu, W.; Liu, L.; Wang, A.; Zhang, Z. Bcl-2/MDM2 Dual Inhibitors Based on Universal Pyramid-Like α -Helical Mimetics. *J. Med. Chem.* **2016**, *59* (7), 3152–3162.
- (25) Szlavik, Z.; Ondi, L.; Csékei, M.; Paczal, A.; Szabó, Z. B.; Radics, G.; Murray, J.; Davidson, J.; Chen, I.; Davis, B.; Hubbard, R. E.; Pedder, C.; Dokurno, P.; Surgenor, A.; Smith, J.; Robertson, A.; LeToumelin-Braizat, G.; Cauquil, N.; Zarka, M.; Demarles, D.; Perron-Sierra, F.; Claperon, A.; Colland, F.; Geneste, O.; Kotschy, A. Structure-Guided Discovery of a Selective Mcl-1 Inhibitor with Cellular Activity. *J. Med. Chem.* **2019**, *62* (15), 6913–6924.
- (26) Kotschy, A.; Szlavik, Z.; Murray, J.; Davidson, J.; Maragno, A. L.; Le Toumelin-Braizat, G.; Chanrion, M.; Kelly, G. L.; Gong, J.-N.; Moujalled, D. M.; Bruno, A.; Csekei, M.; Paczal, A.; Szabo, Z. B.; Sipos, S.; Radics, G.; Prosenyak, A.; Balint, B.; Ondi, L.; Blasko, G.; Robertson, A.; Surgenor, A.; Dokurno, P.; Chen, I.; Matassova, N.; Smith, J.; Pedder, C.; Graham, C.; Studeny, A.; Lysiak-Auvity, G.; Girard, A.-M.; Gravé, F.; Segal, D.; Riffkin, C. D.; Pomilio, G.; Galbraith, L. C. A.; Aubrey, B. J.; Brennan, M. S.; Herold, M. J.; Chang, C.; Guasconi, G.; Cauquil, N.; Melchiorre, F.; Guigal-Stephan, N.; Lockhart, B.; Colland, F.; Hickman, J. A.; Roberts, A. W.; Huang, D. C. S.; Wei, A. H.; Strasser, A.; Lessene, G.; Geneste, O. The MCL1 Inhibitor S63845 Is Tolerable and Effective in Diverse Cancer Models. *Nature* **2016**, *538* (7626), 477–482.

- (27) Conlon, I. L.; Drennen, B.; Lanning, M. E.; Hughes, S.; Rothhaas, R.; Wilder, P. T.; MacKerell Jr., A. D.; Fletcher, S. Rationally Designed Polypharmacology: α -Helix Mimetics as Dual Inhibitors of the Oncoproteins Mcl-1 and HDM2. *ChemMedChem* **2020**, *In Press*.
- (28) Hird, A. W.; Tron, A. E. Recent Advances in the Development of Mcl-1 Inhibitors for Cancer Therapy. *Pharmacology & Therapeutics* **2019**, *198*, 59–67.
- (29) Yu, W.; Lakkaraju, S. K.; Raman, E. P.; MacKerell, A. D. Site-Identification by Ligand Competitive Saturation (SILCS) Assisted Pharmacophore Modeling. *J Comput Aided Mol Des* **2014**, *28* (5), 491–507.
- (30) Ustach, V. D.; Lakkaraju, S. K.; Jo, S.; Yu, W.; Jiang, W.; MacKerell, A. D. Optimization and Evaluation of Site-Identification by Ligand Competitive Saturation (SILCS) as a Tool for Target-Based Ligand Optimization. *J. Chem. Inf. Model.* **2019**, *59* (6), 3018–3035.
- (31) Raman, E. P.; Yu, W.; Lakkaraju, S. K.; MacKerell, A. D. Inclusion of Multiple Fragment Types in the Site Identification by Ligand Competitive Saturation (SILCS) Approach. *J. Chem. Inf. Model.* **2013**, *53* (12), 3384–3398.
- (32) Lee, T.; Bian, Z.; Zhao, B.; Hogdal, L. J.; Sensintaffar, J. L.; Goodwin, C. M.; Belmar, J.; Shaw, S.; Tarr, J. C.; Veerasamy, N.; Matulis, S. M.; Koss, B.; Fischer, M. A.; Arnold, A. L.; Camper, D. V.; Browning, C. F.; Rossanese, O. W.; Budhraj, A.; Opferman, J.; Boise, L. H.; Savona, M. R.; Letai, A.; Olejniczak, E. T.; Fesik, S. W. Discovery and Biological Characterization of Potent Myeloid Cell Leukemia-1 Inhibitors. *FEBS Letters* **2017**, *591* (1), 240–251.
- (33) Yu, W.; Jo, S.; Lakkaraju, S. K.; Weber, D. J.; MacKerell, A. D. Exploring Protein-Protein Interactions Using the Site-Identification by Ligand Competitive Saturation (SILCS) Methodology. *Proteins* **2019**, *87* (4), 289–301.
- (34) Nikolovska-Coleska, Z.; Wang, R.; Fang, X.; Pan, H.; Tomita, Y.; Li, P.; Roller, P. P.; Krajewski, K.; Saito, N. G.; Stucky, J. A.; Wang, S. *Anal. Biochem.* **2004**, *332*, 261–273.

3.11. Supplementary Information

3.11.1. Chemistry

General. Unless otherwise stated, all reactions were performed under an inert atmosphere (N₂). Reagents and solvents were ACS grade, and purchased from Sigma-Aldrich, Alfa Aesar, Oakwood and TCI America. Anhydrous solvents were used as provided from Sigma-Aldrich. Reactions were monitored by thin-layer chromatography (TLC), visualizing with a UV lamp and/or KMnO₄ stain. Flash column chromatography was performed with silica gel 60 Å (70-230 mesh, Merck). ¹H and ¹³C NMR spectra were recorded on a Varian INOVA 400 MHz NMR spectrometer at 25 °C. Chemical shifts are reported in parts per million (ppm). Data for ¹H NMR are reported thus: chemical shift (δ ppm) (multiplicity, coupling constant (Hz), integration), where multiplicities are: s = singlet, d = doublet, t = triplet, m = multiplet. The residual solvent peak was used as an internal reference: CDCl₃ (δ_H 7.26; δ_C 77.21) and *d*₆-DMSO (δ_H 2.50; δ_C 39.51). Mass spectra were obtained on an Electrospray TOF (ESI-TOF) mass spectrometer (Bruker AmaZon X). All final molecules were deemed to be >95% pure by reversed-phased HPLC using a Waters 1525 analytical/preparative HPLC fitted with a C¹⁸ reversed-phase column (Atlantis T3: 4.6 mm x 150 mm) according to the following conditions with solvents (A) H₂O/0.1% TFA, (B) CH₃CN–H₂O, 9:1 with 0.1% TFA at 1 ml min⁻¹: (I) a gradient of 50% A to 100% B over 22 min; (II) an isocratic gradient of 100% B over 22 min. Data are presented as retention time (t_R (min)), purity (%), condition (I or II).

Isoxazoles

General Procedure A: Synthesis of 2,4-dioxobutanoates. An aryl ketone (1 eq) was added to a reaction flask and solubilized in anhydrous THF (0.1 M). The reaction mixture

was cooled to 0°C and NaH (2 eq) was added to the reaction. The reaction stirred for 30 minutes and then diethyl oxalate (1.2 eq) was added and stirred overnight at room temperature. Completion of the reaction was monitored via TLC in a gradient of Hexanes/EtOAc. Once complete, the crude mixture was partitioned between 1M HCl and EtOAc. The organic layer was extracted, dried with Na₂SO₄, filtered and concentrated down. The crude material was then dry loaded onto silica gel and purified via column chromatography. The fractions containing the product were combined, concentrated down and azeotroped with CHCl₃ to yield the 2,4-dioxobutanoates (15- 81% yield).

General Procedure B: Synthesis of isoxazole ethyl esters. A substituted β-keto ester (1 eq) was dissolved in EtOH (0.1 M). NH₂OH · HCl (3 eq) was added and the reaction was refluxed overnight. A TLC in Hexanes/EtOAc revealed completion of the reaction. The reaction mixture was partitioned between CH₂Cl₂ and H₂O. The organic layer was washed with brine and dried with Na₂SO₄, filtered, and concentrated in vacuo. The crude product was dry loaded onto silica gel and columned in a gradient of Hexanes/EtOAc. The fractions were collected and azeotroped with CHCl₃ to yield the isoxazole ethyl esters (54-61% yield).

General Procedure C: Synthesis of 4-iodo isoxazole ethyl esters. Isoxazole ethyl esters (1 eq) was dissolved in Trifluoroacetic acid (0.2 M) at 0°C followed by addition of NIS (1.5 eq). The reaction stirred at room temperature overnight. A TLC in 4:1 Hexanes/EtOAc revealed the reaction was complete. The Trifluoroacetic acid was concentrated in vacuo followed by azeotroping (5x) with CHCl₃. The crude product was dry loaded onto silica gel and columned in 4:1 Hexanes/EtOAc. The fractions were

collected and azeotroped with CHCl_3 to yield the 4-iodo isoxazole ethyl esters (85-92% yield).

General Procedure D: Synthesis of tri-substituted isoxazole ethyl esters. 4-iodo isoxazole ethyl esters (1 eq) was dissolved in a 6:1 mixture of DMF and H_2O (0.15 M). Addition of an aryl boronic ester (or acid) and NaHCO_3 followed and the reaction mixture was degassed with N_2 . Lastly, $\text{PdCl}_2(\text{PPh}_3)_2$ was added. The mixture was stirred at 80°C for four hours and the reaction was monitored by TLC. After TLC in Hexanes/EtOAc revealed the reaction was complete, the reaction was filtered through a pad of Celite with CH_2Cl_2 . The filtrate was concentrated in vacuo. The crude solution was partitioned between EtOAc and H_2O . The organic layer was washed with H_2O (3x) and brine (1x). The organic layer was dried with Na_2SO_4 , filtered, and concentrated in vacuo. The crude product was dry loaded onto silica gel and columned in a gradient of Hexanes/EtOAc. The fractions were collected and azeotroped with CHCl_3 to yield the tri-substituted isoxazole ethyl esters (45-63% yield).

General Procedure E: Synthesis of isoxazole carboxylic acids. The isoxazole ethyl ester (1 eq) was reacted with $\text{LiOH}\cdot\text{H}_2\text{O}$ (4 eq) in 3:1:1 THF/ H_2O /MeOH (0.1 M) at room temperature overnight. A TLC in 92:7:1 CH_2Cl_2 /MeOH/Acetic acid indicated the reaction was complete. EtOAc (30mL) was added to the reaction, washed with 1M HCl (x3, 50mL), dried with Na_2SO_4 , filtered, and concentrated in vacuo. The crude product was columned in 92:7:1 CH_2Cl_2 /MeOH/Acetic acid, concentrated in vacuo to reveal the isoxazole carboxylic acid (53-97% yield).

General Procedure F: Synthesis of isoxazole acyl sulfonamides and amides. An isoxazole carboxylic acid (1 eq) was dissolved in CH_2Cl_2 (0.1 M) and cooled to 0°C .

Then, EDCI (1.5 eq), and DMAP (1 eq) were added and the reaction was stirred for 30 minutes followed by addition of the sulfonamide (1.2 eq). The reaction was stirred at room temperature overnight. Completion of the reaction was monitored via TLC in a gradient of 92:7:1 DCM/MeOH/H₂O. Once complete, the DCE was evaporated and the crude mixture was dry loaded onto silica gel. The product was purified via column chromatography in a gradient of 92:7:1 DCM/MeOH/H₂O. The product fractions were collected, combined, concentrated down and azeotroped with CHCl₃ to yield the isoxazole acyl sulfonamides (13-99% yield).

General Procedure G: Synthesis of functionalized sulfonamides. The sulfonyl chloride (1 eq) was added to a reaction flask and dissolved in dioxane (0.1M). The reaction was cooled to 0°C and NH₄OH (10 eq) was added slowly to the reaction mixture. The reaction was heated to room temperature and stirred for 1 hour. Completion of the reaction was monitored via TLC with a gradient of Hexanes/EtOAc. Once completed, the solvent was evaporated off and the crude material was dissolved in EtOAc. The organic layer was washed 1M HCl three times and collected, dried with Na₂SO₄, filtered, concentrated down and azeotroped with CHCl₃ to yield the functionalized sulfonamides (80-90% yield).

Pyrazoles

General Procedure H: Synthesis of anilines. A 4-nitroaryl (1 eq) was dissolved in EtOAc (0.2 M), followed by addition of SnCl₂ dihydrate (3 eq) and the reaction mixture was stirred overnight at 50°C. A TLC in 1:1 Hexanes/EtOAc revealed the reaction completed. The mixture was partitioned between EtOAc and 3M NaOH. The organic layer was dried with Na₂SO₄, filtered, and concentrated down to dryness. It was dry

loaded onto silica gel and columned in a 1:1 Hexanes/EtOAc gradient. Fractions were combined, concentrated, and azeotroped with CHCl_3 to reveal the aryl anilines (77-93% yield)

General Procedure I: Synthesis of the arylhydrazines. An aniline (1 eq) was added to a reaction flask followed by the addition of 1M HCl (0.1 M) and stirred at 0°C . The reaction stirred for 5 minutes and then was brought to room temperature. The reaction stirred for 20 minutes and then was cooled to -5°C . NaNO_2 (1.05 eq.) dissolved in H_2O was added dropwise to reaction. The reaction stirred for 15 minutes and then SnCl_2 (4.0 eq.) was added to the reaction. The reaction stirred at room temperature for 3 hours and a precipitate formed. The precipitate was filtered out of the reaction and washed with cold H_2O to isolate the desired arylhydrazine (60-70% yield).

General Procedure J: Synthesis of the 2,4-dioxobutanoates. A ketone (1 eq) was added to a reaction flask and solubilized in a mixture of 5:1 anhydrous toluene/anhydrous THF (0.1 M). The reaction was cooled to 0°C and NaH (2 eq) was then added to the reaction. The reactions stirred for 10 minutes and then diethyl oxalate (1.2 eq) was added. The reaction was then heated to 60°C and stirred for 2 hours. Completion of the reaction was monitored via TLC in a gradient of Hexanes/EtOAc. Once complete, the crude mixture was partitioned between 1M HCl and EtOAc. The organic layer was extracted, dried with Na_2SO_4 , filtered and concentrated down. The crude material was then dry loaded onto silica gel and purified via column chromatography. The fractions containing the product were combined, concentrated down and azeotroped with CHCl_3 to yield the 2,4-dioxobutanoates (60-85% yield).

General Procedure K: Synthesis of pyrazole ethyl esters. An arylhydrazine (1 eq) and 2,4-dioxobutanoate (1.2 eq) were added into a reaction flask and solubilized in MeOH (0.1 M). The reaction was refluxed for 3 hours at 65°C. Completion of the reaction was monitored via TLC in a gradient of Hexanes/EtOAc. Once complete, the crude mixture was partitioned between 1M NaOH and EtOAc. The organic layer was extracted, dried with Na₂SO₄, filtered and concentrated down. The crude material was then dry loaded onto silica gel and purified via column. The fractions containing the product were collected, combined, concentrated down and azeotroped with CHCl₃ to yield the pyrazole ethyl esters (80-90% yield).

General Procedure L: Synthesis of pyrazole carboxylic acids. A pyrazole ethyl ester (1 eq) was placed into a reaction flask and solubilized in a 3:1:1 mixture of THF/H₂O/MeOH (0.1 M). LiOH monohydrate (3 eq) was then added and the reaction stirred at room temperature for 3 hours. Additional MeOH and THF were added when needed to homogenize the reaction mixture. Completion of the reaction was monitored via TLC in a gradient of 92:7:1 DCM/MeOH/Acetic acid. Once complete, the crude mixture was partitioned between 1M NaOH and EtOAc. The aqueous layer was collected and then acidified to a pH of 3. EtOAc was added to the acidified aqueous layer. The organic layer was then extracted, dried with Na₂SO₄, filtered, concentrated down and azeotroped with CHCl₃ to yield the pyrazole carboxylic acids (90-95% yield).

General Procedure M: Synthesis of 3-acyl sulfonamide pyrazoles. A pyrazole carboxylic acid (1 eq) was placed into a reaction flask and solubilized in SOCl₂ (0.3 M). The reaction was refluxed for 3 hours to create the acid chloride. Formation of acid chloride was determined via TLC in a gradient of 92:7:1 DCM/MeOH/Acetic acid by

performing a mini-workup in MeOH. Once all the starting acid had become the acid chloride, the SOCl₂ was vacuum evaporated and the acid chloride was re-solubilized in anhydrous DCE (0.3 M). Sulfonamides (1.2 eq) were then added to the reaction followed by DMAP (0.5 eq). The reaction stirred at room temperature for 16 hours. Completion of the reaction was monitored via TLC in a gradient of 92:7:1 DCM/MeOH/H₂O. Once complete, the DCE was evaporated and the crude mixture was dry loaded onto silica gel. The product was purified via column chromatography in a gradient of 92:7:1 DCM/MeOH/H₂O. The product fractions were collected, combined, concentrated down and azeotroped with CHCl₃ to yield the 3-acylsulfonamide pyrazoles (40-65% yield).

3-aryl-2-acyl sulfonamide-1H-indoles

General Procedure N: Synthesis of 3-bromo 1H-indoles. Dissolve 6-chloro 2-ethyl ester 1H-indole (1 eq) in DMF (0.25 M). Add NBS (1.8 eq) dropwise and stir the reaction at room temperature for 1 hour. A TLC of the reaction in 1:1 Hexanes/EtOAc revealed the reaction had completed. The mixture was partitioned between EtOAc and H₂O. After the organic layer was washed four times with H₂O, 50mL of brine was added to wash the organic layer and dried with Na₂SO₄, filtered and concentrated down. The crude material was then dry loaded onto silica gel and purified via column chromatography (4:1 Hexanes/EtOAc) and azeotroped with CHCl₃ to yield 3-bromo-6-chloro-1H-indole (83%).

General Procedure O: Synthesis of 5-bromo-biphenyl ethers. Dissolve 3-chlorophenol (1.5 eq) and 5-bromo-2-fluoropyridine (1 eq) in DMF (0.1 M) followed by addition of K₂CO₃ (2 eq). The reaction was stirred at 100°C overnight. A TLC of the reaction in 1:1 Hexanes/EtOAc revealed the reaction had completed. The mixture was

partitioned between EtOAc and H₂O. After the organic layer was washed four times with H₂O, 50mL of brine was added to wash the organic layer and dried with Na₂SO₄, filtered and concentrated down. The crude material was then dry loaded onto silica gel and purified via column chromatography (2:1 Hexanes/EtOAc) and azeotroped with CHCl₃ to yield 5-bromo-2-(3-chlorophenoxy)pyridine (61%).

General Procedure P: Synthesis of 5-boronic ester-biphenyl ethers. A substituted bromo-halogenated biphenyl ring (1 eq) was dissolved in anhydrous DMF (0.1 M). The mixture was degassed with N₂ followed by addition of AcOK (2 eq), bis(pinacolato)diboron (1.1 eq), and PdCl₂(PPh₃)₂ (5mol%). The reaction was stirred at 80° for 2 hours. A TLC of the reaction in 2:1 Hexanes/EtOAc revealed the reaction had completed. The mixture was filtered through a pad of selite with CH₂Cl₂ and concentrated down. The oil was partitioned between EtOAc and H₂O. After the organic layer was washed four times with H₂O, 50mL of brine was added to wash the organic layer and dried with Na₂SO₄, filtered and concentrated down. The crude material was then dry loaded onto silica gel and purified via column chromatography (4:1 Hexanes/EtOAc) and azeotroped with CHCl₃ to yield a boronic ester substituted biphenyl ring (13-73%).

General Procedure Q: Synthesis of 3-aryl-1H-indole ethyl esters. A 3-bromo-1H-indole (1 eq) and aryl boronic ester (1.5 eq) was dissolved in anhydrous DMF (0.1 M). K₂CO₃ (3 eq) was added and the reaction was degassed with N₂. PdCl₂(PPh₃)₂ was added and the reaction was stirred at 110°C overnight. A TLC of the reaction in 4:1 Hexanes/EtOAc revealed the reaction had completed. The mixture was partitioned between EtOAc and H₂O. After the organic layer was washed four times with H₂O, 50mL

of brine was added to wash the organic layer and dried with Na_2SO_4 , filtered and concentrated down. The crude material was then dry loaded onto silica gel and purified via column chromatography (4:1 Hexanes/EtOAc) and azeotroped with CHCl_3 to yield the 3-aryl-1H-indole ethyl esters (20-25%).

General Procedure R: Synthesis of 3-aryl-1H-indole carboxylic acids. An indole ethyl ester (1 eq) was placed into a reaction flask and dissolved in a 3:1:1 mixture of THF/ H_2O /MeOH (0.1 M). LiOH monohydrate (3 eq) was then added and the reaction stirred at room temperature for overnight. Completion of the reaction was monitored via TLC in a gradient of 92:7:1 DCM/MeOH/Acetic acid. Once complete, the crude mixture was partitioned between 1M HCl and EtOAc. The organic layer was then extracted, dried with Na_2SO_4 , filtered, concentrated down and azeotroped with CHCl_3 to yield the indole carboxylic acids (99% yield).

General Procedure S: Synthesis of 3-aryl-1H-indole acyl sulfonamides. An indole carboxylic acid (1 eq) and sulfonamide (1 eq) was dissolved in CH_2Cl_2 (0.1 M). EDCI (1.3 eq) and DMAP (1eq) was added followed by dropwise addition of DIPEA (2 eq). The reaction was monitored by TLC in mixture of 79:9:1 DCM/MeOH/ H_2O . When complete, the reaction as partitioned between CH_2Cl_2 and saturated NH_4Cl , followed by a wash with brine. The organic layer was then extracted, dried with Na_2SO_4 , filtered, and concentrated down. The crude material was then dry loaded onto silica gel and purified via column chromatography (79:9:1 CH_2Cl_2 /MeOH/ H_2O) and azeotroped with CHCl_3 to yield the 2-acyl sulfonamide indoles (7%).

Reverse sulfonamide 1H-indoles

General Procedure T: Synthesis of 1H-indole sulfonic acids. An indole ethyl ester (1 eq) was dissolved in Acetic Anhydride (1M) and was cooled to 0°C. H₂SO₄ (5 eq) was slowly added dropwise to the reaction mixture and stirred overnight at room temperature. A TLC of the reaction in 1:1 Hexanes/EtOAc revealed the reaction had completed. The reaction underwent vacuum filtration with cold AcOH followed by EtOAc and dried in a vacuum oven overnight to yield the 1H-indole sulfonic acids (68%).

General Procedure U: Synthesis of 1H-indole sulfonyl chlorides. An indole sulfonic acid (1 eq) was dissolved in CH₂Cl₂ (0.2 M) and a catalytic amount of DMF (2 M) was added until the reaction turned clear. Slowly, oxalyl chloride (5 eq) was added and the reaction was stirred at 40°C for 2-3 hours. A TLC of the reaction in 2:1 Hexanes/EtOAc revealed the reaction was complete after 2 hours. The solvent was concentrated down and the crude product was moved forward to yield the indole sulfonyl chlorides (>99%).

General Procedure V: Synthesis of reverse sulfonamide 1H-indole ethyl esters. An indole sulfonyl chloride (1 eq) and a secondary amine (1.5 eq) was dissolved in anhydrous CHCl₃ (0.1 M) followed by addition of DIPEA (3 eq). The reaction was monitored by TLC in 2:1 Hexanes/EtOAc, and when complete the solvent was concentrated down to dryness. The crude material was then dry loaded onto silica gel and purified via column chromatography (2:1 Hexanes/EtOAc) and azeotroped with CHCl₃ to yield the reverse sulfonamide indole ethyl esters(22-68%).

General Procedure W: Synthesis of reverse sulfonamide 1H-indole carboxylic acids. An indole ethyl ester (1 eq) was placed into a reaction flask and dissolved in a 3:1:1 mixture of THF/H₂O/MeOH (0.1 M). LiOH monohydrate (3 eq) was then added and the reaction stirred at room temperature for overnight. Completion of the reaction was

monitored via TLC in a gradient of 92:7:1 DCM/MeOH/Acetic acid. Once complete, the crude mixture was partitioned between 1M HCl and EtOAc. The organic layer was then extracted, dried with Na₂SO₄, filtered, concentrated down. The crude mixture was dry loaded onto silica and columned in a gradient of 92:7:1 DCM/MeOH/Acetic acid and azeotroped with CHCl₃ to yield the indole carboxylic acids (35-73% yield).

General Procedure X: Synthesis of secondary amines. A substituted aryl aldehyde (1eq) was dissolved in DCE (0.25 M) at 0°C followed by a substituted primary amine (1eq). Once dissolved, NaBH(OAc)₃ (1.5 eq) was added and the reaction was stirred overnight at room temperature. Completion of the reaction was monitored via TLC in a gradient of 92:7:1 DCM/MeOH/Ammonium hydroxide. Once complete, the crude mixture was partitioned between saturated NaHCO₃ and EtOAc. The organic layer was then extracted, dried with Na₂SO₄, filtered, concentrated down. The crude mixture was dry loaded onto silica and columned in a gradient of 92:7:1 DCM/MeOH/Ammonium hydroxide and azeotroped with CHCl₃ to yield the indole carboxylic acids.

Isoxazoles

ethyl 4-(3,4-dichlorophenyl)-2,4-dioxobutanoate (2a). General procedure A with 3,4-dichloroacetophenone. Yellow solid (yield = 53%). δ_{H} (400MHz, CDCl₃) 8.07 (s, 1H, Ar), 7.81 (d, 1H, Ar, $J = 8$ Hz), 7.59 (d, 1H, Ar, $J = 8.8$ Hz), 7.01 (s, 1H, Ar), 4.44-4.38 (m, 2H, CH₂CH₃), 1.42 (t, 3H, CH₂CH₃, $J = 7.2$ Hz); δ_{C} (400MHz, d₆-DMSO) 187.8, 170.1, 162.9, 136.6, 135.0, 132.2, 131.2, 129.5, 127.8, 98.1, 61.4, 13.9

ethyl 4-(6-(3-chlorophenoxy)pyridin-3-yl)-2,4-dioxobutanoate (2b). General procedure A with 1-(6-(3-chlorophenoxy)pyridin-3-yl)ethan-1-one. Red solid (yield = 42%). δ_{H} (400MHz, CDCl₃) 8.81 (s, 1H, Ar), 8.30 (d, 1H, Ar, $J = 10.8$ Hz), 7.37 (t, 1H, Ar, $J = 7.6$

Hz), 7.26 (s, 2H, Ar), 7.20 (s, 1H, Ar), 7.06 (t, 2H, Ar, $J = 10.4$ Hz), 6.99 (s, 1H, Ar), 4.43-4.37 (m, 2H, CH_2CH_3), 1.41 (t, 3H, CH_2CH_3 , $J = 7.2$ Hz)

ethyl 5-(3,4-dichlorophenyl)isoxazole-3-carboxylate (3a). General procedure B with 2a.

White solid (yield = 54%). δ_{H} (400MHz, CDCl_3) 7.91 (s, 1H, Ar), 7.65 (d, 1H, Ar, $J = 8.8$ Hz), 7.58 (d, 1H, Ar, $J = 8$ Hz), 6.95 (s, 1H, Ar), 4.51-4.45 (m, 2H, CH_2CH_3), 1.44 (t, 3H, CH_2CH_3 , $J = 6.8$ Hz); δ_{C} (400MHz, CDCl_3) 168.8, 159.2, 156.7, 134.7, 133.3, 130.8, 127.2, 125.8, 124.5, 100.5, 62.0, 13.7

ethyl 5-(6-(3-chlorophenoxy)pyridin-3-yl)isoxazole-3-carboxylate (3b). General

procedure B with 2b. White solid (yield = 81%). δ_{H} (400MHz, CDCl_3) 8.62 (s, 1H, Ar), 8.13 (d, 1H, Ar, $J = 8.8$ Hz), 7.36 (t, 1H, Ar, $J = 7.6$ Hz), 7.26 (s, 2H, Ar), 7.20 (s, 1H, Ar), 7.07 (d, 2H, Ar, $J = 8.8$ Hz), 6.91 (s, 1H, Ar), 4.51-4.45 (m, 2H, CH_2CH_3), 1.44 (t, 3H, CH_2CH_3 , $J = 6.8$ Hz); δ_{C} (400MHz, $\text{d}_6\text{-DMSO}$) 168.5, 163.8, 159.2, 156.8, 153.9, 145.4, 137.6, 133.6, 131.1, 125.2, 121.8, 120.4, 118.4, 112.1, 100.9, 62.0, 13.9

ethyl 5-(3,4-dichlorophenyl)-4-iodoisoxazole-3-carboxylate (4a). General procedure C

with 3a. Light yellow solid (yield = 85%). δ_{H} (400MHz, CDCl_3) 8.18 (s, 1H, Ar), 7.93 (d, 1H, Ar, $J = 8.4$ Hz), 7.62 (d, 1H, Ar, $J = 8.4$ Hz), 4.53-4.48 (m, 2H, CH_2CH_3), 1.46 (t, 3H, CH_2CH_3 , $J = 7.2$ Hz); Moved crude product forward.

ethyl 5-(6-(3-chlorophenoxy)pyridin-3-yl)-4-iodoisoxazole-3-carboxylate (4b). General

procedure C with 3b. Light brown solid (yield = 86%). δ_{H} (400MHz, CDCl_3) 8.60 (s, 1H, Ar), 8.14 (d, 1H, Ar, $J = 8$ Hz), 7.88 (d, 1H, Ar, $J = 8.4$ Hz), 7.33 (s, 1H, Ar), 7.09 (d, 1H, Ar, $J = 8.8$ Hz), 6.91 (s, 1H, Ar), 6.85 (d, 1H, Ar, $J = 5.6$ Hz), 4.49-4.47 (m, 2H, CH_2CH_3), 1.44 (t, 3H, CH_2CH_3 , $J = 6.8$ Hz); Moved crude product forward.

ethyl 5-(3,4-dichlorophenyl)-4-(4-isopropoxyphenyl)isoxazole-3-carboxylate (5a).

General procedure D with 4a and (4-isopropoxyphenyl)boronic acid. White solid (yield = 63%). δ_{H} (400MHz, CDCl_3) 7.66 (s, 1H, Ar), 7.37 (d, 1H, Ar, $J = 8.4$ Hz), 7.28 (obsc, 1H, Ar), 7.21 (d, 2H, Ar, $J = 8.4$ Hz), 6.94 (d, 2H, Ar, $J = 8.8$ Hz), 4.62-4.58 (m, 1H, $\text{CH}(\text{CH}_3)_2$), 4.35-4.30 (m, 2H, CH_2CH_3), 1.37 (d, 6H, $\text{CH}(\text{CH}_3)_2$, $J = 6.4$ Hz), 1.28 (t, 3H, CH_2CH_3 , $J = 7.2$ Hz); δ_{C} (400MHz, d_6 -DMSO) 158.6, 157.1, 134.0, 132.3, 131.5, 131.4, 130.8, 130.5, 129.1, 128.6, 127.6, 126.9, 126.4, 62.3, 13.9

ethyl 4,5-bis(3,4-dichlorophenyl)isoxazole-3-carboxylate (5b). General procedure D with 4a and (3,4-dichlorophenyl)boronic acid. Light yellow solid (yield = 45%). δ_{H} (400MHz, CDCl_3) 7.68 (s, 1H, Ar), 7.53 (d, 1H, Ar, $J = 7.6$ Hz), 7.46 (s, 1H, Ar), 7.42 (d, 1H, Ar, $J = 8$ Hz), 7.22-7.16 (m, 2H, Ar), 4.38-4.32 (m, 2H, CH_2CH_3), 1.31 (t, 3H, CH_2CH_3 , $J = 7.2$ Hz); δ_{C} (400MHz, d_6 -DMSO) 164.6, 158.7, 157.1, 154.9, 133.8, 132.3, 131.5, 130.8, 130.5, 129.1, 128.9, 128.5, 127.6, 126.9, 126.2, 115.3, 61.8, 13.6

ethyl 4-(1-(tert-butoxycarbonyl)-6-methyl-1H-indol-3-yl)-5-(3,4-dichlorophenyl)isoxazole-3-carboxylate (5c). General procedure D with 4a and 1-boc-6-methyl indole-3-boronic acid, pinacol ester. (yield = 47%). δ_{H} (400MHz, CDCl_3) 8.07 (s, 1H, Ar), 7.83 (s, 1H, Ar), 7.64 (s, 1H, Ar), 7.32 (s, 2H, Ar), 7.00 (d, 1H, Ar, $J = 8$ Hz), 6.96 (d, 1H, Ar, $J = 8$ Hz), 4.31-4.29 (m, 2H, CH_2CH_3), 1.69 (s, 10H, $\text{CH}(\text{CH}_3)_3$), 1.56 (s, 3H, CH_3), 1.23 (t, 3H, CH_2CH_3 , $J = 7.2$ Hz); Moved crude product forward.

ethyl 5-(6-(3-chlorophenoxy)pyridin-3-yl)-4-(2,4-dichlorophenyl)isoxazole-3-carboxylate (5d). General procedure D with 4b and 2,4-dichlorophenyl boronic acid. Yellow solid (yield = 35%). δ_{H} (400MHz, CDCl_3) 8.65 (s, 1H, Ar), 8.16 (d, 1H, Ar, $J = 8.4$ Hz), 7.52 (s, 1H, Ar), 7.34 (s, 1H, Ar), 7.32 (d, 3H, Ar, $J = 4$ Hz), 7.27 (obsc, 1H, Ar), 7.18-7.11

(m, 2H, Ar), 6.29 (s, 1H, Ar), 4.51-4.45 (m, 2H, CH₂CH₃), 1.45 (t, 3H, CH₂CH₃, *J* = 7.2 Hz)

ethyl 5-(6-(3-chlorophenoxy)pyridin-3-yl)-4-(3,4-dichlorophenyl)isoxazole-3-carboxylate

(5e). General procedure D with 4b and 3,4-dichlorophenyl boronic acid. Brown-red solid (yield = 71%). δ_H (400MHz, CDCl₃) 8.64 (s, 1H, Ar), 8.16 (d, 1H, Ar, *J* = 8.4 Hz), 7.57 (s, 1H, Ar), 7.52 (d, 1H, Ar, *J* = 7.6 Hz), 7.38-7.33 (m, 3H, Ar), 7.18-7.12 (m, 2H, Ar), 6.92 (s, 1H, Ar), 4.51-4.46 (m, 2H, CH₂CH₃), 1.45 (t, 3H, CH₂CH₃, *J* = 8 Hz)

5-(3,4-dichlorophenyl)-4-(4-isopropoxyphenyl)isoxazole-3-carboxylic acid (6a). General

procedure E with 5a. White solid (yield = 94%). δ_H (400MHz, CDCl₃) 7.68 (s, 1H, Ar), 7.40 (d, 1H, Ar, *J* = 8.8 Hz), 7.30 (d, 1H, Ar, *J* = 8.4 Hz), 7.21 (d, 2H, Ar, *J* = 8.8 Hz), 6.94 (d, 2H, Ar, *J* = 8 Hz), 4.62-4.59 (m, 1H, CH(CH₃)₂), 1.39 (d, 6H, CH(CH₃)₂, *J* = 5.6 Hz); δ_C (400MHz, d₆-DMSO) 163.7, 161.2, 158.1, 157.0, 133.6, 132.3, 131.8, 131.6, 128.8, 127.4, 127.1, 120.0, 117.4, 116.0, 69.6, 22.2

4,5-bis(3,4-dichlorophenyl)isoxazole-3-carboxylic acid (6b). General procedure E with

5b. White solid (yield = 53%). δ_H (400MHz, (CH₃)₂CO) 7.74 (s, 2H, Ar), 7.65 (d, 2H, Ar, *J* = 6.8 Hz), 7.44 (d, 2H, Ar, *J* = 8 Hz); δ_C (400MHz, CDCl₃) 165.1, 156.0, 134.6, 133.0, 132.7, 132.6, 132.4, 131.7, 131.1, 130.8, 129.8, 129.1, 127.2, 116.0

4-(1-(tert-butoxycarbonyl)-6-methyl-1H-indol-3-yl)-5-(3,4-dichlorophenyl)isoxazole-3-carboxylic acid (6c). General procedure E with 5c and 1.1 eq of LiOH monohydrate.

Brown solid (yield = 90%). δ_H (400MHz, CDCl₃) 7.98 (s, 1H, Ar), 7.73 (s, 1H, Ar), 7.24 (obsc, 2H, Ar), 6.89 (s, 2H, Ar), 1.63 (s, 9H, CH(CH₃)₃) 2.41 (s, 3H, CH₃); δ_C (400MHz, CDCl₃) 149.5, 138.7, 136.5, 135.5, 135.1, 134.9, 134.5, 133.1, 130.7, 128.4, 126.6, 125.8, 125.6, 124.4, 119.2, 115.5, 107.8, 84.2, 28.0, 21.8

5-(3,4-dichlorophenyl)-4-(6-methyl-1H-indol-3-yl)isoxazole-3-carboxylic acid (6d).

General procedure E with 5c. (yield = 97%) δ_{H} (400MHz, $(\text{CH}_3)_2\text{CO}$) 10.55 (s, 1H, Ar), 7.80 (s, 1H, Ar), 7.55 (s, 3H, Ar), 7.32 (s, 1H, Ar), 7.01 (d, 1H, Ar, $J = 7.6$ Hz), 6.81 (d, 1H, Ar, $J = 8.8$ Hz), 2.40 (s, 3H, CH_3); δ_{C} (400MHz, CDCl_3) 168.9, 165.7, 162.4, 142.2, 138.5, 137.5, 136.6, 136.1, 133.3, 133.0, 131.4, 130.7, 129.4, 126.6, 123.9, 116.9, 106.5, 25.9

5-(6-(3-chlorophenoxy)pyridin-3-yl)-4-(2,4-dichlorophenyl)isoxazole-3-carboxylic acid

(6e). General procedure E with 5d. White solid (yield = 99%). δ_{H} (400MHz, CDCl_3) 8.68 (s, 1H, Ar), 8.18 (d, 1H, Ar, $J = 8.8$ Hz), 7.52 (s, 1H, Ar), 7.35-7.30 (m, 3H, Ar), 7.26 (obsc, 1H, Ar), 7.16 (t, 2H, Ar, $J = 12$ Hz), 6.98 (s, 1H, Ar); δ_{C} (400MHz, CDCl_3) 178.7, 164.0, 161.7, 156.9, 153.5, 145.4, 137.3, 136.0, 124.6, 134.3, 134.2, 132.0, 129.3, 126.9, 122.4, 119.6, 118.9, 112.3, 100.3

5-(6-(3-chlorophenoxy)pyridin-3-yl)-4-(3,4-dichlorophenyl)isoxazole-3-carboxylic acid

(6f). General procedure E with 5e. Grey solid (yield = 86%). δ_{H} (400MHz, CDCl_3) 8.77 (s, 1H, Ar), 8.43 (d, 1H, Ar, $J = 8.8$ Hz), 7.70 (d, 2H, Ar, $J = 8.4$ Hz), 7.55 (d, 1H, Ar, $J = 8.8$ Hz), 7.50 (d, 2H, Ar, $J = 9.6$ Hz), 7.32 (t, 3H, Ar, $J = 10$ Hz) δ_{C} (400MHz, CDCl_3) 173.8, 169.2, 165.9, 165.2, 159.2, 150.4, 144.2, 142.7, 139.7, 137.3, 136.5, 135.5, 134.8, 128.2, 125.9, 124.3, 117.5, 105.8,

5-(3,4-dichlorophenyl)-4-(4-isopropoxyphenyl)-N-(4-

(trifluoromethoxy)phenyl)sulfonyl)isoxazole-3-carboxamide (7a). General procedure F

with 6a and 4-(trifluoromethyl)benzenesulfonamide. White solid (yield = 77%). δ_{H} (400MHz, d_6 -DMSO) 7.86 (d, 2H, Ar, $J = 8.4$ Hz), 7.71 (d, 1H, Ar, $J = 8.8$ Hz), 7.67 (s, 1H, Ar), 7.41 (br s, 3H, Ar), 7.09 (d, 2H, Ar, $J = 8.8$ Hz), 6.81 (d, 2H, Ar, $J = 8.8$ Hz),

4.62-4.59 (m, 1H, $\underline{\text{CH}}(\text{CH}_3)_2$), 1.28 (d, 6H, $\underline{\text{CH}}(\text{CH}_3)_2$, $J = 6.4$ Hz); δ_{C} (400MHz, d_6 -DMSO) 168.0, 166.5, 166.1, 162.5, 155.0, 147.9, 144.2, 137.9, 136.9, 136.5, 135.8, 134.5, 133.5, 132.7, 132.0, 125., 125.1, 120.7, 120.5, 112.1, 74.2, 26.9

methyl 4-(4,5-bis(3,4-dichlorophenyl)isoxazole-3-carboxamido)benzoate (7b). General procedure F with 6b and methyl 3-aminobenzoate. White solid (yield = 30%). δ_{H} (400MHz, CDCl_3) 7.70 (s, 2H, Ar), 7.54 (d, 2H, Ar, $J = 8$ Hz), 7.45 (obsc, 2H, Ar), 7.22-7.17 (m, 4H, Ar), 3.91 (s, 3H, COOCH_3); Moved crude product forward.

5-(3,4-dichlorophenyl)-4-(6-methyl-1H-indol-3-yl)-N-((4-(trifluoromethoxy)phenyl)sulfonyl)isoxazole-3-carboxamide (7c). General procedure F with 6d and 4-(trifluoromethoxy)benzenesulfonamide. Green solid. (yield = 27%) δ_{H} (400MHz, d_6 -DMSO) 7.74 (t, 3H, Ar, $J = 8.4$ Hz), 7.61 (d, 1H, Ar, $J = 8.4$ Hz), 7.42 (d, 2H, Ar, $J = 14$), 7.32 (d, 2H, Ar, $J = 8$ Hz), 7.22 (s, 1H, Ar), 6.72 (d, 1H, Ar, $J = 8$ Hz), 6.67 (d, 1H, Ar, $J = 8$ Hz), 2.37 (s, 3H, CH_3); δ_{C} (400MHz, d_6 -DMSO) 163.4, 160.5, 149.9, 136.9, 132.6, 132.0, 131.4, 130.8, 129.4, 128.5, 128.3, 126.7, 125.9, 123.6, 121.3, 120.5, 119.1, 112.1, 109.9, 101.7, 21.6

5-(6-(3-chlorophenoxy)pyridin-3-yl)-4-(2,4-dichlorophenyl)-N-((4-(trifluoromethoxy)phenyl)sulfonyl)isoxazole-3-carboxamide (7d). General procedure F with 6e and 4-(trifluoromethoxy)benzenesulfonamide. White solid (yield = 99%). δ_{H} (400MHz, CDCl_3) 8.42 (s, 1H, Ar), 8.04 (d, 2H, Ar, $J = 8.8$ Hz), 7.95 (br s, 1H, Ar), 7.50 (t, 2H, Ar, $J = 6.4$ Hz), 7.33-7.24 (obsc, 3H, Ar), 7.11 (br s, 3H, Ar), 6.98 (d, 1H, Ar, $J = 8.8$ Hz), 6.79 (s, 1H, Ar); δ_{C} (400MHz, CDCl_3) 168.3, 164.9, 164.0, 162.8, 153.2, 151.5, 145.2, 140.3, 138.4, 136.9, 136.0, 133.0, 132.2, 132.0, 131.8, 131.3, 130.1, 128.8, 128.6, 123.0, 120.8, 120.3, 120.2, 118.6, 112.1, 106.5

5-(6-(3-chlorophenoxy)pyridin-3-yl)-4-(3,4-dichlorophenyl)-N-((4-(trifluoromethoxy)phenyl)sulfonyl)isoxazole-3-carboxamide (7e). General procedure F with 6f and *4-(trifluoromethoxy)benzenesulfonamide*. Yellow solid (yield = 13%). δ_{H} (400MHz, CDCl_3) 8.38 (s, 1H, Ar), 8.05 (d, 2H, Ar, $J = 8$ Hz), 7.87 (br s, 1H, Ar), 7.49 (s, 1H, Ar), 7.28 (obsc, 2H, Ar), 7.20 (d, 1H, Ar, $J = 7.6$ Hz), 7.10 (d, 1H, Ar, $J = 8.4$ Hz), 7.03 (br s, 2H, Ar), 6.92 (d, 2H, Ar, $J = 8.4$ Hz), 6.75 (s, 1H, Ar), δ_{C} (400MHz, CDCl_3) 178.1, 163.7, 158.3, 151.2, 145.0, 136.7, 136.0, 134.5, 134.4, 134.3, 134.2, 132.1, 131.9, 129.3, 129.0, 126.9, 122.3, 120.1, 119.5, 118.8, 112.0, 110.7, 102.7, 100.1

4-(4,5-bis(3,4-dichlorophenyl)isoxazole-3-carboxamido)benzoic acid (7e). General procedure E with 7b. White solid (yield = 98%). δ_{H} (400MHz, CDCl_3) 7.80 (s, 1H, Ar), 7.75 (obsc, 4H, Ar), 7.72 (s, 1H, Ar), 7.40 (d, 2H, Ar, $J = 8.8$ Hz), 7.35 (d, 2H, Ar, $J = 7.6$ Hz); δ_{C} (400MHz, $\text{d}_6\text{-DMSO}$) 164.4, 160.4, 155.8, 133.6, 132.1, 132.0, 131.5, 131.2, 131.0, 130.9, 130.8, 130.5, 130.4, 130.3, 129.2, 128.6, 127.4, 127.0, 126.4, 126.1, 115.3

4-(trifluoromethoxy)benzenesulfonamide: Followed General Procedure H with 4-(trifluoromethoxy)benzenesulfonyl chloride (83%). δ_{H} (400MHz, $\text{d}_6\text{-DMSO}$) 7.97 (d, $J = 8.8$ Hz, 2H), 7.61 (d, $J = 8.4$ Hz, 2H), 7.53 (s, 2H); Moved crude product forward.

Pyrazoles

(3,4-dichlorophenyl)aniline (8a). General Procedure H with 1-nitro-3,4-dichlorobenzene. Brown oil (yield = 90 %). δ_{H} (400MHz, $\text{d}_6\text{-DMSO}$) 7.19 (t, 1H, Ar, $J = 8.4$ Hz), 6.98 (d, 1H, Ar, $J = 8$ Hz), 6.80 (d, 2H, Ar, $J = 8.4$ Hz), 6.82 (s, 1H, Ar, $J = 7.6$ Hz), 6.73 (d, 2H, Ar, $J = 8.8$ Hz). Carbon spectrum consistent with Sigma Aldrich.

4-(3-chlorophenoxy)aniline (8b). General Procedure H with 1-nitro-4-phenoxybenzene. Brown solid (yield = 92 %). δ_{H} (400MHz, $\text{d}_6\text{-DMSO}$) 10.30 (bs, 2H, Ar), 8.66 (bs, 1H,

Ar), 7.54 (d, 1H, Ar, $J = 8.8$ Hz), 7.23 (s, 1H, Ar), 6.95 (d, 1H, Ar, $J = 8.8$ Hz). Moved forward with crude product.

(3,4-dichlorophenyl)hydrazine (9a). General Procedure I with 8a (yield = 68%). δ_{H} (400MHz, d_6 -DMSO) 10.30 (bs, 2H, Ar), 8.66 (bs, 1H, Ar), 7.54 (d, 1H, Ar, $J = 8.8$ Hz), 7.23 (s, 1H, Ar), 6.95 (d, 1H, Ar, $J = 8.8$ Hz).

(4-(3-chlorophenoxy)phenyl)hydrazine (9b). General Procedure I with 8b. Black solid. (yield = 65%). δ_{H} NMR (400MHz, CDCl_3) 7.19 (t, 1H, Ar, $J = 8.2$ Hz), 6.99 (d, 1H, Ar, $J = 8.0$ Hz), 6.88 (d, 3H, Ar, $J = 8.4$ Hz), 6.83 (d, 1H, Ar, $J = 7.6$ Hz), 6.73 (d, 2H, Ar, $J = 8.8$ Hz), 3.77 (bs, 2H).

ethyl 4-(6-chloro-1H-indol-3-yl)-2,4-dioxobutanoate (11a). General Procedure J with 1-(6-chloro-1H-indol-3-yl)ethan-1-one. Purple solid. (yield = 65%). δ_{H} (400MHz, d_6 -DMSO) 12.54 (s, 1H, Ar), 8.81 (s, 1H, Ar), 8.21 (d, 1H, Ar, $J = 8.4$ Hz), 7.57 (s, 1H, Ar), 7.30 (d, 1H, Ar, $J = 7.6$ Hz), 7.05 (s, 1H, Ar), 4.34-4.29 (m, 2H, CH_2CH_3), 1.33 (t, 3H, CH_2CH_3 , $J = 7.0$ Hz); Moved crude product forward.

ethyl 4-(3,4-dichlorophenyl)-2,4-dioxobutanoate (11b). General Procedure J with 1-(2,3-dichlorophenyl)ethan-1-one. Purple solid. (yield = 75%). δ_{H} (400MHz, CDCl_3) 8.08 (s, 1H), 7.82 (d, $J = 8.0$ Hz, 1H), 7.59 (d, $J = 8.0$ Hz, 1H), 7.01 (s, 1H), 4.42 (q, $J = 8.4$ Hz, 2H), 1.42 (t, $J = 6.8$ Hz, 3H); Carbon spectrum consistent with compound (2a).

ethyl 5-(6-chloro-1H-indol-3-yl)-1-(3,4-dichlorophenyl)-1H-pyrazole-3-carboxylate (12a). General Procedure K with 9a and 11a. Red solid. (yield = 87%). δ_{H} (400MHz, CDCl_3) 8.65 (s, 1H, Ar), 7.65 (s, 1H, Ar), 7.34-7.33 (m, 3H, Ar), 7.18-7.10 (m, 3H, Ar), 6.96 (s, 1H, Ar), 4.50-4.44 (m, 2H, CH_2CH_3), 1.45 (t, 3H, CH_2CH_3 , $J = 7.0$ Hz); δ_{C}

(400MHz, d₆-DMSO) 161.5, 144.2, 139.1, 139.0, 136.4, 131.5, 131.0, 130.9, 127.3, 127.0 126.7, 125.2, 123.9, 120.4, 120.1, 111.7, 109.4, 103.2, 60.6, 14.2

ethyl 1-(4-(3-chlorophenoxy)phenyl)-5-(3,4-dichlorophenyl)-1H-pyrazole-3-carboxylate

(12b). General Procedure K with 9b and 11b. Brown solid. (yield = 90%). δ_H (400MHz, CDCl₃) 7.41 (d, 1H, Ar, *J* = 8.8 Hz), 7.35 (s, 1H, Ar), 7.30 (t, 3H, Ar, *J* = 7.8 Hz), 7.12 (d, 1H, Ar, *J* = 8.0 Hz), 7.07-7.00 (m, 5H, ar), 6.90 (d, 1H, Ar, *J* = 8.8 Hz), 4.46 (m, 2H, CH₂CH₃), 1.43 (t, 3H, CH₂CH₃, *J* = 7.2 Hz).

5-(6-chloro-1H-indol-3-yl)-1-(4-(3-chlorophenoxy)phenyl)-1H-pyrazole-3-carboxylic acid

(13a). General Procedure L with 12a. Yellow solid. (yield = 93%). δ_H (400MHz, d₆-DMSO) 11.67 (s, 1H, Ar), 7.79 (d, 1H, Ar, *J* = 2.4 Hz), 7.66 (d, 1H, Ar, *J* = 8.4 Hz), 7.50 (d, 1H, Ar, *J* = 1.6 Hz), 7.40 (d, 1H, Ar, *J* = 2.4 Hz), 7.35-7.28 (m, 2H, Ar), 7.02 (t, 2H, Ar, *J* = 4.6 Hz); δ_C (400MHz, d₆-DMSO) 163.0, 145.3, 139.3, 136.6, 136.4, 131.4, 130.9, 130.8, 127.2, 126.8, 126.7, 125.0, 124.0, 120.4, 120.1, 111.7, 109.7, 103.4

1-(4-(3-chlorophenoxy)phenyl)-5-(3,4-dichlorophenyl)-1H-pyrazole-3-carboxylic acid

(13b). General Procedure L with 12b. White solid. (yield = 95%). δ_H (400MHz, CDCl₃) 7.43 (d, 1H, *J* = 7.6 Hz), 7.37 (d, 1H, Ar, *J* = 1.6 Hz), 7.31 (t, 3H, Ar, *J* = 8.0 Hz), 7.14 (d, 2H, Ar, *J* = 5.6 Hz), 7.07-7.02 (m, 4H, Ar), 6.92 (d, 1H, Ar, *J* = 8.4 Hz).

5-(6-chloro-1H-indol-3-yl)-N-((4-chlorophenyl)sulfonyl)-1-(3,4-dichlorophenyl)-1H-pyrazole-3-carboxamide (14a). General Procedure M with 13a and 4-

chlorobenzenesulfonamide. Yellow solid. (yield = 53%). δ_H (400MHz, d₆-DMSO). 11.68 (s, 1H, Ar), 8.04 (d, 2H, Ar, *J* = 8.8 Hz), 7.91 (d, 1H, Ar, *J* = 2.4 Hz), 7.77 (d, 2H, Ar, *J* = 8.8 Hz), 7.67 (d, 1H, Ar, *J* = 8.4 Hz), 7.51 (s, 1H, Ar), 7.36-7.30 (m, 3H, Ar), 7.15 (s, 1H, Ar), 7.04 (d, 1H, Ar, *J* = 8.8 Hz); δ_C (400 MHz, d₆-DMSO) 159.8, 144.1, 139.3, 138.9,

138.7, 136.3, 131.6, 131.0, 130.9, 129.6, 129.3, 127.3, 126.9, 126.8, 124.8, 123.9, 120.5, 120.1, 111.7, 108.7, 103.0

1-(4-(3-chlorophenoxy)phenyl)-N-((4-chlorophenyl)sulfonyl)-5-(3,4-dichlorophenyl)-1H-pyrazole-3-carboxamide (14b). General Procedure M with 13b and 4-chlorobenzenesulfonamide. Light brown solid. (yield = 54%). δ_{H} (400MHz, CDCl_3). 9.47 (s, 1H, Ar), 8.11 (d, 2H, Ar, $J = 8.8$ Hz), 7.52 (d, 2H, Ar, $J = 8.4$ Hz), 7.40 (d, 1H, Ar, $J = 8.8$ Hz), 7.33-7.24 (m, 5H, Ar), 7.15 (d, 1H, Ar, $J = 8.0$ Hz), 7.05-6.98 (m, 5H, Ar), 6.94 (d, 1H, Ar, $J = 8.0$ Hz); δ_{C} (400MHz, CDCl_3) 157.7, 156.8, 156.5, 144.0, 143.0, 140.2, 136.6, 133.4, 132.7, 130.4, 130.4, 130.3, 129.9, 129.6, 128.8, 128.1, 127.4, 127.0, 126.6, 124.0, 119.2, 119.0, 117.0, 108.5

N-((2-(4-chloro-3-fluorobenzamido)ethyl)sulfonyl)-1-(4-(3-chlorophenoxy)phenyl)-5-(3,4-dichlorophenyl)-1H-pyrazole-3-carboxamide (14c). General procedure M with 13b and 4-chloro-3-fluoro-N-(2-sulfamoyl)ethylbenzamide. White solid (yield = 28%). δ_{H} (400MHz, d_6 -DMSO). 8.81 (s, 1H, Ar), 7.69 (t, 2H, Ar, $J = 8.6$ Hz), 7.63 (s, 2H, Ar), 7.47 (d, 2H, Ar, $J = 6$ Hz), 7.40 (d, 1H, Ar, $J = 8.8$ Hz), 7.26 (d, 1H, Ar, $J = 8$ Hz), 7.21 (d, 4H, Ar, $J = 8.8$ Hz), 7.13 (s, 1H, Ar), 7.04 (d, 1H, Ar, $J = 8$ Hz), 3.77 (br s, 2H, $\text{NH}(\text{CH}_2)_2\text{SO}_2$), 3.71 (br s, 2H, $\text{NH}(\text{CH}_2)_2\text{SO}_2$); δ (400MHz, CDCl_3) 165.0, 158.6, 156.9, 156.4, 156.1, 143.2, 134.9, 133.6, 133.6, 133.4, 133.2, 132.8, 130.4, 130.4, 130.3, 129.9, 127.9, 126.5, 124.2, 124.0, 122.9, 119.2, 118.9, 117.0, 115.3, 115.0, 108.7, 52.8, 34.2

4-chlorobenzenesulfonamide. General Procedure G with 4-chlorobenzenesulfonyl chloride. White solid (yield = 86%). Proton and Carbon spectra consistent with *Perjessy, A., Sulfur Letters 2002, 25(2), 71-78.*

4-chloro-3-fluoro-N-(2-sulfamoyl)ethyl)benzamide. General procedure S with 4-chloro-3-fluorobenzoic acid and 2-aminoethanesulfonamide. White solid (yield = 62%). δ_{H} (400 MHz, d_6 -DMSO) 8.82 (br s, 1H, Ar), 7.82 (d, 1H, Ar, $J = 9.6$ Hz), 7.77-7.69 (m, 2H, Ar), 6.97 (s, 2H, Ar), 3.67-3.62 (m, 2H, $\text{NH}(\text{CH}_2)_2\text{SO}_2$), 3.26-3.23 (m, 2H, $\text{NH}(\text{CH}_2)_2\text{SO}_2$); Moved crude product forward.

2-acylsulfonamides 1H-indoles

ethyl 3-bromo-6-chloro-1H-indole-2-carboxylate (16). General procedure N. Orange oil. (yield = 83%) δ_{H} (400 MHz, CDCl_3) 9.05 (s, 1H, Ar), 7.60 (d, 1H, Ar, $J = 8.4$ Hz), 7.42 (s, 1H, Ar), 7.21 (d, 1H, Ar, $J = 8.8$ Hz), 4.50-4.45 (m, 2H, CH_2CH_3), 1.47 (t, 3H, (CH_2CH_3) , $J = 7.2$ Hz); Moved crude product forward.

5-bromo-2-(3-chlorophenoxy)pyridine (18). General procedure O with 5-bromo-2-fluoropyridine and 3-chlorophenol. Light brown oil. (yield = 61%) δ_{H} (400 MHz, CDCl_3) 8.24 (s, 1H, Ar), 7.81 (d, 1H, Ar, $J = 8.8$ Hz), 7.34 (t, 1H, Ar, $J = 7.8$ Hz), 7.21 (d, 1H, Ar, $J = 8.8$ Hz), 7.17 (s, 1H, Ar), 7.04 (d, 1H, Ar, $J = 8.8$ Hz), 6.88 (d, 1H, Ar, $J = 8.4$ Hz); δ_{C} (400MHz, CDCl_3) 161.5, 153.9 147.9, 141.7, 134.5, 130.0, 124.7, 121.2, 118.9, 113.6, 112.9

2-(3-chlorophenoxy)-5-(4,4,5,5-tetramethyl-1,3,2-dioxaborolan-2-yl)pyridine (19).

General Procedure P with 18. White solid (yield = 73%). δ_{H} (400 MHz, d_6 -DMSO) 8.53 (s, 1H, Ar), 8.24 (d, 1H, Ar, $J = 8.8$ Hz), 7.49 (t, 1H, Ar, $J = 8.2$ Hz), 7.33 (d, 2H, Ar, $J = 7.6$ Hz), 7.24- 7.18 (m, 2H, Ar), 1.19 (s, 12H, $(\text{C}(\text{CH}_3)_2)$); δ_{C} (400MHz, CDCl_3) 164.6, 154.1, 145.4, 134.4, 129.9, 124.4, 121.2, 118.9, 110.5, 83.6, 83.0, 24.6, 24.4

ethyl 6-chloro-3-(6-(3-chlorophenoxy)pyridin-3-yl)-1H-indole-2-carboxylate (20).

General Procedure Q with 16 and 19. Yellow solid (yield = 25%). δ_{H} (400 MHz, CDCl_3)

8.37 (s, 1H, Ar), 7.94-7.83 (m, 1H, Ar), 7.53 (d, 1H, Ar, $J = 8.4$ Hz), 7.46 (s, 1H, Ar), 7.34 (t, 1H, Ar, $J = 8.4$ Hz), 7.23 (d, 2H, Ar, $J = 12$ Hz), 7.17-7.05 (m, 4H, Ar).

6-chloro-3-(6-(3-chlorophenoxy)pyridin-3-yl)-1H-indole-2-carboxylic acid (21). General Procedure R with 20. Yellow solid (yield = 99%). δ_{H} (400 MHz, d_6 -DMSO) 8.32 (s, 1H, Ar), 8.08 (d, 1H, Ar, $J = 6.8$ Hz), 7.49 (t, 3H, Ar, $J = 9.6$ Hz), 7.33 (t, 3H, Ar, $J = 7.4$ Hz), 7.21 (d, 1H, Ar, $J = 8.4$ Hz), 7.14 (d, 1H, Ar, $J = 8$ Hz), 7.07 (d, 1H, Ar, $J = 8$ Hz).

6-chloro-3-(6-(3-chlorophenoxy)pyridin-3-yl)-N-((4-fluorophenyl)sulfonyl)-1H-indole-2-carboxamide (22). General procedure S with 20 and 4-fluorobenzenesulfonamide.

Yellow solid. (yield = 7%). δ_{H} (400 MHz, d_6 -DMSO) 8.20 (s, 1H, Ar), 7.95 (d, 1H, Ar, $J = 8.8$ Hz), 7.86 (t, 2H, Ar, $J = 6.8$ Hz), 7.54 (s, 1H, Ar), 7.50-7.42 (m, 2H, Ar), 7.33 (d, 2H, Ar, $J = 6.8$ Hz), 7.27-7.21 (m, 4H, Ar), 7.08 (d, 1H, Ar, $J = 8.8$ Hz), 7.02 (d, 1H, Ar, $J = 7.6$ Hz).

4-fluorobenzenesulfonamide. General Procedure G with 4-fluorobenzenesulfonylchloride. White solid (99%). δ_{H} (400 MHz, d_6 -DMSO) 7.91 (t, 2H, Ar, $J = 6.8$ Hz), 7.44 (t, 4H, Ar, $J = 8.6$ Hz); Carbon spectrum consistent with Sigma Aldrich.

Reverse sulfonamide Indoles

6-chloro-2-(ethoxycarbonyl)-1H-indole-3-sulfonic acid (23). General procedure T with 6-chloro-2-ethyl ester-1H-indole. Color. (yield = 95%) δ_{H} (400 MHz, d_6 -DMSO) 11.94 (s, 1H, Ar), 8.17 (d, 1H, Ar, $J = 9.2$ Hz), 7.1 (s, 1H, Ar), 7.09 (d, 1H, Ar, $J = 8$ Hz), 4.33-4.28 (m, 2H, CH_2CH_3), 1.32 (t, 3H, (CH_2CH_3), $J = 7$ Hz); δ_{C} (400 MHz, d_6 -DMSO) 161.1, 135.1, 129.0, 126.8, 125.7, 125.3, 124.3, 121.0, 111.6, 61.1, 14.5

ethyl 6-chloro-3-(chlorosulfonyl)-1H-indole-2-carboxylate (24). General procedure U with 23. Yellow solid. (yield = 99%). δ_{H} (400 MHz, CDCl_3) 12.05 (s, 1H, Ar), 8.16 (d,

1H, Ar, $J = 8.4$ Hz), 7.44 (s, 1H, Ar), 7.10 (d, 1H, Ar, $J = 8.4$ Hz), 4.47-4.29 (m, 2H, CH_2CH_3), 1.33 (t, 3H, $J = 8$ Hz); δ_{C} (400 MHz, CDCl_3) 164.8, 158.9, 138.6, 134.3, 132.2, 125.3, 122.2, 113.4, 99.8, 63.0, 13.8

N-(4-bromobenzyl)-1-cyclohexylmethanamine. General procedure X with 4-bromobenzaldehyde and cyclohexane methylamine. Light yellow oil. (yield = %). δ_{H} (400 MHz, CDCl_3) 7.50 (s, 1H, Ar), 7.38 (d, 1H, Ar, $J = 6.8$ Hz), 7.25 (s, 1H, Ar), 7.2-7.171 (m, 1H, Ar), 3.75 (d, 2H, NHCH_2), 2.46-2.44 (m, 2H, NHCH_2) 1.78-1.66 (m, 5H, C_6H_{12}), 1.48-1.39 (m, 2H, C_6H_{12}) 1.27-1.14 (m, 3H, C_6H_{12}), 0.097-0.91 (m, 2H, C_6H_{12})

N-(3-bromobenzyl)-2-(4-chlorophenyl)ethan-1-amine. General procedure X with 3-bromobenzaldehyde and 2-(4-chlorophenyl)ethylamine. Yellow oil (yield = %). δ_{H} (400 MHz, CDCl_3) 7.49 (s, 1H, Ar), 7.38 (d, 1H, Ar, $J = 7.6$ Hz), 7.26 (obsc, 3H, Ar), 7.20 (d, 1H, Ar, $J = 6.8$ Hz), 7.12 (d, 2H, Ar, $J = 8$ Hz), 3.81 (d, 2H, NHCH_2), 2.87 (br s, 4H, NHCH_2) 2.17 (s, 3H, ?)

N-(3,4-dichlorobenzyl)-1-(furan-3-yl)methanamine. General procedure X with 3,4-dichlorobenzaldehyde and furfurylamine. Red oil (yield = %). δ_{H} (400 MHz, CDCl_3) 7.45 (s, 1H, Ar), 7.38 (d, 2H, Ar, $J = 7.6$ Hz), 7.17 (d, 1H, Ar, $J = 8.8$ Hz), 6.32 (s, 1H, Ar), 6.18 (s, 1H, Ar), 3.77 (d, 2H, NHCH_2), 3.74 (d, 2H, NHCH_2)

N-(4-bromobenzyl)-2-methylpropan-1-amine. General procedure X with 4-bromobenzaldehyde and isobutylamine. Color (yield = %).

N-(3,4-dichlorobenzyl)-2,2-dimethylpropan-1-amine. General procedure X with 3,4-dichlorobenzaldehyde and neopentylamine. Colorless oil (yield = %).

N-(4-chlorobenzyl)-2,2-dimethylpropan-1-amine. General procedure X with 4-chlorobenzaldehyde and neopentylamine. Colorless oil (yield = %) δ_{H} (400 MHz, CDCl_3) 7.28 (obsc, 4H, Ar), 3.77 (s, 2H, NHCH_2), 2.31 (s, 2H, NHCH_2), 0.91 (s, 9H, $\text{C}(\text{CH}_3)_3$)

N-benzyl-1-(4-chlorophenyl)methanamine. General procedure X with benzylamine and 4-chlorobenzaldehyde. Orange oil (yield = %). δ_{H} (400 MHz, CDCl_3) 7.34 (d, 4H, Ar, $J = 4.4$ Hz), 7.29 (obsc, 5H, Ar), 3.79 (d, 4H, NHCH_2 , $J = 6.8$ Hz); Carbon consistent with *Likhar, Pravin R., European Journal of Organic Chemistry 2009, (31), 5383-5389*

ethyl 3-(N-(4-bromobenzyl)-N-(cyclohexylmethyl)sulfamoyl)-6-chloro-1H-indole-2-carboxylate (25a). General procedure V with 24 and *N*-(4-bromobenzyl)-1-cyclohexylmethanamine. White solid (yield = 68%). δ_{H} (400 MHz, CDCl_3) 8.29 (d, 1H, Ar, $J = 8.8$ Hz), 7.47 (s, 1H, Ar), 7.35 (d, 1H, Ar, $J = 7.2$ Hz), 7.30 (obsc, 2H, Ar), 7.18 (d, 1H, Ar, $J = 7.2$ Hz), 7.13 (d, 1H, Ar, $J = 7.2$ Hz), 4.55 (s, 2H, NHCH_2), 4.51-4.45 (m, 2H, CH_2CH_3), 3.16-3.15 (m, 2H, NHCH_2) 1.60 (br s, 8H, C_6H_{12}), 1.43 (t, 4H, C_6H_{12} , $J = 6.8$ Hz) 1.06 (s, 3H, CH_2CH_3); δ_{C} (400MHz, $\text{d}_6\text{-DMSO}$) 159.3, 140.2, 134.9, 130.3, 130.0, 129.9, 128.9, 126.8, 124.0, 123.3, 123.0, 121.5, 112.6, 62.1, 54.1, 50.6, 35.2, 30.0, 25.8, 25.2, 14.0

ethyl 3-(N-(3-bromobenzyl)-N-(4-chlorophenethyl)sulfamoyl)-6-chloro-1H-indole-2-carboxylate (25b). General procedure V with 24 and *N*-(3-bromobenzyl)-2-(4-chlorophenyl)ethan-1-amine. Yellow oil (yield = 22%). δ_{H} (400 MHz, CDCl_3) 8.26 (d, 1H, Ar, $J = 8.4$ Hz), 7.48 (s, 1H, Ar), 7.39 (s, 2H, Ar), 7.31-7.16 (obsc m, 3H, Ar), 7.04 (2, 1H, Ar, $J = 8.8$ Hz), 6.81 (d, 2H, Ar, $J = 8$ Hz), 4.62 (s, 2H, NHCH_2), 4.46-4.41 (m, 2H, CH_2CH_3), 3.52-3.48 (m, 2H, NHCH_2), 2.69-2.65 (m, 2H, NHCH_2), .60 (br s, 8H, C_6H_{12}), 1.47-1.41 (m, 3H) 0.94 (s, 3H, CH_2CH_3)

ethyl 6-chloro-3-(N-(3,4-dichlorobenzyl)-N-(furan-3-ylmethyl)sulfamoyl)-1H-indole-2-carboxylate (25c). General procedure V with 24 and N-(3,4-dichlorobenzyl)-1-(furan-3-yl)methanamine. White solid (yield = 40%). δ_{H} (400 MHz, CDCl_3) 9.55 (s, 1H, Ar), 8.29 (d, 1H, Ar, $J = 8.8$ Hz), 7.48 (s, 1H, Ar), 7.34 (d, 1H, Ar, $J = 7.6$ Hz), 7.30 (obsc, 1H, Ar), 7.19 (s, 1H, Ar), 7.12 (d, 1H, Ar, $J = 8.4$ Hz), 6.17 (s, 1H, Ar), 5.93 (s, 1H, Ar), 4.51 (s, 2H, NHCH_2), 4.46-4.41 (m, 4H, NHCH_2 and CH_2CH_3), 1.41 (t, 3H, CH_2CH_3 , $J = 7.2$ Hz); δ_{C} (400 MHz, CDCl_3) 158.4, 149.1, 142.6, 136.8, 133.9, 132.6, 131.5, 130.4, 129.9, 127.5, 127.0, 125.1, 124.4, 124.0, 119.0, 111.7, 110.2, 109.6

ethyl 3-(N-(4-bromobenzyl)-N-isobutylsulfamoyl)-6-chloro-1H-indole-2-carboxylate (25d). General procedure V with 24 and N-(4-bromobenzyl)-2-methylpropan-1-amine. (yield = 28%). δ_{H} (400 MHz, CDCl_3) 9.60 (s, 1H, Ar), 8.25 (d, 1H, Ar, $J = 8.4$ Hz), 7.46 (s, 1H, Ar), 7.39 (d, 2H, Ar, $J = 7.6$ Hz), 7.27 (d, 1H, Ar, $J = 7.2$ Hz), 7.14 (d, 2H, Ar, $J = 8$ Hz), 4.56 (s, 2H, NHCH_2), 4.46-4.41 (m, 2H, CH_2CH_3), 3.03 (d, 2H, NHCH_2 , $J = 7.2$ Hz), 1.70 (s, 1H, $\text{CH}(\text{CH}_2)_2$), 1.40 (t, 3H, CH_2CH_3 , $J = 6$ Hz), 0.69 (d, 6H, $\text{CH}(\text{CH}_2)_2$, $J = 6.4$ Hz); δ_{C} (400 MHz, CDCl_3) 158.7, 135.8, 134.0, 132.5, 131.5, 129.8, 126.7, 125.1, 124.3, 124.0, 121.4, 119.8, 111.7, 65.5, 54.9, 51.1, 26.2, 19.8

ethyl 6-chloro-3-(N-(3,4-dichlorobenzyl)-N-neopentylsulfamoyl)-1H-indole-2-carboxylate (25e). General procedure V with 24 and N-(3,4-dichlorobenzyl)-2,2-dimethylpropan-1-amine. Yellow oil (yield = 45%). δ_{H} (400 MHz, CDCl_3) 8.23 (d, 1H, Ar, $J = 8.8$ Hz), 7.44 (s, 1H, Ar), 7.29-7.23 (obsc, 2H, Ar), 7.14 (s, 1H, Ar), 7.01 (d, 1H, Ar, $J = 8.4$ Hz), 4.69 (s, 2H, NHCH_2), 4.50-4.44 (m, 2H, CH_2CH_3), 3.32 (s, 2H, NHCH_2), 1.43 (t, 3H, CH_2CH_3 , $J = 6.8$ Hz), 0.91 (s, 9H, $\text{C}(\text{CH}_3)_3$)

ethyl 6-chloro-3-(N-(4-chlorobenzyl)-N-neopentylsulfamoyl)-1H-indole-2-carboxylate (25f). General procedure V with 24 and N-(4-chlorobenzyl)-2,2-dimethylpropan-1-amine. Yellow oil (yield = 35%). δ_{H} (400 MHz, CDCl_3) 10.15 (s, 1H, Ar), 8.21 (d, 1H, Ar, $J = 9.6$ Hz), 7.44 (s, 1H, Ar), 7.24 (s, 1H, Ar), 7.15 (d, 2H, Ar, $J = 8.4$ Hz), 7.07 (d, 2H, Ar, $J = 8.4$ Hz), 4.70 (s, 2H, NHCH_2), 4.40-4.35 (m, 2H, CH_2CH_3), 3.24 (s, 2H, NHCH_2), 1.34 (t, 3H, CH_2CH_3 , $J = 6.8$ Hz), 0.84 (s, 9H, $\text{C}(\text{CH}_3)_3$)

ethyl 3-(N-benzyl-N-(4-chlorobenzyl)sulfamoyl)-6-chloro-1H-indole-2-carboxylate (25g). General procedure V with 24 and N-benzyl-1-(4-chlorophenyl)methanamine. White solid (yield = 44%). δ_{H} (400 MHz, CDCl_3) 8.30 (d, 1H, Ar, $J = 8.4$ Hz), 7.47 (s, 1H, Ar), 7.26 (obsc, 2H, Ar), 7.26-7.16 (m, 5H, Ar), 7.00 (d, 4H, Ar, $J = 9.6$ Hz), 4.47-4.42 (d, 6H, NHCH_2 and CH_2CH_3), 1.39 (t, 3H, CH_2CH_3 , $J = 7.6$ Hz); δ_{C} (400MHz, CDCl_3) 135.1, 134.1, 133.6, 132.9, 132.2, 129.2, 128.1, 128.0, 127.8, 127.2, 126.5, 124.7, 124.0, 123.5, 111.4, 76.9, 76.2, 62.1, 13.8

3-(N-(4-bromobenzyl)-N-(cyclohexylmethyl)sulfamoyl)-6-chloro-1H-indole-2-carboxylic acid (26a). General procedure W with 25a. Yellow solid (yield = 50%). δ_{H} (400 MHz, d_6 -DMSO) 8.00 (d, 1H, Ar, $J = 8.4$ Hz), 7.52 (s, 1H, Ar), 7.50 (s, 1H, Ar), 7.43 (d, 1H, Ar, $J = 7.6$ Hz), 7.33 (d, 1H, Ar, $J = 7.6$ Hz), 7.28-7.20 (m, 2H, Ar), 4.61 (s, 2H, NHCH_2), 3.02 (d, 2H, NHCH_2), 1.49 (br s, 5H, C_6H_{12}), 1.25 (s, 2H, C_6H_{12}), 0.99-0.87 (m, 3H, C_6H_{12}), 0.64-0.61 (m, 2H, C_6H_{12}); δ_{C} (400 MHz, d_6 -DMSO) 146.8, 139.2, 135.6, 135.4, 134.9, 133.0, 131.9, 129.9, 127.5, 127.1, 126.6, 117.2, 59.9, 56.8, 40.7, 35.2, 31.1, 30.4

3-(N-(3-bromobenzyl)-N-(4-chlorophenethyl)sulfamoyl)-6-chloro-1H-indole-2-carboxylic acid (26b). General procedure W with 25b. Color (yield = 53%). δ_{H} (400 MHz, d_6 -DMSO) 7.94 (d, 1H, Ar, $J = 10$ Hz), 7.50 (d, 2H, Ar, $J = 9.6$ Hz), 7.44 (d, 1H, Ar, $J = 8$

Hz), 7.34 (d, 1H, Ar, $J = 6.8$ Hz), 7.27 (t, 1H, Ar, $J = 7.6$ Hz), 7.18 (d, 3H, Ar, $J = 8$ Hz), 6.98 (d, 2H, Ar, $J = 8$ Hz), 4.69 (NHCH₂), 3.19 (s, 4H, NHCH₂) 2.57 (obsc, 2H, NHCH₂); δ_C (400 MHz, d₆-DMSO) 184.3, 162.3, 141.5, 137.6, 134.7, 133.9, 130.6, 130.5, 130.3, 129.8, 128.0, 127.4, 126.8, 124.5, 123.9, 122.0, 121.6, 112.1, 50.7, 49.0, 33.3

6-chloro-3-(N-(3,4-dichlorobenzyl)-N-(furan-3-ylmethyl)sulfamoyl)-1H-indole-2-

carboxylic acid (26c). General procedure W with 25c. Yellow solid (yield = 35%). δ_H

(400 MHz, d₆-DMSO) 7.98 (d, 1H, Ar, $J = 8.8$ Hz), 7.49 (s, 1H, Ar), 7.45 (d, 2H, Ar, $J = 8.8$ Hz), 7.28 (s, 1H, Ar), 7.18 (d, 1H, Ar, $J = 8.8$ Hz), 7.12 (d, 1H, Ar, $J = 8$ Hz), 6.24 (s, 1H, Ar), 6.10 (s, 1H, Ar), 4.53 (d, 4H, NHCH₂, $J = 8.4$ Hz); δ_C (400 MHz, d₆-DMSO) 149.9, 142.7, 139.1, 134.1, 130.0, 129.6, 129.2, 128.2, 128.0, 127.6, 124.6, 122.4, 122.2, 122.0, 121.5, 112.2, 112.0, 110.3, 109.4,

3-(N-(4-bromobenzyl)-N-isobutylsulfamoyl)-6-chloro-1H-indole-2-carboxylic acid (26d).

General procedure W with 25d. Tan solid (yield = 84%). δ_H (400 MHz, d₆-DMSO) 8.06 (d, 1H, Ar, $J = 9.6$ Hz), 7.56 (s, 1H, Ar), 7.51 (d, 2H, Ar, $J = 8.4$ Hz), 7.31 (s, 2H, Ar), 7.27 (d, 2H, Ar, $J = 8.8$ Hz), 4.42 (s, 2H, NHCH₂), 2.96 (d, 2H, NHCH₂, $J = 7.6$ Hz), 1.60 (s, 1H, CH(CH₂)₂), 0.61 (d, 6H, CH(CH₂)₂), $J = 6.4$ Hz); δ_C (400 MHz, d₆-DMSO) 162.3, 138.1, 134.0, 131.0, 130.1, 128.5, 127.9, 124.8, 122.3, 122.0, 120.0, 112.3, 111.7, 55.8, 51.5, 29.0, 26.2, 19.8

6-chloro-3-(N-(3,4-dichlorobenzyl)-N-neopentylsulfamoyl)-1H-indole-2-carboxylic acid

(26e). General procedure W with 25e. Yellow solid (yield = 73%). δ_H (400 MHz, d₆-DMSO) 7.96 (d, 1H, Ar, $J = 8.8$ Hz), 7.51 (d, 2H, Ar, $J = 8.8$ Hz), 7.46 (s, 1H, Ar), 7.28 (br s, 1H, Ar), 7.22 (d, 1H, Ar, $J = 8.8$ Hz), 4.76 (s, 2H, NHCH₂), 3.19 (s, 2H, NHCH₂),

0.79 (s, 9H, C(CH₃)₃); δ_C (400 MHz, d₆-DMSO) 188.4, 140.2, 140.2, 134.1, 130.6, 130.1, 129.1, 129.0, 128.2, 127.6, 124.8, 122.4, 122.3, 112.2, 60.7, 53.1, 32.5, 28.1

6-chloro-3-(N-(4-chlorobenzyl)-N-neopentylsulfamoyl)-1H-indole-2-carboxylic acid

(26f). General procedure W with 25f. Yellow solid (yield = 37%). δ_H (400 MHz, d₆-DMSO) 7.96 (d, 1H, Ar, *J* = 8.8 Hz), 7.53 (s, 1H, Ar), 7.32 (br s, 4H, Ar), 7.20 (d, 1H, Ar, *J* = 8.4 Hz), 4.74 (s, 2H, NHCH₂), 3.69 (s, 2H, NHCH₂), 0.76 (s, 9H, C(CH₃)₃); δ_C (400 MHz, d₆-DMSO) 172.1, 162.3, 138.0, 134.0, 131.1, 129.2, 127.9, 127.0, 125.0, 122.3, 122.0, 112.3, 111.5, 60.3, 53.6, 32.5, 28.1

3-(N-benzyl-N-(4-chlorobenzyl)sulfamoyl)-6-chloro-1H-indole-2-carboxylic acid (26g).

General procedure W with 25g. Yellow solid (yield = 65%). δ_H (400 MHz, d₆-DMSO) 8.04 (d, 1H, Ar, *J* = 8.8 Hz), 7.61 (s, 1H, Ar), 7.17 (d, 6H, Ar, *J* = 13.6), 7.10 (br s, 4H, Ar), 4.51 (br s, 4H, N(CH₂)₂); δ_C (400 MHz, d₆-DMSO) 136.9, 136.4, 134.1, 131.4, 129.6, 128.1, 128.0, 127.9, 127.9, 127.0, 124.6, 122.4, 122.1, 112.2, 51.1, 50.2

3.11.2. Biology

Materials. All chemical reagents were ACS grade or higher unless otherwise indicated.

The D₂O, D₆-DMSO, and ¹⁵NH₄Cl were purchased from Cambridge Isotope Laboratories, Inc. (Andover, MA). All other chemicals were purchased from Sigma-Aldrich (St. Louis, MO).

Proteins. The pLM302 expression vector was constructed to produce His6-MBP (maltose binding protein) tagged recombinant human Mcl-1 residues 172 to 327 (Mcl-1 172-327) in HMS174 (DE3) cells (EMD Millipore) using either LB or minimal media supplemented with ¹⁵NH₄Cl to produce unlabeled or ¹⁵N-labeled Mcl-1, respectively. The tagged protein was initially purified from the crude cell lysate by IMAC chromatography (GE Healthcare Life Sciences), and after dialysis to remove the imidazole the affinity tag was cleaved using PreScission Protease (GE Healthcare Life Sciences). A Sephacryl S-200 size exclusion column was used as a final purification step before the protein was concentrated with a 10,000 MWCO centrifugal filter concentrator (EMD Millipore). The concentration of the protein was determined using the Bio-Rad Protein Assay (Bio-Rad Inc., Hercules, CA) using BSA of a known concentration as the standard (Pierce). The purity of the protein was confirmed using SDS-PAGE analysis and NMR HSQC experiments were done to confirm the protein was properly folded (data not shown).

Peptides. A 6-aminohexanoic acid linker was conjugated to the N-terminus of the Bak BH3 peptide (GQVGRQLAIIGDDINR), capped with fluorescein (on the amino group of the linker), and the peptide was amidated on the C-terminus to give FITC-Ahx-GQVGRQLAIIGDDINR-CONH₂, hereafter referred to as “FITC-Bak⁷¹⁻⁸⁹” (synthesized by Neo BioScience in >95% purity). The peptide was soluble and stored in H₂O at pH 7. The concentration of the stock

solution of unlabeled peptides were determined by quantitative amino acid analysis (Biosynthesis Inc., Lewisville, TX), the concentration of FITC peptide was determined at pH 8.0 using the extinction coefficient for amide-linked FITC, $\epsilon_{494} = 68,000 \text{ cm}^{-1}\text{M}^{-1}$. The peptide was synthesized using solid-state peptide synthesis and the purity was determined to be >95% by high pressure liquid chromatography and mass spectrometry.

Fluorescence anisotropy experiments. Fluorescence anisotropy experiments were conducted using a PHERAstar FS (BMG Labtech) multimode microplate reader equipped with two PMTs for simultaneous measurements of the perpendicular and parallel fluorescence emission. In addition, the absolute anisotropy measurements were made on a Cary Eclipse Fluorescence Spectrophotometer (Agilent Technologies) equipped with automated polarizers.

The fluorescence anisotropy assays were performed in black polypropylene 384-well microplate (Costar) with a final volume of 20 μL . Initially the affinity (K_d) of the FITC-Bak⁷¹⁻⁸⁹ peptide was determined by titrating Mcl-1¹⁷²⁻³²⁷ into 10 nM FITC-Bak⁷¹⁻⁸⁹ peptide in 20 mM HEPES, pH 6.8, 50 mM NaCl, 3 mM DTT, 0.01% Triton X-100 and 5% DMSO at room temperature while monitoring the perpendicular and parallel fluorescence emission with a 485 nm excitation and 520 nm emission filters. The fluorescence anisotropy competition assay was performed using 100 nM Mcl-1¹⁷²⁻³²⁷ in the same buffer (10 nM FITC-Bak⁷¹⁻⁸⁹ peptide in 20 mM HEPES, pH 6.8, 50 mM NaCl, 3 mM DTT, 0.01% Triton X-100 and 5% DMSO) with varying concentrations of either unlabeled peptide or experimental compounds.

The initial binding affinities (K_d) were determined by fitting the binding data to the Dose Response function in the Origin software (OriginLab, Northampton, MA): $y = A_1 + (A_2 -$

$A_1) / (1+10^{(\text{LOGx}^{0-x})p})$ such that dynamic range = $\text{abs}(A_1-A_2)$ and the $K_d = 10^{\text{LOGx}^0}$. The IC_{50} in the competition assays were determined by fitting the binding data to the One Site Competition function in the Origin software (OriginLab, Northampton, MA): $y = A_2 + (A_1 - A_2) / (1+10^{(x-\text{logx}_0)})$ such that dynamic range = $\text{abs}(A_1-A_2)$ and the $IC_{50} = 10^{\wedge}(\text{logx}0)$. It has been shown that each of the proteins used here binds a single target peptide (1:1 stoichiometry) at the concentrations used in the competition assays¹⁻³. Therefore, we are able to use an equation derived by Nikolovska-Coleska et al.⁴ to calculate the K_d from the IC_{50} from the anisotropy competition assays. The affinity (K_d) of TAMRA-p53¹⁵⁻²⁹ for Hdm²¹⁻¹¹⁵ was determined to be $6.51 \pm 0.44 \mu\text{M}$, and the affinity of FITC-Bak⁷¹⁻⁸⁹ for Mcl-1¹⁷²⁻³²⁷ was determined to be $41.96 \pm 2.78 \text{ nM}$ and $6.67 \pm 0.05 \text{ nM}$, respectively, in the assay conditions used.

The quality and suitability of the fluorescence anisotropy competition assays were evaluated using the Z-factor developed by Zhang et al.⁵ The Z-factor = $1 - (3SD_b + 3SD_f) / (|\mu_b - \mu_f|)$ where μ_b and μ_f are the mean anisotropy (mA) values of the bound and free probe, respectively, and SD_b and SD_f are the standard deviations of those values for bound and free probe, respectively. The Z-factor can be any value ≤ 1 , with a value of 1 being an ideal assay, ≥ 0.5 but < 1.0 being an excellent assay, and a value < 0.5 being unacceptable for our application.

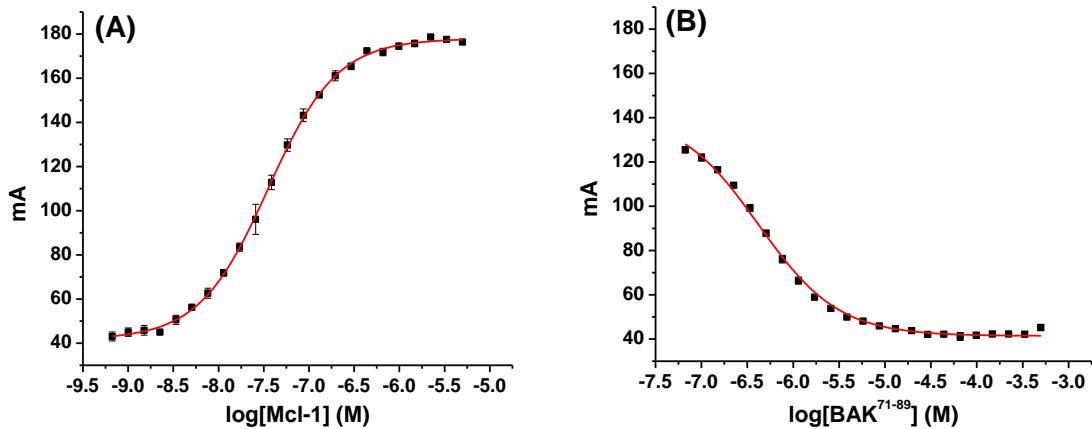


Figure S1. (A) Titration of Mcl-1¹⁷²⁻³²⁷ into 10 nM FITC-BAK⁷¹⁻⁸⁹ gives a K_D of 41.96 ± 2.78 nM with the free FITC-BAK peptide having an absolute anisotropy value of 41.4 ± 1.4 mA (this is the same as Mcl-1 assay b/c same peptide, buffer and conditions) and the Mcl-1 bound peptide 178.0 ± 1.4 mA. (B) The FITC-BAK⁷¹⁻⁸⁹ was competed off Mcl-1¹⁷²⁻³²⁷ with unlabeled BAK⁷¹⁻⁸⁹ peptide with an IC_{50} of 418.19 ± 37.77 nM giving a calculated K_D of 101.84 ± 12.37 nM. For this competition assay 60 nM Mcl-1¹⁷²⁻³²⁷ was used and gives an excellent Z-factor of 0.79 with a dynamic range of 86.96 ± 0.32 mA.

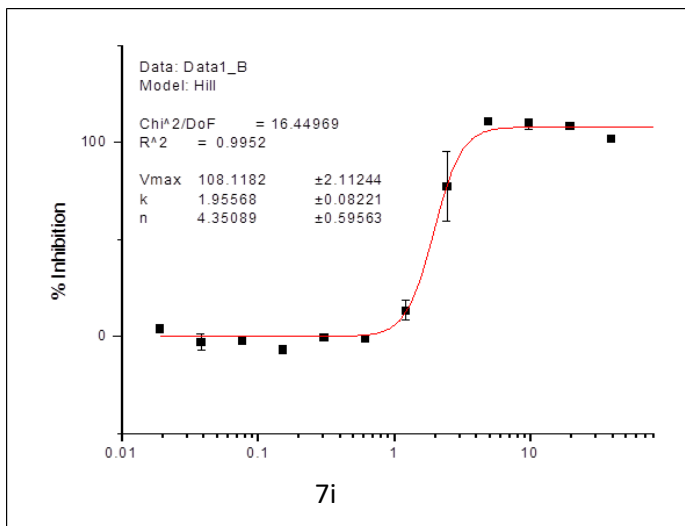


Figure S2. The FITC Bak⁷¹⁻⁸⁹ was competed off Mcl-1¹⁷²⁻³²⁷ with **7i**, giving an estimated IC₅₀ of 1.96 ± 0.08 μM. For all the competition assays used to test compounds, 100 nM Mcl-1¹⁷²⁻³²⁷ was used giving an excellent Z-factor of 0.82 with a dynamic range of 101.8 ± 2.85 mA.

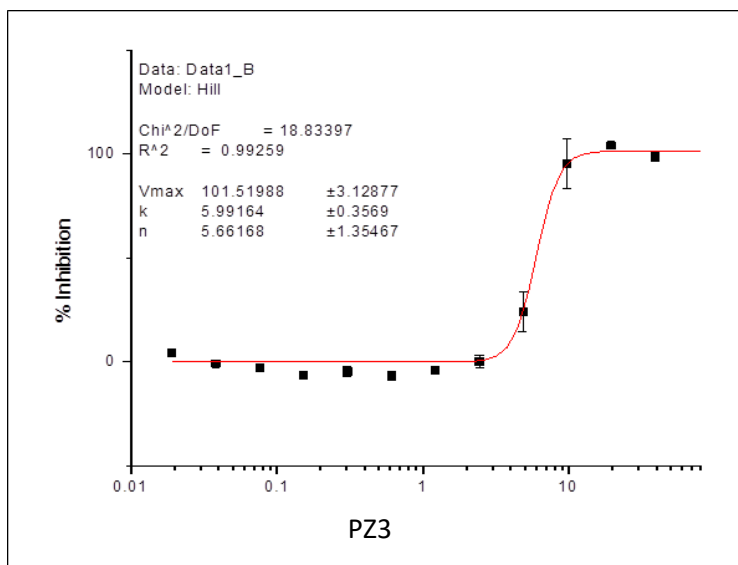


Figure S3. The FITC Bak⁷¹⁻⁸⁹ was competed off Mcl-1¹⁷²⁻³²⁷ with **PZ3**, giving an estimated IC₅₀ of 5.99 ± 0.36 μM. For all the competition assays used to test compounds, 100 nM Mcl-1¹⁷²⁻³²⁷ was used giving an excellent Z-factor of 0.82 with a dynamic range of 101.8 ± 2.85 mA.

3.11.3. References

- (1) Willis S.N., Chen, L., Dewson, G., Wei, A., Naik E., Fletcher J. I., Adams, J. M., Huang, D. C. S. Proapoptotic Bak is sequestered by Mcl-1 and Bcl-xL, but not Bcl-2, until displaced by BH3-only proteins. *Genes Dev.* **2005**, 19 (11), 1294-1305
- (2) Stewart, M. L., Fire, E., Keating, A. E., Walensky, L. D. The Mcl-1 BH3 helix is an exclusive Mcl-1 inhibitor and apoptosis sensitizer. *Nat Chem Biol.* **2010**. 6 (8), 595-601.
- (3) Nikolovska-Coleska Z., Wang R., Fang X., Pan H., Tomita Y., Li P., et al. Development and optimization of a binding assay for the XIAP BIR3 domain using fluorescence polarization. *Anal Biochem.* **2004**, 332 (2), 261-73.

- (4) Zhang J.H., Chung T.D., Oldenburg K.R. A Simple Statistical Parameter for Use in Evaluation and Validation of High Throughput Screening Assays. *J Biomol Screen.* **1999**, 4 (2), 67-73.

3.12. Acknowledgements

I would like to thank Dr. Alexander MacKerell Jr.'s lab for performing SILCS.

Chapter 4. Kröhnke pyridines: Rapid and facile access to Mcl-1 inhibitors

Protein–protein interactions (PPIs) play key roles in cell differentiation, homeostasis, and apoptosis, among others.¹ Given their significance, it is unsurprising that their dysregulations can lead to a plethora of diseases, such as cancer and Alzheimer's. The Bcl-2 family of proteins controls mitochondrial (intrinsic) apoptosis through several PPIs, and is composed of anti-apoptotic and pro-apoptotic members, the latter of which are further divided into effector and BH3-only proteins.²⁻⁴ There are now six recognized anti-apoptotic proteins each of which is comprised of four BH domains: Bcl-2 itself, Bcl-x_L, Bcl-W, Mcl-1, Bfl-1 and Bcl-b. The effector proteins, which include Bcl-2 antagonist killer (Bak), Bcl-2-associated x (Bax) and Bcl-2-related ovarian killer (Bok), are also made up of four BH domains and assume similar globular structures: particularly, a hydrophobic groove on the surface that recognizes the BH3 α -helical domain of pro-apoptotic family members. Lastly, the BH3-only proteins, also referred to as the death initiators, which include Bim, Noxa and Puma, comprise only the BH3 amphipathic α -helical domain.

The BH3-only proteins promote cell death through neutralizing the pro-survival proteins, as well as directly activating the effectors Bax and Bak, which themselves are also neutralized by the pro-survival proteins.^{5,6} In this tripartite apoptotic switch, once Bax and Bak levels are sufficiently elevated, the proteins homodimerize in the outer mitochondrial membrane, so beginning the apoptosis cascade. The pro-apoptotic proteins recognize their pro-survival counterparts through a BH3 α -helical amphipathic helix on the former with a hydrophobic surface groove on the latter.⁷ Particularly, this protein–protein interaction (PPI) is mediated by a conserved pattern of hydrophobic residues on

one face of the α -helix at positions i , $i+3/4$, $i+7$, $i+11$ that probe into four hydrophobic sub-pockets, and a conserved aspartate on the opposing face at position $i+5$ that recognizes a conserved arginine.⁸

The pro-survival Bcl-2 proteins are upregulated in several human cancers, including acute myeloid leukemia and multiple myeloma.^{9,10} Mcl-1 overexpression, in particular, has been linked to acquired drug resistance to current chemotherapeutics such as gemcitabine and microtubule-directed agents like vinblastine.¹¹ Furthermore, upon the inhibition of Bcl-2 and Bcl-x_L, a compensatory upregulation of Mcl-1 results.¹² Accordingly, the development of Mcl-1 inhibitors has become an intense area of research, with two inhibitors recently advancing into clinical trials for refractory or relapsed multiple myeloma, lymphoma and acute myeloid leukemia.¹³⁻¹⁵ In the event these trials are unsuccessful, it is important that the discovery of Mcl-1 inhibitors is sustained, ideally with novel scaffolds and straightforward syntheses towards increased chances of success and at a minimum cost so that treatments are affordable. Herein, we disclose Mcl-1 inhibitors based on 4,6-disubstituted picolinic acid, which are readily accessible through a convergent, three-step synthesis that exploits Kröhnke pyridine chemistry.

Commonalities between Mcl-1 inhibitors include a functional group to engage Arg263, most often a carboxylic acid, and appropriately-positioned hydrophobic groups that delve into the p2 and p4 pockets.¹⁶⁻²¹ For example, as shown in Figure 4.1, Abbvie has disclosed the inhibitor A1210477 based on an indole core with a carboxylic acid at the 2-position and a hydrophobic group at the 3-position that binds in the p2 pocket.¹⁸ Meanwhile, Fesik and co-workers have generated more elaborate structures, such as

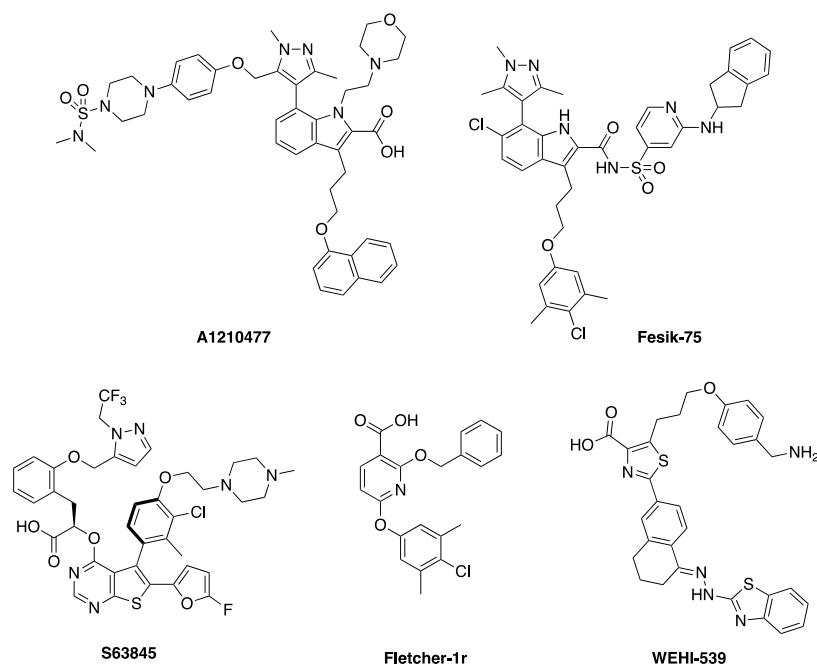


Figure 4. 1. Some Mcl-1 inhibitors and the Bcl-x_L-selective inhibitor WEHI-539.

Fesik-75, that can additionally bind the p4 pocket by virtue of substitutions of an acyl sulfonamide carboxylic acid surrogate.^{17b} Geneste and colleagues have described the Mcl-1 inhibitor S63845 based on a thienopyrimidine core;¹⁹ the 2-fluorofuranyl moiety engages the p2 pocket, the 2,2,2-trifluoroethylpyrazole the p4 pocket and the carboxylic acid forms a salt bridge with Arg263. By deconstructing one of our previously reported oligoamide-based BH3 mimetics, we discovered moderately potent Mcl-1 inhibitors centered on a 2,6-disubstituted nicotinic acid core; our most potent compound **1r** is depicted in Figure 1.²² We rationalized that similarly di-substituted picolinic acids may also be effective Mcl-1 inhibitors, perhaps even more so due to the *ortho* relationship of the pyridine nitrogen and the carboxylic acid that might permit an additional electrostatic interaction with Arg263 akin to the thiazole-2-carboxylic acid core of the Bcl-x_L selective inhibitor WEHI-539.²³ Moreover, such 2,4,6-tri-substituted pyridines may be rapidly accessed by the Kröhnke pyridine synthesis,²⁴ which would facilitate the assembly of a

library. In fact, Kröhnke pyridines have already demonstrated bioactivity as inhibitors of c-Myc–Max dimerization and topoisomerase I.^{25,26} Our generic design is shown in Figure 4.2A. We next designed the target molecule **1** in which both the R¹ and R² groups are 4-isopropoxyphenyl moieties. Overlay of MM2-energy minimized **1** with the Bim-BH3 α -helix (Figure 4.2B) revealed good mimicry of the side chains of Leu62 and Phe69 by the 4-isopropoxy groups, and of Asp67 by the carboxylic acid, as predicted.

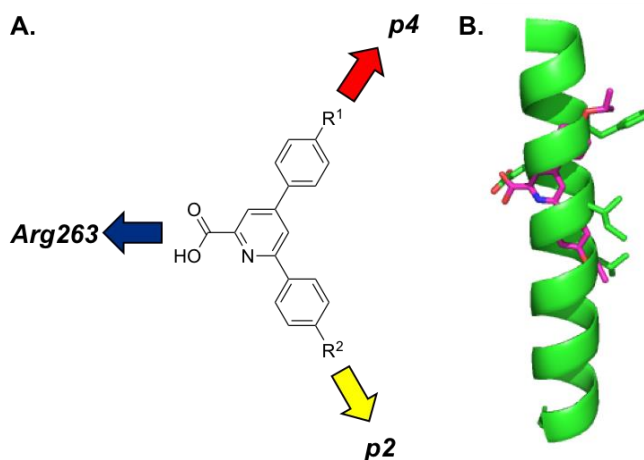


Figure 4. 2. A. Generic inhibitor structure; B. MM2-energy minimized ligand **1** (R¹ = R² = OiPr, magenta, coloured by atom type) overlaid with Bim-BH3 α -helix (key residues highlighted).

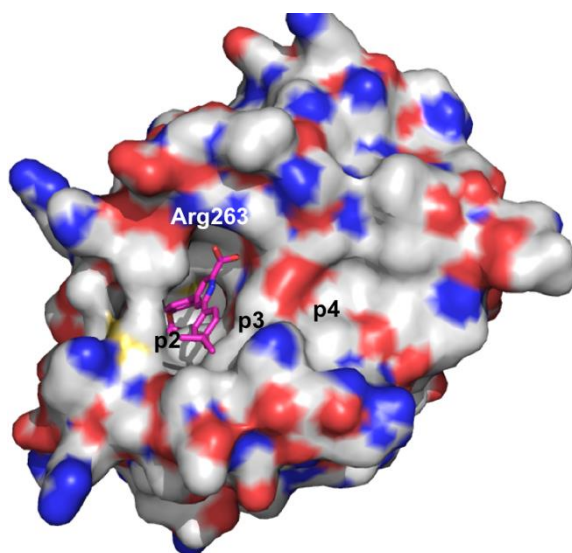


Figure 4. 3. A low-energy GOLD docking solution of **1** (magenta) with Mcl-1 extracted from PDB ID: 4HW2. Ligand and protein coloured by atom type. White label indicates key Mcl-1 residue Arg263, black labels describe sub-pockets within the BH3-binding crevice.

We performed molecular docking experiments with **1** using GOLD, wherein the binding site was taken to be 10 Å about Met231, which is located on the surface of the protein between the p2 and p3 pockets of the BH3 binding crevice. All of the highest ranked solutions exhibited very similar binding modes, and a representative docking is provided in Figure 4.3. As illustrated, the carboxylic acid is close to Arg263. In contrast to the design, the isopropoxy groups are directed into the p2 and p3 pockets, as opposed to the p2 and p4 pockets. We believe this finding is due to our use of the 4HW2 PDB file in which the p2 pocket is substantially opened up such that the entire isopropoxyphenyl group is accommodated instead of just the isopropoxy substituent. Nevertheless, compound **1** demonstrates good complementarity to the BH3 binding crevice. Accordingly, we synthesized **1** and a series of analogues by following the chemistry depicted in Figure 4.4. First, aldehydes R¹CHO (**2**) underwent Knoevenagel condensations with sodium pyruvate to deliver vinylidene acids **3**. Meanwhile, methyl ketones R²COCH₃ (**4**) were converted into their corresponding arylketo α-pyridinium iodide salts **5** by refluxing in pyridine in the presence of iodine. Finally, vinylidene acids **3** were condensed with salts **5** to furnish Kröhnke pyridines **1** and the ILC series, which were isolated by crystallization.

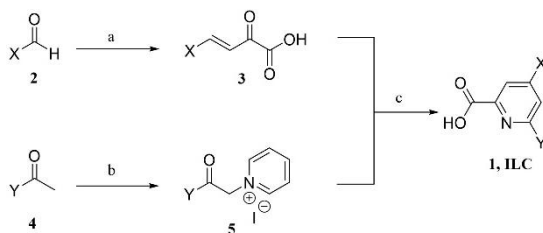


Figure 4. 4. a) sodium pyruvate, NaOH, EtOH/H₂O, 1:1, RT, 1 h; b) I₂, pyridine, Δ, 16 h; c) NH₄OAc, MeOH, 60 °C, 16 h.

Compounds were evaluated in a fluorescence polarization competition assay (Table 4.1) for their abilities to disrupt the PPI interaction between Mcl-1 and fluorescently-labeled Bak-BH3 peptide GQVGRQLAIGDDINR, as described by us previously.²⁰ Unfortunately, fluorescence overlap between fluorescein-Bak-BH3 and compound **1** rendered the determination of an IC₅₀ value challenging. However, this was remedied by shifting to the TAMRA fluorophore. The IC₅₀ data acquired from the competition assay were converted to K_i values using the Nikolovska-Coleska equation.²⁷ ILC-1-098 inhibited Mcl-1 with a K_i of 28.8 μM, which was improved upon by the addition of a second isopropoxy group in the R² group (ILC-1-094: K_i = 19.7 μM), and



Code Number	W	X	Y	Z	K _i (μM)	Code Number	W	X	Y	Z	K _i (μM)
ILC-1-098	CH			N	28.8 ± 3.5	ILC-1-166	CH			N	10.9 ± 0.70
ILC-1-094	CH			N	19.7 ± 0.49	ILC-1-172	CH			N	38.2 ± 6.55
ILC-1-107	CH			N	9.77 ± 1.04	ILC-1-203	CH			N	10.3 ± 0.36
ILC-1-192	CH			N	~100	ILC-1-210	CH			N	8.47 ± 0.32
ILC-1-167	CH			N	~40	ILC-1-200	CH			N	7.44 ± 0.47
ILC-1-197	CH			N	~40	ILC-1-178	CH			N	7.33 ± 0.55
ILC-1-176	CH			N	~40	ILC-1-174	CH			N	6.10 ± 0.59
ILC-1-193	CH			N	>100	ILC-1-168	CH			N	13.7 ± 0.89
ILC-1-169	CH			N	7.60 ± 0.62	ILC-1-102	CH			N	9.22 ± 0.48
ILC-1-170	CH			N	9.24 ± 0.53	ILC-1-199	N			CH	4.43 ± 0.33

Table 4.1. Mcl-1 inhibitory structure–activity relationships of Kröhnke pyridines. IC₅₀ data from a fluorescence polarization assay with Mcl-1¹⁷²⁻³⁷¹ and TAMRA-labeled Bak-BH3 peptide were converted to K_i values using the Nikolovska-Coleska equation.²⁶

further still by the replacement of the R² isopropyl group with a benzyl group: ILC-1-107, $K_i = 9.77 \mu\text{M}$. For the series of Kröhnke pyridines with R¹ = *p*-4-bromophenyl, significant inhibitory activity was only observed with ILC-1-169 which bears the largest hydrophobic group in the *para* position of the R² phenyl ring. We next prepared a series of pyridines in which R¹ was fixed as a *p*-phenoxyphenyl moiety; all demonstrated appreciable inhibition of Mcl-1. In general, the larger and more hydrophobic the R² group, the greater the inhibition of Mcl-1, with ILC-1-174 the most potent of all the compounds evaluated ($K_i = 6.10 \mu\text{M}$). Finally, we wanted to probe the importance of the position of the pyridine nitrogen, and so we prepared compound ILC-1-199, where the nitrogen was shifted into the position *para* to the carboxylic acid. The K_i of ILC-1-199 was determined to be $4.43 \pm 0.33 \mu\text{M}$, suggesting the position of the nitrogen atom apparently has no impact on binding. It should be noted that the majority of inhibitors plateaued at ~80% inhibition. We believe this may be related to solubility since at higher concentrations, inhibition began to rapidly reduce, suggesting possible aggregation. That being said, ILC-1-199, our most potent inhibitor, accomplished complete displacement of the TAMRA-Bak peptide. Therefore, we selected this compound for further evaluation.

Two-dimensional ¹H-¹⁵N HSQC NMR spectra was collected for ¹⁵N-labeled MCL-1 in the absence (black) and presence (red) of ILC-1-199 (Figure 4.5). This experiment provides ¹H-¹⁵N correlations for each amino acid of ¹⁵N-isotope labeled protein and addition of compounds that directly interact with the protein result in the perturbation of those chemical shifts and/or the loss of the correlation due to chemical exchange broadening. Regardless, any change in chemical shift values confirm the direct interaction of the small molecules and ¹⁵N-labeled protein and may provide an indication

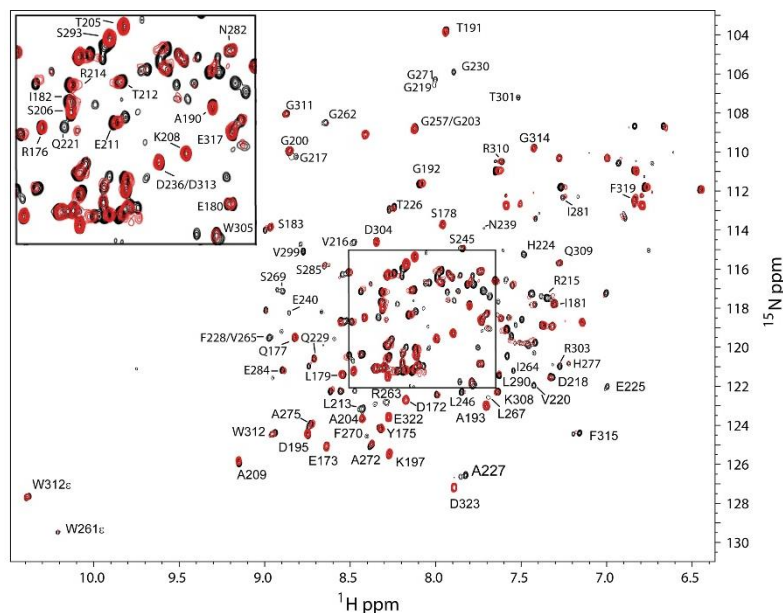


Figure 4. 5. Two-dimensional ^1H , ^{15}N -fast heteronuclear single quantum coherence (HSQC) spectra of MCL1¹⁷²⁻³²⁷ in the absence (black) and in the presence (red) of ILC-1-199 showing clear changes in the ^1H - ^{15}N correlations for multiple amino acids indicating direct interaction of the compound and the protein. The majority of the correlation peaks are weakened or lost complete due to intermediate chemical exchange broadening. Some amino acid assignments have been made based on the chemical shift values freely available in the Biological Magnetic Resonance Data Bank (BMRB) for MCL1 (BMRB Entry 19654).

about where the compounds bind. The addition of ILC-1-199 caused perturbation of multiple correlation peaks assuring it directly interacts with MCL-1. However, due to the interaction being in intermediate exchange, the correlation peaks were lost or weakened and could not be assigned to specific amino acids with this experiment.

In summary, we have discovered novel inhibitors of Mcl-1 based on a 4,6-disubstituted picolinic acid core. The compounds were rapidly and readily synthesized using the Kröhnke pyridine synthesis. It is surmised that the carboxylic acid binds Arg263, and the hydrophobic R¹ and R² groups bind two of the four hydrophobic subpockets of the BH3-binding groove. Future work will focus on the expansion of our compound library, as well as the addition of solubilizing groups, such as a morpholino moiety. Furthermore, conversion of the carboxylic acid to substituted acyl sulfonamides,

as reported by Fesik and colleagues,^{17a} may permit occupation of a third hydrophobic sub-pocket to afford additional improvements in binding affinities. It is envisaged that the simplicity of the chemistry will expedite the discovery of more potent derivatives, and our efforts in this regard shall be reported in due course.

4.1. References

- (1) (a) Fletcher, S.; Hamilton, A. D. *Curr. Opin. Chem. Biol.* **2005**, *9*, 632–638; (b) Arkin, M. R.; Wells, J. A. *Nat. Rev. Drug Discov.* **2004**, *3*, 301–317.
- (2) Reed, J. C. *Nat. Rev. Drug Discov.* **2002**, *2*, 111-121.
- (3) Youle, R. J.; Strasser, A. *Nat. Rev. Mol. Cell Biol.* **2008**, *1*, 47-59.
- (4) Czabotar, P. E.; Lessene, G.; Strasser, A.; Adams, J. M. *Nat. Rev. Mol. Cell Biol.* **2014**, *1*, 49-63.
- (5) Willis, S. N.; Fletcher, J. I.; Kaufmann, T.; van Delft, M. F.; Chen, L.; Czabotar, P. E.; Ierino, H.; Lee, E. F.; Fairlie, W. D.; Bouillet, P.; Strasser, A.; Kluck, R. M.; Adams, J. M.; Huang, D. C. *Science* **2007**, *5813*, 856-859.
- (6) Kim, H.; Rafiuddin-Shah, M.; Tu, H. C.; Jeffers, J. R.; Zambetti, G. P.; Hsieh, J. J.; Cheng, E. H. *Nat. Cell Biol.* **2006**, *12*, 1348-1358.
- (7) Sattler, M.; Liang, H.; Nettlesheim, D.; Meadows, R. P.; Harlan, J. E.; Eberstadt, M.; Yoon, H. S.; Shuker, S. B.; Chang, B. S.; Minn, A. J.; Thompson, C. B.; Fesik, S. W. *Science* **1997**, *5302*, 983-986.
- (8) Yap, J. L.; Chen, L.; Lanning, M. E.; Fletcher, S. *J. Med. Chem.* **2017**, doi: 10.1021/acs.jmedchem.5b01888
- (9) Cerella, C.; Gaigneaux, A.; Mazumder, A.; Lee, J.-Y.; Saland, E.; Radogna, F.; Farge, T.; Vergez, F.; Récher, C.; Sarry, J.-E.; Kim, K.-W.; Shin, H. Y.; Dicato, M.; Deiderich, M. *Leukemia* **2017**, *31*, 755–759.
- (10) Punnoose, E. A.; Levenson, J. D.; Peale, F.; Boghaert, E. R.; Belmont, L. D.; Tan, N.; Young, A.; Mitten, M.; Ingalla, E.; Darbonne, W. C.; Oleksijew, A.; Tapang, P.; Yue, P.; Oeh, J.; Lee, L. Maiga, S.; Fairbrother, W. J.; Aimot, M.; Souers, A. J.; Sampath, D. *Mol. Cancer Ther.* **2016**, *15*, 1132–1144.
- (11) Salerni, B. L.; Bates, D. J.; Albershardt, T. C.; Lowrey, C. H.; Eastman, A. *Mol. Cancer Ther.* **2010**, *9*, 791–802.

- (12) Luedtke, D. A.; Niu, X.; Pan, Y.; Zhao, J.; Liu, S.; Edwards, H.; Chen, K.; Lin, H.; Taub, J. W.; Ge, Y. *Signal Trans.. Targeted Ther.* **2017**, 17012.
- (13) Chen, L.; Fletcher, S. *Expert. Opin. Ther. Pat.* **2017**, 27, 163–178.
- (14) <https://www.cancer.gov/about-cancer/treatment/clinical-trials/search/v?id=NCI-2016-00888&r=1>
- (15) <https://www.cancer.gov/about-cancer/treatment/clinical-trials/search/v?id=NCI-2017-00472&r=1>
- (16) Belmar, J.; Fesik, S. W. *Pharmacol. Ther.* **2015**, 145, 76 – 84.
- (17) (a) Friberg, A.; Vigil, D.; Zhao, B.; Daniels, R. N.; Burke, J. P.; Garcia-Barrantes, P. M.; Camper, D.; Chauder, B. A.; Lee, T.; Olejniczak, E. T.; Fesik, S. W. *J. Med. Chem.* **2013**, 56, 15–30; (b) Pelz, N. F.; Bian, Z.; Zhao, B.; Shaw, S.; Tarr, J. C.; Belmar, J.; Gregg, C.; Camper, D. V.; Goodwin, C. M.; Arnold, A. L.; Sensintaffar, J. L.; Friberg, A.; Rossanese, O. W.; Lee, T.; Olejniczak, E. T.; Fesik, S. W. *J. Med. Chem.* **2016**, 59, 2054–2066; (c) Shaw, S.; Bian, Z.; Zhao, B.; Tarr, J. C.; Veerasamy, N.; Jeon, K.; Belmar, J.; Arnold, A. L.; Fogarty, S. A.; Perry, E.; Sensintaffar, J. L.; Camper, D. V.; Rossanese, O. W.; Lee, T.; Olejniczak, E. T.; Fesik, S. W.; *J. Med. Chem.* **2018**; DOI: 10.1021/acs.jmedchem.7b01155
- (18) Levenson, J. D.; Zhang, H.; Chen, J.; Tahir, S. K.; Phillips, D. C.; Xue, J.; Nimmer, P.; Jin, S.; Smith, M.; Xiao, Y.; Kovar, P.; Tanaka, A.; Bruncko, M.; Sheppard, G. S.; Wang, L.; Gierke, S.; Kategaya, L.; Anderson, D. J.; Wong, C.; Eastham-Anderson, J.; Ludlam, M. J. C.; Sampath, D.; Fairbrother, W. J.; Wertz, I.; Rosenberg, S. H.; Tse, C.; Elmore, S. W.; Souers, A. J. *Cell Death Dis.* **2015**, 6, e1590.
- (19) Kotschy, A.; Szlavik, Z.; Murray, J.; Davidson, J.; Maragno, A. L.; Le Toumelin-Braizat, G.; Chanrion, M.; Kelly, G. L.; Gong, J.-N.; Moujalled, D. M.; Bruno, A.; Csekei, M.; Paczal, A.; Szabo, Z. B.; Sipos, S.; Radics, G.; Prosenyak, A.; Balint, B.; Ondi, L.; Blasko, G.; Robertson, A.; Surgenor, A.; Dokurno, P.; Chen, I.; Matassova, N.; Smith, J.; Pedder, C.; Graham, C.; Studeny, A.; Lysiak-Auvity, G.; Gravé, F.; Segal, D.; Riffkin, C. D.; Pomilio, G.; Galbraith, L. C. A.; Aubrey, B. J.; Brennan, M. S.; Herold, M. J.; Chang, C.; Guasconi, G.; Cauquil, N.; Melchiorre, F.; Guigal-Stephan, N.; Lockhart, B.; Colland, F.; Hickman, J. A.; Roberts, A. W.; Huang, D. C. S.; Wei, A. H.; Strasser, A.; Lessene, G.; Geneste, O. *Nature* **2016**, 538, 477–482.
- (20) Chen, L.; Wilder, P. T.; Drennen, B.; Tran, J.; Roth, B. M.; Chesko, K.; Shapiro, P.; Fletcher, S. *Org. Biomol. Chem.* **2016**, 14, 5505–5510; (b) Lanning, M. E.; Yu, W.; Yap, J. L.; Chauhan, J.; Chen, L.; Whiting, E.; Pidugu, L. S.; Atkinson, T.; Bailey, H.; Li, W.; Roth, B. M.; Hynicka, L.; Chesko, K.; Toth, E. A.;

- Shapiro, P.; MacKerell, A. D.; Wilder, P. T.; Fletcher, S. *Eur. J. Med. Chem.* **2016**, *113*, 273–292; (c) Whiting, E.; Raje, M. R.; Chauhan, J.; Wilder, P. T.; Van Eker, D.; Hughes, S. J.; Bowen, N. G.; Vickers, G. E. A.; Fenimore, I. C.; Fletcher, S. *Bioorg. Med. Chem. Lett.* **2018**.
- (21) (a) Akcay, G.; Belmonte, M. A.; Aquila, B.; Chauhui, C.; Hird, A. W.; Lamb, M. L.; Rawlins, R. B.; Su, N.; Tentarelli, S.; Grimster, N. P.; Su, O. *Nat. Chem. Biol.* **2016**, *12*, 931–936; (b) Lee, S.; Wales, T. E.; Escudero, S.; Cohen, D. T.; Luccarelli, J.; Gallagher, C. G.; Cohen, N. A.; Huhn, A. J.; Bird, G. H.; Engen, J. R.; Walensky, L. D. *Nat. Struct. Mol. Biol.* **2016**, *23*, 600–607.
- (22) Drennen, B.; Scheenstra, J. A.; Yap, J. L.; Chen, L.; Lanning, M. E.; Roth, B. M.; Wilder, P. T.; Fletcher, S. *ChemMedChem* **2016**, *11*, 827–833.
- (23) Lessene, G.; Czabotar, P. E.; Sleebs, B. E.; Zobel, K.; Loews, K. N.; Adams, J. M.; Baell, J. B.; Colman, P. M.; Deshaves, K.; Fairbrother, W. J.; Flygare, J. A.; Gibbons, P.; Kersten, W. J.; Kulasegaram, S.; Moss, R. M.; Parisot, J. P.; Smith, B. J.; Street, I. P.; Yang, H.; Huang, D. C.; Watson, K. G. *Nat. Chem. Biol.* **2013**, *9*, 390–397.
- (24) Kröhnke, F.; Zecher, W. *Angew. Chem.* **1962**, *74*, 811–817.
- (25) Hart, J. R.; Garner, A. L.; Yu, J.; Ito, Y.; Sun, M.; Ueno, L.; Rhee, J. K.; Baksh, M. M.; Stefan, E.; Hartl, M.; Bister, K.; Vogt, P. K.; Janda, K. D. *Proc. Natl. Acad. Sci. USA* **2014**, *111*, 12556–12561.
- (26) Karki, R.; Park, C.; Jun, K. Y.; Kadayat, T. M.; Lee, E. S.; Kwon, Y. *Eur. J. Med. Chem.* **2015**, *90*, 360–378.
- (27) Nikolovska-Coleska, Z.; Wang, R.; Fang, X.; Pan, H.; Tomita, Y.; Li, P.; Roller, P. P.; Krajewski, K.; Saito, N. G.; Stucky, J. A.; Wang, S. *Anal. Biochem.* **2004**, *332*, 261–273.

4.2. Supplementary Information

4.2.1. Chemistry: General.

Unless otherwise stated, all reactions were performed under an inert (N₂) atmosphere.

Reagents and solvents were reagent grade and purchased from Sigma-Aldrich, Alfa

Aesar, Oakwood, and TCI America. Anhydrous solvents were purchased from Sigma-

Aldrich and used as provided. Reactions were monitored by TLC, visualizing with a UV

lamp and/or KMnO₄ stain. Silica gel 60 (70–230 mesh, Merck) was used for flash

column chromatography. ^1H and ^{13}C NMR spectra were recorded on Varian INOVA 400 MHz NMR spectrometers at 25 °C. Chemical shifts are reported in parts per million (ppm). Data for ^1H NMR are reported as follows: chemical shift (δ ppm) (multiplicity, coupling constant (Hz), integration, identity). Multiplicities are reported as follows: s = singlet, d = doublet, t = triplet, q = quartet, dd = doublet of doublets, m = multiplet. Data for ^{13}C are reported in terms of chemical shifts (δ ppm). The residual solvent peak was used as an internal reference. Mass spectrometry was performed on a Bruker AmaZon X quadrupole ion trap mass spectrometer using either electrospray ionization (ESI) or atmospheric pressure chemical ionization (APCI). All final molecules were $\geq 95\%$ pure according to reversed-phased HPLC using a Waters 1525 analytical/preparative HPLC fitted with a C18 reversed-phase column (Atlantis T3: 4.6 mm x 150 mm) and employing an isocratic gradient of $\text{CH}_3\text{CN-H}_2\text{O}$, 9:1 over 22 min. Data are presented as retention time (t_{R} (min), purity (%)). The D_2O , $\text{D}_6\text{-DMSO}$, and $^{15}\text{NH}_4\text{Cl}$ were purchased from Cambridge Isotope Laboratories, Inc. (Andover, MA).

General Procedure A: Formation of Pyridinium Iodide Salts. The appropriate ketone (1 eq) was reacted with iodine (1 eq) in refluxing pyridine (0.25 M) overnight. In most cases, a heavy precipitate had formed. The reaction was allowed to cool to room temperature, then over ice. The precipitated solid was isolated by vacuum filtration, washed with cold pyridine and then ether to give the pyridinium iodide salts, which were used without further purification.

General Procedure B: Knoevenagel Condensations. NaOH (2.5 eq) was dissolved in a 1:1 mixture of $\text{H}_2\text{O/EtOH}$ (0.20 M) solution. Sodium pyruvate (2 eq) was added, followed by the appropriate aldehyde (1 eq). The resulting mixture was stirred at room

temperature for 1 h. The resulting white precipitate was collected by vacuum filtration, then washed with cold EtOH to deliver the potassium *trans*- γ,β -unsaturated α -keto acid salt. The ppt was partitioned between 1M HCl and EtOAc, the organic layer was dried over Na₂SO₄, filtered and concentrated to afford the corresponding *trans*- γ,β -unsaturated α -keto acid.

General Procedure C: Kröhnke Pyridine Cyclizations. The appropriate *trans*- γ,β -unsaturated α -keto acid (1 eq) was dissolved in MeOH (0.1 M), followed by the addition of the appropriate pyridinium iodide salt (1 eq). Lastly, NH₄OAc (10 eq) was added to the reaction mixture. The reaction was gently refluxed overnight. The next day, the reaction mixture was cooled to room temperature, concentrated to ca. 5 mL if necessary, then partitioned between CH₂Cl₂ and 1M HCl. The organic layer was dried over Na₂SO₄, filtered and concentrated. The residue was purified either by recrystallization in hot acetic acid or hot EtOH, or by silica gel flash column chromatography, eluting with 92:7:1, CH₂Cl₂/MeOH/acetic acid.

(E)-2-Oxo-4-(4-phenoxyphenyl)but-3-enoic acid (**3a**) was prepared by reacting aldehyde (2a) with sodium pyruvate on a 10 mmol scale following general procedure A. Yield = 52%. Yellow solid: δ_{H} (400 MHz, DMSO-*d*₆) 7.84 (d, 1H, Ar, *J* = 7.6 Hz), 7.74 (d, 1H, Ar, *J* = 15.6 Hz), 7.45 (t, 1H, Ar, *J* = 8 Hz), 7.37 (t, 1H, Ar, *J* = 7.4 Hz), 7.28-7.19 (m, 2H, Ar), 7.12 (d, 2H, Ar, *J* = 8 Hz), 7.03-6.85 (m, 3H, Ar); δ_{C} (400 MHz, DMSO-*d*₆) 137.1, 136.6, 135.3, 135.2, 134.2, 133.3, 128.5, 126.1, 124.5, 124.0, 123.7, 123.4

(E)-4-Oxo-4-(4-phenoxyphenyl)but-2-enoic acid (**3b**) was prepared by reacting diphenyl ether (1g, 5.87 mmol, 1 eq.) with maleic anhydride (576 mg, 5.87 mmol, 1 eq.) and anhydrous aluminium chloride (783 mg, 5.87 mmol, 1 eq.) in 1,2-dichloroethane (20 mL)

at 0 °C. The reaction was stirred overnight and allowed to warm to RT. The organic layer was diluted with CH₂Cl₂, extracted with 1M NaOH, then the aqueous was acidified with 1M HCl and the product extracted into EtOAc (x2). The combined EtOAc extractions were washed with brine, dried (Na₂SO₄), filtered and concentrated to yield a light yellow solid that was sufficiently pure to be carried forward. Yield = 494 mg (32%). White solid: δ_{H} (400 MHz, DMSO-d₆) 8.08 (d, 2H, Ar, $J = 8.4$ Hz), 7.88 (d, 1H, Ar, $J = 15.6$ Hz), 7.28 (t, 2H, Ar, $J = 7.4$ Hz), 7.17-7.03 (m, 4H, Ar), 6.68 (d, 1H, COCH₂, $J = 15.6$ Hz); δ_{C} (400 MHz, DMSO-d₆) 192.8, 171.5, 167.2, 159.8, 141.2, 137.8, 136.7, 136.0, 135.8, 135.6, 130.2, 129.9, 125.4, 125.2, 122.4

(*E*)-4-(4-Bromophenyl)-2-oxobut-3-enoic acid (**3c**) was prepared by reacting 4-bromobenzaldehyde with sodium pyruvate on a 20 mmol scale following general procedure A. Yield = quant. Yellow solid: δ_{H} (400 MHz, DMSO-d₆) 7.75 (t, 3H, Ar, $J = 8.8$ Hz), 7.69 (s, 1H, Ar), 7.65 (d, 2H, Ar, $J = 8$ Hz); δ_{C} consistent with previous data (Rezvanian, A. An Expedient Synthesis Strategy to the 1,4-Dihydropyridines and Pyrido[1,2-*a*]Quinoxalines: Iodine Catalyzed One-Pot Four-Component Domino Reactions. *Tetrahedron* **2016**, 72 (41), 6428–6435.)

1-(2-(2,4-Diisopropoxyphenyl)-2-oxoethyl)pyridin-1-ium bromide (**5a**) was prepared by refluxing 2-bromo-1-(2,4-diisopropoxyphenyl)ethan-1-one with pyridine on a 2 mmol scale following general procedure B. Yield = 36%. White solid: δ_{H} (400 MHz, CDCl₃-d₆) 9.20 (d, 2H, Ar, $J = 6.4$ Hz), 8.49 (t, 1H, Ar, $J = 7.8$ Hz), 8.06 (t, 2H, Ar, $J = 7$ Hz), 7.91 (d, 1H, Ar, $J = 8.8$ Hz), 6.54 (s, 2H, Ar), 6.51 (s, 1H, COCH₂), 6.46 (s, 1H, COCH₂), 4.81-4.75 (m, 1H, CH(CH₃)₂), 4.68-4.62 (m, 1H, CH(CH₃)₂), 1.63 (t, 6H, CH(CH₃)₂), $J =$

6.2 Hz), 1.38 (d, 6H, CH(CH₃)₂, *J* = 6.4 Hz); δ_C (400 MHz, DMSO-d₆) 193.3, 169.4, 165.7, 151.4, 151.7, 137.8, 132.6, 121.6, 113.3, 105.8, 76.3, 75.2, 74.9, 26.9, 26.8

1-(2-(4-Isopropoxyphenyl)-2-oxoethyl)pyridin-1-ium bromide (5b) was prepared by refluxing 2-bromo-1-(4-isopropoxyphenyl)ethan-1-one with pyridine on a 2 mmol scale following general procedure B. Yield = 87%. White solid: δ_H (400 MHz, CDCl₃-d₆) 9.32 (d, 2H, Ar, *J* = 5.2 Hz), 8.46 (t, 1H, Ar, *J* = 8 Hz), 8.07 (d, 2H, Ar, *J* = 8.4 Hz), 8.02 (t, 2H, Ar, *J* = 7 Hz), 7.07 (s, 2H, Ar), 6.89 (d, 1H, COCH₂, *J* = 8.8 Hz), 4.65-4.59 (m, 1H, CH(CH₃)₂), 1.34 (d, 6H, CH(CH₃)₂, *J* = 6.4 Hz); δ_C (400 MHz, DMSO-d₆) 194.0, 167.8, 151.5, 135.9, 132.9, 131.0, 120.7, 75.1, 71.0, 26.7

1-(2-Oxo-2-phenylethyl)pyridin-1-ium iodide (5c) was prepared by refluxing acetophenone with pyridine on a 10 mmol scale following general procedure B. Yield = quant. Light brown solid: δ_H (400 MHz, DMSO-d₆) 8.99 (d, 2H, Ar, *J* = 6 Hz), 8.75 (t, 1H, Ar, *J* = 7.8 Hz), 8.29 (t, 2H, Ar, *J* = 7 Hz), 8.08 (d, 2H, Ar, *J* = 6.8 Hz), 7.81 (t, 1H, Ar, *J* = 7.4 Hz), 7.68 (t, 2H, Ar, *J* = 7.6 Hz), 6.47 (s, 2H, COCH₂); δ_C consistent with previous data (Liu, J.; Zhang, F.; Wang, T.; Qing, X.; Wang, C. Selective Hydrolysis of 1-Cyanocyclopropane-1-Carboxylates: Concise Preparation of 1-Carbamoylcyclopropane-1-Carboxylates. *J. Chem. Res.* **2016**, *40* (11), 694–697.)

1-(2-(4-Chlorophenyl)-2-oxoethyl)pyridin-1-ium iodide (5d) was prepared by refluxing 1-(4-chlorophenyl)ethan-1-one with pyridine on a 13 mmol scale following general procedure B. Yield = quant. Light brown solid: δ_H (400 MHz, DMSO-d₆) 8.99-8.94 (m, 4H, Ar), 8.75 (t, 1H, Ar, *J* = 7.8 Hz), 8.60 (t, 1H, Ar, *J* = 7.6 Hz), 8.29 (t, 2H, Ar, *J* = 7 Hz), 8.08 (d, 4H, Ar, *J* = 7.2), 7.77 (d, 2H, Ar, *J* = 8.8 Hz), 6.47 (s, 2H, COCH₂); δ_C consistent with previous data (Baharfar, R.; Asghari, S.; Zaheri, F.; Shariati, N. Three-

Component Synthesis of Novel Spirooxindole–furan Derivatives Using Pyridinium Salts.

Comptes Rendus Chim. **2017**, *20* (4), 359–364.)

1-(2-(2-Bromophenyl)-2-oxoethyl)pyridin-1-ium iodide (5e) was prepared by refluxing 1-(2-bromophenyl)ethan-1-one with pyridine on a 10 mmol scale following general procedure B. Yield = 75%. Light beige solid: δ_{H} (400 MHz, DMSO- d_6) 9.01 (d, 2H, Ar, $J = 6.4$ Hz), 8.76 (t, 1H, Ar, $J = 7.8$ Hz), 8.30 (t, 2H, Ar, $J = 7$ Hz), 8.11 (d, 1H, Ar, $J = 8$ Hz), 7.89 (d, 1H, Ar, $J = 7.6$ Hz), 7.69 (t, 1H, Ar, $J = 7$ Hz), 7.63 (t, 1H, Ar, $J = 7$ Hz), 6.40 (s, 2H, COCH₂); δ_{C} consistent with previous data (Sham, K.-C.; Lee, C.-S.; Chan, K.-Y.; Yiu, S.-M.; Wong, W.-T.; Kwong, H.-L. Coordination Properties of Axially Unfixed Chiral Dipyridine Ligands towards Metal and Ammonium Ions. *Polyhedron* **2011**, *30* (6), 1149–1156.)

1-(2-(3-Bromophenyl)-2-oxoethyl)pyridin-1-ium iodide (5f) was prepared by refluxing 1-(3-bromophenyl)ethan-1-one with pyridine on a 10 mmol scale following general procedure B. Yield = quant. Beige solid: δ_{H} (400 MHz, DMSO- d_6) 8.97 (d, 2H, Ar, $J = 6.4$ Hz), 8.76 (t, 1H, Ar, $J = 7.8$ Hz), 8.30 (t, 2H, Ar, $J = 7$ Hz), 8.23 (s, 1H, Ar), 8.06 (d, 1H, Ar, $J = 7.6$ Hz), 8.02 (d, 1H, Ar, $J = 8.4$ Hz), 7.65 (t, 1H, Ar, $J = 7.8$ Hz), 6.48 (s, 2H, COCH₂); δ_{C} consistent with previous data (Shu, W.-M.; Ma, J.-R.; Yang, Y.; Wu, A.-X. An Efficient Synthesis of Novel Fused Cycloheptatrienes through Mn(II)-Mediated Formal Intermolecular [2 + 2 + 2 + 1] Cycloaddition. *Org. Lett.* **2014**, *16* (5), 1286–1289.)

1-(2-(4-Methoxyphenyl)-2-oxoethyl)pyridin-1-ium iodide (5g) was prepared by refluxing 1-(4-methoxyphenyl)ethan-1-one with pyridine on a 10mmol scale following general procedure B. Orange-brown solid. δ_{H} (400 MHz, DMSO- d_6) 8.98 (d, 2H, Ar, $J = 5.6$ Hz),

8.73 (t, 1H, Ar, $J = 7.8$ Hz), 8.27 (t, 2H, Ar, $J = 7$ Hz), 8.05 (d, 2H, Ar, $J = 8.8$ Hz), 7.20 (d, 2H, Ar, $J = 8.4$), 6.41 (s, 1H, COCH₂), 3.91 (s, 3H, COCH₃); δ_C consistent with previous data (Hu, R.-B.; Sun, S.; Su, Y. Visible-Light-Induced Carbo-2-Pyridylation of Electron-Deficient Alkenes with Pyridinium Salts. *Angew. Chem. Int. Ed.* **2017**, *56* (36), 10877–10880.)

1-(2-(4-Nitrophenyl)-2-oxoethyl)pyridin-1-ium iodide salt (5h) was prepared by refluxing 1-(4-nitrophenyl)ethan-1-one with pyridine on a 10 mmol scale following general procedure B. Yield = 40%. Dark orange solid: δ_H (400 MHz, DMSO-*d*₆) 8.98 (d, 2H, Ar, $J = 5.6$ Hz), 8.76 (t, 1H, Ar, $J = 7.8$ Hz), 8.49 (d, 2H, Ar, $J = 8.4$ Hz), 8.32-8.29 (m, 4H, Ar), 6.51 (s, 2H, COCH₂); δ_C consistent with previous data (Galenko, E. E.; Galenko, A. V.; Khlebnikov, A. F.; Novikov, M. S.; Shakirova, J. R. Synthesis and Intramolecular Azo Coupling of 4-Diazopyrrole-2-Carboxylates: Selective Approach to Benzo and Hetero [c]-Fused 6H-Pyrrolo[3,4-c]Pyridazine-5-Carboxylates. *J. Org. Chem.* **2016**, *81* (18), 8495–8507.)

1-(2-(Benzo[d][1,3]dioxol-5-yl)-2-oxoethyl)pyridin-1-ium iodide (5i) was prepared by refluxing 1-(benzo[d][1,3]dioxol-5-yl)ethan-1-one with pyridine on a 6 mmol scale following general procedure B. Yield = 65%. Burnt orange solid: δ_H (400 MHz, DMSO-*d*₆) 8.97 (d, 2H, Ar, $J = 5.6$ Hz), 8.73 (t, 1H, Ar, $J = 7.8$ Hz), 8.27 (t, 2H, Ar, $J = 7$ Hz), 7.73 (d, 1H, Ar, $J = 10.4$ Hz), 7.54 (s, 1H, Ar), 7.21 (d, 1H, Ar, $J = 8$ Hz), 6.37 (s, 2H, OCH₂O) 6.22 (s, 2H, COCH₂); δ_C consistent with previous data (Shu, W.-M.; Ma, J.-R.; Yang, Y.; Wu, A.-X. An Efficient Synthesis of Novel Fused Cycloheptatrienes through Mn(II)-Mediated Formal Intermolecular [2 + 2 + 2 + 1] Cycloaddition. *Org. Lett.* **2014**, *16* (5), 1286–1289.)

1-(2-(4-(Benzyloxy)phenyl)-2-oxoethyl)pyridin-1-ium iodide (5j) was prepared by refluxing 1-(4-(benzyloxy)phenyl)ethan-2-one with pyridine on a 7 mmol scale following general procedure B. Yield = 75%. Burnt orange solid: δ_{H} (400 MHz, DMSO- d_6) 8.97 (d, 2H, Ar, $J = 5.6$ Hz), 8.73 (t, 1H, Ar, $J = 7.8$ Hz), 8.27 (t, 2H, Ar, $J = 7$ Hz), 8.04 (d, 2H, Ar, $J = 8.8$ Hz), 7.49 (d, 2H, Ar, $J = 7.2$ Hz), 7.42 (t, 2H, Ar, $J = 7.4$ Hz), 7.37 (d, 1H, Ar, $J = 7.2$ Hz), 7.27 (d, 2H, Ar, $J = 8.8$ Hz), 6.41 (s, 2H, CH_2O), 5.29 (s, 2H, COCH_2); δ_{C} consistent with previous data (Fuglseth, E.; Thvedt, T. H. K.; Møll, M. F.; Hoff, B. H. Electrophilic and Nucleophilic Side Chain Fluorination of Para-Substituted Acetophenones. *Tetrahedron* **2008**, *64* (30), 7318–7323.)

1-(2-(4-Bromophenyl)-2-oxoethyl)pyridin-1-ium iodide (5k) was prepared by refluxing 1-(4-bromophenyl)ethan-1-one with pyridine on a 10 mmol scale following general procedure B. Yield = quant. Yellow solid: δ_{H} (400 MHz, DMSO- d_6) 8.97 (d, 2H, Ar, $J = 5.6$ Hz), 8.74 (t, 1H, Ar, $J = 7.2$ Hz), 8.00 (d, 2H, Ar, $J = 8$ Hz), 7.91 (d, 2H, Ar, $J = 8.8$ Hz), 6.43 (s, 2H, COCH_2); δ_{C} consistent with previous data (Galenko, E. E.; Galenko, A. V.; Khlebnikov, A. F.; Novikov, M. S.; Shakirova, J. R. Synthesis and Intramolecular Azo Coupling of 4-Diazopyrrole-2-Carboxylates: Selective Approach to Benzo and Hetero [c]-Fused 6H-Pyrrolo[3,4-c]Pyridazine-5-Carboxylates. *J. Org. Chem.* **2016**, *81* (18), 8495–8507.)

Final Products

6-(2,4-Diisopropoxyphenyl)-4-(4-isopropoxyphenyl)picolinic acid (ILC-1-094, 1) was prepared by refluxing 4-[4-(isopropoxy)phenyl]-2-oxo-3-butanoic acid with pyridinium iodide salt **5a** and ammonium acetate on a 0.5 mmol scale following general procedure C. Yield = 11%. Green-brown solid: δ_{H} (400 MHz, CDCl_3 - d_6) 8.33 (s, 2H, Ar), 7.80 (d, 1H,

Ar, $J = 7.6$ Hz), 7.71 (d, 2H, Ar, $J = 8.4$ Hz), 7.01 (d, 2H, Ar, $J = 8.4$ Hz), 6.64 (d, 1H, Ar, $J = 7.6$ Hz), 6.58 (s, 1H, Ar), 4.69-4.62 (m, 3H, $\underline{\text{C}}\text{H}(\text{CH}_3)_2$), 1.43-1.38 (m, 18H, $\text{CH}(\underline{\text{C}}\text{H}_3)_2$); δ_{C} (400 MHz, DMSO- d_6) 163.9, 160.9, 159.7, 157.0, 153.7, 151.3, 146.0, 131.7, 128.7, 128.5, 124.5, 118.1, 116.3, 107.2, 102.5, 71.2, 70.2, 70.0, 29.6, 22.1, 22.0, 21.9; $t_{\text{R}} = 40.7$ min (100%)

4,6-Bis(4-isopropoxyphenyl)picolinic acid (ILC-1-098) was prepared by refluxing 4-[4-(isopropoxy)phenyl]-2-oxo-3-butanoic acid with pyridinium iodide salt **5b** and ammonium acetate on a 0.75 mmol scale following general procedure C. Yield = 30%. Light yellow solid: δ_{H} (400 MHz, $\text{CDCl}_3\text{-d}_6$) 8.29 (s, 1H, Ar), 8.05 (s, 1H, Ar), 7.97 (d, 2H, Ar, $J = 8$ Hz), 7.69 (d, 2H, Ar, $J = 8.8$ Hz), 7.02 (d, 4H, Ar, $J = 7.6$ Hz), 4.64 (t, 2H, $\underline{\text{C}}\text{H}(\text{CH}_3)_2$, $J = 5.6$ Hz), 1.39 (d, 12H, $\text{CH}(\underline{\text{C}}\text{H}_3)_2$, $J = 6.4$ Hz); δ_{C} (400 MHz, DMSO- d_6) 164.6, 159.5, 156.5, 151.3, 146.1, 129.4, 128.7, 128.4, 120.8, 118.4, 116.3, 115.9, 70.0, 21.9; $t_{\text{R}} = 41.2$ min (100%)

4,6-Bis(4-(benzyloxy)phenyl)picolinic acid (ILC-1-102) was prepared by refluxing 2-oxo-4-[4-(benzyloxy)phenyl]-3-butenoic acid with pyridinium iodide salt **5j** and ammonium acetate on a 0.20 mmol following general procedure C. Yield = 75%. Brown solid: δ_{H} (400 MHz, DMSO- d_6) 8.27 (d, 3H, Ar, $J = 8.8$ Hz), 8.16 (s, 1H, Ar), 7.58 (s, 1H, Ar), 7.52-7.33 (m, 12H, Ar), 7.15 (d, 3H, Ar, $J = 6.8$ Hz), 5.21 (d, 4H, COCH_2 , $J = 20.4$ Hz); δ_{C} (400 MHz, DMSO- d_6) 164.7, 164.2, 161.6, 154.2, 154.2, 143.7, 142.1, 142.0, 135.9, 135.5, 133.8, 133.6, 133.0, 132.9, 124.8, 121.2, 120.0, 118.6, 74.6, 74.4; $t_{\text{R}} = 49.6$ min (100%)

6-(4-(Benzyloxy)phenyl)-4-(4-isopropoxyphenyl)picolinic acid (ILC-1-107) was prepared by refluxing 4-[4-(isobutoxy)phenyl]-2-oxo-3-butanoic acid with pyridinium iodide salt

5j and ammonium acetate on a 0.50 mmol scale following general procedure C. Yield = 62%. Brown solid: δ_{H} (400 MHz, $\text{CDCl}_3\text{-d}_6$) 8.32 (s, 1H, Ar), 8.07 (s, 1H, Ar), 8.00 (d, 2H, Ar, $J = 8.8$ Hz), 7.71 (d, 2H, Ar, $J = 8.4$ Hz), 7.47 (d, 2H, Ar, $J = 6.8$ Hz), 7.42 (t, 2H, Ar, $J = 7.4$ Hz), 7.37 (d, 1H, Ar, $J = 7.2$ Hz), 7.13 (d, 2H, Ar, $J = 8.8$ Hz), 7.04 (d, 2H, Ar, $J = 8.8$ Hz), 5.17 (s, 2H, COCH_2), 3.80 (d, 2H, $\text{CH}_2\text{CH}(\text{CH}_3)_2$, $J = 6.4$ Hz), 2.15-2.12 (m, 1H, $\text{CH}_2\text{CH}(\text{CH}_3)_2$), 1.06 (d, 6H, $\text{CH}_2\text{CH}(\text{CH}_3)_2$, $J = 6.4$ Hz); δ_{C} (400 MHz, DMSO-d_6) 167.2, 160.4, 159.9, 156.8, 150.2, 149.2, 137.3, 131.2, 129.3, 128.8, 128.3, 128.1, 119.4, 119.1, 115.5, 115.2, 114.9, 74.2, 69.7, 39.3, 19.4; $t_{\text{R}} = 50.0$ min (99.0%)

6-(4-Methoxyphenyl)-4-(4-phenoxyphenyl)picolinic acid (ILC-1-166) was prepared by refluxing acid **3a** with pyridinium iodide salt **5g** and ammonium acetate on a 0.56 mmol scale following general procedure C. Yield = 15%. Brown solid: δ_{H} (400 MHz, DMSO-d_6) 8.37 (s, 1H, Ar), 8.28 (d, 2H, Ar, $J = 8.8$ Hz), 8.15 (s, 1H, Ar), 8.02 (d, 2H, Ar, $J = 8.4$ Hz), 7.46 (t, 2H, Ar, $J = 7.8$ Hz), 7.22 (t, 1H, Ar, $J = 7.6$ Hz), 7.16-7.08 (m, 6H, Ar), 3.85 (s, 3H, OCH_3); δ_{C} (400 MHz, DMSO-d_6) 171.5, 165.7, 163.5, 161.8, 161.0, 154.2, 153.8, 136.8, 135.5, 135.4, 134.2, 133.8, 129.3, 125.4, 124.5, 123.7, 119.2, 60.4; $t_{\text{R}} = 42.5$ min (96.2%)

4,6-Bis(4-bromophenyl)picolinic acid (ILC-1-167) was prepared by refluxing acid **3c** with pyridinium iodide salt **5k** and ammonium acetate on a 0.60 mmol scale following general procedure C. Yield = 26%. Green solid: δ_{H} (400 MHz, DMSO-d_6) 8.51 (s, 1H, Ar), 8.29 (t, 3H, Ar, $J = 9.4$ Hz), 7.98 (d, 2H, Ar, $J = 8.4$ Hz), 7.76 (t, 4H, Ar, $J = 7.4$ Hz), 7.46 (t, 2H, Ar, $J = 7.8$ Hz), 7.22 (t, 1H, Ar, $J = 7.6$ Hz), 7.16-7.08 (m, 6H, Ar), 3.85 (s, 3H, OCH_3); δ_{C} (400 MHz, DMSO-d_6) 166.4, 156.2, 149.7, 148.9, 137.3, 136.1, 132.5, 132.1, 129.8, 129.7, 123.8, 121.1, 120.9; $t_{\text{R}} = 45.0$ min (99.7%)

6-(4-Nitrophenyl)-4-(4-phenoxyphenyl)picolinic acid (ILC-1-168) was prepared by refluxing acid **3a** with pyridinium iodide salt **5e** and ammonium acetate on a 0.56 mmol scale following general procedure C. Yield = 30%. Burnt orange solid: δ_{H} (400 MHz, DMSO- d_6) 8.61 (d, 2H, Ar, $J = 8$ Hz), 8.41-8.32 (m, 3H, Ar), 8.20 (d, 1H, Ar, $J = 8.8$ Hz), 8.07 (d, 2H, Ar, $J = 8.4$ Hz), 7.47 (t, 2H, Ar, $J = 7.8$ Hz), 7.23 (t, 1H, Ar, $J = 7.4$ Hz), 7.18-7.12 (m, 4H, Ar); δ_{C} (400 MHz, DMSO- d_6) 166.5, 158.9, 156.2, 154.9, 149.6, 148.4, 144.3, 131.5, 131.0, 130.6, 129.6, 128.8, 124.6, 124.3, 121.8, 119.8, 119.0; $t_{\text{R}} = 44.8$ min (91.2%)

6-(4-(Benzyloxy)phenyl)-4-(4-bromophenyl)picolinic acid (ILC-1-169) was prepared by refluxing acid **3c** with pyridinium iodide salt **5j** and ammonium acetate on a 0.60 mmol scale following general procedure C. Yield = 65%. Dark green solid. δ_{H} (400 MHz, DMSO- d_6) 8.40 (s, 1H, Ar), 8.29 (d, 2H, Ar, $J = 8$ Hz), 8.17 (s, 1H, Ar), 7.96 (d, 2H, Ar, $J = 8.8$ Hz), 7.76 (d, 2H, Ar, $J = 8$ Hz), 7.50 (d, 2H, Ar, $J = 8$ Hz), 7.42 (t, 2H, Ar, $J = 7.4$ Hz), 7.36 (d, 1H, Ar, $J = 7.2$ Hz), 7.18 (d, 2H, Ar, $J = 8.8$ Hz), 5.22 (s, 2H, OCH $_2$); δ_{C} (400 MHz, DMSO- d_6) 166.6, 160.1, 158.3, 157.1, 149.4, 148.6, 137.3, 136.4, 132.5, 130.8, 129.8, 129.1, 128.8, 128.3, 128.2, 132.7, 120.1, 120.0 115.3, 69.7; $t_{\text{R}} = 48.1$ min (98.3%)

4-(4-Phenoxyphenyl)-6-phenylpicolinic acid (ILC-1-170) was prepared by refluxing acid **3a** with pyridinium iodide salt **5c** and ammonium acetate on a 1.0 mmol scale following general procedure C. Yield = 33%. Brown solid: δ_{H} (400 MHz, DMSO- d_6) 8.44 (s, 1H, Ar), 8.31 (d, 2H, Ar, $J = 7.6$ Hz), 8.23 (s, 1H, Ar), 8.04 (d, 2H, Ar, $J = 8.8$ Hz), 7.57-7.45 (m, 5H, Ar), 7.24 (d, 1H, Ar, $J = 3.4$ Hz), 7.15 (t, 4H, Ar, $J = 9$ Hz); δ_{C} (400 MHz,

DMSO-d₆) 158.1, 157.1, 150.0, 139.1, 132.6, 131.5, 130.8, 130.4, 129.9, 128.4, 125.4, 121.5, 121.4, 120.6, 119.8; t_R = 43.4 min (100%)

6-(Benzo[d][1,3]dioxol-5-yl)-4-(4-phenoxyphenyl)picolinic acid (ILC-1-172) was prepared by refluxing acid **3a** with pyridinium iodide salt **5i** and ammonium acetate on a 1.0 mmol scale following general procedure C. Yield = 27%. Light orange solid: δ_H (400 MHz, DMSO-d₆) 8.38 (s, 1H, Ar), 8.17 (s, 1H, Ar), 8.03 (d, 2H, Ar, J = 8.4 Hz), 7.95 (s, 1H, Ar), 7.91 (d, 1H, Ar, J = 8.8 Hz), 7.46 (t, 2H, Ar, J = 7.8 Hz), 7.23 (d, 1H, Ar, J = 6.8 Hz), 7.14 (t, 4H, Ar, J = 7.8 Hz), 7.08 (d, 1H, Ar, J = 8 Hz), 6.13 (s, 2H, OCH₂O); δ_C (400 MHz, DMSO-d₆) 166.6, 158.7, 156.7, 156.3, 149.2, 149.0, 148.4, 132.5, 131.9, 130.6, 129.5, 124.5, 122.0, 120.1, 120.0, 119.7, 119.0, 108.8, 107.8, 101.8; t_R = 43.1 min (100%)

6-(4-(Benzyloxy)phenyl)-4-(4-phenoxyphenyl)picolinic acid (ILC-1-174) was prepared by refluxing acid **3a** with pyridinium iodide salt **5j** and ammonium acetate on a 1.0 mmol scale following general procedure C. Yield = 25%. Brown solid: δ_H (400 MHz, DMSO-d₆) 8.37 (s, 1H, Ar), 8.29 (d, 2H, Ar, J = 8 Hz), 8.16 (s, 1H, Ar), 8.02 (d, 2H, Ar, J = 8.4 Hz), 7.51-7.40 (m, 7H, Ar), 7.36 (d, 1H, Ar, J = 7.2 Hz), 7.22-7.12 (m, 7H, Ar), 5.21 (s, 2H, OCH₂); δ_C (400 MHz, DMSO-d₆) 166.7, 160.0, 158.7, 157.0, 156.3, 149.3, 149.1, 137.3, 131.9, 130.9, 130.6, 129.5, 129.1, 128.8, 128.3, 128.2, 123.5, 119.7, 119.0, 115.3 69.7; t_R = 49.3 min (97.4%)

4-(4-Bromophenyl)-6-(4-methoxyphenyl)picolinic acid (ILC-1-176) was prepared by refluxing acid **3c** with pyridinium iodide salt **5g** and ammonium acetate on a 1.0 mmol scale following general procedure C. Yield = 38%. Green solid: δ_H (400 MHz, DMSO-d₆) 8.39 (s, 1H, Ar), 8.28 (d, 2H, Ar, J = 8.8 Hz), 8.17 (s, 1H, Ar), 7.95 (d, 2H, Ar, J =

8.8 Hz), 7.76 (d, 2H, Ar, $J = 8.4$ Hz), 7.09 (d, 2H, Ar, $J = 8.8$ Hz), 3.85 (s, 3H, OCH₃); δ_C (400 MHz, DMSO-d₆) 171.4, 165.8, 161.9, 154.2, 153.4, 141.2, 137.2, 135.3, 134.5, 133.8, 128.4, 124.7, 119.2, 60.4; $t_R = 40.0$ min (98.5%)

6-(4-Isopropoxyphenyl)-4-(4-phenoxyphenyl)picolinic acid (ILC-1-178) was prepared by refluxing acid **3a** with pyridinium iodide salt **5b** and ammonium acetate on a 0.74 mmol scale following general procedure C. Yield = 31%. Dark brown solid: δ_H (400 MHz, DMSO-d₆) 8.35 (s, 1H, Ar), 8.25 (d, 2H, Ar, $J = 8.4$ Hz), 8.15 (s, 1H, Ar), 8.01 (d, 2H, Ar, $J = 8.8$ Hz), 7.46 (t, 2H, Ar, $J = 7.8$ Hz), 7.22 (t, 1H, Ar, $J = 7.8$ Hz), 7.14 (t, 4H, Ar, $J = 8.2$ Hz), 7.06 (d, 2H, Ar, $J = 8.4$ Hz), 4.75-4.72 (m, 1H, OCH(CH₃)₂), 1.31 (d, 6H, OCH(CH₃)₂); δ_C (400 MHz, DMSO-d₆) 171.5, 164.0, 163.5, 161.9, 153.8, 136.7, 135.4, 134.2, 133.9, 129.3, 124.5, 123.7, 120.6, 116.9, 74.4, 60.0, 26.9; $t_R = 46.5$ min (98.9%)

4-(4-Bromophenyl)-6-phenylpicolinic acid (ILC-1-192) was prepared by refluxing acid **3c** with pyridinium iodide salt **5c** and ammonium acetate on a 1.0 mmol scale following general procedure C. Yield = 20%. Green solid: δ_H (400 MHz, DMSO-d₆) 8.47 (s, 1H, Ar), 8.31 (d, 2H, Ar, $J = 6.8$ Hz), 8.24 (s, 1H, Ar), 7.98 (d, 2H, Ar, $J = 7.6$ Hz), 7.77 (d, 2H, Ar, $J = 8.8$ Hz), 7.57-7.51 (m, 3H, Ar), 7.15 (t, 4H, Ar, $J = 9$ Hz); δ_C (400 MHz, DMSO-d₆) 171.4, 162.2, 154.5, 153.5, 142.9, 141.1, 137.3, 134.8, 134.6, 133.9, 132.4, 128.5, 125.7, 125.5; $t_R = 40.5$ min (95.2%)

6-(Benzo[d][1,3]dioxol-5-yl)-4-(4-bromophenyl)picolinic acid (ILC-1-193) was prepared by refluxing acid **3c** with pyridinium iodide salt **5i** and ammonium acetate on a 1.0 mmol scale following general procedure C. Yield = 42%. Grey solid: δ_H (400 MHz, DMSO-d₆) 8.40 (s, 1H, Ar), 8.18 (s, 1H, Ar), 7.97 (d, 3H, Ar, $J = 9.6$ Hz), 7.91 (d, 1H, Ar, $J = 8.8$ Hz), 7.76 (d, 2H, Ar, $J = 7.6$ Hz), 7.08 (d, 1H, Ar, $J = 8.8$ Hz), 6.13 (s, 2H, OCH₂O); δ_C

(400 MHz, DMSO- d_6) 171.3, 161.6, 153.8, 153.4, 153.1, 137.2, 134.6, 128.5, 126.8, 125.1, 124.9, 119.4, 113.6, 112.5, 106.6; t_R = 39.2 min (100%)

4-(4-Bromophenyl)-6-(4-chlorophenyl)picolinic acid (ILC-1-197) was prepared by refluxing acid **3c** with pyridinium iodide salt **5d** and ammonium acetate on a 1.0 mmol scale following general procedure C. Yield = 16%. Green solid: δ_H (400 MHz, DMSO- d_6) 8.50 (s, 1H, Ar), 8.36 (d, 2H, Ar, J = 8.8 Hz), 8.26 (s, 1H, Ar), 7.97 (d, 2H, Ar, J = 7.6 Hz), 7.76 (d, 2H, Ar, J = 8 Hz), 7.61 (d, 2H, Ar, J = 8.4 Hz); δ_C (400 MHz, DMSO- d_6) 171.2, 160.9, 154.4, 153.7, 141.7, 140.9, 139.7, 134.6, 134.2, 133.9, 128.6, 125.8; t_R = 45.2 min (98.9%)

2-(4-Bromophenyl)-6-(4-phenoxyphenyl)isonicotinic acid (ILC-1-199) was prepared by refluxing acid **3b** with pyridinium iodide salt **5k** and ammonium acetate on a 1.0 mmol scale following general procedure C. Yield = 37%. Brown solid: δ_H (400 MHz, DMSO- d_6) 8.26 (d, 4H, Ar, J = 10.8 Hz), 8.21 (d, 2H, Ar, J = 7.6 Hz), 7.73 (d, 2H, Ar, J = 8.8 Hz), 7.45 (t, 2H, Ar, J = 8 Hz), 7.21 (t, 1H, Ar, J = 7.4 Hz), 7.13 (t, 4H, Ar, J = 8.6 Hz); δ_C (400 MHz, DMSO- d_6) 171.5, 163.6, 161.6, 161.3, 160.8, 146.3, 142.4, 138.1, 137.1, 135.5, 134.1, 134.0, 129.3, 128.6, 124.5, 123.7, 122.9, 122.5; t_R = 51.9 min (97.9%)

6-(4-Bromophenyl)-4-(4-phenoxyphenyl)picolinic acid (ILC-1-200) was prepared by refluxing acid **3a** with pyridinium iodide salt **5k** and ammonium acetate on a 1.0 mmol scale following general procedure C. Yield = 33%. Light orange solid: δ_H (400 MHz, DMSO- d_6) 8.47 (s, 1H, Ar), 8.29 (d, 2H, Ar, J = 8.4 Hz), 8.24 (s, 1H, Ar), 8.03 (d, 2H, Ar, J = 7.6 Hz), 7.74 (d, 2H, Ar, J = 7.6 Hz), 7.46 (t, 2H, Ar, J = 7.8 Hz), 7.22 (t, 1H, Ar, J = 7.6 Hz), 7.14 (t, 4H, Ar, J = 9 Hz); δ_C (400 MHz, DMSO- d_6) 171.3, 163.6, 160.8,

154.3, 154.2, 142.2, 136.8, 136.4, 135.4, 143.3, 129.3, 128.5, 125.6, 125.4, 124.5, 123.7;
 $t_R = 48.2$ min (96.5%)

6-(2-Bromophenyl)-4-(4-phenoxyphenyl)picolinic acid (ILC-1-203) was prepared by refluxing acid **3a** with pyridinium iodide salt **5e** and ammonium acetate on a 1.0 mmol scale following general procedure C. Yield = 11%. Brown-orange solid: δ_H (400 MHz, DMSO- d_6) 8.30 (s, 1H, Ar), 8.12 (s, 1H, Ar), 7.97 (d, 2H, Ar, $J = 7.6$ Hz), 7.80 (d, 1H, Ar, $J = 7.6$ Hz), 7.66 (d, 1H, Ar, $J = 6.8$ Hz), 7.56 (t, 1H, Ar, $J = 7.4$ Hz), 7.48-7.42 (m, 4H, Ar), 7.22 (t, 1H, Ar, $J = 7.4$ Hz), 7.13 (d, 4H, Ar, $J = 8$ Hz); δ_C (400 MHz, DMSO- d_6) 171.4, 163.7, 163.5, 160.8, 152.9, 145.5, 138.1, 136.9, 136.1, 135.7, 135.4, 134.2, 133.0, 129.6, 129.4, 126.5, 125.6, 124.6, 123.7; $t_R = 44.7$ min (95.3%)

6-(3-Bromophenyl)-4-(4-phenoxyphenyl)picolinic acid (ILC-1-210) was prepared by refluxing acid **3a** with pyridinium iodide salt **5f** and ammonium acetate on a 1.0 mmol scale following general procedure C. Yield = 25%. Brown-orange solid: δ_H (400 MHz, DMSO- d_6) 8.57 (s, 1H, Ar), 8.25 (s, 1H, Ar), 8.35 (d, 1H, Ar, $J = 7.6$ Hz), 8.26 (s, 1H, Ar), 8.06 (d, 1H, Ar, $J = 9.2$ Hz), 7.70 (d, 1H, Ar, $J = 7.6$ Hz), 7.53 (d, 1H, Ar, $J = 7.6$ Hz), 7.50-7.44 (m, 2H, Ar), 7.23 (t, 1H, Ar, $J = 7.4$ Hz), 7.15 (t, 4H, Ar, $J = 9.4$ Hz); δ_C (400 MHz, DMSO- d_6) 171.3, 163.6, 161.0, 160.3, 154.2, 145.3, 137.4, 136.4, 136.0, 135.4, 134.9, 134.4, 131.3, 129.3, 127.5, 125.8, 124.5, 123.7; $t_R = 47.7$ min (98.0%)

4.2.2. Biology

Protein purification. We regularly express and purify recombinant human Mcl-1 residues 172 to 327 (MCL1¹⁷²⁻³²⁷) protein in *E. coli* of high purity (>95% pure) and milligram quantity for use in all the applications proposed including FPCA and stable isotopically labeled (¹⁵N) protein for NMR studies. The pLM302 expression vector was constructed to produce His6-MBP (maltose

binding protein) tagged recombinant human Mcl-1 residues 172 to 327 (MCL1¹⁷²⁻³²⁷) in HMS174 (DE3) cells (EMD Millipore) using either LB or minimal media supplemented with ¹⁵NH₄Cl to produce unlabeled or ¹⁵N-labeled MCL1, respectively. The tagged protein was initially purified from the crude cell lysate by IMAC chromatography (GE Healthcare Life Sciences), and after dialysis to remove the imidazole the affinity tag was cleaved using PreScission Protease (GE Healthcare Life Sciences). A Sephacryl S-200 size exclusion column was used as a final purification step before the protein was concentrated with a 10,000 MWCO centrifugal filter concentrator (EMD Millipore). The concentrations of the proteins were determined using the Bio-Rad Protein Assay (Bio-Rad Inc., Hercules, CA) using BSA of a known concentration as the standard (Pierce). The purity of the protein was confirmed using SDS-PAGE analysis and NMR HSQC experiments were done to confirm the protein was properly folded.

Peptides. A 6-aminohexanoic acid linker was conjugated to the N-terminus of the Bak BH3 peptide amino acids 71 to 89 (GQVGRQLAIIGDDINR), capped with fluorescein (on the amino group of the linker), and the peptide was amidated on the C-terminus to give FITC-Ahx-GQVGRQLAIIGDDINR-CONH₂, hereafter referred to as “FITC-Bak” was synthesized and purity determined to be >95% (Neo BioScience). In addition, 5-Carboxytetramethylrhodamine (5-TAMRA) labeled version was purchase, 5-TAMRA-GQVGRQLAIIGDDINR-COH, hereafter “TAMRA-Bak” (Anaspec, Fremont, CA). The concentrated peptide stocks were prepared in DMSO and the concentration of the peptide was determined in water at pH 8.0 using the extinction coefficient for amide-linked FITC and for TAMRA of $\epsilon_{494} = 68,000 \text{ cm}^{-1}\text{M}^{-1}$, and $\epsilon_{547} = 65,000 \text{ cm}^{-1}\text{M}^{-1}$, respectively.

Protein NMR. Uniformly ^{15}N -labeled MCL-1¹⁷²⁻³²⁷ was used to collect two-dimensional ^1H , ^{15}N -fast heteronuclear single quantum coherence (HSQC) [1] spectra at 25°C with a Bruker AVANCE III 950 US2 NMR spectrometer (950.029 MHz for protons) equipped with pulsed-field gradients, four frequency channels, and triple resonance, z-axis gradient cryogenic probes. A one-second relaxation delay was used, and quadrature detection in the indirect dimensions was obtained with states-TPPI phase cycling; initial delays in the indirect dimensions were set to give zero- and first-order phase corrections of 90° and –180°, respectively [2, 3]. Data were processed using the processing program nmrPipe on Linux workstations [4]. All proton chemical shifts are reported with respect to the H₂O or HDO signal, taken to be 4.658 ppm relative to external TSP (0.0 ppm) at 25°C. The ^{15}N chemical shifts were indirectly referenced using the zero-point frequency at 25°C of 0.10132905 for ^{15}N - ^1H , as previously described [5-7]. The MCL-1 sample contained 73.3 μM ^{15}N -labeled MCL-1¹⁷²⁻³²⁷, 20 mM HEPES, pH 6.8, 50 mM NaCl, 10% D₂O, and 5% D₆-DMSO with and without 150 μM ILC-1-199.

Fluorescence polarization competition assay (FPCA). Fluorescence polarization experiments were conducted using a BMG PHERAstar FS multimode microplate reader equipped with two PMTs for simultaneous measurements of the perpendicular and parallel fluorescence emission. The assays were performed in black polypropylene 384-well microplate (Costar) with a final volume of 20 μL at room temperature with a 485 nm excitation while monitoring the perpendicular and parallel fluorescence emission at 520 nm. Using the FITC-Bak peptide, the fluorescence polarization competition assay (FPCA) was performed using 100 nM MCL-1¹⁷²⁻³²⁷, 10 nM FITC-Bak peptide, 20 mM HEPES, pH 6.8, 50 mM NaCl, 0.01% Triton X-100 and 2.5% DMSO with varying concentrations of compound. Using the TAMRA-Bak peptide, the

FPCA was performed using 800 nM MCL-1¹⁷²⁻³²⁷, 10 nM TAMRA-Bak peptide, 20 mM HEPES, pH 6.8, 50 mM NaCl, 0.01% Triton X-100 and 2.5% DMSO with varying concentrations of compound. Curve fitting was carried out using Origin (OriginLab, Northampton, MA) to determine the IC₅₀. The K_i was determined from the IC₅₀ using the Nikolovska-Coleska equation [8]. The affinity (K_D) of FITC-Bak and TAMRA-Bak for MCL-1¹⁷²⁻³²⁷ were previously determined to be 33.8 ± 0.50 nM and 852.3 ± 10.4 nM in the assay conditions used.

4.2.3. References

- (1) Mori, S., et al., Improved sensitivity of HSQC spectra of exchanging protons at short interscan delays using a new fast HSQC (FHSQC) detection scheme that avoids water saturation. *J Magn Reson B*, 1995. **108**(1): p. 94-8.
- (2) Marion, D., et al., Overcoming the overlap problem in the assignment of ¹H NMR spectra of larger proteins by use of three-dimensional heteronuclear ¹H-¹⁵N Hartmann-Hahn-multiple quantum coherence and nuclear Overhauser-multiple quantum coherence spectroscopy: application to interleukin 1 beta. *Biochemistry*, 1989. **28**(15): p. 6150-6.
- (3) Bax, A. and M. Ikura, An efficient 3D NMR technique for correlating the proton and ¹⁵N backbone amide resonances with the alpha-carbon of the preceding residue in uniformly ¹⁵N/¹³C enriched proteins. *J Biomol NMR*, 1991. **1**(1): p. 99-104.
- (4) Delaglio, F., et al., NMRPipe: a multidimensional spectral processing system based on UNIX pipes. *J Biomol NMR*, 1995. **6**(3): p. 277-93.
- (5) Edison, A.S., et al., Practical introduction to theory and implementation of multinuclear, multidimensional nuclear magnetic resonance experiments. *Methods Enzymol*, 1994. **239**: p. 3-79.
- (6) Live, D.H., Davis, D.G., Agosta, W.C., and Cowburn, D., *J. Am. Chem. Soc.*, 1984(106): p. 1939-1941.
- (7) Spera, S., M. Ikura, and A. Bax, Measurement of the exchange rates of rapidly exchanging amide protons: application to the study of calmodulin and its complex with a myosin light chain kinase fragment. *J Biomol NMR*, 1991. **1**(2): p. 155-65.
- (8) Nikolovska-Coleska, Z., et al., Development and optimization of a binding assay for the XIAP BIR3 domain using fluorescence polarization. *Analytical biochemistry*, 2004. **332**(2): p. 261-73.

4.3. Acknowledgement

I would like to thank Drs. Varney and Godoy-Ruiz for performing the HSQC NMR experiments and Dr. Paul T. Wilder for performing the fluorescence polarization competition assays.

Reproduced with permission from I.L. Conlon, D. Van Eker, S. Abdelmalak, W. A. Murphy, H. Bashir, M. Sun, J. Chauhan, K.M. Varney, R. Godoy-Ruiz, P.T. Wilder, and S. Fletcher., *Bioorganic & Medicinal Chemistry Letters* 2018, 28 (10), 1949-1953.

Copyright © 2018 Elsevier Ltd. Published by Elsevier Ltd. All rights Reserved.

Chapter 5. Construction of 1*H*-indazoles from *ortho*-aminobenzoximes by the Mitsunobu reaction.

1*H*-Indazoles are incredibly rare in nature but the diverse pharmacological properties imparted to molecules containing this nucleus has catapulted them firmly into the drug designer's toolkit. Indeed, molecules presenting the 1*H*-indazole motif have featured in the development of drugs spanning a range of pathophysiologies, such as inflammation

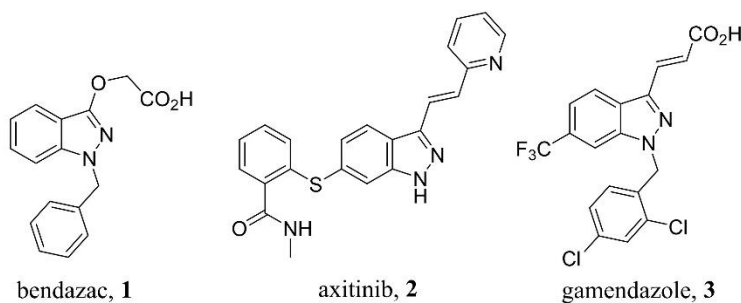


Figure 5.1. Drug molecules featuring a 1*H*-indazole motif.

(bendazac, **1**) and renal cell carcinoma (axitinib, **2**), as well as towards the discovery of a male contraceptive (gamendazole, **3**) (Figure 5.1.¹⁻⁴ Traditional routes to 1*H*-indazoles involve severe and/or inconvenient conditions,^{5,6} for example diazotization, or suffer from poor functional group tolerance.⁷ Given the significance of 1*H*-indazoles in medicinal chemistry,^{1,2} it is becoming increasingly important to develop milder routes to their synthesis that are compatible with a range of functional groups.

Towards this end, there have been several reports of alternative strategies to access 1*H*-indazoles. Methods include iodine-⁸ or PIFA-mediated⁹ C-H amination of aryl hydrazones, although yields may be poor or moderate at best, cyclizations of *o*-haloaryl hydrazones, but this requires the *o*-haloaryl aldehyde/ketone,¹⁰ as well as metal-catalyzed C-H activations of various precursors, including imidate esters and NH imines with nitrosoarenes.¹¹ In addition, CsF-mediated 1,3-dipolar cycloadditions with an α -

substituted diazomethylphosphonates and arynes also affords 1*H*-indazoles.¹² A mild procedure was published in 2008 wherein the *in situ* *O*-mesylation of *ortho*-aminobenzoximes results in a transient intermediate that cyclizes to the 1*H*-indazole nucleus.¹³ More recently, Manna and colleagues effected the cyclodehydration of *ortho*-aminobenzoximes to 1*H*-indazoles with the highly electrophilic triphenylphosphine-I₂ system,¹⁴ which is a commonly employed ring-closing strategy employed in the synthesis of oxazoles, for example.¹⁵ Given these reports, we considered that the Mitsunobu reaction might effect the same transformation, offering another mild synthesis of 1*H*-indazoles. Indeed, we recently utilized the Mitsunobu reaction to effect the heterocyclization of salicylhydroxamic acids into 3-hydroxybenzisoxazoles,¹⁶ as well as salicylaldoximes into salicylonitriles via *in situ*-generated 1,2-benzisoxazoles.¹⁷

The Mitsunobu reaction is a mild and essentially neutral alkylation, with clean inversion, of an acidic (pro)nucleophile, whose p*K*_a should be around 12 or lower, such as a carboxylic acid, phenol or sulfonamide with a primary or secondary alcohol.¹⁸⁻²⁰ A remarkably versatile reaction, it has been employed in the construction of C-O, C-N, C-S as well as C-C bonds.¹⁸⁻²⁰ Due to its mildness, the Mitsunobu reaction is compatible with a wide range of functional groups. The reaction typically involves an azodicarboxylate, such as diethyl azodicarboxylate (DEAD) or diisopropyl azodicarboxylate (DIAD), and a phosphine, usually triphenylphosphine. The phosphine reacts with DEAD/DIAD in a phospho-Michael reaction to generate a betaine intermediate, which is the key species that promotes the reaction between the (pro)nucleophile and the alcohol.

According to the pK_a rule, a primary aromatic amine is unable to engage in the Mitsunobu reaction because its pK_a is too high. Therefore, we elected to reduce the pK_a of the amino functionality by transforming it into a Boc-protected carbamate, which we have observed likewise activates an analogous 2-aminopyrimidine derivative to Mitsunobu chemistry.²¹ Briefly, Boc protection of 2'-aminoacetophenone (**4**) was achieved with Boc_2O in hot EtOH; crucially, base was excluded from the reaction mixture to prevent the undesired formation of the corresponding 4-methylene-3,1-benzoaxin-2-one.²² The requisite oxime functional group was next installed by treatment

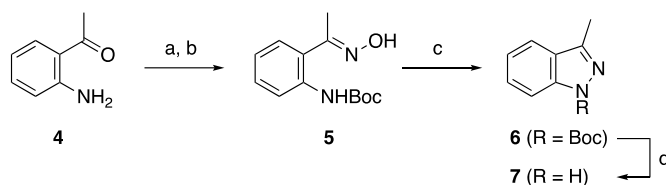
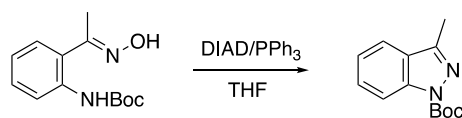


Figure 5.2. a) Boc_2O , EtOH, 50 °C, 48 h; (b) $NH_2OH.HCl$, pyridine; (c) DIAD, PPh_3 , THF, 60 °C, 4 h; (d) TFA/ CH_2Cl_2 , rt, 1 h.

with hydroxylamine.HCl in pyridine to deliver **5** almost exclusively as the (*E*)-isomer, wherein the hydroxyl and NHBoc are distal to each other; only a trace amount of the readily separable (*Z*)-isomer was observed, consistent with the literature.¹³ Pleasingly, treatment of **5** with 1.2 eq of PPh_3 and DIAD effected cyclization to the desired indazole



Entry	DIAD (eq.)	Time (h)	Temp. (°C)	Yield (%) ^a
1	1.2	16	25	65
2	2	16	25	77
3	2	16	40	78
4	2	16	50	88
5	2	16	60	95
6	2	4	60	95
7	2	2	60	78

Table 5.1. Optimization of the Mitsunobu-triggered cyclodehydration. ^aisolated yield after purification by flash column chromatography

6 in 65% isolated yield with the mass balance being unreacted starting material (Figure 5.2). After some experimentation (see Table 5.1), we arrived at optimal reaction conditions of 2 eq PPh₃ and 2 eq DIAD at 60 °C for 4 h.

Note that extending the reaction time from 4 h to 16 h had no benefit to the yield of the indazole (compare entries 5 and 6), likely owing to decomposition of the intermediate betaine. Activation of an oxime's hydroxy can result in its conversion to the corresponding amide or nitrile via the Beckmann rearrangement²³ or, in the case of oximes with α -protons, to the α -aminoketone via the Neber rearrangement.²⁴ However, the almost-quantitative yield of **6** (entry 6) suggests little or no such rearrangements

Entry	Oxime	1H-Indazole	Yield (%) ^b	Entry	Oxime	1H-Indazole	Yield (%) ^b
1			95	7			94
2			68	8			70
3			84	9			82
4			79	10			77
5			74 ^c	11			0
6			97				

Table 5.2. Substrate scope for Mitsunobu reaction with NHBoc oximes. ^aReagents and conditions: The oxime (1 eq) is dissolved in anhydrous THF (0.1 M), then PPh₃ (2 eq) and DIAD (2 eq) are added. The reaction is heated at 60 °C for 4 h; ^bisolated yield after purification by flash column chromatography; ^ccontaminated with DIAD-H₂, yield determined by NMR.

occurred. Therefore, these conditions were then applied to a range of *N*-Boc-activated *ortho*-aminobenzoximes, and the yields are presented in Table 5.2.

The Mitsunobu reaction was successful with the aldoxime in entry 2 (Table 5.2), generating the anticipated 3-unsubstituted 1*H*-indazole; the moderate yield was due largely to incomplete consumption of the starting material as no significant by-products were observed. In contrast, Stambuli's conditions led to the dehydration of their analogous aldoxime to the corresponding nitrile.¹³ A variety of ketoximes wherein the NHBoc and hydroxyl were distal to one another (entries 3 – 10) – all of which happened to be the (*E*)-isomers were then treated with DIAD and PPh₃; all cyclized in good to excellent yields to the corresponding 1*H*-indazoles. However, the (*Z*)-oxime in entry 11, isomeric to the successful reaction in entry 10, failed to deliver any 1*H*-indazole, indicating that the NHBoc and hydroxyl must be distal to each other for the reaction to proceed.

Deprotection of the Boc group of **6** proceeded smoothly and quantitatively with a 1:1 mixture of TFA/CH₂Cl₂, or 4 M HCl/dioxane in under 1 h at RT to furnish **7**. To our

Entry	R	Yield (%) ^a
1	—H	29 ^b
2	—H	11 ^c
3	—Me	82 ^b
4	—allyl	71
5	—isopropyl	0

Table 5.3. Substrate scope for Mitsunobu reaction with *NHR* oximes utilizing optimized reaction conditions. ^aIsolated yield; ^bcontaminated with DIAD-H₂, yield determined by ¹H NMR; ^cADDM substituted for DIAD.

surprise, unprotected 1*H*-indazole **7** could also be generated by conducting the Mitsunobu reaction on the non-Boc-protected/activated analogue of **5**, albeit in low yield (Table 5.3, entry 1), highlighting the significance of the activating group. We surmise this unexpected Mitsunobu reaction was promoted by the close proximity of the activated oxime hydroxyl. Replacement of DIAD with azodicarbonyl dimorpholide (ADDM), which can tolerate less acidic pronucleophiles and has the added benefit of excellent water solubility,^{19,25} did not improve the yield. The finding in entry 1 motivated us to apply the optimized reaction conditions to a range of secondary anilines (entry 2). Pleasingly, (unactivated) secondary anilines afforded high yields of the *N*¹-substituted 1*H*-indazoles, although the hindered *N*-isopropyl oxime (entry 5) did not react. The *N*-aryl oxime in entry 6 cyclized efficiently under the optimized conditions, which is especially noteworthy as alternative, newer 1*H*-indazole synthetic strategies either do not report on such oximes or report that the chemistry was unsuccessful.^{13,14} The tosylated substrate yielded a mixture of products.

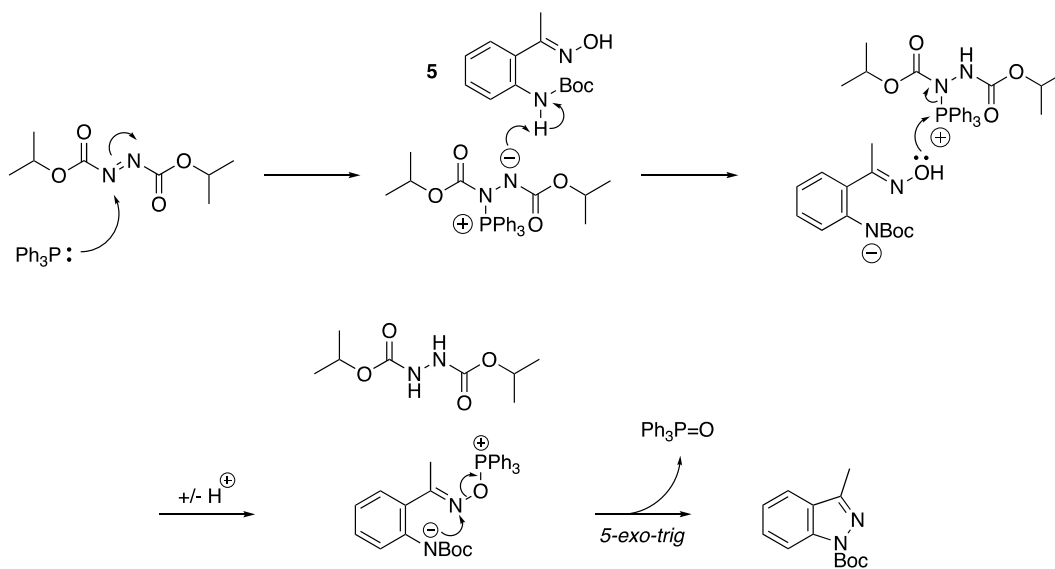


Figure 5.3. Proposed mechanism for construction of the 1*H*-indazole nucleus under Mitsunobu conditions.

The proposed mechanism for the Mitsunobu-triggered cyclodehydration is given in Figure 5.3. Upon the standard activation of the oxime's hydroxyl group, here playing the role of the alcohol, and deprotonation of the pronucleophile, intermediate 8 is generated. The aniline nitrogen then attacks the oxime nitrogen, displacing the activated alcohol in a *5-exo-trig* heterocyclization that is allowed by Baldwin's rules. This mechanism is also consistent with the observation that the (*Z*)-oxime (Table 5.2, entry 11) did not afford any of the corresponding *1H*-indazole because (a) the hydroxyl of the oxime is especially hindered, rendering its activation difficult and (b) the oxime nitrogen is sterically inaccessible and so the cyclization reaction is not possible under these conditions.

5.1. Conclusions

In summary, we have further expanded the utility of the Mitsunobu reaction to include the construction of *1H*-indazoles from *ortho*-aminobenzoximes. Primary amines required pre-activation with a Boc group to deliver the *N*¹-Boc protected *1H*-indazoles in good to excellent yields, whilst secondary amines furnished *N*¹-substituted *1H*-indazoles directly. The chemistry exhibits a strict geometric criterion – the amino group and hydroxyl must be distal to each other. We proposed a mechanism consistent with these observations wherein the cyclization step is a *5-exo-trig* reaction that is permitted by Baldwin's rules. This chemistry provides not only an alternative to several of the approaches to *1H*-indazoles that have emerged recently but distinct advantages as well. First, the ability to prepare 3-unsubstituted *1H*-indazoles from the precursor aldoxime opens the door to a variety of chemical transformations at the 3-position, including halogenation and acylation. Second, this methodology permits the synthesis of *1H*-indazoles substituted at

the N1 position with aryl groups. Since Mitsunobu chemistry is mild and occurs under essentially neutral conditions, it is predicted that this work will become a popular strategy in the synthesis of the 1*H*-indazole motif.

5.2. References

- (1) Zhang, S.-G.; Liang, C.-G.; Zhang, W.-H. *Molecules* **2018**, *23*, 2783.
- (2) Gaikwada, D. D.; Chapolikara, A. D.; Devkatea, C. G.; Warada, K. D.; Tayadea, A. P.; Pawarb, R. P.; Dombc, A. J. *Eur. J. Med. Chem.* **2015**, *90*, 707–731.
- (3) Wilmes, L. J.; Pallavicini, M. G.; Fleming, L. M.; Gibbs, J.; Wang, D.; Li, K. L.; Partridge, S. C.; Henry, R. G.; Shalinsky, D. R.; Hu-Lowe, D.; Park, J. W.; McShane, T. M.; Lu, Y.; Brasch, R. C.; Hylton, N. M. *Magn. Reson. Imaging* **2007**, *25*, 319–27.
- (4) Tash, J. S.; Attardi, B.; Hild, S. A.; Chakrasali, R.; Jakkaraj, S. R.; Georg, G. I. *Biol. Reprod.* **2008**, *78*, 1127–1138.
- (5) Eicher, T.; Hauptmann, S.; Speicher, A. *Structures, Reactions, Synthesis, and Applications*, 3rd, Completely Revised and Enlarged Edition; Wiley-VCH: Weinheim, 2013.
- (6) O'Dell, D. K.; Nicholas, K. M. *Heterocycles* **2004**, *63*, 373–382.
- (7) Cho, C. S.; Lim, D. W.; Heo, N. H.; Kim, T.-J.; Sim, S. C. *Chem. Commun.* **2004**, 104–105.
- (8) Wei, W.; Wang, Z.; Yang, X.K.; Yu, W.Q.; Chang, J.B. *Adv. Synth. Catal.* **2017**, *359*, 3378–3387.
- (9) Zhang, Z. G.; Huang, Y. Y.; Huang, G. Q.; Zhang, G. S.; Liu, Q. F. *J. Heterocyclic. Chem.* **2017**, *54*, 2426–2433
- (10) Lukin, K.; Hsu, M. C.; Fernando, D.; Leanna, M. R. *J. Org. Chem.* **2006**, *71*, 8166–8172
- (11) Wang, Q.; Li, X. W. *Org. Lett.* **2016**, *18*, 2102–2105.
- (12) Chen, G. H.; Hu, M. L.; Peng, Y. G. *J. Org. Chem.* **2018**, *83*, 1591–1597.
- (13) Counciller, C. M.; Eichman, C. C.; Wray, B. C.; Stambuli, J. P. *Org. Lett.* **2008**, *10*, 1021–1023.

- (14) Paul, S.; Panda, S.; Manna, D. *Tetrahedron Lett.* **2014**, *55*, 2480–2483.
- (15) Wipf, P.; Miller, C. P. *J. Org. Chem.* **1993**, *58*, 3604–3606.
- (16) Van Eker, D.; Chauhan, J.; Murphy, W. A.; Conlon, I. L.; Fletcher, S. *Tetrahedron Lett.* **2016**, *57*, 5301–5303.
- (17) Whiting, E.; Lanning, M. E.; Scheenstra, J. A.; Fletcher, S. *J. Org. Chem.* **2015**, *80*, 1229–1234.
- (18) Mitsunobu, O.; Yamada, M. *Bull. Chem. Soc. Jpn.* **1967**, *40*, 2380–2382.
- (19) Kumara Swamy, K. C.; Bhuvan Kumar, N. N.; Balaraman, E.; Pavan Kumar, K. V. P.; *Chem. Rev.* **2009**, *109*, 2551–2651.
- (20) Fletcher, S. *Org. Chem. Front.* **2015**, *2*, 739–752.
- (21) Fletcher, S.; Shahani, V. M.; Gunning, P. T. *Tetrahedron Lett.* **2009**, *50*, 4258–4261.
- (22) P.-E. Broutin, P. Hilty and A. W. Thomas, *Tetrahedron Lett.* **2003**, *44*, 6429–6432.
- (23) Luca, L. D.; Giacomelli, G.; Porcheddu, A. *J. Org. Chem.* **2002**, *67*, 6272–6274.
- (24) Taber, D. F.; Tian, W. *J. Am. Chem. Soc.* **2006**, *128*, 1058–1059.
- (25) Lanning, M. E.; Fletcher, S. *Tetrahedron Lett.* **2013**, *54*, 4624–4628.

5.3. Supplementary Information

Preparation of (*E*)-*N*-Boc-*ortho*-aminobenzoxime: 2-aminoacetophenone (**4**; 1 g, 7.40 mmol, 1 eq) was heated at 50°C with Boc₂O (1.78 g, 8.14 mmol, 1.1eq) in ethanol (12 mL) for 48 h. TLC confirmed the reaction was complete. The reaction mixture was concentrated to dryness, reconstituted in CH₂Cl₂, adsorbed to silica gel, then purified by flash column chromatography (eluent: Hex/EtOAc, 2:1) to deliver *tert*-butyl (2-acetylphenyl)carbamate (1.5 g, 88%): δ_H (400 MHz, CDCl₃) 10.95 (s, 1H, NH), 8.47 (d, 1H, Ar, *J* = 8.8 Hz), 7.86 (d, 1H, Ar, *J* = 7.6 Hz), 7.52 (t, 1H, Ar, *J* =

7.6 Hz), 7.26 (s, 1H, Ar), 7.03 (t, 1H, Ar, $J = 8.0$ Hz), 2.65 (s, 3H, COCH₃), 1.52 (s, 9H, C(CH₃)₃); δ_C (100 MHz, CDCl₃) 202.2, 153.1, 141.8, 134.9, 131.6, 121.4, 120.9, 119.1, 80.5, 28.5, 28.3.

tert-Butyl (2-acetylphenyl)carbamate (400 mg, 1.70 mmol, 1 eq) were refluxed with NH₂OH.HCl (472 mg, 6.80 mmol, 4 eq) and pyridine (1.51 mL, 18.7 mmol, 11 eq) in methanol (6 mL) overnight. The reaction was then cooled to room temperature, and partitioned between 1M HCl and EtOAc. The organic layer was collected, and the aqueous was extracted once more with further EtOAc. The combined organic layers were washed with H₂O, brine, dried over Na₂SO₄, filtered and concentrated. The crude residue was adsorbed onto silica gel from CH₂Cl₂, then purified by flash column chromatography, eluting with Hex/EtOAc, 2:1 to furnish *tert-butyl (E)-(2-(1-(hydroxyimino)ethyl)phenyl)carbamate* **5** (91%): δ_H (400 MHz, DMSO-*d*₆) 8.05 (d, 1H, Ar, $J = 8.8$ Hz), 7.50 (d, 1H, Ar, $J = 8$ Hz), 7.32 (t, 1H, Ar, $J = 8.4$ Hz), 7.09 (t, 1H, Ar, $J = 7.6$ Hz), 2.21 (s, 3H, CH₃), 1.47 (s, 9H, C(CH₃)₃); δ_C (100 MHz, CDCl₃) 183.3, 157.9, 153.2, 137.2, 129.7, 128.4, 121.9, 119.8, 80.2, 28.4, 13.4.

Typical Mitsunobu procedure: To a solution of *tert*-butyl (*E*)-(2-(1-(hydroxyimino)ethyl)phenyl)carbamate (125 mg, 0.5 mmol, 1 eq) in anhydrous THF (5 mL) were added PPh₃ (262 mg, 1 mmol, 2 eq) and DIAD (197 μ L, 1 mmol, 2 eq). The reaction was heated at 60 °C for 4 h. The solvent was removed *in vacuo*, the crude residue was adsorbed to silica gel from CH₂Cl₂, and then purified by flash column chromatography (eluent: Hex/EtOAc, 3:1) to afford *tert-butyl 3-methyl-1H-indazole-1-carboxylate* **6** (110 mg, 95%): δ_H (400 MHz, CDCl₃) 8.07 (d, 1H, Ar, $J = 7.6$ Hz), 7.60 (d, 1H, Ar, $J = 8$ Hz), 7.47 (t, 1H, Ar, $J = 7.6$ Hz), 7.26 (t, 1H, Ar, $J = 8$

Hz), 2.56 (s, 3H, CH₃), 1.69 (s, 9H, C(CH₃)₃); 149.3, δ_{H} (100 MHz, CDCl₃) 149.3, 148.5, 140.1, 128.8, 125.9, 123.2, 120.3, 114.6, 84.5, 28.2, 12.3.

5.4. Acknowledgement

I would like to thank Katie Konsein for the massive help with the organic chemistry of this project.

Reproduced with permission from I.L. Conlon, K. Konsein, Y. Morel, A. Chan, and S. Fletcher., *Tetrahedron Letters* 2019, 60 (37), 150929. Copyright © 2019 Elsevier Ltd.

Published by Elsevier Ltd. All rights Reserved.

Chapter 6. Ongoing and future small molecule inhibitors targeting the Bcl-2 Anti-apoptotic Proteins

6.1. Introduction

Challenges remain finding efficacious strategies of targeting the undruggable proteome. These are proteins that are considered difficult to target due to factors such as not having well-defined binding pockets, including non-enzymatic proteins or transcription factors, or their intracellular nature, making antibody development near impossible¹.

Traditionally these proteins are targeted with small molecules which have led to dosing and long drug exposure issues, which may cause a mutation of the target protein causing resistance or compensatory upregulation of other proteins¹. Lastly, developing nucleic acid-based drugs are also challenging due to their instability in serum, potential immunogenicity, or eliciting off-target effects². However, novel strategies including targeted protein degradation and covalent inhibition have recently emerged to overcome the limitations of these traditional therapies.

6.2. Targeted Protein Degradation

Protein degradation hijacks the cells machinery to degrade proteins, specifically the ubiquitin proteasome system (UPS). The UPS is the main pathway of degrading intracellular proteins due to misfolding, damage, aggregation, or excess protein in the cell³. It is a tightly-controlled post-translational mechanism that utilizes a group of enzymes and ubiquitin, a small 76 amino acid protein, to carry out its function^{4,5}. First, ubiquitin is activated through an ATP-dependent reaction of a thioester bond between the ubiquitin-activating enzyme E1 and the carboxyl terminus of ubiquitin. Next, ubiquitin is transferred from the active site cysteine of the E1 enzyme to the ubiquitin conjugating

enzyme E2. Finally, an E3 ubiquitin ligase enzyme catalyzes the transfer of ubiquitin from the E2 enzyme to a lysine residue on the target protein through covalent bond formation. This cycle is repeated until a poly-ubiquitin chain has been generated, which functions as a signal that is recognized by the 26S proteasome for degradation⁵⁻⁷ (Figure 6.1).

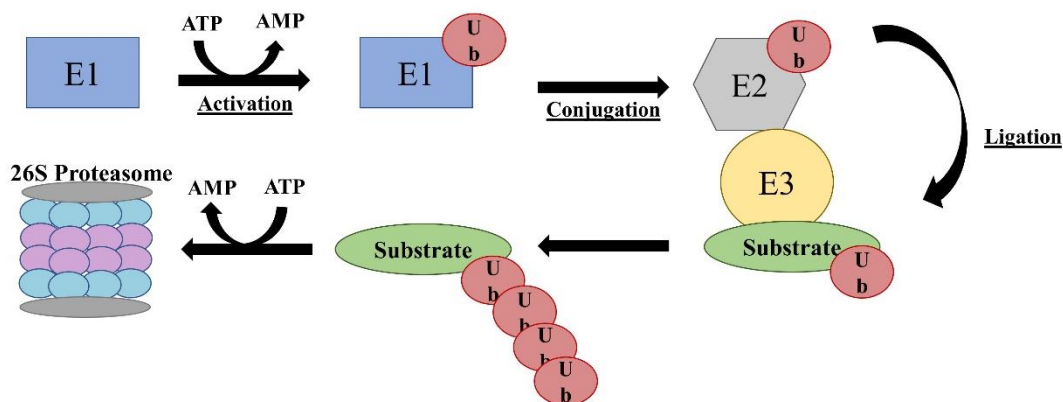


Figure 6.1. The ubiquitin proteasome system (*Ub* = ubiquitin).

Proteolysis targeting chimeras (PROTACs) are an emerging field of targeted protein degradation. They are hetero-bifunctional molecules comprised of three key features: 1) a distinct binding moiety specific to the E3 ligase, 2) a chemical linker, and 3) a ligand that binds to the protein of interest (POI) (Figure 6.2)^{5,8}. The chemical composition of PROTACs drive their catalytic mode of action and serve as a bridge to bring the E3 ligase and POI in close proximity to ultimately trigger protein degradation⁵. A ternary complex is formed when one side of the degrader binds to the E3 ligase and another ligand binds to the POI, while a linker joins the two ligands together (Figure 6.2). Once the complex is formed, the E3 ligase recruits the E2 ubiquitin-conjugating enzyme to transfer ubiquitin to the target protein. Various cycles produce a poly-ubiquitin chain

that serves as a signal for recognition by the 26S proteasome for degradation. Once degradation occurs, the PROTAC can continue its cycle of recruitment¹ (Figure 6.2).

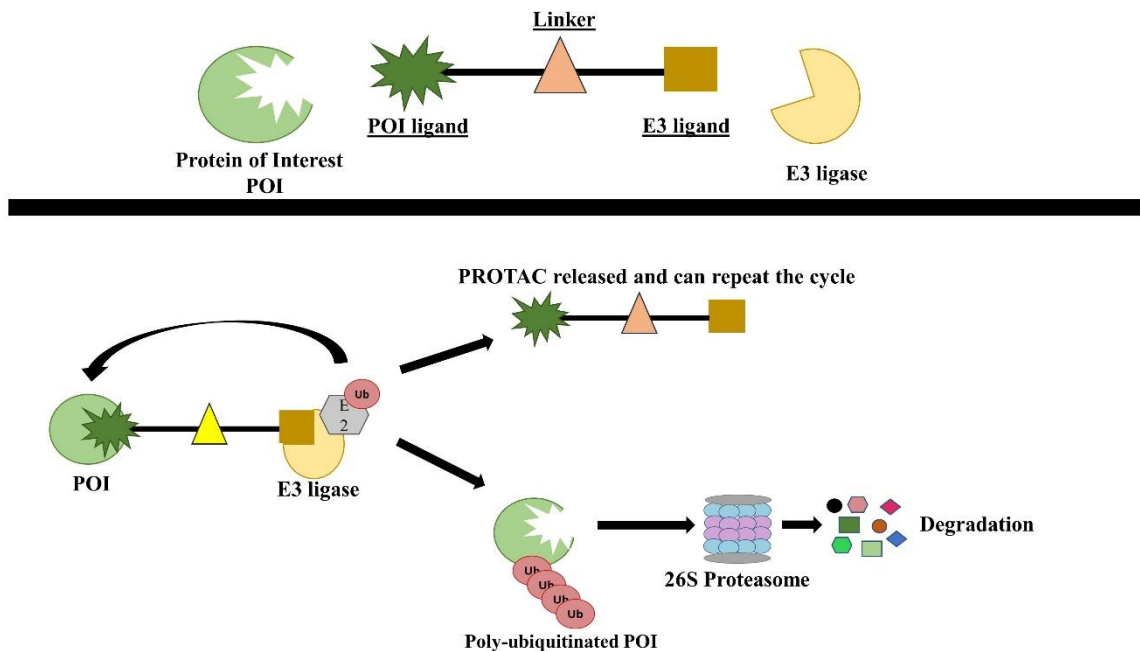


Figure 6.2. PROTAC design (top) and the mechanism of the PROTAC technology (bottom).

Interestingly, this mode-of-action serves under an “event-driven” model, which is in stark contrast to the traditional occupancy-driven model, which maintains that high drug concentrations are needed to maintain a constant level of target occupancy for a clinical effect⁵. However, this can lead to issues such as off-target effects or resistance. Conversely, the “event-driven” model states that the activity of these degraders is not based on stoichiometric occupancy of the target protein, and may only require a transient moment for binding to achieve activity^{1,2}. For example, studies have shown that reduced protein levels of more than 90% can be achieved at nanomolar concentrations of the PROTAC⁵.

The first PROTAC compound was described in 2001 by Sakamoto *et al.* They focused on the E3 ligase SCF^{β-TRCP}, a Cullin protein family member, that promotes the ubiquitination of IκBα in response to inflammatory signals⁹. The degradation of this protein leads to the activation of NFκB. In this proof-of-concept paper, they wanted to recruit an unrelated protein, in this case methionine aminopeptidase-2 (MetAP-2), to SCF^{β-TRCP} for protein degradation. They chose MetAP-2 as it is a target of potent angiogenesis inhibitors and it is not known to be ubiquitinated by the SCF complex. They utilized the IκBα peptide (IPP) to bind the E3 ligase connected to ovalicin by a chemical

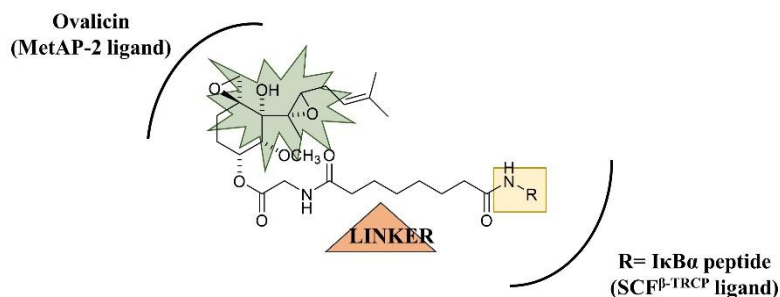


Figure 6.3. The first PROTAC developed by Sakamoto *et al.*⁹

linker, which is a potent MetAP-2 inhibitor. Studies revealed that Compound 1 (Figure 6.3) did recruit MetAP-2 to SCF^{β-TRCP}, resulting in its ubiquitination and subsequent degradation, while MetAP-2 was not ubiquitinated by SCF^{β-TRCP} in the absence of the PROTAC⁹. Since its discovery, numerous research groups have further characterized PROTAC molecules and revealed its broad application with a number of different E3 ligases including mouse double minute 2 (MDM2), von Hippel-Lindau (VHL), and cereblon (CRBN) as well as numerous target proteins^{5,6}.

PROTAC technology has led to the creation of the pharmaceutical company Arvinas, which currently has two compounds in phase I clinical trials. The first, ARV-110, is an orally bioavailable drug that targets the androgen receptor (AR) in metastatic

castration-resistant prostate cancer, while ARV-471 functions as an estrogen receptor (ER) degrader in patients with ER(+)/HER2(-) metastatic breast cancer^{10,11}. Recently, Arvinas has released results of their Phase 1/2 study with ARV-110 showing favorable safety and tolerability in patients as well as evidence of in-tumor AR reduction¹². This is the first clinical study demonstrating the use of PROTAC technology in humans¹³.

6.3. Advantages and Disadvantages of PROTAC design

Since its discovery almost twenty years ago, PROTACs have become a rapidly emerging field in drug development. There are numerous advantages and disadvantages that have been described and will be further explained. PROTACs are unique in that they utilize the cells own degradation machinery. As such, they are catalytic in nature and present an advantageous way to destroy unwanted proteins, such as those that are overexpressed in cancer, including BRD4, Mcl-1, and various kinases as well as demonstrating sensitivity to drug-resistant targets^{2,12,14-18}. In fact, studies show that PROTACs can target cancer cells that previously showed resistance to the parent compound. This is attributed to the fact that degraders they have the potential to completely eliminate the target and thus its function entirely¹⁴. For example, cancer cells resistant to the kinase inhibitor ibrutinib respond to an ibrutinib-based PROTAC compound, suggesting these may be used as alternative therapies⁷.

In addition, as seen within the Bcl-2 family, when certain protein family members are antagonized, it results in compensatory upregulation of other proteins. However, because the PROTAC mechanism of action involves a transient binding event, it may eliminate this issue through stabilizing the protein's half-life or depleting the protein reserve within the cell while the small molecule can return for another cycle of

degradation^{1,8,19}. Depending on the time it takes to resynthesize the target protein, it could potentially eliminate the existing levels of protein. This can result in a number of different pharmacokinetic and pharmacodynamic differences. For example, they may have a longer duration of action that extends beyond the clearance time of the drug and only substoichiometric doses are needed to achieve therapeutic effect^{7,8,14,19}.

However, the chemical composition of these degraders has revealed critical issues related to compound development. These are large molecules, with molecular weights ranging between 700 and 1000 Daltons, making them difficult for oral delivery due to poor cell permeability. Oral delivery is the most desirable method for small molecules due to patient compliance and frequent dosing, allowing for a continuous maintenance of drug exposure in the body. However, studies show that once PROTACs reach circulation, they exhibit small molecule behaviors including good tissue distribution and low hepatic clearance¹⁹. Importantly, dosing issues must be addressed early, as higher doses of PROTAC molecules can inhibit the PROTAC-protein complexes to the target protein partner, effectively stopping catalytic degradation, which is known as the hook effect.

There is also a possibility of resistance due to genomic alterations involving the E3 ligase complex or the protein of interest⁷. First and foremost, not only must both proteins be present in the affected tissues, but the target must be responsive to PROTAC degradation. For example, targeting certain proteins for degradation may lead to large increases of the protein in the event of quick turn-around of protein biosynthesis¹⁹. Importantly, both proteins must also have high affinity ligands and selection of the E3 ligase and target protein ligands is crucial., but many potent inhibitors have already been developed for a number of different targets and E3 ligases, which can aid in compound

development^{7,8}. In addition, the linker length, flexibility, and chemical composition must be considered because one single linker is not universal among PROTAC compounds. In fact, the hydrophobicity and length of different linkers can affect the efficacy of the inhibitors for different targets^{6,14,20,21}. The disadvantages highlighted here reveal there is still much to learn in the field of targeted protein degradation including how to rationally design a PROTAC molecule.

6.4. Venetoclax-based PROTACs

The Bcl-2 anti-apoptotic protein is overexpressed in numerous hematological malignancies including acute myeloid leukemia (AML) and chronic lymphocytic leukemia (CLL). Bcl-2 is governed by α -helix mediated protein-protein interactions (PPIs) that are comprised of large, shallow hydrophobic contact points. However, years of research culminated in the approval of venetoclax, a Bcl-2 selective inhibitor (Figure 6.4, left). It was initially approved for CLL and it has since expanded to patients with small lymphocytic lymphoma (SLL). Recently, the approval was further extended to

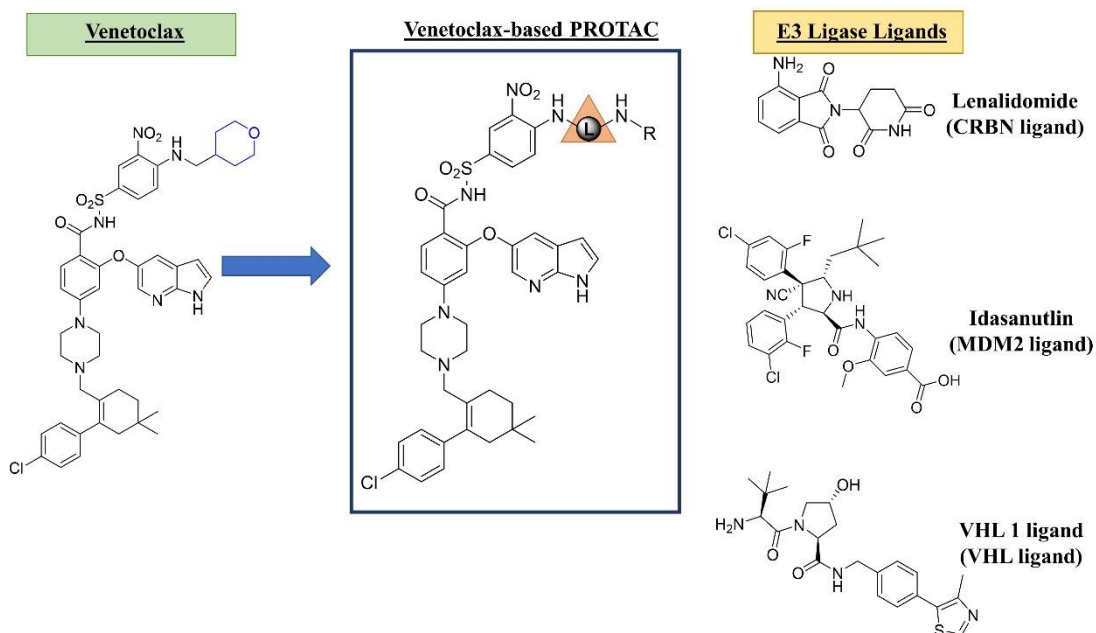


Figure 6.4. Our venetoclax based PROTAC design. “L” represents linker.

combination therapies with hypomethylating agents or low-dose cytarabine for adults with newly-diagnosed AML²². AML is an aggressive blood cancer that requires quick, intense chemotherapy; however, older adults may be unable to tolerate it. In fact, a recent press release revealed that venetoclax in combination with the hypomethylating agent azacitidine showed a statistically significant improvement in survival with patients with previously untreated AML who were not able to receive intense chemotherapy²³. These promising results and subsequent approval of venetoclax for AML is a promising targeted therapy for these patients²⁴.

Recent reports reveal that patients acquire resistance to venetoclax in CLL. Although the overall response rate with venetoclax monotherapy is 79%, relapses are seen in many patients and as many as 50 percent become refractory after continuous treatment, which has been attributed to resistance. Importantly, studies have reported a range of Bcl-2 mutations, such as Gly101Val and Asp103Tyr²⁵⁻²⁷. In fact, a genomic evaluation study of patients with relapsed CLL revealed the Gly101Val mutation had occurred and was not present at the beginning of treatment. This is a detrimental mutation as it binds venetoclax 180 times less than wt Bcl-2. Of note, they did not find this mutation in the general population or in patients with other B-cell malignancies who did not receive venetoclax treatment²⁶. Venetoclax has proven its importance in treating a range of detrimental hematological diseases, therefore it is imperative to find a way to manage these acquired resistances.

6.4.1. Venetoclax PROTAC approach

There is a therapeutic need to develop an inhibitor that binds both the wild type and mutant forms of Bcl-2. As previously explained, PROTACs have a catalytic mechanism

of action and only sub-stoichiometric amounts of compound are needed to achieve protein degradation. Therefore, low target occupancy may be achieved with low affinity ligands. In addition, PROTACs do not rely on inhibiting the function of the protein, rather they only need to bind it long enough to allow for ubiquitination. Therefore, theoretically a lower affinity ligand may be adequate to neutralize targets related to these proteins²⁸. Accordingly, we have developed venetoclax-based PROTACs and anticipate they will bind both the wild type and mutant Bcl-2 proteins.

6.4.2. Design

Currently, rationally designing PROTAC compounds is a challenge, therefore our design takes flexibility, hydrophobicity, and differing E3 ligases into account. In order to retain binding affinity towards wt Bcl-2, we will keep the core of the venetoclax compound and replace the tetrahydropyran motif. This functional group has revealed to be solvent exposed in the crystal structure, suggesting replacement may offer minimal detriment to Bcl-2 binding affinity. This group will be replaced with linkers of varying lengths and hydrophobicities and we will install both short and long alkyl chains and PEG linkers. In addition, we will target the most common E3 ligases in PROTAC development: CRBN, MDM2, and VHL. These will be targeted with corresponding ligands thalidomide, idasanutlin, and VHL ligand 1 (Figure 6.4). These PROTACs will be evaluated in a fluorescence polarization competition assay as described in Chapters 2, 3, and 4, as well as cell-based toxicity assays. To test viability of cells resistant to venetoclax, we will test AML cell lines such as venetoclax-sensitive MV4;11 and MOLM13, as well as venetoclax-resistant OCI-AML2 and OCI-AML3.

6.5 Targeting the Bcl-2 family anti-apoptotic protein Bfl-1 through covalent inhibition

6.6. Current strategies to target Bfl-1

Bfl-1 is a poorly understood anti-apoptotic protein within the Bcl-2 family of proteins, however, due to its implication in the development of numerous cancers as well as chemoresistance, it remains an important target in the field of drug discovery (See Chapter 1.10). Many research groups have developed small molecule inhibitors and stapled peptides designed to target the BH3-binding groove of Bfl-1. Mathieu *et al.* described two compounds that target the BH3-binding groove of Bfl-1 with low micromolar binding affinities, while displacing pro-apoptotic proteins to induce apoptosis (Figure 6.5).

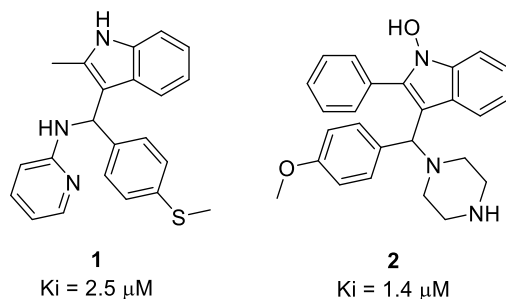


Figure 6.5. Mathieu *et al.* Bfl-1 inhibitors with corresponding binding affinities.

They also describe *in cell* results revealing these compounds can alleviate resistance in malignant B cells to the pan Bcl-2 family inhibitor ABT-737, showcasing its ability to synergize with a previously developed BH3 mimetic²⁹. Additionally, RNA interference strategies have demonstrated that Bfl-1 inhibition can sensitize different lymphoma cell lines to the chemotherapy drugs cisplatin and fludarabine, validating the efficacy of targeting Bfl-1³⁰.

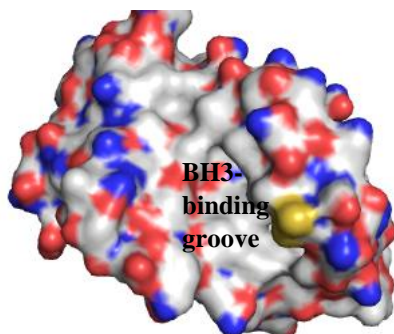


Figure 6.6. Solvent accessible Cys highlighted in Bfl-1. PDB 3MPQ

Recently, there has been a resurgence in the development of covalent inhibitors, which utilize an electrophilic warhead such as acrylamide or boronic acid to target a cysteine, serine, or threonine in the protein-of-interest (POI)³¹. A recent crystal structure of Bfl-1 revealed it has a surface-accessible cysteine in the BH3-binding groove that can be targeted with covalent inhibition (highlighted yellow, Figure 6.6)³².

Cysteine is one of the least abundant amino acids, yet the ionizable thiol group has properties that can impart specialized or increased reactivity related to protein structure and function. These include the formation of disulfide bonds, alkylation by electrophiles, and oxidation by reactive oxygen and nitrogen species³³. Previously, the development of cysteine reactive drugs was difficult and avoided, due to a number of different liabilities: the potential toxicity of the protein adducts, immunogenicity causing an allergic response or hypersensitivity to the drug owing to the protein adduct, or reactive species that may be targeted by endogenous nucleophiles such as glutathione leading to off-target effects^{34,35}.

However, the FDA approval of small molecule covalent inhibitors, such as kinase inhibitors ibrutinib and afatinib (Figure 6.7), demonstrates that covalent inhibition without severe liabilities is possible³⁶. A cysteine-reactive small molecule inhibitor must be selective and potent to limit liabilities and produce on-target effects. However, no

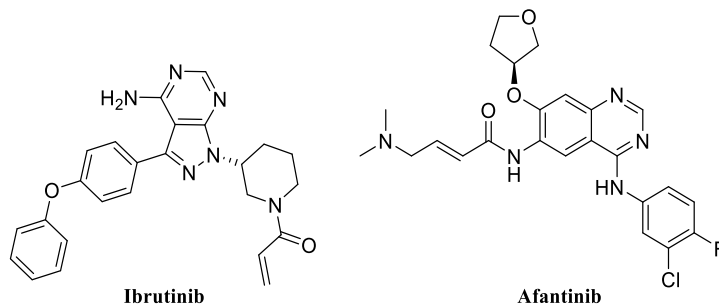


Figure 6.7. FDA approved covalent kinase inhibitors.

other anti-apoptotic protein contains a cysteine in the BH3-binding domain, so incorporation of cysteine-reactive electrophilic warheads may lead to increased selectivity of Bfl-1 inhibitors^{32,36}.

6.7. Stapled α -helix Covalent Inhibitors of Bfl-1

Walensky *et al.* have developed irreversible covalent stapled peptides that selectively target Bfl-1^{32,36}. A crystal structure of Noxa and Bfl-1 revealed a unique positioning of cysteines at the binding interface of Bfl-1 (C55) and Noxa (C25), which they reasoned was compatible with disulfide bond formation (highlighted yellow, Figure 6.8). They

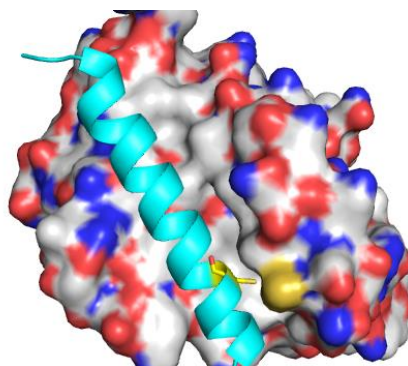


Figure 6.8. Noxa (cyan) C25 (yellow stick) and Bfl-1 C55 highlighted. PDB 3MPQ

developed a stapled α -helix that would retain the noncovalent interactions of the hydrophobic BH3-binding domain with an electrophilic warhead capable of interacting with Bfl-1 C55. To test whether this was experimentally viable, they developed serine mutants of the cysteines in Noxa (C25S) and Bfl-1 (C4S, C19S, and C55S) and incubated

them under oxidizing conditions, which would reveal if a disulfide bond was present. They showed that a disulfide bond was feasible between the Noxa and Bfl-1 C55 by showing that when the wildtype Bfl-1 was incubated with wildtype Noxa, a shift in molecular weight consistent with protein binding was present and was later confirmed by FITC scan. Additionally, when FITC-Noxa peptides were incubated with other anti-apoptotic proteins with cysteines (Mcl-1 and Bcl-xL), they found no molecular weight shift⁸. This revealed that the protein adducts formed may include the disulfide bond between Noxa C25 and Bfl-1 C55³².

Next, they developed peptides with various electrophilic warheads (Figure 6.9)

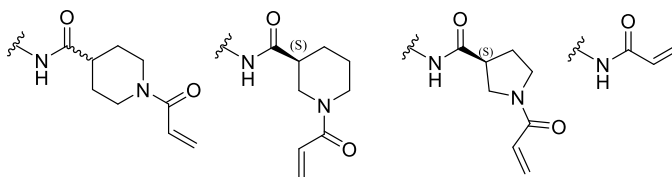


Figure 6.9. Representative acrylamide moieties used in Walensky *et al.* experiments.

because an intracellular disulfide bond cannot be relied on for protein inhibition. In addition, they saw optimal interactions of Bim with an adjacent Trp17 to Cys55 of Bfl-1, so they developed both Bim and Noxa stapled peptides capped with non-natural acrylamide moieties. They found D-nipecotic acid was the most effective (Figure 6.9, left) and incubated these peptides with wildtype Bfl-1 as well as the serine mutant (C4S/C19S and C55), which revealed exclusive reactivity with C55 only. Mass spectrometry experiments also revealed conversion to the appropriate adduct with D-nipecotic acid-Noxa peptide and Bfl-1 mutant (C4S/C19S and C55)³². This represents that the peptides are capable of selectivity targeting the cysteine in the BH3 domain. A crystal structure between D-nipecotic acid-Noxa peptide and wildtype Bfl-1 reveals that

it binds within the BH3 domain and shows the nipecotic acid covalently bonded to C55 (Figure 6.10)³². Additionally, they saw no nonspecific reactivity upon incubation with

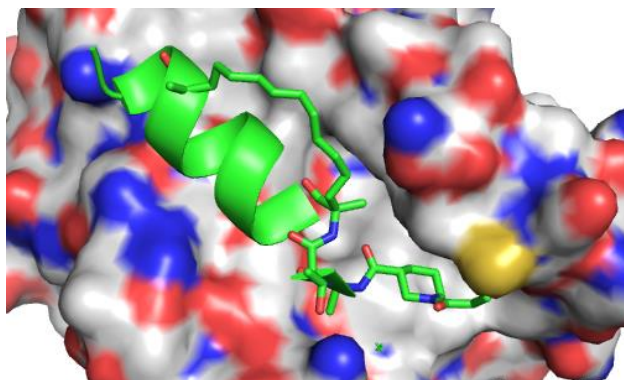


Figure 6.10. *D-nipecotic-acid-Noxa peptide-Bfl-1 complex. Sticks showcase the nipecotic acid moiety in contact with Bfl-1 C55 (yellow). PDB 5HWW.*

Mcl-1 and Bcl-xL. Experiments revealed that these peptides irreversibly decreased anti-apoptotic function and increased apoptosis in Bfl-1 dependent melanoma cells. In addition, they found the stapled Bim peptide was more potent compared to Noxa, and induced cytochrome *c* release and caspase 3/7 activation, indicating it was acting in an apoptosis-dependent manner³⁶.

These stapled peptides capable of reacting with C55 of Bfl-1 in the BH3-binding domain reveals that a covalent, selective Bfl-1 inhibitor can be developed. Therefore, we have designed two tris-aryl α -helix mimetic inhibitors with different electrophilic warheads to probe the Bfl-1 BH3 domain while interacting with the surface-accessible C55 within the binding interface.

6.8. Design

Targeting protein-protein interactions is difficult due to the hydrophobic, shallow binding region of the binding interfaces³⁷. However, experimental tools have identified residues within the protein complex that cause an increase in binding free energy when mutated, revealing key interactions³⁸. These residues occur at the *i*, *i*+3/4, and *i*+7 position of the

α -helix. Specifically, these residues in the Bim-BH3 binding domain include Leu62 (i), Ile65 ($i+3$), and Phe69 ($i+7$). In addition, a conserved arginine residue on pro-life proteins forms a salt bridge with Asp67 on the Bim α -helix at the $i+5$ position that has

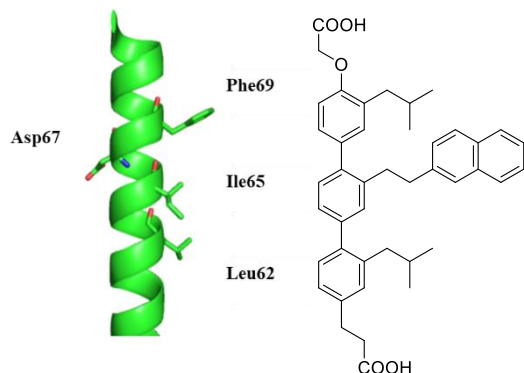


Figure 6.11. Bim-BH3 with highlighted residues (left). Hamilton *et al.* representative terphenyl scaffold α -helix mimetic (right).

proven to be important in binding affinity^{37,39-41} (Figure 6.11). As previously shown with Walensky's stapled α -helical peptides, mimicry of these residues can lead to a potent, selective inhibitor. In addition to Walensky's peptidomimetics, tris-aryl scaffolds have been extensively used as α -helix mimetics, which are small molecules that mimic the residues of α -helix⁴²⁻⁴⁴. Tris-aryl scaffolds are used because they project functional groups in a similar spatial orientation to the native α -helix. Hamilton *et al.* pioneered the field of α -helix mimetics with terphenyl scaffolds functioning as Bcl-xL inhibitors (Figure 6.11)^{42,43}.

We have developed two tris-aryl scaffolds that function as α -helix mimetics based on two non-peptidic scaffolds: JY-1-106, an oligoamide-foldamer-based Bcl-xL and Mcl-1 inhibitor, as well as a triazene based scaffold, based on a previously described bridged small molecule α -helix mimetic^{45,46} (Figure 6.12). We will also incorporate

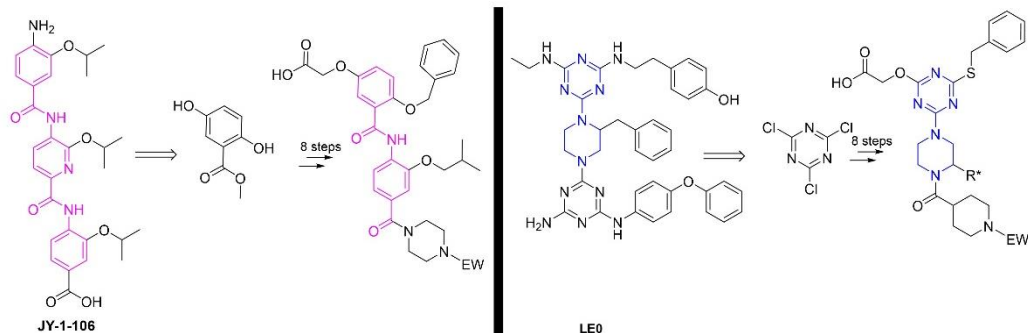


Figure 6.12. Our general workflow of design. EW denotes electrophilic warhead.

electrophilic warheads in these scaffolds to probe Cys55 of Bfl-1 in the BH3-binding domain. These will be discussed below. Given the success of these scaffolds as helix mimetics and the success of Walensky's covalent inhibitors, we hypothesize that our scaffolds will act as potent, selective Bfl-1 covalent inhibitors.

6.8.1. JY-1-106

Hamilton's lab initially developed terphenyls as α -helix mimetics^{42,47,48}. Further, they introduced an oligoamide-foldamer scaffold comprised of bifurcated hydrogen bonds used to maintain the integrity of the helical structure⁴⁹ (Figure 6.13, **1**). Although a crystal structure showed that the rigidity of the backbone was due to the bifurcated hydrogen bonds of the pyridine nitrogens, it was unclear whether they would be present

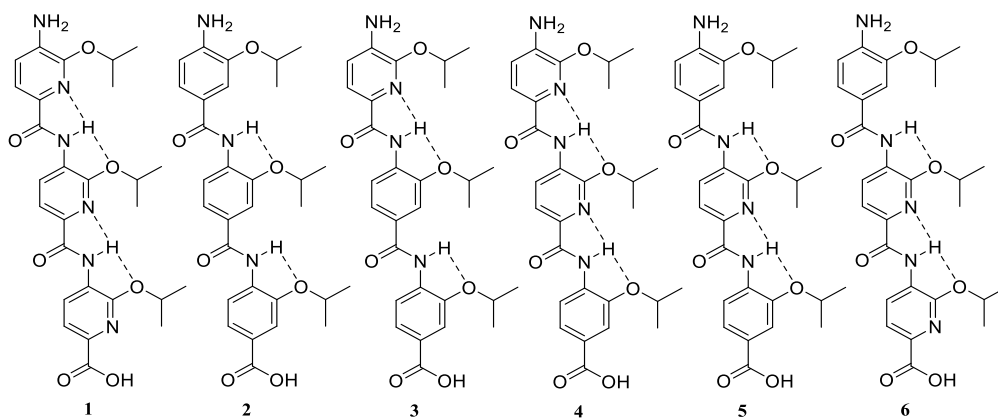


Figure 6.13. Oligoamide-foldamer compounds with bifurcated hydrogen bonds.

under physiological conditions⁴⁶. Therefore, Yap *et al.* used molecular dynamics (MD) simulations with the CHARMM General Force Field on Hamilton's oligoamide-foldamers (**1** and **2**, Figure 6.13). Experimentally, the NH---N hydrogen bonds in **1** were more stable than the NH---O interactions. Additionally, experiments were performed to evaluate the propensity of the isopropyl ether groups and the geometry of the ether oxygens, which revealed both the rigid picolinamide and flexible benzamide are both good mimetics of the Bak-BH3 peptide⁴⁶.

To further explore the preferred intramolecular bifurcated hydrogen bonding, which is directly related to the flexibilities of the scaffold, they synthesized compounds **3,4,5** and **6**. As seen in Figure 6.13, they replaced pyridine subunits in a stepwise manner to further probe the flexibility of the scaffolds *in vitro*. A fluorescence polarization competition assay with Bcl-xL and FITC-Bak revealed that replacement of the pyridine subunits with benzene led to increased inhibition of Bcl-xL. They suggest that the increased flexibility coupled with the increased hydrophobicity of Hamilton's compound **2** allowed for more favorable interactions with Bcl-xL⁴⁶. Nonetheless, these studies resulted in the Bcl-xL and Mcl-1 inhibitor JY-1-106 (**5**).

Our oligoamide-foldamer scaffold derives from both Hamilton and JY-1-106, such that the first two subunits offer bifurcated hydrogen bonds between the two oxygens and the amide hydrogen (Figure 6.12, pink compound). In addition, we have chosen benzene subunits in place of pyridine to decrease rigidity of the backbone for more favorable interactions with Bfl-1. We also will introduce isonipecotic acid or piperidine as the last subunit of the scaffold, as the flexibility they offer may allow for potential increased interactions with Cys55 of Bfl-1. Representative compound **OA1** was manually

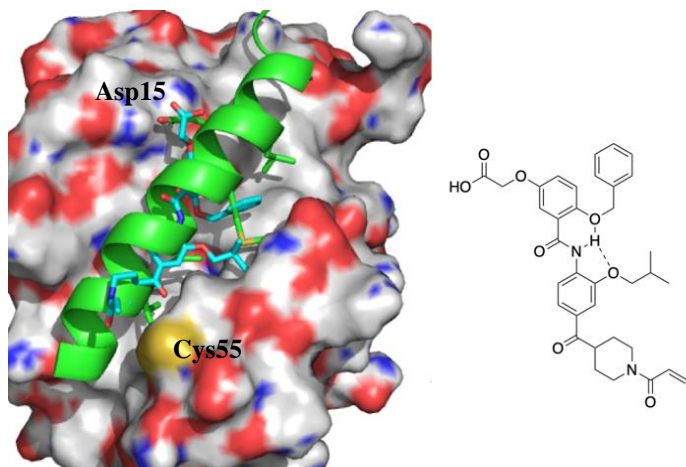


Figure 6.14. Representative compound *OAI* manually docked in *Puma-Bfl-1*. PDB: 5UUL.

docked in Bfl-1 shown in Figure 6.14, which reveals good mimicry of the pro-apoptotic Puma-BH3 peptide, while the carboxylic acid offers good mimicry of Asp15. The acrylamide moiety, acting as the electrophilic warhead, is also near Cys55 of Bfl-1, indicating the placement may allow for effective covalent inhibition.

The synthesis for our oligoamide-foldamer scaffold is described as follows in Figure 6.15:

First, methyl 2,5-dihydroxybenzoate (**1**) was reacted with *t*-butyl bromoacetate and selectively alkylated the 5-hydroxy group to give (**2**). Alkylation of the 2-phenoxy group with benzyl bromide gives (**3**). **3** will undergo saponification with LiOH H₂O to reveal

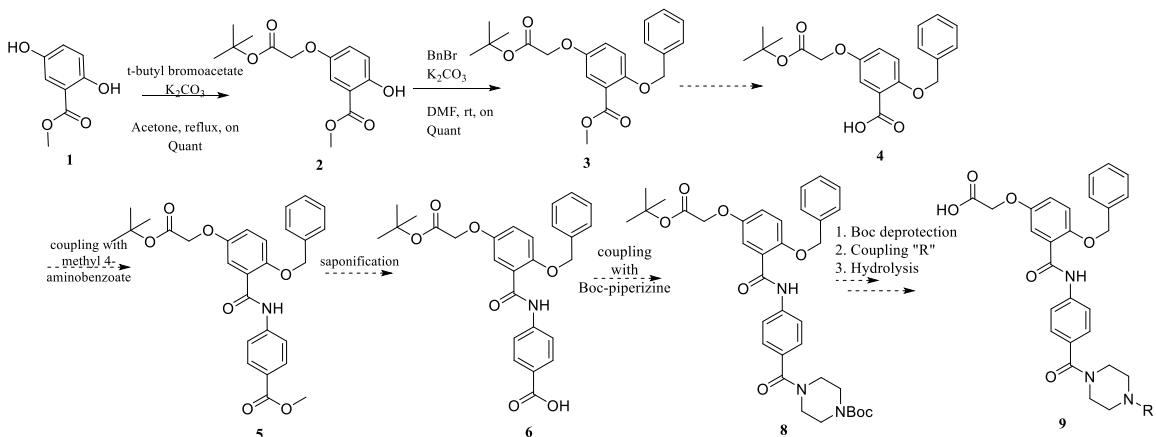


Figure 6.15 Oligoamide-foldamer based α -helix mimetic synthesis.

the carboxylic acid (**4**) and will be coupled with methyl 4-aminobenzoate to give the two functionalized oligoamide-foldamer subunits (**5**). Next, **5** will be saponified to reveal the carboxylic acid **6**, which will be coupled with Boc-piperazine (**7**). The Boc group will be deprotected with 4M HCl, coupled with various electrophilic warheads, and hydrolyzed to reveal the final deprotected oligoamide-foldamer covalent inhibitor (**8**).

6.8.2. Triazene based scaffold

Previously developed tris-aryl compounds had poor water solubility and difficult syntheses; therefore, Lim *et al.* described the development of a triazine-piperazine-triazene scaffold as Mcl-1 inhibitors⁴⁵ (Figure 6.12, blue scaffold). The triazine is a privileged scaffold that was used due to the ease of functionalization, while the piperazine was previously used as an isostere of terphenyl structures. In addition, the calculated cLogP value of this scaffold was superior to the previous α -helix based tris-aryl compounds, showcasing the potential increase in physicochemical properties needed to improve aqueous solubility (1.36 vs 6.21, respectively). This indicates that this scaffold may possess more “drug-like” properties in comparison to previous terphenyl scaffolds. Computational studies also revealed that the functional groups effectively mimicked the i , $i+3/4$, $i+7$ residues of an α -helix. Through development of a combinatorial library, coupled with a high-throughput screen against Mcl-1, they discovered **LE0** (Figure 6.12, blue compound), with a $K_i = 9.3 \mu\text{M}$ ⁴⁵.

We have developed a triazine-piperazine-piperidine scaffold based on the triazene scaffold due to the correct spatial orientation of the functional groups described by Lim *et al.* We have utilized a piperazine and piperidine in place of the piperazine-triazene

subunits due to the ease of synthesis and increased flexibility. In addition, the final piperidine moiety will allow for the introduction of an electrophilic warhead in one step.

The synthesis is described briefly in Figure 6.16:

Cyanuric chloride (**1**) will undergo three stepwise S_NAR reactions with methyl glycolate (**2**), benzyl mercaptan (**3**), and boc-substituted piperazine to give the tri-substituted triazine (**4**). The piperazine will be deprotected with 4M HCl (**5**) and coupled with boc-isonipectic acid (**6**) and subsequently deprotected again (**7**). The various electrophilic warheads will be coupled to **8** and lastly, saponification of the carboxylic acid will reveal the triazine α -helix mimetic scaffold (**9**).

Lim *et al.* described that poor binding affinity to Mcl-1 was in part due to the

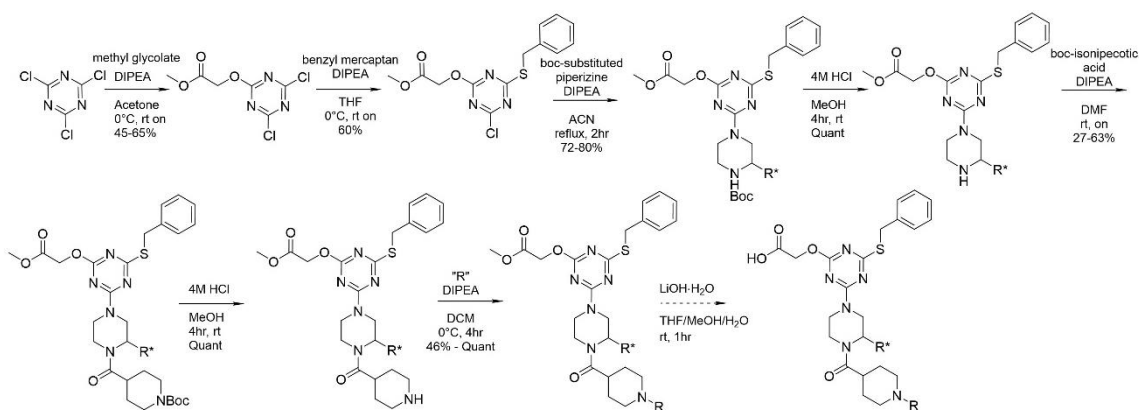


Figure 6.16. Triazine based α -helix mimetic synthesis.

conformational flexibility of the compound, which may have introduced a large entropic loss upon binding⁴⁵. However, we hypothesize that the introduction of an electrophilic warhead will not only impart selectivity, but will also increase binding affinity, which may offset the potential reduced affinity caused by the entropic loss upon binding.

Manual docking of representative compound **TR1** overlaid with the Puma-BH3 peptide reveals good mimicry of the Puma-BH3 peptide (Figure 6.17). The carboxylic

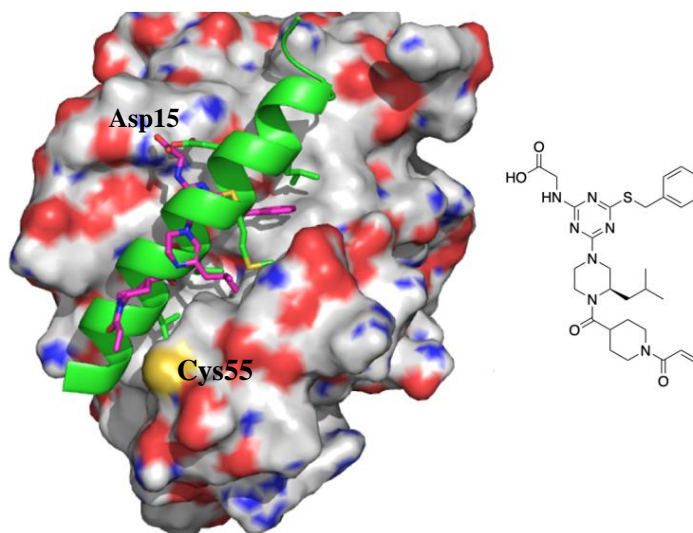


Figure 6.17. Representative compound **TR1** (pink) manually docked in *Bfl-1-Puma-BH3*. PDB: 5UUL.

acid effectively mimics Asp15, while the (*R*)-isopropyl group probes into the same pocket as Leu10. Further, we will synthesize both the *R* and *S* compounds with various groups such as methyl and isopropyl to probe the Leu10 pocket. In addition, the piperidine subunit with the acrylamide moiety is in close contact with Cys55 of Bfl-1. This docking figure reveals that our compounds are comparable to the native α -helix and may offer effective covalent inhibition of Bfl-1.

6.8.3. Electrophilic warheads

For covalent inhibition to be successful, the electrophilic warhead must be considered. This is a functional moiety that will directly react with the cysteine in the protein-of-interest. The reactivity and selectivity must be carefully balanced due to the potential off-target binding, as the electrophilic warhead can react with endogenous nucleophiles, creating toxic protein adducts. We will explore both reversible and irreversible moieties

to further probe the Bfl-1 interaction. Initially, we will utilize three groups to show our proof-of-concept works. The irreversible warheads will be acrylamide and pentafluorobenzenesulfonamide, while acrylonitrile will serve as the reversible moiety (Figure 6.18). Acrylamide moieties have been used in FDA approved covalent inhibitors,

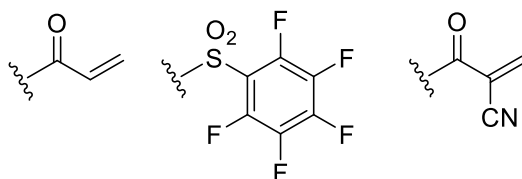


Figure 6.18. The electrophilic warheads we will use in our compound design. Acrylamide (left), pentafluorobenzenesulfonamide (center) and acrylonitrile (right).

such as the Bruton's tyrosine kinase inhibitor Ibrutinib as well as the Epidermal growth factor receptor tyrosine kinase inhibitor Osimertinib⁵⁰. The pentafluorobenzenesulfonamide was utilized in a STAT3 inhibitor as an effective covalent inhibitor. A metabolic stability study revealed that the para-fluorine reacted with glutathione via nucleophilic aromatic substitution, showing that it is capable of reacting covalently with an endogenous ligand. They suggest that it may behave as an electrophilic warhead toward thiol nucleophiles *in vivo*⁵¹.

The strategy of using reversible covalent inhibitors was developed to avoid potential toxicity issues associated with irreversible inhibitors. Taunton *et al.* found that 2-cyanoacrylates could react reversibly with cysteine at physiological pH. They described that the reversibility was caused by β -elimination via an E1cB mechanism (Figure 6.19).

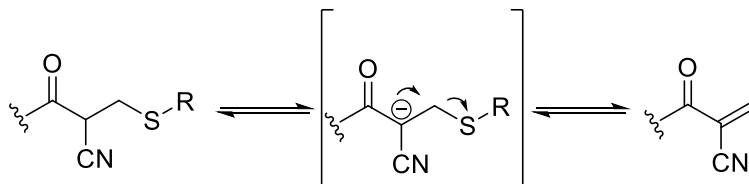


Figure 6.19. E1cB mechanism describing thiol elimination of reversible α -cyanoacrylate covalent moiety.

In fact, they experimentally showed that different electron withdrawing groups could increase the intrinsic reversibility of the compound by monitoring the disappearance of the adducts and reappearance of the acrylonitrile compounds with NMR or LC/MS. For example, a methylthiazole exhibited an elimination rate of $t_{1/2} < 1$ minute⁵². We will functionalize the piperidine ring with an acrylonitrile group substituted with simple alkyl groups to probe the potential of a reversible covalent inhibitor against Bfl-1.

6.7. Discussion

The resurgence of covalent inhibition has led to the development of many FDA approved inhibitors. Bfl-1, a Bcl-2 anti-apoptotic protein, has recently seen has become an important target due to its implication in chemoresistance and cancer progression. Herein, we have described two α -helix mimetic covalent inhibitors in development to target this understudied protein.

6.8. Future Work and Introspection

The work presented here showcases numerous scaffolds that have been developed to target multiple protein-protein interactions. Although we were unsuccessful in developing a potent small molecule inhibitor towards two different proteins, Mcl-1 and HDM2, these scaffolds can be used as starting points to further develop selective inhibitors. In particular, it would be beneficial to focus efforts on developing a more potent Mcl-1 selective inhibitor. Not only does our lab focus on targeting the Bcl-2 protein family, but the most potent scaffolds that were developed within this work target Mcl-1. In addition, it may be useful to start further development with the most potent scaffold, the isoxazoles.

However, it is imperative to perform experiments to find the binding mode of these compounds. In this work we have utilized the *in silico* method SILCS (Site Identification by Ligand Competitive Saturation), but it would be useful to couple this with a biophysical method such as HSQC NMR or X-ray Crystallography. Not only would we be able to further validate the binding mode described by SILCS, but we can further optimize compounds for more potent inhibitors. It is also important that these are tested against other Bcl-2 anti-apoptotic proteins to assess the selectivity. As stated in Chapter 1, inhibiting one or more anti-apoptotic proteins can lead to a compensatory upregulation of others, so it will be important to assess which proteins these compounds inhibit. In addition, these compounds need to be tested for toxicity and potency in a range of cancerous and non-cancerous cells, as we currently only have data assessing the potency in the fluorescence polarization competition assay. At this point, it would be important to make sure these compounds are inducing apoptosis in the cell through the intrinsic apoptosis pathway, which can be done through pull-down experiments including western blots. In the event we have a potent compound in cells, it would be interesting to further assess the pathway of these compounds utilizing a proteomics approach, to get a larger picture of how these compounds work in the cell.

Further, we have moved forward with targeting the anti-apoptotic protein Bfl-1. Today, pharmaceutical companies are working on selective Mcl-1 inhibitors that have reached both in preclinical and clinical studies and many have developed potent inhibitors in the picomolar range (See Chapter 1). Therefore, we have decided that it will be useful to look at less competitive targets, such as Bfl-1.

6.9. Conclusion

Developing inhibitors against the Bcl-2 anti-apoptotic proteins remains challenging, due to the inherent difficulties of targeting PPIs. However, their importance in various hematological diseases and solid tumors showcase the urgent need to find new therapeutics. Although the field has been highlighted with successes such as the approval of venetoclax, there are still compensatory resistance and overexpression mechanisms revealing themselves. Utilizing medicinal chemistry techniques such as covalent inhibition and PROTAC technology may pave a way to new efficacious antineoplastics targeting the Bcl-2 protein family.

6.9. References

- (1) Pei, H.; Peng, Y.; Zhao, Q.; Chen, Y. Small Molecule PROTACs: An Emerging Technology for Targeted Therapy in Drug Discovery. *RSC Advances* **2019**, *9* (30), 16967–16976.
- (2) Lai, A. C.; Crews, C. M. Induced Protein Degradation: An Emerging Drug Discovery Paradigm. *Nat Rev Drug Discov* **2017**, *16* (2), 101–114.
- (3) Meyer-Schwesinger, C. The Ubiquitin–Proteasome System in Kidney Physiology and Disease. *Nature Reviews Nephrology* **2019**, *15* (7), 393–411.
- (4) Sakamoto, K. M.; Kim, K. B.; Verma, R.; Ransick, A.; Stein, B.; Crews, C. M.; Deshaies, R. J. Development of Protacs to Target Cancer-Promoting Proteins for Ubiquitination and Degradation. *Molecular & Cellular Proteomics* **2003**, *2* (12), 1350–1358.
- (5) Konstantinidou, M.; Li, J.; Zhang, B.; Wang, Z.; Shaabani, S.; Ter Brake, F.; Essa, K.; Dömling, A. PROTACs— a Game-Changing Technology. *Expert Opinion on Drug Discovery* **2019**, *14* (12), 1255–1268.
- (6) Bondeson, D. P.; Crews, C. M. Targeted Protein Degradation by Small Molecules. *Annu. Rev. Pharmacol. Toxicol.* **2017**, *57*, 107–123.
- (7) Schapira, M.; Calabrese, M. F.; Bullock, A. N.; Crews, C. M. Targeted Protein Degradation: Expanding the Toolbox. *Nature Reviews Drug Discovery* **2019**, *18* (12), 949–963.
- (8) Wu, T.; Yoon, H.; Xiong, Y.; Dixon-Clarke, S. E.; Nowak, R. P.; Fischer, E. S. Targeted Protein Degradation as a Powerful Research Tool in Basic Biology and Drug Target Discovery. *Nature Structural & Molecular Biology* **2020**.
- (9) Sakamoto, K. M.; Kim, K. B.; Kumagai, A.; Mercurio, F.; Crews, C. M.; Deshaies, R. J. Protacs: Chimeric Molecules That Target Proteins to the Skp1-Cullin-F Box Complex for Ubiquitination and Degradation. *Proceedings of the National Academy of Sciences* **2001**, *98* (15), 8554–8559.
- (10) Arvinas Inc. *A Phase 1, Open-Label, Dose Escalation Clinical Trial to Evaluate the Safety, Tolerability and Pharmacokinetics of ARV-471 in Patients With Estrogen Receptor Positive/Human Epidermal Growth Factor Receptor 2 Negative (ER+/HER2-) Locally Advanced or Metastatic Breast Cancer, Who Have Received Prior Hormonal Therapy and Chemotherapy in the Locally Advanced/Metastatic Setting*; Clinical trial registration NCT04072952; clinicaltrials.gov, 2020.

- (11) Arvinas Inc. *A Phase I, Open-Label, Dose Escalation Clinical Trial to Evaluate the Safety, Tolerability, Pharmacokinetics, and Pharmacodynamics of ARV-110 in Patients With Metastatic Castration-Resistant Prostate Cancer Who Have Progressed on at Least Two Prior Systemic Therapies.*; Clinical trial registration NCT03888612; clinicaltrials.gov, 2019.
- (12) Gao, H.; Sun, X.; Rao, Y. PROTAC Technology: Opportunities and Challenges. *ACS Medicinal Chemistry Letters* **2020**, *11* (3), 237–240.
- (13) Inc, A. Arvinas Releases Updated Dose Escalation Data from Clinical Trial of PROTAC® Protein Degradar ARV-110 in Patients with Metastatic Castration-Resistant Prostate Cancer <http://www.globenewswire.com/news-release/2020/05/29/2040817/0/en/Arvinas-Releases-Updated-Dose-Escalation-Data-from-Clinical-Trial-of-PROTAC-Protein-Degrader-ARV-110-in-Patients-with-Metastatic-Castration-Resistant-Prostate-Cancer.html> (accessed Jul 15, 2020).
- (14) Sun, X.; Gao, H.; Yang, Y.; He, M.; Wu, Y.; Song, Y.; Tong, Y.; Rao, Y. PROTACs: Great Opportunities for Academia and Industry. *Signal Transduction and Targeted Therapy* **2019**, *4* (1), 1–33.
- (15) Papatzimas, J. W.; Gorobets, E.; Maity, R.; Muniyat, M. I.; MacCallum, J. L.; Neri, P.; Bahlis, N. J.; Derksen, D. J. From Inhibition to Degradation: Targeting the Antiapoptotic Protein Myeloid Cell Leukemia 1 (MCL1). *J. Med. Chem.* **2019**, *62* (11), 5522–5540.
- (16) Tinworth, C. P.; Lithgow, H.; Dittus, L.; Bassi, Z. I.; Hughes, S. E.; Muelbaier, M.; Dai, H.; Smith, I. E. D.; Kerr, W. J.; Burley, G. A.; Bantscheff, M.; Harling, J. D. PROTAC-Mediated Degradation of Bruton's Tyrosine Kinase Is Inhibited by Covalent Binding. *ACS Chem. Biol.* **2019**, *14* (3), 342–347.
- (17) Tovell, H.; Testa, A.; Zhou, H.; Shpiro, N.; Crafter, C.; Ciulli, A.; Alessi, D. R. Design and Characterization of SGK3-PROTAC1, an Isoform Specific SGK3 Kinase PROTAC Degradar. *ACS Chem Biol* **2019**, *14* (9), 2024–2034.
- (18) Zhang, F.; Wu, Z.; Chen, P.; Zhang, J.; Wang, T.; Zhou, J.; Zhang, H. Discovery of a New Class of PROTAC BRD4 Degradars Based on a Dihydroquinazolinone Derivative and Lenalidomide/Pomalidomide. *Bioorganic & Medicinal Chemistry* **2020**, *28* (1), 115228.
- (19) Neklesa, T. K.; Winkler, J. D.; Crews, C. M. Targeted Protein Degradation by PROTACs. *Pharmacology & Therapeutics* **2017**, *174*, 138–144.
- (20) Smith, B. E.; Wang, S. L.; Jaime-Figueroa, S.; Harbin, A.; Wang, J.; Hamman, B. D.; Crews, C. M. Differential PROTAC Substrate Specificity Dictated by Orientation of Recruited E3 Ligase. *Nature Communications* **2019**, *10* (1), 131.

- (21) Cyrus, K.; Wehenkel, M.; Choi, E.-Y.; Han, H.-J.; Lee, H.; Swanson, H.; Kim, K.-B. Impact of Linker Length on the Activity of PROTACs. *Mol Biosyst* **2011**, *7* (2), 359–364.
- (22) VENCLEXTA® (venetoclax tablets): CLL/SLL and AML Treatment
<https://www.venclexta.com/>
- (23) Genentech: Press Releases | Monday, Mar 23, 2020
<https://www.gene.com/media/press-releases/14842/2020-03-23/genentech-announces-venclexta-combinatio>
- (24) Pollyea, D. A.; Amaya, M.; Strati, P.; Konopleva, M. Y. Venetoclax for AML: Changing the Treatment Paradigm. *Blood Adv* **2019**, *3* (24), 4326–4335.
- (25) Tausch, E.; Close, W.; Dolnik, A.; Bloehdorn, J.; Chyla, B.; Bullinger, L.; Döhner, H.; Mertens, D.; Stilgenbauer, S. Venetoclax Resistance and Acquired BCL2 Mutations in Chronic Lymphocytic Leukemia. *Haematologica* **2019**, *104* (9), e434–e437.
- (26) Thangavadivel, S.; Byrd, J. C. Gly101Val BCL2 Mutation: One Step Closer to Understanding Venetoclax Resistance in CLL. *Cancer Discov* **2019**, *9* (3), 320–322.
- (27) Novel mutations contribute to progression of venetoclax-treated CLL
<https://www.mdedge.com/hematology-oncology/article/216519/cll/novel-mutations-contribute-to-progression-venetoclax-treated-cll>
- (28) Scheepstra, M.; Hekking, K. F. W.; van Hijfte, L.; Folmer, R. H. A. Bivalent Ligands for Protein Degradation in Drug Discovery. *Comput Struct Biotechnol J* **2019**, *17*, 160–176.
- (29) Mathieu, A.-L.; Sperandio, O.; Pottiez, V.; Balzarín, S.; Herlédan, A.; Elkaïm, J. O.; Fogeron, M.-L.; Piveteau, C.; Dassonneville, S.; Deprez, B.; Villoutreix, B. O.; Bonnefoy, N.; Leroux, F. Identification of Small Inhibitory Molecules Targeting the Bfl-1 Anti-Apoptotic Protein That Alleviates Resistance to ABT-737. *J Biomol Screen* **2014**, *19* (7), 1035–1046.
- (30) Barile, E.; Marconi, G. D.; De, S. K.; Baggio, C.; Gambini, L.; Salem, A. F.; Kashyap, M. K.; Castro, J. E.; Kipps, T. J.; Pellicchia, M. HBfl-1/HNOXA Interaction Studies Provide New Insights on the Role of Bfl-1 in Cancer Cell Resistance and for the Design of Novel Anticancer Agents. *ACS Chem. Biol.* **2017**, *12* (2), 444–455.
- (31) Bandyopadhyay, A.; Gao, J. Targeting Biomolecules with Reversible Covalent Chemistry. *Curr Opin Chem Biol* **2016**, *34*, 110–116.

- (32) Harvey, E. P.; Seo, H.-S.; Guerra, R. M.; Bird, G. H.; Dhe-Paganon, S.; Walensky, L. D. Crystal Structures of Anti-Apoptotic BFL-1 and Its Complex with a Covalent Stapled Peptide Inhibitor. *Structure* **2018**, *26* (1), 153-160.e4.
- (33) Poole, L. B. The Basics of Thiols and Cysteines in Redox Biology and Chemistry. *Free Radic. Biol. Med.* **2015**, *80*, 148–157.
- (34) Johnson, D. S.; Weerapana, E.; Cravatt, B. F. Strategies for Discovering and Derisking Covalent, Irreversible Enzyme Inhibitors. *Future Med Chem* **2010**, *2* (6), 949–964.
- (35) Lopes, F.; Santos, M. M. M.; Moreira, R. *1.2 Designing Covalent Inhibitors: A Medicinal Chemistry Challenge*; De Gruyter, 2015; pp 44–60.
- (36) Huhn, A. J.; Guerra, R. M.; Harvey, E. P.; Bird, G. H.; Walensky, L. D. Selective Covalent Targeting of Anti-Apoptotic BFL-1 by Cysteine-Reactive Stapled Peptide Inhibitors. *Cell Chem Biol* **2016**, *23* (9), 1123–1134.
- (37) Lanning, M. E.; Fletcher, S. Recapitulating the α -Helix: Nonpeptidic, Low-Molecular-Weight Ligands for the Modulation of Helix-Mediated Protein–Protein Interactions. *Future Medicinal Chemistry* **2013**, *5* (18), 2157–2174.
- (38) Boersma, M. D.; Sadowsky, J. D.; Tomita, Y. A.; Gellman, S. H. Hydrophile Scanning as a Complement to Alanine Scanning for Exploring and Manipulating Protein–Protein Recognition: Application to the Bim BH3 Domain. *Protein Sci* **2008**, *17* (7), 1232–1240.
- (39) Petros, A. M.; Olejniczak, E. T.; Fesik, S. W. Structural Biology of the Bcl-2 Family of Proteins. *Biochim. Biophys. Acta* **2004**, *1644* (2–3), 83–94.
- (40) Azzarito, V.; Long, K.; Murphy, N. S.; Wilson, A. J. Inhibition of α -Helix-Mediated Protein–Protein Interactions Using Designed Molecules. *Nat Chem* **2013**, *5* (3), 161–173.
- (41) Barnard, A.; Long, K.; Yeo, D. J.; Miles, J. A.; Azzarito, V.; Burslem, G. M.; Prabhakaran, P.; A Edwards, T.; Wilson, A. J. Orthogonal Functionalisation of α -Helix Mimetics. *Org. Biomol. Chem.* **2014**, *12* (35), 6794–6799.
- (42) Orner, B. P.; Ernst, J. T.; Hamilton, A. D. Toward Proteomimetics: Terphenyl Derivatives as Structural and Functional Mimics of Extended Regions of an α -Helix. *J. Am. Chem. Soc.* **2001**, *123* (22), 5382–5383.
- (43) Yin, H.; Lee, G.-I.; Sedey, K. A.; Kutzki, O.; Park, H. S.; Orner, B. P.; Ernst, J. T.; Wang, H.-G.; Sebt, S. M.; Hamilton, A. D. Terphenyl-Based Bak BH3 Alpha-Helical Proteomimetics as Low-Molecular-Weight Antagonists of Bcl-XL. *J. Am. Chem. Soc.* **2005**, *127* (29), 10191–10196.

- (44) Lanning, M. E.; Fletcher, S. Multi-Facial, Non-Peptidic α -Helix Mimetics. *Biology (Basel)* **2015**, *4* (3), 540–555.
- (45) Lee, Y.; Im, H.; Das, S.; Oh, M.; Lee, J. H.; Ham, S.; Lim, H.-S. Bridged α -Helix Mimetic Small Molecules. *Chem. Commun.* **2019**, *55* (88), 13311–13314.
- (46) Yap, J. L.; Cao, X.; Vanommeslaeghe, K.; Jung, K.-Y.; Peddaboina, C.; Wilder, P. T.; Nan, A.; MacKerell, A. D.; Smythe, W. R.; Fletcher, S. Relaxation of the Rigid Backbone of an Oligoamide-Foldamer-Based α -Helix Mimetic: Identification of Potent Bcl-XL Inhibitors. *Org. Biomol. Chem.* **2012**, *10* (15), 2928–2933.
- (47) Saraogi, I.; Hamilton, A. D. α -Helix Mimetics as Inhibitors of Protein–Protein Interactions. *Biochem Soc Trans* **2008**, *36* (6), 1414–1417.
- (48) Fletcher, S.; Hamilton, A. D. Protein Surface Recognition and Proteomimetics: Mimics of Protein Surface Structure and Function. *Current Opinion in Chemical Biology* **2005**, *9* (6), 632–638.
- (49) Ernst, J. T.; Becerril, J.; Park, H. S.; Yin, H.; Hamilton, A. D. Design and Application of an Alpha-Helix-Mimetic Scaffold Based on an Oligoamide-Foldamer Strategy: Antagonism of the Bak BH3/Bcl-XL Complex. *Angew. Chem. Int. Ed. Engl.* **2003**, *42* (5), 535–539.
- (50) Martín-Gago, P.; Olsen, C. A. Arylfluorosulfate-Based Electrophiles for Covalent Protein Labeling: A New Addition to the Arsenal. *Angewandte Chemie International Edition* **2019**, *58* (4), 957–966.
- (51) Ali, A. M.; Gómez-Biagi, R. F.; Rosa, D. A.; Lai, P.-S.; Heaton, W. L.; Park, J.; Eiring, A. M.; Vellore, N. A.; de Araujo, E. D.; Ball, D. P.; Shouksmith, A. E.; Patel, A. B.; Deininger, M. W.; O’Hare, T.; Gunning, P. T. Disarming an Electrophilic Warhead: Retaining Potency in Tyrosine Kinase Inhibitor (TKI)-Resistant CML Lines, While Circumventing Pharmacokinetic Liabilities. *ChemMedChem* **2016**, *11* (8), 850–861.
- (52) Krishnan, S.; Miller, R. M.; Tian, B.; Mullins, R. D.; Jacobson, M. P.; Taunton, J. Design of Reversible, Cysteine-Targeted Michael Acceptors Guided by Kinetic and Computational Analysis. *J Am Chem Soc* **2014**, *136* (36), 12624–12630.

Chapter 7. References

- (1) Pentimalli, F. BCL2: A 30-Year Tale of Life, Death and Much More to Come. *Cell Death Differ.* **2018**, *25* (1), 7–9.
- (2) Tzifi, F.; Economopoulou, C.; Gourgiotis, D.; Ardavanis, A.; Papageorgiou, S.; Scorilas, A. The Role of BCL2 Family of Apoptosis Regulator Proteins in Acute and Chronic Leukemias <https://www.hindawi.com/journals/ah/2012/524308/> (accessed Mar 21, 2020).
- (3) Vaux, D. L.; Cory, S.; Adams, J. M. Bcl-2 Gene Promotes Haemopoietic Cell Survival and Cooperates with c-Myc to Immortalize Pre-B Cells. *Nature* **1988**, *335* (6189), 440–442.
- (4) Hardwick, J. M.; Soane, L. Multiple Functions of BCL-2 Family Proteins. *Cold Spring Harb. Perspect. Biol.* **2013**, *5* (2).
- (5) Youle, R. J.; Strasser, A. The BCL-2 Protein Family: Opposing Activities That Mediate Cell Death. *Nat. Rev. Mol. Cell Biol.* **2008**, *9* (1), 47–59.
- (6) Czabotar, P. E.; Lessene, G.; Strasser, A.; Adams, J. M. Control of Apoptosis by the BCL-2 Protein Family: Implications for Physiology and Therapy. *Nat. Rev. Mol. Cell Biol.* **2014**, *15* (1), 49–63.
- (7) Muchmore, S. W.; Sattler, M.; Liang, H.; Meadows, R. P.; Harlan, J. E.; Yoon, H. S.; Nettlesheim, D.; Chang, B. S.; Thompson, C. B.; Wong, S.-L.; Ng, S.-C.; Fesik, S. W. X-Ray and NMR Structure of Human Bcl-x L , an Inhibitor of Programmed Cell Death. *Nature* **1996**, *381* (6580), 335–341.
- (8) Petros, A. M.; Olejniczak, E. T.; Fesik, S. W. Structural Biology of the Bcl-2 Family of Proteins. *Biochim. Biophys. Acta* **2004**, *1644* (2–3), 83–94.
- (9) Wong, C.; Anderson, D. J.; Lee, E. F.; Fairlie, W. D.; Ludlam, M. J. C. Direct Visualization of Bcl-2 Family Protein Interactions Using Live Cell Fluorescent Protein Redistribution Assays. *Cell Death Dis.* **2012**, *3* (3), e288.
- (10) van Delft, M. F.; Huang, D. C. S. How the Bcl-2 Family of Proteins Interact to Regulate Apoptosis. *Cell Res.* **2006**, *16* (2), 203–213.
- (11) Shimizu, S.; Konishi, A.; Kodama, T.; Tsujimoto, Y. BH4 Domain of Antiapoptotic Bcl-2 Family Members Closes Voltage-Dependent Anion Channel and Inhibits Apoptotic Mitochondrial Changes and Cell Death. *Proc. Natl. Acad. Sci. U. S. A.* **2000**, *97* (7), 3100–3105.

- (12) Dewson, G.; Kluck, R. M. Mechanisms by Which Bak and Bax Permeabilise Mitochondria during Apoptosis. *J. Cell Sci.* **2009**, *122* (16), 2801–2808.
- (13) Letai, A.; Bassik, M. C.; Walensky, L. D.; Sorcinelli, M. D.; Weiler, S.; Korsmeyer, S. J. Distinct BH3 Domains Either Sensitize or Activate Mitochondrial Apoptosis, Serving as Prototype Cancer Therapeutics. *Cancer Cell* **2002**, *2* (3), 183–192.
- (14) Willis, S. N.; Fletcher, J. I.; Kaufmann, T.; van Delft, M. F.; Chen, L.; Czabotar, P. E.; Ierino, H.; Lee, E. F.; Fairlie, W. D.; Bouillet, P.; Strasser, A.; Kluck, R. M.; Adams, J. M.; Huang, D. C. S. Apoptosis Initiated When BH3 Ligands Engage Multiple Bcl-2 Homologs, Not Bax or Bak. *Science* **2007**, *315* (5813), 856–859.
- (15) Lanning, M. E.; Fletcher, S. Recapitulating the α -Helix: Nonpeptidic, Low-Molecular-Weight Ligands for the Modulation of Helix-Mediated Protein–Protein Interactions. *Future Med. Chem.* **2013**, *5* (18), 2157–2174.
- (16) Boersma, M. D.; Sadowsky, J. D.; Tomita, Y. A.; Gellman, S. H. Hydrophile Scanning as a Complement to Alanine Scanning for Exploring and Manipulating Protein–Protein Recognition: Application to the Bim BH3 Domain. *Protein Sci. Publ. Protein Soc.* **2008**, *17* (7), 1232–1240.
- (17) Moreira, I. S.; Fernandes, P. A.; Ramos, M. J. Hot Spots--a Review of the Protein-Protein Interface Determinant Amino-Acid Residues. *Proteins* **2007**, *68* (4), 803–812.
- (18) Azzarito, V.; Long, K.; Murphy, N. S.; Wilson, A. J. Inhibition of α -Helix-Mediated Protein-Protein Interactions Using Designed Molecules. *Nat. Chem.* **2013**, *5* (3), 161–173.
- (19) Barnard, A.; Long, K.; Yeo, D. J.; Miles, J. A.; Azzarito, V.; Burslem, G. M.; Prabhakaran, P.; A Edwards, T.; Wilson, A. J. Orthogonal Functionalisation of α -Helix Mimetics. *Org. Biomol. Chem.* **2014**, *12* (35), 6794–6799.
- (20) Drennen, B.; Scheenstra, J. A.; Yap, J. L.; Chen, L.; Lanning, M. E.; Roth, B. M.; Wilder, P. T.; Fletcher, S. Structural Re-Engineering of the α -Helix Mimetic JY-1-106 into Small-Molecules: Disruption of the Mcl-1–Bak-BH3 Protein–Protein Interaction with 2,6-Di-Substituted Nicotinates. *ChemMedChem* **2016**, *11* (8), 827–833.
- (21) Sattler, M.; Liang, H.; Nettlesheim, D.; Meadows, R. P.; Harlan, J. E.; Eberstadt, M.; Yoon, H. S.; Shuker, S. B.; Chang, B. S.; Minn, A. J.; Thompson, C. B.; Fesik, S. W. Structure of Bcl-XL-Bak Peptide Complex: Recognition Between Regulators of Apoptosis. *Science* **1997**, *275* (5302), 983–986.
- (22) Cosentino, K.; García-Sáez, A. J. Bax and Bak Pores: Are We Closing the Circle? *Trends Cell Biol.* **2017**, *27* (4), 266–275.

- (23) Renehan, A. G.; Booth, C.; Potten, C. S. What Is Apoptosis, and Why Is It Important? *BMJ* **2001**, *322* (7301), 1536–1538.
- (24) Campbell, K. J.; Tait, S. W. G. Targeting BCL-2 Regulated Apoptosis in Cancer. *Open Biol.* **2018**, *8* (5).
- (25) Westphal, D.; Kluck, R. M.; Dewson, G. Building Blocks of the Apoptotic Pore: How Bax and Bak Are Activated and Oligomerize during Apoptosis. *Cell Death Differ.* **2014**, *21* (2), 196–205.
- (26) Flores-Romero, H.; Landeta, O.; Ugarte-Uribe, B.; Cosentino, K.; García-Porras, M.; García-Sáez, A. J.; Basañez, G. BFL1 Modulates Apoptosis at the Membrane Level through a Bifunctional and Multimodal Mechanism Showing Key Differences with BCLXL. *Cell Death Differ.* **2019**, *26* (10), 1880–1894.
- (27) Czabotar, P. E.; Westphal, D.; Dewson, G.; Ma, S.; Hockings, C.; Fairlie, W. D.; Lee, E. F.; Yao, S.; Robin, A. Y.; Smith, B. J.; Huang, D. C. S.; Kluck, R. M.; Adams, J. M.; Colman, P. M. Bax Crystal Structures Reveal How BH3 Domains Activate Bax and Nucleate Its Oligomerization to Induce Apoptosis. *Cell* **2013**, *152* (3), 519–531.
- (28) Hanahan, D.; Weinberg, R. A. Hallmarks of Cancer: The next Generation. *Cell* **2011**, *144* (5), 646–674.
- (29) Um, H.-D. Bcl-2 Family Proteins as Regulators of Cancer Cell Invasion and Metastasis: A Review Focusing on Mitochondrial Respiration and Reactive Oxygen Species. *Oncotarget* **2015**, *7* (5), 5193–5203.
- (30) Lopez, J.; Tait, S. W. G. Mitochondrial Apoptosis: Killing Cancer Using the Enemy Within. *Br. J. Cancer* **2015**, *112* (6), 957–962.
- (31) Ortíz-Maldonado, V.; Mozas, P.; Delgado, J. The Biology behind B-Cell Lymphoma 2 as a Target in Chronic Lymphocytic Leukemia. *Ther. Adv. Hematol.* **2016**, *7* (6), 321–329.
- (32) Green, D. R. A BH3 Mimetic for Killing Cancer Cells. *Cell* **2016**, *165* (7), 1560.
- (33) Oltersdorf, T.; Elmore, S. W.; Shoemaker, A. R.; Armstrong, R. C.; Augeri, D. J.; Belli, B. A.; Bruncko, M.; Deckwerth, T. L.; Dinges, J.; Hajduk, P. J.; Joseph, M. K.; Kitada, S.; Korsmeyer, S. J.; Kunzer, A. R.; Letai, A.; Li, C.; Mitten, M. J.; Nettesheim, D. G.; Ng, S.; Nimmer, P. M.; O'Connor, J. M.; Oleksijew, A.; Petros, A. M.; Reed, J. C.; Shen, W.; Tahir, S. K.; Thompson, C. B.; Tomaselli, K. J.; Wang, B.; Wendt, M. D.; Zhang, H.; Fesik, S. W.; Rosenberg, S. H. An Inhibitor of Bcl-2 Family Proteins Induces Regression of Solid Tumours. *Nature* **2005**, *435* (7042), 677–681.

- (34) Shuker, S. B.; Hajduk, P. J.; Meadows, R. P.; Fesik, S. W. Discovering High-Affinity Ligands for Proteins: SAR by NMR. *Science* **1996**, *274* (5292), 1531–1534.
- (35) Oral Bioavailability (F%)
https://www.pharmainformatic.com/html/oral_bioavailability__f__.html (accessed Mar 25, 2020).
- (36) Park, C.-M.; Bruncko, M.; Adickes, J.; Bauch, J.; Ding, H.; Kunzer, A.; Marsh, K. C.; Nimmer, P.; Shoemaker, A. R.; Song, X.; Tahir, S. K.; Tse, C.; Wang, X.; Wendt, M. D.; Yang, X.; Zhang, H.; Fesik, S. W.; Rosenberg, S. H.; Elmore, S. W. Discovery of an Orally Bioavailable Small Molecule Inhibitor of Prosurvival B-Cell Lymphoma 2 Proteins. *J. Med. Chem.* **2008**, *51* (21), 6902–6915.
- (37) Souers, A. J.; Levenson, J. D.; Boghaert, E. R.; Ackler, S. L.; Catron, N. D.; Chen, J.; Dayton, B. D.; Ding, H.; Enschede, S. H.; Fairbrother, W. J.; Huang, D. C. S.; Hymowitz, S. G.; Jin, S.; Khaw, S. L.; Kovar, P. J.; Lam, L. T.; Lee, J.; Maecker, H. L.; Marsh, K. C.; Mason, K. D.; Mitten, M. J.; Nimmer, P. M.; Oleksijew, A.; Park, C. H.; Park, C.-M.; Phillips, D. C.; Roberts, A. W.; Sampath, D.; Seymour, J. F.; Smith, M. L.; Sullivan, G. M.; Tahir, S. K.; Tse, C.; Wendt, M. D.; Xiao, Y.; Xue, J. C.; Zhang, H.; Humerickhouse, R. A.; Rosenberg, S. H.; Elmore, S. W. ABT-199, a Potent and Selective BCL-2 Inhibitor, Achieves Antitumor Activity While Sparing Platelets. *Nat. Med.* **2013**, *19* (2), 202–208.
- (38) Tse, C.; Shoemaker, A. R.; Adickes, J.; Anderson, M. G.; Chen, J.; Jin, S.; Johnson, E. F.; Marsh, K. C.; Mitten, M. J.; Nimmer, P.; Roberts, L.; Tahir, S. K.; Xiao, Y.; Yang, X.; Zhang, H.; Fesik, S.; Rosenberg, S. H.; Elmore, S. W. ABT-263: A Potent and Orally Bioavailable Bcl-2 Family Inhibitor. *Cancer Res.* **2008**, *68* (9), 3421–3428.
- (39) Cang, S.; Iragavarapu, C.; Savooji, J.; Song, Y.; Liu, D. ABT-199 (Venetoclax) and BCL-2 Inhibitors in Clinical Development. *J. Hematol. Oncol. J Hematol Oncol* **2015**, *8*.
- (40) Clinical Study Report Synopsis S55746, **2019**. <https://clinicaltrials.servier.com/wp-content/uploads/CL1-55746-001-anonymisedsynopsis-2019.09.16-1.pdf>
- (41) Juárez-Salcedo, L. M.; Desai, V.; Dalia, S. Venetoclax: Evidence to Date and Clinical Potential. *Drugs Context* **2019**, *8*.
- (42) Pivotal Phase II Study Showed Nearly 80 Percent of People with Hard-to-treat Type of Chronic Lymphocytic Leukemia Responded to Investigational Medicine Venetoclax https://www.drugs.com/nda/venetoclax_151206.html (accessed Mar 26, 2020).
- (43) AbbVie Announces US FDA Approval of Venclaxta (venetoclax) as a Chemotherapy-Free Combination Regimen for Previously Untreated Chronic

Lymphocytic Leukemia Patients <https://www.drugs.com/newdrugs/abbvie-announces-us-fda-approval-venclerxa-venetoclax-chemotherapy-free-combination-regimen-4974.html>

- (44) Ran, X.; Gestwicki, J. E. Inhibitors of Protein-Protein Interactions (PPIs): An Analysis of Scaffold Choices and Buried Surface Area. *Curr. Opin. Chem. Biol.* **2018**, *44*, 75–86.
- (45) Lipinski, C. A. Rule of Five in 2015 and beyond: Target and Ligand Structural Limitations, Ligand Chemistry Structure and Drug Discovery Project Decisions. *Adv. Drug Deliv. Rev.* **2016**, *101*, 34–41.
- (46) Lessene, G.; Czabotar, P. E.; Colman, P. M. BCL-2 Family Antagonists for Cancer Therapy. *Nat. Rev. Drug Discov.* **2008**, *7* (12), 989–1000.
- (47) Diguarher, T. L.; Casara, P.; STARCK, J.-B.; Henlin, J.-M.; Davidson, J. E. P.; Murray, J. B.; Graham, C. J.; Chen, I.-J.; Geneste, O.; Hickman, J.; Depil, S.; Tiran, A. L.; Nyerges, M.; Nanteuil, G. D. New Indolizine Derivatives, Method for Preparing Same and Pharmaceutical Compositions Containing Same. WO2013110890A1, August 1, 2013.
- (48) Casara, P.; Davidson, J.; Claperon, A.; Le Toumelin-Braizat, G.; Vogler, M.; Bruno, A.; Chanrion, M.; Lysiak-Auvity, G.; Le Diguarher, T.; Starck, J.-B.; Chen, I.; Whitehead, N.; Graham, C.; Matassova, N.; Dokurno, P.; Pedder, C.; Wang, Y.; Qiu, S.; Girard, A.-M.; Schneider, E.; Gravé, F.; Studeny, A.; Guasconi, G.; Rocchetti, F.; Maïga, S.; Henlin, J.-M.; Colland, F.; Kraus-Berthier, L.; Le Gouill, S.; Dyer, M. J. S.; Hubbard, R.; Wood, M.; Amiot, M.; Cohen, G. M.; Hickman, J. A.; Morris, E.; Murray, J.; Geneste, O. S55746 Is a Novel Orally Active BCL-2 Selective and Potent Inhibitor That Impairs Hematological Tumor Growth. *Oncotarget* **2018**, *9* (28), 20075–20088.
- (49) Ferenczy, G. G.; Keserű, G. M. Enthalpic Efficiency of Ligand Binding. *J. Chem. Inf. Model.* **2010**, *50* (9), 1536–1541.
- (50) Yang, Y.; Zhao, S.; Song, J. Caspase-Dependent Apoptosis and -Independent Poly(ADP-Ribose) Polymerase Cleavage Induced by Transforming Growth Factor B1. *Int. J. Biochem. Cell Biol.* **2004**, *36* (2), 223–234.
- (51) Birkinshaw, R. W.; Gong, J.; Luo, C. S.; Lio, D.; White, C. A.; Anderson, M. A.; Blombery, P.; Lessene, G.; Majewski, I. J.; Thijssen, R.; Roberts, A. W.; Huang, D. C. S.; Colman, P. M.; Czabotar, P. E. Structures of BCL-2 in Complex with Venetoclax Reveal the Molecular Basis of Resistance Mutations. *Nat. Commun.* **2019**, *10* (1), 1–10.

- (52) Daly, A. K. Chapter 24 - Pharmacogenomics of Warfarin. In *Handbook of Pharmacogenomics and Stratified Medicine*; Padmanabhan, S., Ed.; Academic Press: San Diego, 2014; pp 497–507.
- (53) GUO, Y.; Xue, H.; Wang, Z.; SUN, H. Bcl-2 INHIBITORS. WO2019210828A1, November 7, 2019.
- (54) Study of Bcl-2 Inhibitor BGB-11417 in Participants With Mature B-Cell Malignancies - Full Text View - ClinicalTrials.gov
<https://clinicaltrials.gov/ct2/show/NCT04277637>
- (55) Yang, D.; Zhai, Y.; Wang, G. Combination Product of Bcl-2 Inhibitor and Chemotherapeutic Agent and Use Thereof in the Prevention and/or Treatment of Diseases. WO2020024834A1, February 6, 2020.
- (56) Yang, D.; Zhai, Y.; TANG, Q.; Fang, D. D. Combination Product of Bcl-2 Inhibitor and Mdm2 Inhibitor and Use Thereof in the Prevention and/or Treatment of Diseases. WO2020024820A1, February 6, 2020.
- (57) Yang, D.; Zhai, Y.; Wang, G. Synergistic Antitumor Effect of Bcl-2 Inhibitor Combined with Rituximab and/or Bendamustine or Bcl-2 Inhibitor Combined with Chop. WO2020024826A1, February 6, 2020.
- (58) Ascentage Pharma Announces First Patient Dosed in the Global Phase Ib/II Clinical Study of Bcl-2 Inhibitor APG-2575 in the United States
<https://www.biospace.com/article/ascentage-pharma-announces-first-patient-dosed-in-the-global-phase-ib-ii-clinical-study-of-bcl-2-inhibitor-apg-2575-in-the-united-states/> (accessed Mar 27, 2020).
- (59) Pharma, A. Ascentage Pharma Announces Clearances for Three Phase Ib/II Clinical Studies of APG-2575 in China and the U.S., Beginning Simultaneous Clinical Development in Three Hematologic Malignancy Indications
<https://www.prnewswire.com/news-releases/ascentage-pharma-announces-clearances-for-three-phase-ib-ii-clinical-studies-of-apg-2575-in-china-and-the-us-beginning-simultaneous-clinical-development-in-three-hematologic-malignancy-indications-301019683.html>
- (60) Yang, D.; Zhai, Y.; Wang, G.; Fang, D. D.; DENG, J.; QIU, M.; Zhang, L. Combination of Bcl-2/Bcl-xL Inhibitors and Chemotherapeutic Agent and Use Thereof. WO2020024976A1, February 6, 2020.
- (61) Bai, L.; Chen, J.; Liu, L.; McEachern, D.; Aguilar, A.; Zhou, H.; Yang, C. Y.; Wang, H.; Wen, J.; Wang, G.; Zhai, Y.; Guo, M.; Yang, D.; Wang, S. 338 BM-1252 (APG-1252): A Potent Dual Specific Bcl-2/Bcl-XL Inhibitor That Achieves Complete Tumor Regression with Minimal Platelet Toxicity. *Eur. J. Cancer* **2014**, *50*, 109–110.

- (62) Wang, J.; Yang, D.; Luo, Q.; Qiu, M.; Zhang, L.; Li, B.; Chen, H.; Yi, H.; Yan, X.; Li, S.; Sun, J. APG-1252-12A Induces Mitochondria-Dependent Apoptosis through Inhibiting the Antiapoptotic Proteins Bcl-2/Bcl-xL in HL-60 Cells. *Int. J. Oncol.* **2017**, *51* (2), 563–572.
- (63) Lakhani, N. J.; Rasco, D. W.; Tolcher, A. W.; Huang, Y.; Ji, J.; Wang, H.; Dong, Q.; Men, L.; O'Rourke, T. J.; Chandana, S. R.; Amaya, A.; Cole, Y.; Kaiser, B.; Mays, T. A.; Patnaik, A.; Papadopoulos, K. P.; Yang, D.; Zhai, Y. A Phase I Study of Novel Dual Bcl-2/Bcl-XL Inhibitor APG-1252 in Patients with Advanced Small Cell Lung Cancer (SCLC) or Other Solid Tumor. *J. Clin. Oncol.* **2018**, *36*, 2594–2594.
- (64) Study of Combination APG-1252 Plus Paclitaxel in Patients With Relapsed/Refractory Small Cell Lung Cancer - Full Text View - ClinicalTrials.gov <https://clinicaltrials.gov/ct2/show/NCT04210037>
- (65) A Study of APG-1252 in Patients With SCLC or Other Solid Tumors - Full Text View - ClinicalTrials.gov <https://clinicaltrials.gov/ct2/show/NCT03080311>
- (66) APG-1252 in Patients With SCLC or Advanced Solid Tumors - Full Text View - ClinicalTrials.gov <https://clinicaltrials.gov/ct2/show/NCT03387332>
- (67) A Study of APG-1252 Plus Osimertinib(AZD9291) in EGFR TKI Resistant NSCLC Patients - Full Text View - ClinicalTrials.gov <https://clinicaltrials.gov/ct2/show/NCT04001777>
- (68) Tao, Z.-F.; Hasvold, L.; Wang, L.; Wang, X.; Petros, A. M.; Park, C. H.; Boghaert, E. R.; Catron, N. D.; Chen, J.; Colman, P. M.; Czabotar, P. E.; Deshayes, K.; Fairbrother, W. J.; Flygare, J. A.; Hymowitz, S. G.; Jin, S.; Judge, R. A.; Koehler, M. F. T.; Kovar, P. J.; Lessene, G.; Mitten, M. J.; Ndubaku, C. O.; Nimmer, P.; Purkey, H. E.; Oleksijew, A.; Phillips, D. C.; Sleeb, B. E.; Smith, B. J.; Smith, M. L.; Tahir, S. K.; Watson, K. G.; Xiao, Y.; Xue, J.; Zhang, H.; Zobel, K.; Rosenberg, S. H.; Tse, C.; Levenson, J. D.; Elmore, S. W.; Souers, A. J. Discovery of a Potent and Selective BCL-XL Inhibitor with in Vivo Activity. *ACS Med. Chem. Lett.* **2014**, *5* (10), 1088–1093.
- (69) Wang, L.; Doherty, G. A.; Judd, A. S.; Tao, Z.-F.; Hansen, T. M.; Frey, R. R.; Song, X.; Bruncko, M.; Kunzer, A. R.; Wang, X.; Wendt, M. D.; Flygare, J. A.; Catron, N. D.; Judge, R. A.; Park, C. H.; Shekhar, S.; Phillips, D. C.; Nimmer, P.; Smith, M. L.; Tahir, S. K.; Xiao, Y.; Xue, J.; Zhang, H.; Le, P. N.; Mitten, M. J.; Boghaert, E. R.; Gao, W.; Kovar, P.; Choo, E. F.; Diaz, D.; Fairbrother, W. J.; Elmore, S. W.; Sampath, D.; Levenson, J. D.; Souers, A. J. Discovery of A-1331852, a First-in-Class, Potent, and Orally-Bioavailable BCL-X_L Inhibitor. *ACS Med. Chem. Lett.* **2020**.

- (70) Levenson, J. D.; Phillips, D. C.; Mitten, M. J.; Boghaert, E. R.; Diaz, D.; Tahir, S. K.; Belmont, L. D.; Nimmer, P.; Xiao, Y.; Ma, X. M.; Lowes, K. N.; Kovar, P.; Chen, J.; Jin, S.; Smith, M.; Xue, J.; Zhang, H.; Oleksijew, A.; Magoc, T. J.; Vaidya, K. S.; Albert, D. H.; Tarrant, J. M.; La, N.; Wang, L.; Tao, Z.-F.; Wendt, M. D.; Sampath, D.; Rosenberg, S. H.; Tse, C.; Huang, D. C. S.; Fairbrother, W. J.; Elmore, S. W.; Souers, A. J. Exploiting Selective BCL-2 Family Inhibitors to Dissect Cell Survival Dependencies and Define Improved Strategies for Cancer Therapy. *Sci. Transl. Med.* **2015**, *7* (279), 279ra40-279ra40.
- (71) Besbes, S.; Pocard, M.; Mirshahi, M.; Billard, C. The First MCL-1-Selective BH3 Mimetics Have Therapeutic Potential for Chronic Lymphocytic Leukemia. *Crit. Rev. Oncol. Hematol.* **2016**, *100* (Supplement C), 32–36.
- (72) Fire, E.; Gullá, S. V.; Grant, R. A.; Keating, A. E. Mcl-1–Bim Complexes Accommodate Surprising Point Mutations via Minor Structural Changes. *Protein Sci. Publ. Protein Soc.* **2010**, *19* (3), 507–519.
- (73) Akgul, C. Mcl-1 Is a Potential Therapeutic Target in Multiple Types of Cancer. *Cell. Mol. Life Sci.* **2009**, *66* (8), 1326–1336.
- (74) Kotschy, A.; Szlavik, Z.; Murray, J.; Davidson, J.; Maragno, A. L.; Le Toumelin-Braizat, G.; Chanrion, M.; Kelly, G. L.; Gong, J.-N.; Moujalled, D. M.; Bruno, A.; Csekei, M.; Paczal, A.; Szabo, Z. B.; Sipos, S.; Radics, G.; Prosenyak, A.; Balint, B.; Ondi, L.; Blasko, G.; Robertson, A.; Surgenor, A.; Dokurno, P.; Chen, I.; Matassova, N.; Smith, J.; Pedder, C.; Graham, C.; Studeny, A.; Lysiak-Auvity, G.; Girard, A.-M.; Gravé, F.; Segal, D.; Riffkin, C. D.; Pomilio, G.; Galbraith, L. C. A.; Aubrey, B. J.; Brennan, M. S.; Herold, M. J.; Chang, C.; Guasconi, G.; Cauquil, N.; Melchiorre, F.; Guigal-Stephan, N.; Lockhart, B.; Colland, F.; Hickman, J. A.; Roberts, A. W.; Huang, D. C. S.; Wei, A. H.; Strasser, A.; Lessene, G.; Geneste, O. The MCL1 Inhibitor S63845 Is Tolerable and Effective in Diverse Cancer Models. *Nature* **2016**, *538* (7626), 477–482.
- (75) Xiang, W.; Yang, C.-Y.; Bai, L. MCL-1 Inhibition in Cancer Treatment. *OncoTargets Ther.* **2018**, *11*, 7301–7314.
- (76) Levenson, J. D.; Zhang, H.; Chen, J.; Tahir, S. K.; Phillips, D. C.; Xue, J.; Nimmer, P.; Jin, S.; Smith, M.; Xiao, Y.; Kovar, P.; Tanaka, A.; Bruncko, M.; Sheppard, G. S.; Wang, L.; Gierke, S.; Kategaya, L.; Anderson, D. J.; Wong, C.; Eastham-Anderson, J.; Ludlam, M. J. C.; Sampath, D.; Fairbrother, W. J.; Wertz, I.; Rosenberg, S. H.; Tse, C.; Elmore, S. W.; Souers, A. J. Potent and Selective Small-Molecule MCL-1 Inhibitors Demonstrate on-Target Cancer Cell Killing Activity as Single Agents and in Combination with ABT-263 (Navitoclax). *Cell Death Dis.* **2015**, *6* (1), e1590.
- (77) Derenne, S.; Monia, B.; Dean, N. M.; Taylor, J. K.; Rapp, M.-J.; Harousseau, J.-L.; Bataille, R.; Amiot, M. Antisense Strategy Shows That Mcl-1 Rather than Bcl-2 or

Bcl-x(L) Is an Essential Survival Protein of Human Myeloma Cells. *Blood* **2002**, *100* (1), 194–199.

- (78) Chen, L.; Fletcher, S. Mcl-1 Inhibitors: A Patent Review. *Expert Opin. Ther. Pat.* **2017**, *27* (2), 163–178.
- (79) Ramsey, H. E.; Fischer, M. A.; Lee, T.; Gorska, A. E.; Arrate, M. P.; Fuller, L.; Boyd, K. L.; Strickland, S. A.; Sensintaffar, J.; Hogdal, L. J.; Ayers, G. D.; Olejniczak, E. T.; Fesik, S. W.; Savona, M. R. A Novel MCL1 Inhibitor Combined with Venetoclax Rescues Venetoclax-Resistant Acute Myelogenous Leukemia. *Cancer Discov.* **2018**, *8* (12), 1566–1581.
- (80) Beekman, A. M.; Howell, L. A. Small-Molecule and Peptide Inhibitors of the Pro-Survival Protein Mcl-1. *Chemmedchem* **2016**, *11* (8), 802–813.
- (81) Tron, A. E.; Belmonte, M. A.; Adam, A.; Aquila, B. M.; Boise, L. H.; Chiarparin, E.; Cidado, J.; Embrey, K. J.; Gangl, E.; Gibbons, F. D.; Gregory, G. P.; Hargreaves, D.; Hendricks, J. A.; Johannes, J. W.; Johnstone, R. W.; Kazmirski, S. L.; Kettle, J. G.; Lamb, M. L.; Matulis, S. M.; Nooka, A. K.; Packer, M. J.; Peng, B.; Rawlins, P. B.; Robbins, D. W.; Schuller, A. G.; Su, N.; Yang, W.; Ye, Q.; Zheng, X.; Secrist, J. P.; Clark, E. A.; Wilson, D. M.; Fawell, S. E.; Hird, A. W. Discovery of Mcl-1-Specific Inhibitor AZD5991 and Preclinical Activity in Multiple Myeloma and Acute Myeloid Leukemia. *Nat. Commun.* **2018**, *9*.
- (82) Caenepeel, S.; Brown, S. P.; Belmontes, B.; Moody, G.; Keegan, K. S.; Chui, D.; Whittington, D. A.; Huang, X.; Poppe, L.; Cheng, A. C.; Cardozo, M.; Houze, J.; Li, Y.; Lucas, B.; Paras, N. A.; Wang, X.; Taygerly, J. P.; Vimolratana, M.; Zancanella, M.; Zhu, L.; Cajulis, E.; Osgood, T.; Sun, J.; Damon, L.; Egan, R. K.; Greninger, P.; McClanaghan, J. D.; Gong, J.; Moujalled, D.; Pomilio, G.; Beltran, P.; Benes, C. H.; Roberts, A. W.; Huang, D. C.; Wei, A.; Canon, J.; Coxon, A.; Hughes, P. E. AMG 176, a Selective MCL1 Inhibitor, Is Effective in Hematologic Cancer Models Alone and in Combination with Established Therapies. *Cancer Discov.* **2018**, *8* (12), 1582–1597.
- (83) KYPROLIS® (carfilzomib) for Relapsed Multiple Myeloma Treatment
<https://www.kyprolis.com/>
- (84) Spencer, A.; Rosenberg, A. S.; Jakubowiak, A.; Raje, N.; Chatterjee, M.; Trudel, S.; Bahlis, N. J.; Siegel, D. S.; Wilop, S.; Harrison, S. J.; NagaKrishna, M.; Dhuria, S.; Hindoyan, A.; McIver, Z.; Henary, H.; Morrow, P. K.; Roberts, A. A Phase 1, First-in-Human Study of AMG 176, a Selective MCL-1 Inhibitor, in Patients With Relapsed or Refractory Multiple Myeloma. *Clin. Lymphoma Myeloma Leuk.* **2019**, *19* (10), e53–e54.

- (85) Safety, Tolerability, Pharmacokinetics and Efficacy of AMG 397 in Subjects With Multiple Myeloma, NHL, and AML - Full Text View - ClinicalTrials.gov <https://clinicaltrials.gov/ct2/show/NCT03465540>
- (86) Amgen shares hit after analysts expose buried FDA trial halt <https://www.fiercebitech.com/biotech/amgen-shares-hit-after-analysts-expose-buried-fda-trial-halt>
- (87) Agrawal, P. NMR Spectroscopy in Drug Discovery and Development. *Mater. Methods* **2019**.
- (88) Szlávik, Z.; Ondi, L.; Csékei, M.; Paczal, A.; Szabó, Z. B.; Radics, G.; Murray, J.; Davidson, J.; Chen, I.; Davis, B.; Hubbard, R. E.; Pedder, C.; Dokurno, P.; Surgenor, A.; Smith, J.; Robertson, A.; LeToumelin-Braizat, G.; Cauquil, N.; Zarka, M.; Demarles, D.; Perron-Sierra, F.; Claperon, A.; Colland, F.; Geneste, O.; Kotschy, A. Structure-Guided Discovery of a Selective Mcl-1 Inhibitor with Cellular Activity. *J. Med. Chem.* **2019**, *62* (15), 6913–6924.
- (89) Li, Z.; He, S.; Look, A. T. The MCL1-Specific Inhibitor S63845 Acts Synergistically with Venetoclax/ABT-199 to Induce Apoptosis in T-Cell Acute Lymphoblastic Leukemia Cells. *Leukemia* **2019**, *33* (1), 262–266.
- (90) Prukova, D.; Andera, L.; Nahacka, Z.; Karolova, J.; Svaton, M.; Klanova, M.; Havranek, O.; Soukup, J.; Svobodova, K.; Zemanova, Z.; Tuskova, D.; Pokorna, E.; Helman, K.; Forsterova, K.; Pacheco-Blanco, M.; Vockova, P.; Berkova, A.; Fronkova, E.; Trneny, M.; Klener, P. Co-Targeting of BCL2 with Venetoclax and MCL1 with S63845 Is Synthetically Lethal in Vivo in Relapsed Mantle Cell Lymphoma. *Clin. Cancer Res.* **2019**.
- (91) Wei, A. H.; Roberts, A. W.; Spencer, A.; Rosenberg, A. S.; Siegel, D.; Walter, R. B.; Caenepeel, S.; Hughes, P.; McIver, Z.; Mezzi, K.; Morrow, P. K.; Stein, A. Targeting MCL-1 in Hematologic Malignancies: Rationale and Progress. *Blood Rev.* **2020**, 100672.
- (92) Hird, A. W.; Tron, A. E. Recent Advances in the Development of Mcl-1 Inhibitors for Cancer Therapy. *Pharmacol. Ther.* **2019**, *198*, 59–67.
- (93) Study of AZD5991 in Relapsed or Refractory Haematologic Malignancies. - Full Text View - ClinicalTrials.gov <https://clinicaltrials.gov/ct2/show/NCT03218683> (accessed Apr 2, 2020).
- (94) A Study of the Safety and Tolerability of ABBV-467 in Adult Participants With Relapsed/Refractory Multiple Myeloma - Full Text View - ClinicalTrials.gov <https://clinicaltrials.gov/ct2/show/NCT04178902>

- (95) Brady, P. B.; Braje, W.; Dai, Y.; Doherty, G. A.; Gong, J.; Jantos, K.; Ji, C.; Judd, A. S.; Kunzer, A. R.; Lai, C.; Mastracchio, A.; Risi, R. M.; Song, X.; Souers, A. J.; Sullivan, G. M.; Tao, Z.-F.; Teske, J. A.; Wang, X.; Wendt, M. D.; Yu, Y.; Zhu, G.; Penning, T. D. Macrocyclic MCL-1 Inhibitors and Methods of Use. US20200010480A1, January 9, 2020.
- (96) Elmore, S. W.; Souers, A. J.; Bruncko, M.; Song, X.; Wang, X.; Hasvold, L. A.; Wang, L.; Kunzer, A. R.; Park, C.-M.; Wendt, M. D.; Tao, Z.-F.; Madar, D. 7-Substituted Indole as Mcl-1 Inhibitors. EP3243814B1, October 17, 2018.
- (97) Bruncko, M.; Wang, L.; Sheppard, G. S.; Phillips, D. C.; Tahir, S. K.; Xue, J.; Erickson, S.; Fidanze, S.; Fry, E.; Hasvold, L.; Jenkins, G. J.; Jin, S.; Judge, R. A.; Kovar, P. J.; Madar, D.; Nimmer, P.; Park, C.; Petros, A. M.; Rosenberg, S. H.; Smith, M. L.; Song, X.; Sun, C.; Tao, Z.-F.; Wang, X.; Xiao, Y.; Zhang, H.; Tse, C.; Levenson, J. D.; Elmore, S. W.; Souers, A. J. Structure-Guided Design of a Series of MCL-1 Inhibitors with High Affinity and Selectivity. *J. Med. Chem.* **2015**, *58* (5), 2180–2194.
- (98) Wang, Q.; Hao, S. A-1210477, a Selective MCL-1 Inhibitor, Overcomes ABT-737 Resistance in AML. *Oncol. Lett.* **2019**, *18* (5), 5481–5489.
- (99) Ottina, E.; Tischner, D.; Herold, M. J.; Villunger, A. A1/Bfl-1 in Leukocyte Development and Cell Death. *Exp. Cell Res.* **2012**, *318* (11), 1291–1303.
- (100) Flores-Romero, H.; Landeta, O.; Ugarte-Uribe, B.; Cosentino, K.; García-Porras, M.; García-Sáez, A. J.; Basañez, G. BFL1 Modulates Apoptosis at the Membrane Level through a Bifunctional and Multimodal Mechanism Showing Key Differences with BCLXL. *Cell Death Differ.* **2019**, *26* (10), 1880–1894.
- (101) Gangoda, L.; Teh, C. E.; Dengler, M. A.; Best, S. A.; Weeden, C. E.; Tai, L.; Lee, E. F.; Fairlie, W. D.; Sutherland, K. D.; Harrison, L. C.; Gray, D. H.; Strasser, A.; Herold, M. J. Characterization of a Novel Human BFL-1-Specific Monoclonal Antibody. *Cell Death Differ.* **2020**, *27* (2), 826–828.
- (102) Barile, E.; Marconi, G. D.; De, S. K.; Baggio, C.; Gambini, L.; Salem, A. F.; Kashyap, M. K.; Castro, J. E.; Kipps, T. J.; Pellicchia, M. HBfl-1/HNOXA Interaction Studies Provide New Insights on the Role of Bfl-1 in Cancer Cell Resistance and for the Design of Novel Anticancer Agents. *ACS Chem. Biol.* **2017**, *12* (2), 444–455.
- (103) Vogler, M. BCL2A1: The Underdog in the BCL2 Family. *Cell Death Differ.* **2012**, *19* (1), 67–74.
- (104) Choi, S. S.; Park, I. C.; Yun, J. W.; Sung, Y. C.; Hong, S. I.; Shin, H. S. A Novel Bcl-2 Related Gene, Bfl-1, Is Overexpressed in Stomach Cancer and Preferentially Expressed in Bone Marrow. *Oncogene* **1995**, *11* (9), 1693–1698.

- (105) Zong, W.-X.; Edelman, L. C.; Chen, C.; Bash, J.; Gélinas, C. The Prosurvival Bcl-2 Homolog Bfl-1/A1 Is a Direct Transcriptional Target of NF- κ B That Blocks TNF α -Induced Apoptosis. *Genes Dev.* **1999**, *13* (4), 382–387.
- (106) Fan, G.; Simmons, M. J.; Ge, S.; Dutta-Simmons, J.; Kucharczak, J.; Ron, Y.; Weissmann, D.; Chen, C.-C.; Mukherjee, C.; White, E.; Gélinas, C. Defective Ubiquitin-Mediated Degradation of Antiapoptotic Bfl-1 Predisposes to Lymphoma. *Blood* **2010**, *115* (17), 3559–3569.
- (107) Vier, J.; Groth, M.; Sochalska, M.; Kirschnek, S. The Anti-Apoptotic Bcl-2 Family Protein A1/Bfl-1 Regulates Neutrophil Survival and Homeostasis and Is Controlled via PI3K and JAK/STAT Signaling. *Cell Death Dis.* **2016**, *7*, e2103.
- (108) Herman, M. D.; Nyman, T.; Welin, M.; Lehtiö, L.; Flodin, S.; Trésaugues, L.; Kotenyova, T.; Flores, A.; Nordlund, P. Completing the Family Portrait of the Anti-Apoptotic Bcl-2 Proteins: Crystal Structure of Human Bfl-1 in Complex with Bim. *FEBS Lett.* **2008**, *582* (25–26), 3590–3594.
- (109) Olsson, A.; Norberg, M.; ökvist, A.; Derkow, K.; Choudhury, A.; Tobin, G.; Celsing, F.; österborg, A.; Rosenquist, R.; Jondal, M.; Osorio, L. M. Upregulation of Bfl-1 Is a Potential Mechanism of Chemoresistance in B-Cell Chronic Lymphocytic Leukaemia. *Br. J. Cancer* **2007**, *97* (6), 769–777.
- (110) Huhn, A. J.; Guerra, R. M.; Harvey, E. P.; Bird, G. H.; Walensky, L. D. Selective Covalent Targeting of Anti-Apoptotic BFL-1 by Cysteine-Reactive Stapled Peptide Inhibitors. *Cell Chem. Biol.* **2016**, *23* (9), 1123–1134.
- (111) Mathieu, A.-L.; Sperandio, O.; Pottiez, V.; Balzarini, S.; Herlédan, A.; Elkaïm, J. O.; Fogeron, M.-L.; Piveteau, C.; Dassonneville, S.; Deprez, B.; Villoutreix, B. O.; Bonnefoy, N.; Leroux, F. Identification of Small Inhibitory Molecules Targeting the Bfl-1 Anti-Apoptotic Protein That Alleviates Resistance to ABT-737. *J. Biomol. Screen.* **2014**, *19* (7), 1035–1046.
- (112) Esteve-Arenys, A.; Roue, G. BFL-1 Expression Determines the Efficacy of Venetoclax in MYC+/BCL2+ Double Hit Lymphoma. *Oncoscience* **2018**, *5* (3–4), 59–61.
- (113) Janda, A. L. G. and K. D. Protein-Protein Interactions and Cancer: Targeting the Central Dogma <http://www.eurekaselect.com/87258/article>
- (114) Mabonga, L.; Kappo, A. P. Protein-Protein Interaction Modulators: Advances, Successes and Remaining Challenges. *Biophys. Rev.* **2019**, *11* (4), 559–581.
- (115) Akhtar, R. S.; Ness, J. M.; Roth, K. A. Bcl-2 Family Regulation of Neuronal Development and Neurodegeneration. *Biochim. Biophys. Acta BBA - Mol. Cell Res.* **2004**, *1644* (2), 189–203.

- (116) Sassone, J.; Maraschi, A.; Sassone, F.; Silani, V.; Ciammola, A. Defining the Role of the Bcl-2 Family Proteins in Huntington's Disease. *Cell Death Dis.* **2013**, *4* (8), 772–772.
- (117) Luciani, D. S.; White, S. A.; Widenmaier, S. B.; Saran, V. V.; Taghizadeh, F.; Hu, X.; Allard, M. F.; Johnson, J. D. Bcl-2 and Bcl-XL Suppress Glucose Signaling in Pancreatic β -Cells. *Diabetes* **2013**, *62* (1), 170–182.
- (118) Fletcher, S.; Hamilton, A. D. Protein Surface Recognition and Proteomimetics: Mimics of Protein Surface Structure and Function. *Curr. Opin. Chem. Biol.* **2005**, *9* (6), 632–638.
- (119) Lanning, M. E.; Fletcher, S. Recapitulating the α -Helix: Nonpeptidic, Low-Molecular-Weight Ligands for the Modulation of Helix-Mediated Protein–Protein Interactions. *Future Med. Chem.* **2013**, *5* (18), 2157–2174.
- (120) Azzarito, V.; Long, K.; Murphy, N. S.; Wilson, A. J. Inhibition of α -Helix-Mediated Protein-Protein Interactions Using Designed Molecules. *Nat. Chem.* **2013**, *5* (3), 161–173.
- (121) Arkin, M. Protein–Protein Interactions and Cancer: Small Molecules Going in for the Kill. *Curr. Opin. Chem. Biol.* **2005**, *9* (3), 317–324.
- (122) Lampson, B. L.; Davids, M. S. The Development and Current Use of BCL-2 Inhibitors for the Treatment of Chronic Lymphocytic Leukemia. *Curr. Hematol. Malign. Rep.* **2017**, *12* (1), 11–19.
- (123) Tisato, V.; Voltan, R.; Gonelli, A.; Secchiero, P.; Zauli, G. MDM2/X Inhibitors under Clinical Evaluation: Perspectives for the Management of Hematological Malignancies and Pediatric Cancer. *J. Hematol. Oncol. J Hematol Oncol* **2017**, *10* (1), 133.
- (124) Phase I Study of MIK665, a Mcl-1 Inhibitor, in Patients With Refractory or Relapsed Lymphoma or Multiple Myeloma. <https://clinicaltrials.gov/ct2/show/NCT02992483>
- (125) Study of Safety and Efficacy of HDM201 in Combination With LEE011 in Patients With Liposarcoma. <https://clinicaltrials.gov/ct2/show/NCT02343172>
- (126) Lanning, M. E.; Wilder, P. T.; Bailey, H.; Drennen, B.; Cavalier, M.; Chen, L.; Yap, J. L.; Raje, M.; Fletcher, S. Towards More Drug-like Proteomimetics: Two-Faced, Synthetic α -Helix Mimetics Based on a Purine Scaffold. *Org. Biomol. Chem.* **2015**, *13* (32), 8642–8646.

- (127) Petros, A. M.; Olejniczak, E. T.; Fesik, S. W. Structural Biology of the Bcl-2 Family of Proteins. *Biochim. Biophys. Acta* **2004**, *1644* (2–3), 83–94.
- (128) Barnard, A.; Long, K.; Yeo, D. J.; Miles, J. A.; Azzarito, V.; Burslem, G. M.; Prabhakaran, P.; A Edwards, T.; Wilson, A. J. Orthogonal Functionalisation of α -Helix Mimetics. *Org. Biomol. Chem.* **2014**, *12* (35), 6794–6799.
- (129) Czabotar, P. E.; Lessene, G.; Strasser, A.; Adams, J. M. Control of Apoptosis by the BCL-2 Protein Family: Implications for Physiology and Therapy. *Nat. Rev. Mol. Cell Biol.* **2014**, *15* (1), 49–63.
- (130) Vousden, K. H.; Lane, D. P. P53 in Health and Disease. *Nat. Rev. Mol. Cell Biol.* **2007**, *8* (4), 275–283.
- (131) Youle, R. J.; Strasser, A. The BCL-2 Protein Family: Opposing Activities That Mediate Cell Death. *Nat. Rev. Mol. Cell Biol.* **2008**, *9* (1), 47–59.
- (132) Adams, C. M.; Clark-Garvey, S.; Porcu, P.; Eischen, C. M. Targeting the Bcl-2 Family in B Cell Lymphoma. *Front. Oncol.* **2019**, *8*.
- (133) Lee, M.-S.; Ha, J.-H.; Yoon, H. S.; Lee, C.-K.; Chi, S.-W. Structural Basis for the Conserved Binding Mechanism of MDM2-Inhibiting Peptides and Anti-Apoptotic Bcl-2 Family Proteins. *Biochem. Biophys. Res. Commun.* **2014**, *445* (1), 120–125.
- (134) Vu, B.; Wovkulich, P.; Pizzolato, G.; Lovey, A.; Ding, Q.; Jiang, N.; Liu, J.-J.; Zhao, C.; Glenn, K.; Wen, Y.; Tovar, C.; Packman, K.; Vassilev, L.; Graves, B. Discovery of RG7112: A Small-Molecule MDM2 Inhibitor in Clinical Development. *ACS Med. Chem. Lett.* **2013**, *4* (5), 466–469.
- (135) Saha, M. N.; Jiang, H.; Chang, H. Molecular Mechanisms of Nutlin-Induced Apoptosis in Multiple Myeloma. *Cancer Biol. Ther.* **2010**, *10* (6), 567–578.
- (136) Toufektchan, E.; Toledo, F. The Guardian of the Genome Revisited: P53 Downregulates Genes Required for Telomere Maintenance, DNA Repair, and Centromere Structure. *Cancers* **2018**, *10* (5).
- (137) Teoh, G.; Urashima, M.; Ogata, A.; Chauhan, D.; DeCaprio, J. A.; Treon, S. P.; Schlossman, R. L.; Anderson, K. C. MDM2 Protein Overexpression Promotes Proliferation and Survival of Multiple Myeloma Cells. *Blood* **1997**, *90* (5), 1982–1992.
- (138) Kojima, K.; Konopleva, M.; McQueen, T.; O'Brien, S.; Plunkett, W.; Andreeff, M. Mdm2 Inhibitor Nutlin-3a Induces P53-Mediated Apoptosis by Transcription-Dependent and Transcription-Independent Mechanisms and May Overcome Atm-Mediated Resistance to Fludarabine in Chronic Lymphocytic Leukemia. *Blood* **2006**, *108* (3), 993–1000.

- (139) Leu, J. I.-J.; Dumont, P.; Hafey, M.; Murphy, M. E.; George, D. L. Mitochondrial P53 Activates Bak and Causes Disruption of a Bak–Mcl1 Complex. *Nat. Cell Biol.* **2004**, *6* (5), 443–450.
- (140) Kojima, K.; McQueen, T.; Chen, Y.; Jacamo, R.; Konopleva, M.; Shinojima, N.; Shpall, E.; Huang, X.; Andreeff, M. P53 Activation of Mesenchymal Stromal Cells Partially Abrogates Microenvironment-Mediated Resistance to FLT3 Inhibition in AML through HIF-1 α -Mediated down-Regulation of CXCL12. *Blood* **2011**, *118* (16), 4431–4439.
- (141) Chipuk, J. E.; Kuwana, T.; Bouchier-Hayes, L.; Droin, N. M.; Newmeyer, D. D.; Schuler, M.; Green, D. R. Direct Activation of Bax by P53 Mediates Mitochondrial Membrane Permeabilization and Apoptosis. *Science* **2004**, *303* (5660), 1010–1014.
- (142) Besbes, S.; Billard, C. First MCL-1-Selective BH3 Mimetics as Potential Therapeutics for Targeted Treatment of Cancer. *Cell Death Dis.* **2015**, *6* (7), e1810–e1810.
- (143) Kotschy, A.; Szlavik, Z.; Murray, J.; Davidson, J.; Maragno, A. L.; Le Toumelin-Braizat, G.; Chanrion, M.; Kelly, G. L.; Gong, J.-N.; Moujalled, D. M.; Bruno, A.; Csekei, M.; Paczal, A.; Szabo, Z. B.; Sipos, S.; Radics, G.; Proszenyak, A.; Balint, B.; Ondi, L.; Blasko, G.; Robertson, A.; Surgenor, A.; Dokurno, P.; Chen, I.; Matassova, N.; Smith, J.; Pedder, C.; Graham, C.; Studeny, A.; Lysiak-Auvity, G.; Girard, A.-M.; Gravé, F.; Segal, D.; Riffkin, C. D.; Pomilio, G.; Galbraith, L. C. A.; Aubrey, B. J.; Brennan, M. S.; Herold, M. J.; Chang, C.; Guasconi, G.; Cauquil, N.; Melchiorre, F.; Guigal-Stephan, N.; Lockhart, B.; Colland, F.; Hickman, J. A.; Roberts, A. W.; Huang, D. C. S.; Wei, A. H.; Strasser, A.; Lessene, G.; Geneste, O. The MCL1 Inhibitor S63845 Is Tolerable and Effective in Diverse Cancer Models. *Nature* **2016**, *538* (7626), 477–482.
- (144) Carry, J.-C.; Garcia-Echeverria, C. Inhibitors of the P53/Hdm2 Protein–Protein Interaction—Path to the Clinic. *Bioorg. Med. Chem. Lett.* **2013**, *23* (9), 2480–2485.
- (145) Drennen, B.; Scheenstra, J. A.; Yap, J. L.; Chen, L.; Lanning, M. E.; Roth, B. M.; Wilder, P. T.; Fletcher, S. Structural Re-Engineering of the α -Helix Mimetic JY-1-106 into Small-Molecules: Disruption of the Mcl-1–Bak-BH3 Protein–Protein Interaction with 2,6-Di-Substituted Nicotinates. *ChemMedChem* **2016**, *11* (8), 827–833; E. Whiting, M. R. Raje, J. Chauhan, P. T. Wilder, D. Van Eker, S. J. Hughes, N. G. Bowen, G. E. A. Vickers, I. C. Fenimore, S. Fletcher, Discovery of Mcl-1 inhibitors based on a thiazolidine-2,4-dione scaffold. *Bioorg. Med. Chem. Lett.* **2018**, *28*, 523–528; I. L. Conlon, D. Van Eker, S. Abdelmalak, W. A. Murphy, H. Bashir, M. Sun, J. Chauhan, K. M. Varney, R. GodoyRuiz, P. T. Wilder, S. Fletcher, Kröhnke pyridines: Rapid and facile access to Mcl-1

- inhibitors. *Bioorg. Med. Chem. Lett.* **2018**, *28*, 1949–1953; M. E. Lanning, W. Yu, J. L. Yap, J. Chauhan, L. Chen, E. Whiting, L. S. Pidugu, T. Atkinson, H. Bailey, W. Li, B. M. Roth, L. Hynicka, K. Chesko, E. A. Toth, P. Shapiro, A. D. MacKerell Jr, P. T. Wilder, S. Fletcher, Structure-based design of N-substituted 1-hydroxy-4-sulfamoyl-2-naphthoates as selective inhibitors of the Mcl-1 oncoprotein. *Eur. J. Med. Chem.* **2016**, *113*, 273–292; M. E. Lanning, P. T. Wilder, H. Bailey, B. Drennen, M. Cavalier, L. Chen, J. L. Yap, M. Raje, S. Fletcher, Towards more drug-like proteomimetics: two-faced, synthetic α -helix mimetics based on a purine scaffold. *Org. Biomol. Chem.* **2015**, *13*, 8642–8646.
- (146) Fletcher, S. MCL-1 Inhibitors - Where Are We Now (2019)? *Expert Opin. Ther. Pat.* **2019**, *29* (11), 909–919; J. L. Yap, L. Chen, M. E. Lanning, S. Fletcher, *J. Med. Chem.* **2017**, *60*, 821–838.
- (147) Beloglazkina, A.; Zyk, N.; Majouga, A.; Beloglazkina, E. Recent Small-Molecule Inhibitors of the P53–MDM2 Protein–Protein Interaction. *Molecules* **2020**, *25* (5) <https://doi.org/10.3390/molecules25051211>.
- (148) AbbVie Announces US FDA Approval of Venclexta (venetoclax) as a Chemotherapy-Free Combination Regimen for Previously Untreated Chronic Lymphocytic Leukemia Patients <https://www.drugs.com/newdrugs/abbvie-announces-us-fda-approval-venclexta-venetoclax-chemotherapy-free-combination-regimen-4974.html>
- (149) Friberg, A.; Vigil, D.; Zhao, B.; Daniels, R. N.; Burke, J. P.; Garcia-Barrantes, P. M.; Camper, D.; Chauder, B. A.; Lee, T.; Olejniczak, E. T.; Fesik, S. W. Discovery of Potent Myeloid Cell Leukemia 1 (Mcl-1) Inhibitors Using Fragment-Based Methods and Structure-Based Design. *J. Med. Chem.* **2013**, *56* (1), 15–30.
- (150) Punnoose, E. A.; Levenson, J. D.; Peale, F.; Boghaert, E. R.; Belmont, L. D.; Tan, N.; Young, A.; Mitten, M.; Ingalla, E.; Darbonne, W. C.; Oleksijew, A.; Tapang, P.; Yue, P.; Oeh, J.; Lee, L.; Maiga, S.; Fairbrother, W. J.; Amiot, M.; Souers, A. J.; Sampath, D. Expression Profile of BCL-2, BCL-XL, and MCL-1 Predicts Pharmacological Response to the BCL-2 Selective Antagonist Venetoclax in Multiple Myeloma Models. *Mol. Cancer Ther.* **2016**, *15* (5), 1132–1144.
- (151) Konopleva, M.; Pollyea, D. A.; Potluri, J.; Chyla, B.; Hogdal, L.; Busman, T.; McKeegan, E.; Salem, A. H.; Zhu, M.; Ricker, J. L.; Blum, W.; DiNardo, C. D.; Kadia, T.; Dunbar, M.; Kirby, R.; Falotico, N.; Levenson, J.; Humerickhouse, R.; Mabry, M.; Stone, R.; Kantarjian, H.; Letai, A. Efficacy and Biological Correlates of Response in a Phase II Study of Venetoclax Monotherapy in Patients with Acute Myelogenous Leukemia. *Cancer Discov.* **2016**, *6* (10), 1106–1117.
- (152) Research, A. A. for C. BCL2/MDM2 Inhibitor Combo Effective in AML. *Cancer Discov.* **2019**, *9* (2), 156–156.

- (153) Seipel, K.; Schmitter, K.; Bacher, U.; Pabst, T. Rationale for a Combination Therapy Consisting of MCL1- and MEK-Inhibitors in Acute Myeloid Leukemia. *Cancers* **2019**, *11* (11). <https://doi.org/10.3390/cancers11111779>.
- (154) Reddy, A. S.; Zhang, S. Polypharmacology: Drug Discovery for the Future. *Expert Rev. Clin. Pharmacol.* **2013**, *6* (1). <https://doi.org/10.1586/ecp.12.74>.
- (155) Anighoro, A.; Bajorath, J.; Rastelli, G. Polypharmacology: Challenges and Opportunities in Drug Discovery. *J. Med. Chem.* **2014**, *57* (19), 7874–7887.
- (156) Rautureau, G. J. P.; Yabal, M.; Yang, H.; Huang, D. C. S.; Kvensakul, M.; Hinds, M. G. The Restricted Binding Repertoire of Bcl-B Leaves Bim as the Universal BH3-Only Prosurvival Bcl-2 Protein Antagonist. *Cell Death Dis.* **2012**, *3* (12), e443.
- (157) Wang, Z.; Song, T.; Feng, Y.; Guo, Z.; Fan, Y.; Xu, W.; Liu, L.; Wang, A.; Zhang, Z. Bcl-2/MDM2 Dual Inhibitors Based on Universal Pyramid-Like α -Helical Mimetics. *J. Med. Chem.* **2016**, *59* (7), 3152–3162.
- (158) Vaupel, A.; Bold, G.; De Pover, A.; Stachyra-Valat, T.; Hergovich Lisztwan, J.; Kallen, J.; Masuya, K.; Furet, P. Tetra-Substituted Imidazoles as a New Class of Inhibitors of the P53–MDM2 Interaction. *Bioorg. Med. Chem. Lett.* **2014**, *24* (9), 2110–2114.
- (159) Mady, A. S. A.; Liao, C.; Bajwa, N.; Kump, K. J.; Abulwerdi, F. A.; Lev, K. L.; Miao, L.; Grigsby, S. M.; Perdih, A.; Stuckey, J. A.; Du, Y.; Fu, H.; Nikolovska-Coleska, Z. Discovery of Mcl-1 Inhibitors from Integrated High Throughput and Virtual Screening. *Sci. Rep.* **2018**, *8*. <https://doi.org/10.1038/s41598-018-27899-9>.
- (160) Li, C.; Pazgier, M.; Li, C.; Yuan, W.; Liu, M.; Wei, G.; Lu, W.-Y.; Lu, W. Systematic Mutational Analysis of Peptide Inhibition of the P53-MDM2/MDMX Interactions. *J. Mol. Biol.* **2010**, *398* (2), 200–213.
- (161) Yin, H.; Lee, G.; Sedey, K. A.; Kutzki, O.; Park, H. S.; Orner, B. P.; Ernst, J. T.; Wang, H.-G.; Sebti, S. M.; Hamilton, A. D. Terphenyl-Based Bak BH3 α -Helical Proteomimetics as Low-Molecular-Weight Antagonists of Bcl-XL. *J. Am. Chem. Soc.* **2005**, *127* (29), 10191–10196.
- (162) Vassilev, L. T.; Vu, B. T.; Graves, B.; Carvajal, D.; Podlaski, F.; Filipovic, Z.; Kong, N.; Kammlott, U.; Lukacs, C.; Klein, C.; Fotouhi, N.; Liu, E. A. In Vivo Activation of the P53 Pathway by Small-Molecule Antagonists of MDM2. *Science* **2004**, *303* (5659), 844–848.

- (163) Bold, G.; Furet, P.; Gessier, F.; Kallen, J.; Lisztwan, J. H.; Masuya, K.; Vaupel, A. Tetra-Substituted Heteroaryl Compounds and Their Use as Mdm2 and/or Mdm4 Modulators. CA2771936A1, March 3, 2011.
- (164) Pelz, N. F.; Bian, Z.; Zhao, B.; Shaw, S.; Tarr, J. C.; Belmar, J.; Gregg, C.; Camper, D. V.; Goodwin, C. M.; Arnold, A. L.; Sensintaffar, J. L.; Friberg, A.; Rossanese, O. W.; Lee, T.; Olejniczak, E. T.; Fesik, S. W. Discovery of 2-Indole-Acylsulfonamide Myeloid Cell Leukemia 1 (Mcl-1) Inhibitors Using Fragment-Based Methods. *J. Med. Chem.* **2016**, *59* (5), 2054–2066.
- (165) Kapadiya, Dr. K.; Kavadia, K.; Manvar, P.; Kotadiya, R.; Kothari, R.; Ranjan, K. Catalyst Free Synthesis of Thiazole Derivatives Bearing Azo Imine Linkage as Antimicrobial Agents. *Chem. Biol. Interface* **2015**, *5*, 258–266.
- (166) Miyamoto, D. K.; Flaxman, H. A.; Wu, H.-Y.; Gao, J.; Woo, C. M. Discovery of a Celecoxib Binding Site on Prostaglandin E Synthase (PTGES) with a Cleavable Chelation-Assisted Biotin Probe. *ACS Chem. Biol.* **2019**, *14* (12), 2527–2532.
- (167) Gierse, J. K.; Zhang, Y.; Hood, W. F.; Walker, M. C.; Trigg, J. S.; Maziasz, T. J.; Koboldt, C. M.; Muhammad, J. L.; Zweifel, B. S.; Masferrer, J. L.; Isakson, P. C.; Seibert, K. Valdecoxib: Assessment of Cyclooxygenase-2 Potency and Selectivity. *J. Pharmacol. Exp. Ther.* **2005**, *312* (3), 1206–1212.
- (168) Guvench, O.; Jr, A. D. M. Computational Fragment-Based Binding Site Identification by Ligand Competitive Saturation. *PLoS Comput. Biol.* **2009**, *5* (7), e1000435.
- (169) Raman, E. P.; Yu, W.; Lakkaraju, S. K.; MacKerell, A. D. Inclusion of Multiple Fragment Types in the Site Identification by Ligand Competitive Saturation (SILCS) Approach. *J. Chem. Inf. Model.* **2013**, *53* (12), 3384–3398.
- (170) Ustach, V. D.; Lakkaraju, S. K.; Jo, S.; Yu, W.; Jiang, W.; MacKerell, A. D. Optimization and Evaluation of Site-Identification by Ligand Competitive Saturation (SILCS) as a Tool for Target-Based Ligand Optimization. *J. Chem. Inf. Model.* **2019**, *59* (6), 3018–3035.
- (171) Raman, E. P.; Yu, W.; Guvench, O.; MacKerell, A. D. Reproducing Crystal Binding Modes of Ligand Functional Groups Using Site-Identification by Ligand Competitive Saturation (SILCS) Simulations. *J. Chem. Inf. Model.* **2011**, *51* (4), 877–896.
- (172) Small, M.; MacKerell, A. D. Force Field Representation of Biomolecular Systems. In *In Silico Drug Discovery and Design: Theory, Methods, Challenges, and Applications*; Cavasotto, C. N., Series Ed.; CRC Press, 2015.

- (173) Z. Nikolovska-Coleska, R. Wang, X. Fang, H. Pan, Y. Tomita, P. Li, P. P. Roller, K. Krajewski, N. G. Saito, J. A. Stuckey, S. Wang, *Anal. Biochem.* **2004**, *332*, 261-273.
- (174) Willis S.N., Chen, L., Dewson, G., Wei, A., Naik E., Fletcher J. I., Adams, J. M., Huang, D. C. S. Proapoptotic Bak is sequestered by Mcl-1 and Bcl-xL, but not Bcl-2, until displaced by BH3-only proteins. *Genes Dev.* **2005**, *19* (11), 1294-1305.
- (175) Stewart, M. L., Fire, E., Keating, A. E., Walensky, L. D. The Mcl-1 BH3 helix is an exclusive Mcl-1 inhibitor and apoptosis sensitizer. *Nat Chem Biol.* **2010**, *6* (8), 595-601.
- (176) Popowicz G.M., Czarna A., Holak T.A.. Structure of the human Mdmx protein bound to the p53 tumor suppressor transactivation domain. *Cell Cycle.* **2008**, *7* (15), 2441-3.
- (177) Nikolovska-Coleska Z., Wang R., Fang X., Pan H., Tomita Y., Li P., et al. Development and optimization of a binding assay for the XIAP BIR3 domain using fluorescence polarization. *Anal Biochem.* **2004**, *332* (2), 261-73.
- (178) Zhang J.H., Chung T.D., Oldenburg K.R. A Simple Statistical Parameter for Use in Evaluation and Validation of High Throughput Screening Assays. *J Biomol Screen.* **1999**, *4* (2), 67-73.
- (179) Akgul, C. Mcl-1 Is a Potential Therapeutic Target in Multiple Types of Cancer. *Cellular and Molecular Life Sciences* **2009**, *66* (8), 1326–1336.
- (180) Lee, E. F.; Harris, T. J.; Tran, S.; Evangelista, M.; Arulananda, S.; John, T.; Ramnac, C.; Hobbs, C.; Zhu, H.; Gunasingh, G.; Segal, D.; Behren, A.; Cebon, J.; Dobrovic, A.; Mariadason, J. M.; Strasser, A.; Rohrbeck, L.; Haass, N. K.; Herold, M. J.; Fairlie, W. D. BCL-XL and MCL-1 Are the Key BCL-2 Family Proteins in Melanoma Cell Survival. *Cell Death Dis* **2019**, *10* (5), 342.
- (181) Derenne, S.; Monia, B.; Dean, N. M.; Taylor, J. K.; Rapp, M.-J.; Harousseau, J.-L.; Bataille, R.; Amiot, M. Antisense Strategy Shows That Mcl-1 Rather than Bcl-2 or Bcl-x(L) Is an Essential Survival Protein of Human Myeloma Cells. *Blood* **2002**, *100* (1), 194–199.
- (182) Abulwerdi, F.; Liao, C.; Liu, M.; Azmi, A. S.; Aboukameel, A.; Mady, A. S. A.; Gulappa, T.; Cierpicki, T.; Owens, S.; Zhang, T.; Sun, D.; Stuckey, J. A.; Mohammad, R. M.; Nikolovska-Coleska, Z. A Novel Small-Molecule Inhibitor of Mcl-1 Blocks Pancreatic Cancer Growth in Vitro and in Vivo. *Mol. Cancer Ther.* **2014**, *13* (3), 565–575.

- (183) Friberg, A.; Vigil, D.; Zhao, B.; Daniels, R. N.; Burke, J. P.; Garcia-Barrantes, P. M.; Camper, D.; Chauder, B. A.; Lee, T.; Olejniczak, E. T.; Fesik, S. W. Discovery of Potent Myeloid Cell Leukemia 1 (Mcl-1) Inhibitors Using Fragment-Based Methods and Structure-Based Design. *J. Med. Chem.* **2013**, *56* (1), 15–30.
- (184) Punnoose, E. A.; Levenson, J. D.; Peale, F.; Boghaert, E. R.; Belmont, L. D.; Tan, N.; Young, A.; Mitten, M.; Ingalla, E.; Darbonne, W. C.; Oleksijew, A.; Tapang, P.; Yue, P.; Oeh, J.; Lee, L.; Maiga, S.; Fairbrother, W. J.; Amiot, M.; Souers, A. J.; Sampath, D. Expression Profile of BCL-2, BCL-XL, and MCL-1 Predicts Pharmacological Response to the BCL-2 Selective Antagonist Venetoclax in Multiple Myeloma Models. *Mol Cancer Ther* **2016**, *15* (5), 1132–1144.
- (185) Pelz, N. F.; Bian, Z.; Zhao, B.; Shaw, S.; Tarr, J. C.; Belmar, J.; Gregg, C.; Camper, D. V.; Goodwin, C. M.; Arnold, A. L.; Sensintaffar, J. L.; Friberg, A.; Rossanese, O. W.; Lee, T.; Olejniczak, E. T.; Fesik, S. W. Discovery of 2-Indole-Acylsulfonamide Myeloid Cell Leukemia 1 (Mcl-1) Inhibitors Using Fragment-Based Methods. *J. Med. Chem.* **2016**, *59* (5), 2054–2066.
- (186) Phase I Study of S64315 Administred Intravenously in Patients With Acute Myeloid Leukaemia or Myelodysplastic Syndrome - Full Text View - ClinicalTrials.gov <https://clinicaltrials.gov/ct2/show/NCT02979366>
- (187) Phase I Study of MIK665, a Mcl-1 Inhibitor, in Patients With Refractory or Relapsed Lymphoma or Multiple Myeloma - Full Text View - ClinicalTrials.gov <https://clinicaltrials.gov/ct2/show/NCT02992483>
- (188) Lanning, M. E.; Fletcher, S. Recapitulating the α -Helix: Nonpeptidic, Low-Molecular-Weight Ligands for the Modulation of Helix-Mediated Protein–Protein Interactions. *Future Medicinal Chemistry* **2013**, *5* (18), 2157–2174.
- (189) Amgen halts trials on cardiac toxicity <https://www.evaluate.com/vantage/articles/news/snippets/amgen-halts-trials-cardiac-toxicity>
- (190) Beekman, A. M.; Howell, L. A. Small-Molecule and Peptide Inhibitors of the Pro-Survival Protein Mcl-1. *ChemMedChem* **2016**, *11* (8), 802–813.
- (191) Barnard, A.; Long, K.; Yeo, D. J.; Miles, J. A.; Azzarito, V.; Burslem, G. M.; Prabhakaran, P.; A Edwards, T.; Wilson, A. J. Orthogonal Functionalisation of α -Helix Mimetics. *Org. Biomol. Chem.* **2014**, *12* (35), 6794–6799.
- (192) Petros, A. M.; Olejniczak, E. T.; Fesik, S. W. Structural Biology of the Bcl-2 Family of Proteins. *Biochim. Biophys. Acta* **2004**, *1644* (2–3), 83–94.

- (193) Azzarito, V.; Long, K.; Murphy, N. S.; Wilson, A. J. Inhibition of α -Helix-Mediated Protein-Protein Interactions Using Designed Molecules. *Nat Chem* **2013**, *5* (3), 161–173.
- (194) Lanning, M. E.; Fletcher, S. Multi-Facial, Non-Peptidic α -Helix Mimetics. *Biology (Basel)* **2015**, *4* (3), 540–555.
- (195) Jayatunga, M. K. P.; Thompson, S.; Hamilton, A. D. α -Helix Mimetics: Outwards and Upwards. *Bioorganic & Medicinal Chemistry Letters* **2014**, *24* (3), 717–724.
- (196) Yin, H.; Lee, G.-I.; Sedey, K. A.; Kutzki, O.; Park, H. S.; Orner, B. P.; Ernst, J. T.; Wang, H.-G.; Sebti, S. M.; Hamilton, A. D. Terphenyl-Based Bak BH3 Alpha-Helical Proteomimetics as Low-Molecular-Weight Antagonists of Bcl-XL. *J. Am. Chem. Soc.* **2005**, *127* (29), 10191–10196.
- (197) Kazi, A.; Sun, J.; Doi, K.; Sung, S.-S.; Takahashi, Y.; Yin, H.; Rodriguez, J. M.; Becerril, J.; Berndt, N.; Hamilton, A. D.; Wang, H.-G.; Sebti, S. M. The BH3 α -Helical Mimic BH3-M6 Disrupts Bcl-XL, Bcl-2, and MCL-1 Protein-Protein Interactions with Bax, Bak, Bad, or Bim and Induces Apoptosis in a Bax- and Bim-Dependent Manner. *J Biol Chem* **2011**, *286* (11), 9382–9392.
- (198) Yap, J. L.; Cao, X.; Vanommeslaeghe, K.; Jung, K.-Y.; Peddaboina, C.; Wilder, P. T.; Nan, A.; MacKerell, A. D.; Smythe, W. R.; Fletcher, S. Relaxation of the Rigid Backbone of an Oligoamide-Foldamer-Based α -Helix Mimetic: Identification of Potent Bcl-XL Inhibitors. *Org. Biomol. Chem.* **2012**, *10* (15), 2928–2933.
- (199) Drennen, B.; Scheenstra, J. A.; Yap, J. L.; Chen, L.; Lanning, M. E.; Roth, B. M.; Wilder, P. T.; Fletcher, S. Structural Re-Engineering of the α -Helix Mimetic JY-1-106 into Small-Molecules: Disruption of the Mcl-1–Bak-BH3 Protein–Protein Interaction with 2,6-Di-Substituted Nicotinates. *ChemMedChem* **2016**, *11* (8), 827–833.
- (200) Lanning, M. E.; Wilder, P. T.; Bailey, H.; Drennen, B.; Cavalier, M.; Chen, L.; Yap, J. L.; Raje, M.; Fletcher, S. Towards More Drug-like Proteomimetics: Two-Faced, Synthetic α -Helix Mimetics Based on a Purine Scaffold. *Org. Biomol. Chem.* **2015**, *13* (32), 8642–8646.
- (201) Tron, A. E.; Belmonte, M. A.; Adam, A.; Aquila, B. M.; Boise, L. H.; Chiarparin, E.; Cidado, J.; Embrey, K. J.; Gangl, E.; Gibbons, F. D.; Gregory, G. P.; Hargreaves, D.; Hendricks, J. A.; Johannes, J. W.; Johnstone, R. W.; Kazmirski, S. L.; Kettle, J. G.; Lamb, M. L.; Matulis, S. M.; Nooka, A. K.; Packer, M. J.; Peng, B.; Rawlins, P. B.; Robbins, D. W.; Schuller, A. G.; Su, N.; Yang, W.; Ye, Q.; Zheng, X.; Secrist, J. P.; Clark, E. A.; Wilson, D. M.; Fawell, S. E.; Hird, A. W. Discovery of Mcl-1-Specific Inhibitor AZD5991 and Preclinical Activity in Multiple Myeloma and Acute Myeloid Leukemia. *Nat Commun* **2018**, *9*.

- (202) Wang, Z.; Song, T.; Feng, Y.; Guo, Z.; Fan, Y.; Xu, W.; Liu, L.; Wang, A.; Zhang, Z. Bcl-2/MDM2 Dual Inhibitors Based on Universal Pyramid-Like α -Helical Mimetics. *J. Med. Chem.* **2016**, *59* (7), 3152–3162.
- (203) Szlávik, Z.; Ondi, L.; Csékei, M.; Paczal, A.; Szabó, Z. B.; Radics, G.; Murray, J.; Davidson, J.; Chen, I.; Davis, B.; Hubbard, R. E.; Pedder, C.; Dokurno, P.; Surgenor, A.; Smith, J.; Robertson, A.; LeToumelin-Braizat, G.; Cauquil, N.; Zarka, M.; Demarles, D.; Perron-Sierra, F.; Claperon, A.; Colland, F.; Geneste, O.; Kotschy, A. Structure-Guided Discovery of a Selective Mcl-1 Inhibitor with Cellular Activity. *J. Med. Chem.* **2019**, *62* (15), 6913–6924.
- (204) Kotschy, A.; Szlavik, Z.; Murray, J.; Davidson, J.; Maragno, A. L.; Le Toumelin-Braizat, G.; Chanrion, M.; Kelly, G. L.; Gong, J.-N.; Moujalled, D. M.; Bruno, A.; Csekei, M.; Paczal, A.; Szabo, Z. B.; Sipos, S.; Radics, G.; Prosenyak, A.; Balint, B.; Ondi, L.; Blasko, G.; Robertson, A.; Surgenor, A.; Dokurno, P.; Chen, I.; Matassova, N.; Smith, J.; Pedder, C.; Graham, C.; Studeny, A.; Lysiak-Auvity, G.; Girard, A.-M.; Gravé, F.; Segal, D.; Riffkin, C. D.; Pomilio, G.; Galbraith, L. C. A.; Aubrey, B. J.; Brennan, M. S.; Herold, M. J.; Chang, C.; Guasconi, G.; Cauquil, N.; Melchiorre, F.; Guigal-Stephan, N.; Lockhart, B.; Colland, F.; Hickman, J. A.; Roberts, A. W.; Huang, D. C. S.; Wei, A. H.; Strasser, A.; Lessene, G.; Geneste, O. The MCL1 Inhibitor S63845 Is Tolerable and Effective in Diverse Cancer Models. *Nature* **2016**, *538* (7626), 477–482.
- (205) Conlon, I. L.; Drennen, B.; Lanning, M. E.; Hughes, S.; Rothhaas, R.; Wilder, P. T.; MacKerell Jr., A. D.; Fletcher, S. Rationally Designed Polypharmacology: α -Helix Mimetics as Dual Inhibitors of the Oncoproteins Mcl-1 and HDM2. *ChemMedChem* **2020**, *In Press*.
- (206) Hird, A. W.; Tron, A. E. Recent Advances in the Development of Mcl-1 Inhibitors for Cancer Therapy. *Pharmacology & Therapeutics* **2019**, *198*, 59–67.
- (207) Yu, W.; Lakkaraju, S. K.; Raman, E. P.; MacKerell, A. D. Site-Identification by Ligand Competitive Saturation (SILCS) Assisted Pharmacophore Modeling. *J. Comput Aided Mol Des* **2014**, *28* (5), 491–507.
- (208) Ustach, V. D.; Lakkaraju, S. K.; Jo, S.; Yu, W.; Jiang, W.; MacKerell, A. D. Optimization and Evaluation of Site-Identification by Ligand Competitive Saturation (SILCS) as a Tool for Target-Based Ligand Optimization. *J. Chem. Inf. Model.* **2019**, *59* (6), 3018–3035.
- (209) Raman, E. P.; Yu, W.; Lakkaraju, S. K.; MacKerell, A. D. Inclusion of Multiple Fragment Types in the Site Identification by Ligand Competitive Saturation (SILCS) Approach. *J. Chem. Inf. Model.* **2013**, *53* (12), 3384–3398.

- (210) Lee, T.; Bian, Z.; Zhao, B.; Hogdal, L. J.; Sensintaffar, J. L.; Goodwin, C. M.; Belmar, J.; Shaw, S.; Tarr, J. C.; Veerasamy, N.; Matulis, S. M.; Koss, B.; Fischer, M. A.; Arnold, A. L.; Camper, D. V.; Browning, C. F.; Rossanese, O. W.; Budhraj, A.; Opferman, J.; Boise, L. H.; Savona, M. R.; Letai, A.; Olejniczak, E. T.; Fesik, S. W. Discovery and Biological Characterization of Potent Myeloid Cell Leukemia-1 Inhibitors. *FEBS Letters* **2017**, *591* (1), 240–251.
- (211) Yu, W.; Jo, S.; Lakkaraju, S. K.; Weber, D. J.; MacKerell, A. D. Exploring Protein-Protein Interactions Using the Site-Identification by Ligand Competitive Saturation (SILCS) Methodology. *Proteins* **2019**, *87* (4), 289–301.
- (212) Nikolovska-Coleska, Z.; Wang, R.; Fang, X.; Pan, H.; Tomita, Y.; Li, P.; Roller, P. P.; Krajewski, K.; Saito, N. G.; Stucky, J. A.; Wang, S. *Anal. Biochem.* **2004**, *332*, 261–273.
- (213) Willis S.N., Chen, L., Dewson, G., Wei, A., Naik E., Fletcher J. I., Adams, J. M., Huang, D. C. S. Proapoptotic Bak is sequestered by Mcl-1 and Bcl-xL, but not Bcl-2, until displaced by BH3-only proteins. *Genes Dev.* **2005**, *19* (11), 1294-1305
- (214) Stewart, M. L., Fire, E., Keating, A. E., Walensky, L. D. The Mcl-1 BH3 helix is an exclusive Mcl-1 inhibitor and apoptosis sensitizer. *Nat Chem Biol.* **2010**, *6* (8), 595-601.
- (215) Nikolovska-Coleska Z., Wang R., Fang X., Pan H., Tomita Y., Li P., et al. Development and optimization of a binding assay for the XIAP BIR3 domain using fluorescence polarization. *Anal Biochem.* **2004**, *332* (2), 261-73.
- (216) Zhang J.H., Chung T.D., Oldenburg K.R. A Simple Statistical Parameter for Use in Evaluation and Validation of High Throughput Screening Assays. *J Biomol Screen.* **1999**, *4* (2), 67-73.
- (217) (a) Fletcher, S.; Hamilton, A. D. *Curr. Opin. Chem. Biol.* **2005**, *9*, 632–638; (b) Arkin, M. R.; Wells, J. A. *Nat. Rev. Drug Discov.* **2004**, *3*, 301–317.
- (218) Reed, J. C. *Nat. Rev. Drug Discov.* **2002**, *2*, 111-121.
- (219) Youle, R. J.; Strasser, A. *Nat. Rev. Mol. Cell Biol.* **2008**, *1*, 47-59.
- (220) Czabotar, P. E.; Lessene, G.; Strasser, A.; Adams, J. M. *Nat. Rev. Mol. Cell Biol.* **2014**, *1*, 49-63.
- (221) Willis, S. N.; Fletcher, J. I.; Kaufmann, T.; van Delft, M. F.; Chen, L.; Czabotar, P. E.; Ierino, H.; Lee, E. F.; Fairlie, W. D.; Bouillet, P.; Strasser, A.; Kluck, R. M.; Adams, J. M.; Huang, D. C. *Science* **2007**, *5813*, 856-859.

- (222) Kim, H.; Rafiuddin-Shah, M.; Tu, H. C.; Jeffers, J. R.; Zambetti, G. P.; Hsieh, J. J.; Cheng, E. H. *Nat. Cell Biol.* **2006**, *12*, 1348-1358.
- (223) Sattler, M.; Liang, H.; Nettessheim, D.; Meadows, R. P.; Harlan, J. E.; Eberstadt, M.; Yoon, H. S.; Shuker, S. B.; Chang, B. S.; Minn, A. J.; Thompson, C. B.; Fesik, S. W. *Science* **1997**, *5302*, 983-986.
- (224) Yap, J. L.; Chen, L.; Lanning, M. E.; Fletcher, S. *J. Med. Chem.* **2017**, doi: 10.1021/acs.jmedchem.5b01888
- (225) Cerella, C.; Gaigneaux, A.; Mazumder, A.; Lee, J.-Y.; Saland, E.; Radogna, F.; Farge, T.; Vergez, F.; Récher, C.; Sarry, J.-E.; Kim, K.-W.; Shin, H. Y.; Dicato, M.; Deiderich, M. *Leukemia* **2017**, *31*, 755–759.
- (226) Punnoose, E. A.; Levenson, J. D.; Peale, F.; Boghaert, E. R.; Belmont, L. D.; Tan, N.; Young, A.; Mitten, M.; Ingalla, E.; Darbonne, W. C.; Oleksijew, A.; Tapang, P.; Yue, P.; Oeh, J.; Lee, L. Maiga, S.; Fairbrother, W. J.; Aimot, M.; Souers, A. J.; Sampath, D. *Mol. Cancer Ther.* **2016**, *15*, 1132–1144.
- (227) Salerni, B. L.; Bates, D. J.; Albershardt, T. C.; Lowrey, C. H.; Eastman, A. *Mol. Cancer Ther.* **2010**, *9*, 791–802.
- (228) Luedtke, D. A.; Niu, X.; Pan, Y.; Zhao, J.; Liu, S.; Edwards, H.; Chen, K.; Lin, H.; Taub, J. W.; Ge, Y. *Signal Trans.. Targeted Ther.* **2017**, 17012.
- (229) Chen, L.; Fletcher, S. *Expert. Opin. Ther. Pat.* **2017**, *27*, 163–178.
- (230) <https://www.cancer.gov/about-cancer/treatment/clinical-trials/search/v?id=NCI-2016-00888&r=1>
- (231) <https://www.cancer.gov/about-cancer/treatment/clinical-trials/search/v?id=NCI-2017-00472&r=1>
- (232) Belmar, J.; Fesik, S. W. *Pharmacol. Ther.* **2015**, *145*, 76 – 84.
- (233) (a) Friberg, A.; Vigil, D.; Zhao, B.; Daniels, R. N.; Burke, J. P.; Garcia-Barrantes, P. M.; Camper, D.; Chauder, B. A.; Lee, T.; Olejniczak, E. T.; Fesik, S. W. *J. Med. Chem.* **2013**, *56*, 15–30; (b) Pelz, N. F.; Bian, Z.; Zhao, B.; Shaw, S.; Tarr, J. C.; Belmar, J.; Gregg, C.; Camper, D. V.; Goodwin, C. M.; Arnold, A. L.; Sensintaffar, J. L.; Friberg, A.; Rossanese, O. W.; Lee, T.; Olejniczak, E. T.; Fesik, S. W. *J. Med. Chem.* **2016**, *59*, 2054–2066; (c) Shaw, S.; Bian, Z.; Zhao, B.; Tarr, J. C.; Veerasamy, N.; Jeon, K.; Belmar, J.; Arnold, A. L.; Fogarty, S. A.; Perry, E.; Sensintaffar, J. L.; Camper, D. V.; Rossanese, O. W.; Lee, T.; Olejniczak, E. T.; Fesik, S. W.; *J. Med. Chem.* **2018**; DOI: 10.1021/acs.jmedchem.7b01155

- (234) Levenson, J. D.; Zhang, H.; Chen, J.; Tahir, S. K.; Phillips, D. C.; Xue, J.; Nimmer, P.; Jin, S.; Smith, M.; Xiao, Y.; Kovar, P.; Tanaka, A.; Bruncko, M.; Sheppard, G. S.; Wang, L.; Gierke, S.; Kategaya, L.; Anderson, D. J.; Wong, C.; Eastham-Anderson, J.; Ludlam, M. J. C.; Sampath, D.; Fairbrother, W. J.; Wertz, I.; Rosenberg, S. H.; Tse, C.; Elmore, S. W.; Souers, A. J. *Cell Death Dis.* **2015**, *6*, e1590.
- (235) Kotschy, A.; Szlavik, Z.; Murray, J.; Davidson, J.; Maragno, A. L.; Le Toumelin-Braizat, G.; Chanrion, M.; Kelly, G. L.; Gong, J.-N.; Moujalled, D. M.; Bruno, A.; Csekei, M.; Paczal, A.; Szabo, Z. B.; Sipos, S.; Radics, G.; Proszenyak, A.; Balint, B.; Ondi, L.; Blasko, G.; Robertson, A.; Surgenor, A.; Dokurno, P.; Chen, I.; Matassova, N.; Smith, J.; Pedder, C.; Graham, C.; Studeny, A.; Lysiak-Auvity, G.; Gravé, F.; Segal, D.; Riffkin, C. D.; Pomilio, G.; Galbraith, L. C. A.; Aubrey, B. J.; Brennan, M. S.; Herold, M. J.; Chang, C.; Guasconi, G.; Cauquil, N.; Melchiorre, F.; Guigal-Stephan, N.; Lockhart, B.; Colland, F.; Hickman, J. A.; Roberts, A. W.; Huang, D. C. S.; Wei, A. H.; Strasser, A.; Lessene, G.; Geneste, O. *Nature* **2016**, *538*, 477–482.
- (236) Chen, L.; Wilder, P. T.; Drennen, B.; Tran, J.; Roth, B. M.; Chesko, K.; Shapiro, P.; Fletcher, S. *Org. Biomol. Chem.* **2016**, *14*, 5505–5510; (b) Lanning, M. E.; Yu, W.; Yap, J. L.; Chauhan, J.; Chen, L.; Whiting, E.; Pidugu, L. S.; Atkinson, T.; Bailey, H.; Li, W.; Roth, B. M.; Hynicka, L.; Chesko, K.; Toth, E. A.; Shapiro, P.; MacKerell, A. D.; Wilder, P. T.; Fletcher, S. *Eur. J. Med. Chem.* **2016**, *113*, 273–292; (c) Whiting, E.; Raje, M. R.; Chauhan, J.; Wilder, P. T.; Van Eker, D.; Hughes, S. J.; Bowen, N. G.; Vickers, G. E. A.; Fenimore, I. C.; Fletcher, S. *Bioorg. Med. Chem. Lett.* **2018**.
- (237) (a) Akcay, G.; Belmonte, M. A.; Aquila, B.; Chauhui, C.; Hird, A. W.; Lamb, M. L.; Rawlins, R. B.; Su, N.; Tentarelli, S.; Grimster, N. P.; Su, O. *Nat. Chem. Biol.* **2016**, *12*, 931–936; (b) Lee, S.; Wales, T. E.; Escudero, S.; Cohen, D. T.; Luccarelli, J.; Gallagher, C. G.; Cohen, N. A.; Huhn, A. J.; Bird, G. H.; Engen, J. R.; Walensky, L. D. *Nat. Struct. Mol. Biol.* **2016**, *23*, 600–607.
- (238) Drennen, B.; Scheenstra, J. A.; Yap, J. L.; Chen, L.; Lanning, M. E.; Roth, B. M.; Wilder, P. T.; Fletcher, S. *ChemMedChem* **2016**, *11*, 827–833.
- (239) Lessene, G.; Czabotar, P. E.; Sleebs, B. E.; Zobel, K.; Loews, K. N.; Adams, J. M.; Baell, J. B.; Colman, P. M.; Deshaves, K.; Fairbrother, W. J.; Flygare, J. A.; Gibbons, P.; Kersten, W. J.; Kulasegaram, S.; Moss, R. M.; Parisot, J. P.; Smith, B. J.; Street, I. P.; Yang, H.; Huang, D. C.; Watson, K. G. *Nat. Chem. Biol.* **2013**, *9*, 390–397.
- (240) Kröhnke, F.; Zecher, W. *Angew. Chem.* **1962**, *74*, 811–817.

- (241) Hart, J. R.; Garner, A. L.; Yu, J.; Ito, Y.; Sun, M.; Ueno, L.; Rhee, J. K.; Baksh, M. M.; Stefan, E.; Hartl, M.; Bister, K.; Vogt, P. K.; Janda, K. D. *Proc. Natl. Acad. Sci. USA* **2014**, *111*, 12556–12561.
- (242) Karki, R.; Park, C.; Jun, K. Y.; Kadayat, T. M.; Lee, E. S.; Kwon, Y. *Eur. J. Med. Chem.* **2015**, *90*, 360–378.
- (243) Nikolovska-Coleska, Z.; Wang, R.; Fang, X.; Pan, H.; Tomita, Y.; Li, P.; Roller, P. P.; Krajewski, K.; Saito, N. G.; Stucky, J. A.; Wang, S. *Anal. Biochem.* **2004**, *332*, 261–273.
- (244) Mori, S., et al., Improved sensitivity of HSQC spectra of exchanging protons at short interscan delays using a new fast HSQC (FHSQC) detection scheme that avoids water saturation. *J Magn Reson B*, 1995. **108**(1): p. 94-8.
- (245) Marion, D., et al., Overcoming the overlap problem in the assignment of ¹H NMR spectra of larger proteins by use of three-dimensional heteronuclear ¹H-¹⁵N Hartmann-Hahn-multiple quantum coherence and nuclear Overhauser-multiple quantum coherence spectroscopy: application to interleukin 1 beta. *Biochemistry*, 1989. **28**(15): p. 6150-6.
- (246) Bax, A. and M. Ikura, An efficient 3D NMR technique for correlating the proton and ¹⁵N backbone amide resonances with the alpha-carbon of the preceding residue in uniformly ¹⁵N/¹³C enriched proteins. *J Biomol NMR*, 1991. **1**(1): p. 99-104.
- (247) Delaglio, F., et al., NMRPipe: a multidimensional spectral processing system based on UNIX pipes. *J Biomol NMR*, 1995. **6**(3): p. 277-93.
- (248) Edison, A.S., et al., Practical introduction to theory and implementation of multinuclear, multidimensional nuclear magnetic resonance experiments. *Methods Enzymol*, 1994. **239**: p. 3-79.
- (249) Live, D.H., Davis, D.G., Agosta, W.C., and Cowburn, D., *J. Am. Chem. Soc.*, 1984(106): p. 1939-1941.
- (250) Spera, S., M. Ikura, and A. Bax, Measurement of the exchange rates of rapidly exchanging amide protons: application to the study of calmodulin and its complex with a myosin light chain kinase fragment. *J Biomol NMR*, 1991. **1**(2): p. 155-65.
- (251) Nikolovska-Coleska, Z., et al., Development and optimization of a binding assay for the XIAP BIR3 domain using fluorescence polarization. *Analytical biochemistry*, 2004. **332**(2): p. 261-73.
- (252) Zhang, S.-G.; Liang, C.-G.; Zhang, W.-H. *Molecules* **2018**, *23*, 2783.

- (253) Gaikwada, D. D.; Chapolikara, A. D.; Devkatea, C. G.; Warada, K. D.; Tayadea, A. P.; Pawarb, R. P.; Dombc, A. J. *Eur. J. Med. Chem.* **2015**, *90*, 707–731.
- (254) Wilmes, L. J.; Pallavicini, M. G.; Fleming, L. M.; Gibbs, J.; Wang, D.; Li, K. L.; Partridge, S. C.; Henry, R. G.; Shalinsky, D. R.; Hu-Lowe, D.; Park, J. W.; McShane, T. M.; Lu, Y.; Brasch, R. C.; Hylton, N. M. *Magn. Reson. Imaging* **2007**, *25*, 319–27.
- (255) Tash, J. S.; Attardi, B.; Hild, S. A.; Chakrasali, R.; Jakkaraj, S. R.; Georg, G. I. *Biol. Reprod.* **2008**, *78*, 1127–1138.
- (256) Eicher, T.; Hauptmann, S.; Speicher, A. Structures, Reactions, Synthesis, and Applications, 3rd, Completely Revised and Enlarged Edition; Wiley-VCH: Weinheim, 2013.
- (257) O'Dell, D. K.; Nicholas, K. M. *Heterocycles* **2004**, *63*, 373–382.
- (258) Cho, C. S.; Lim, D. W.; Heo, N. H.; Kim, T.-J.; Sim, S. C. *Chem. Commun.* **2004**, 104–105.
- (259) Wei, W.; Wang, Z.; Yang, X.K.; Yu, W.Q.; Chang, J.B. *Adv. Synth. Catal.* **2017**, *359*, 3378–3387.
- (260) Zhang, Z. G.; Huang, Y. Y.; Huang, G. Q.; Zhang, G. S.; Liu, Q. F. *J. Heterocyclic Chem.* **2017**, *54*, 2426–2433
- (261) Lukin, K.; Hsu, M. C.; Fernando, D.; Leanna, M. R. *J. Org. Chem.* **2006**, *71*, 8166–8172
- (262) Wang, Q.; Li, X. W. *Org. Lett.* **2016**, *18*, 2102–2105.
- (263) Chen, G. H.; Hu, M. L.; Peng, Y. G. *J. Org. Chem.* **2018**, *83*, 1591–1597.
- (264) Counciller, C. M.; Eichman, C. C.; Wray, B. C.; Stambuli, J. P. *Org. Lett.* **2008**, *10*, 1021–1023.
- (265) Paul, S.; Panda, S.; Manna, D. *Tetrahedron Lett.* **2014**, *55*, 2480–2483.
- (266) Wipf, P.; Miller, C. P. *J. Org. Chem.* **1993**, *58*, 3604–3606.
- (268) Van Eker, D.; Chauhan, J.; Murphy, W. A.; Conlon, I. L.; Fletcher, S. *Tetrahedron Lett.* **2016**, *57*, 5301–5303.
- (269) Whiting, E.; Lanning, M. E.; Scheenstra, J. A.; Fletcher, S. *J. Org. Chem.* **2015**, *80*, 1229–1234.

- (270) Mitsunobu, O.; Yamada, M. *Bull. Chem. Soc. Jpn.* **1967**, *40*, 2380–2382.
- (271) Kumara Swamy, K. C.; Bhuvan Kumar, N. N.; Balaraman, E.; Pavan Kumar, K. V. P.; *Chem. Rev.* **2009**, *109*, 2551–2651.
- (272) Fletcher, S. *Org. Chem. Front.* **2015**, *2*, 739–752.
- (273) Fletcher, S.; Shahani, V. M.; Gunning, P. T. *Tetrahedron Lett.* **2009**, *50*, 4258–4261.
- (274) P.-E. Broutin, P. Hilty and A. W. Thomas, *Tetrahedron Lett.* **2003**, *44*, 6429–6432.
- (275) Luca, L. D.; Giacomelli, G.; Porcheddu, A. *J. Org. Chem.* **2002**, *67*, 6272–6274.
- (276) Taber, D. F.; Tian, W. *J. Am. Chem. Soc.* **2006**, *128*, 1058–1059.
- (277) Lanning, M. E.; Fletcher, S. *Tetrahedron Lett.* **2013**, *54*, 4624–4628.
- (278) Pei, H.; Peng, Y.; Zhao, Q.; Chen, Y. Small Molecule PROTACs: An Emerging Technology for Targeted Therapy in Drug Discovery. *RSC Advances* **2019**, *9* (30), 16967–16976.
- (279) Lai, A. C.; Crews, C. M. Induced Protein Degradation: An Emerging Drug Discovery Paradigm. *Nat Rev Drug Discov* **2017**, *16* (2), 101–114.
- (280) Meyer-Schwesinger, C. The Ubiquitin–Proteasome System in Kidney Physiology and Disease. *Nature Reviews Nephrology* **2019**, *15* (7), 393–411.
- (281) Sakamoto, K. M.; Kim, K. B.; Verma, R.; Ransick, A.; Stein, B.; Crews, C. M.; Deshaies, R. J. Development of Protacs to Target Cancer-Promoting Proteins for Ubiquitination and Degradation. *Molecular & Cellular Proteomics* **2003**, *2* (12), 1350–1358.
- (282) Konstantinidou, M.; Li, J.; Zhang, B.; Wang, Z.; Shaabani, S.; Ter Brake, F.; Essa, K.; Dömling, A. PROTACs– a Game-Changing Technology. *Expert Opinion on Drug Discovery* **2019**, *14* (12), 1255–1268.
- (283) Bondeson, D. P.; Crews, C. M. Targeted Protein Degradation by Small Molecules. *Annu. Rev. Pharmacol. Toxicol.* **2017**, *57*, 107–123.
- (284) Schapira, M.; Calabrese, M. F.; Bullock, A. N.; Crews, C. M. Targeted Protein Degradation: Expanding the Toolbox. *Nature Reviews Drug Discovery* **2019**, *18* (12), 949–963.

- (285) Wu, T.; Yoon, H.; Xiong, Y.; Dixon-Clarke, S. E.; Nowak, R. P.; Fischer, E. S. Targeted Protein Degradation as a Powerful Research Tool in Basic Biology and Drug Target Discovery. *Nature Structural & Molecular Biology* **2020**.
- (286) Sakamoto, K. M.; Kim, K. B.; Kumagai, A.; Mercurio, F.; Crews, C. M.; Deshaies, R. J. Protacs: Chimeric Molecules That Target Proteins to the Skp1-Cullin-F Box Complex for Ubiquitination and Degradation. *Proceedings of the National Academy of Sciences* **2001**, *98* (15), 8554–8559.
- (287) Arvinas Inc. *A Phase 1, Open-Label, Dose Escalation Clinical Trial to Evaluate the Safety, Tolerability and Pharmacokinetics of ARV-471 in Patients With Estrogen Receptor Positive/Human Epidermal Growth Factor Receptor 2 Negative (ER+/HER2-) Locally Advanced or Metastatic Breast Cancer, Who Have Received Prior Hormonal Therapy and Chemotherapy in the Locally Advanced/Metastatic Setting*; Clinical trial registration NCT04072952; clinicaltrials.gov, 2020.
- (288) Arvinas Inc. *A Phase 1, Open-Label, Dose Escalation Clinical Trial to Evaluate the Safety, Tolerability, Pharmacokinetics, and Pharmacodynamics of ARV-110 in Patients With Metastatic Castration-Resistant Prostate Cancer Who Have Progressed on at Least Two Prior Systemic Therapies.*; Clinical trial registration NCT03888612; clinicaltrials.gov, 2019.
- (289) Gao, H.; Sun, X.; Rao, Y. PROTAC Technology: Opportunities and Challenges. *ACS Medicinal Chemistry Letters* **2020**, *11* (3), 237–240.
- (290) Inc, A. Arvinas Releases Updated Dose Escalation Data from Clinical Trial of PROTAC® Protein Degradator ARV-110 in Patients with Metastatic Castration-Resistant Prostate Cancer <http://www.globenewswire.com/news-release/2020/05/29/2040817/0/en/Arvinas-Releases-Updated-Dose-Escalation-Data-from-Clinical-Trial-of-PROTAC-Protein-Degradator-ARV-110-in-Patients-with-Metastatic-Castration-Resistant-Prostate-Cancer.html> (accessed Jul 15, 2020).
- (291) Sun, X.; Gao, H.; Yang, Y.; He, M.; Wu, Y.; Song, Y.; Tong, Y.; Rao, Y. PROTACs: Great Opportunities for Academia and Industry. *Signal Transduction and Targeted Therapy* **2019**, *4* (1), 1–33.
- (292) Papatzimas, J. W.; Gorobets, E.; Maity, R.; Muniyat, M. I.; MacCallum, J. L.; Neri, P.; Bahlis, N. J.; Derksen, D. J. From Inhibition to Degradation: Targeting the Antiapoptotic Protein Myeloid Cell Leukemia 1 (MCL1). *J. Med. Chem.* **2019**, *62* (11), 5522–5540.
- (293) Tinworth, C. P.; Lithgow, H.; Dittus, L.; Bassi, Z. I.; Hughes, S. E.; Muelbaier, M.; Dai, H.; Smith, I. E. D.; Kerr, W. J.; Burley, G. A.; Bantscheff, M.; Harling,

- J. D. PROTAC-Mediated Degradation of Bruton's Tyrosine Kinase Is Inhibited by Covalent Binding. *ACS Chem. Biol.* **2019**, *14* (3), 342–347.
- (294) Tovell, H.; Testa, A.; Zhou, H.; Shpiro, N.; Crafter, C.; Ciulli, A.; Alessi, D. R. Design and Characterization of SGK3-PROTAC1, an Isoform Specific SGK3 Kinase PROTAC Degrader. *ACS Chem Biol* **2019**, *14* (9), 2024–2034.
- (295) Zhang, F.; Wu, Z.; Chen, P.; Zhang, J.; Wang, T.; Zhou, J.; Zhang, H. Discovery of a New Class of PROTAC BRD4 Degraders Based on a Dihydroquinazolinone Derivative and Lenalidomide/Pomalidomide. *Bioorganic & Medicinal Chemistry* **2020**, *28* (1), 115228.
- (296) Neklesa, T. K.; Winkler, J. D.; Crews, C. M. Targeted Protein Degradation by PROTACs. *Pharmacology & Therapeutics* **2017**, *174*, 138–144.
- (297) Smith, B. E.; Wang, S. L.; Jaime-Figueroa, S.; Harbin, A.; Wang, J.; Hamman, B. D.; Crews, C. M. Differential PROTAC Substrate Specificity Dictated by Orientation of Recruited E3 Ligase. *Nature Communications* **2019**, *10* (1), 131.
- (298) Cyrus, K.; Wehenkel, M.; Choi, E.-Y.; Han, H.-J.; Lee, H.; Swanson, H.; Kim, K.-B. Impact of Linker Length on the Activity of PROTACs. *Mol Biosyst* **2011**, *7* (2), 359–364.
- (299) VENCLEXTA® (venetoclax tablets): CLL/SLL and AML Treatment
<https://www.venclexta.com/>
- (300) Genentech: Press Releases | Monday, Mar 23, 2020
<https://www.gene.com/media/press-releases/14842/2020-03-23/genentech-announces-venclexta-combinatio>
- (301) Pollyea, D. A.; Amaya, M.; Strati, P.; Konopleva, M. Y. Venetoclax for AML: Changing the Treatment Paradigm. *Blood Adv* **2019**, *3* (24), 4326–4335.
- (302) Tausch, E.; Close, W.; Dolnik, A.; Bloehdorn, J.; Chyla, B.; Bullinger, L.; Döhner, H.; Mertens, D.; Stilgenbauer, S. Venetoclax Resistance and Acquired BCL2 Mutations in Chronic Lymphocytic Leukemia. *Haematologica* **2019**, *104* (9), e434–e437.
- (303) Thangavadivel, S.; Byrd, J. C. Gly101Val BCL2 Mutation: One Step Closer to Understanding Venetoclax Resistance in CLL. *Cancer Discov* **2019**, *9* (3), 320–322.
- (304) Novel mutations contribute to progression of venetoclax-treated CLL
<https://www.mdedge.com/hematology-oncology/article/216519/cll/novel-mutations-contribute-progression-venetoclax-treated-cll>

- (305) Scheepstra, M.; Hekking, K. F. W.; van Hijfte, L.; Folmer, R. H. A. Bivalent Ligands for Protein Degradation in Drug Discovery. *Comput Struct Biotechnol J* **2019**, *17*, 160–176.
- (306) Mathieu, A.-L.; Sperandio, O.; Pottiez, V.; Balzarín, S.; Herlédan, A.; Elkaïm, J. O.; Fogeron, M.-L.; Piveteau, C.; Dassonneville, S.; Deprez, B.; Villoutreix, B. O.; Bonnefoy, N.; Leroux, F. Identification of Small Inhibitory Molecules Targeting the Bfl-1 Anti-Apoptotic Protein That Alleviates Resistance to ABT-737. *J Biomol Screen* **2014**, *19* (7), 1035–1046.
- (307) Barile, E.; Marconi, G. D.; De, S. K.; Baggio, C.; Gambini, L.; Salem, A. F.; Kashyap, M. K.; Castro, J. E.; Kipps, T. J.; Pellicchia, M. HBfl-1/HNOXA Interaction Studies Provide New Insights on the Role of Bfl-1 in Cancer Cell Resistance and for the Design of Novel Anticancer Agents. *ACS Chem. Biol.* **2017**, *12* (2), 444–455.
- (308) Bandyopadhyay, A.; Gao, J. Targeting Biomolecules with Reversible Covalent Chemistry. *Curr Opin Chem Biol* **2016**, *34*, 110–116.
- (309) Harvey, E. P.; Seo, H.-S.; Guerra, R. M.; Bird, G. H.; Dhe-Paganon, S.; Walensky, L. D. Crystal Structures of Anti-Apoptotic BFL-1 and Its Complex with a Covalent Stapled Peptide Inhibitor. *Structure* **2018**, *26* (1), 153-160.e4.
- (310) Poole, L. B. The Basics of Thiols and Cysteines in Redox Biology and Chemistry. *Free Radic. Biol. Med.* **2015**, *80*, 148–157.
- (311) Johnson, D. S.; Weerapana, E.; Cravatt, B. F. Strategies for Discovering and Derisking Covalent, Irreversible Enzyme Inhibitors. *Future Med Chem* **2010**, *2* (6), 949–964.
- (312) Lopes, F.; Santos, M. M. M.; Moreira, R. *1.2 Designing Covalent Inhibitors: A Medicinal Chemistry Challenge*; De Gruyter, 2015; pp 44–60.
- (313) Huhn, A. J.; Guerra, R. M.; Harvey, E. P.; Bird, G. H.; Walensky, L. D. Selective Covalent Targeting of Anti-Apoptotic BFL-1 by Cysteine-Reactive Stapled Peptide Inhibitors. *Cell Chem Biol* **2016**, *23* (9), 1123–1134.
- (314) Lanning, M. E.; Fletcher, S. Recapitulating the α -Helix: Nonpeptidic, Low-Molecular-Weight Ligands for the Modulation of Helix-Mediated Protein–Protein Interactions. *Future Medicinal Chemistry* **2013**, *5* (18), 2157–2174.
- (315) Boersma, M. D.; Sadowsky, J. D.; Tomita, Y. A.; Gellman, S. H. Hydrophile Scanning as a Complement to Alanine Scanning for Exploring and Manipulating Protein–Protein Recognition: Application to the Bim BH3 Domain. *Protein Sci* **2008**, *17* (7), 1232–1240.

- (316) Petros, A. M.; Olejniczak, E. T.; Fesik, S. W. Structural Biology of the Bcl-2 Family of Proteins. *Biochim. Biophys. Acta* **2004**, *1644* (2–3), 83–94.
- (317) Azzarito, V.; Long, K.; Murphy, N. S.; Wilson, A. J. Inhibition of α -Helix-Mediated Protein-Protein Interactions Using Designed Molecules. *Nat Chem* **2013**, *5* (3), 161–173.
- (318) Barnard, A.; Long, K.; Yeo, D. J.; Miles, J. A.; Azzarito, V.; Burslem, G. M.; Prabhakaran, P.; A Edwards, T.; Wilson, A. J. Orthogonal Functionalisation of α -Helix Mimetics. *Org. Biomol. Chem.* **2014**, *12* (35), 6794–6799.
- (319) Orner, B. P.; Ernst, J. T.; Hamilton, A. D. Toward Proteomimetics: Terphenyl Derivatives as Structural and Functional Mimics of Extended Regions of an α -Helix. *J. Am. Chem. Soc.* **2001**, *123* (22), 5382–5383.
- (320) Yin, H.; Lee, G.-I.; Sedey, K. A.; Kutzki, O.; Park, H. S.; Orner, B. P.; Ernst, J. T.; Wang, H.-G.; Sebt, S. M.; Hamilton, A. D. Terphenyl-Based Bak BH3 Alpha-Helical Proteomimetics as Low-Molecular-Weight Antagonists of Bcl-XL. *J. Am. Chem. Soc.* **2005**, *127* (29), 10191–10196.
- (321) Lanning, M. E.; Fletcher, S. Multi-Facial, Non-Peptidic α -Helix Mimetics. *Biology (Basel)* **2015**, *4* (3), 540–555.
- (322) Lee, Y.; Im, H.; Das, S.; Oh, M.; Lee, J. H.; Ham, S.; Lim, H.-S. Bridged α -Helix Mimetic Small Molecules. *Chem. Commun.* **2019**, *55* (88), 13311–13314.
- (323) Yap, J. L.; Cao, X.; Vanommeslaeghe, K.; Jung, K.-Y.; Peddaboina, C.; Wilder, P. T.; Nan, A.; MacKerell, A. D.; Smythe, W. R.; Fletcher, S. Relaxation of the Rigid Backbone of an Oligoamide-Foldamer-Based α -Helix Mimetic: Identification of Potent Bcl-XL Inhibitors. *Org. Biomol. Chem.* **2012**, *10* (15), 2928–2933.
- (324) Saraogi, I.; Hamilton, A. D. α -Helix Mimetics as Inhibitors of Protein–Protein Interactions. *Biochem Soc Trans* **2008**, *36* (6), 1414–1417.
- (325) Fletcher, S.; Hamilton, A. D. Protein Surface Recognition and Proteomimetics: Mimics of Protein Surface Structure and Function. *Current Opinion in Chemical Biology* **2005**, *9* (6), 632–638.
- (326) Ernst, J. T.; Becerril, J.; Park, H. S.; Yin, H.; Hamilton, A. D. Design and Application of an Alpha-Helix-Mimetic Scaffold Based on an Oligoamide-Foldamer Strategy: Antagonism of the Bak BH3/Bcl-XL Complex. *Angew. Chem. Int. Ed. Engl.* **2003**, *42* (5), 535–539.
- (327) Martín-Gago, P.; Olsen, C. A. Arylfluorosulfate-Based Electrophiles for Covalent Protein Labeling: A New Addition to the Arsenal. *Angewandte Chemie International Edition* **2019**, *58* (4), 957–966.

- (328) Ali, A. M.; Gómez-Biagi, R. F.; Rosa, D. A.; Lai, P.-S.; Heaton, W. L.; Park, J.; Eiring, A. M.; Vellore, N. A.; de Araujo, E. D.; Ball, D. P.; Shouksmith, A. E.; Patel, A. B.; Deininger, M. W.; O'Hare, T.; Gunning, P. T. Disarming an Electrophilic Warhead: Retaining Potency in Tyrosine Kinase Inhibitor (TKI)-Resistant CML Lines, While Circumventing Pharmacokinetic Liabilities. *ChemMedChem* **2016**, *11* (8), 850–861.
- (329) Krishnan, S.; Miller, R. M.; Tian, B.; Mullins, R. D.; Jacobson, M. P.; Taunton, J. Design of Reversible, Cysteine-Targeted Michael Acceptors Guided by Kinetic and Computational Analysis. *J Am Chem Soc* **2014**, *136* (36), 12624–12630.